

AFFDL-TR-69-111

AD070 2528

20090521 014

FRACTURE MECHANICS GUIDELINES FOR AIRCRAFT STRUCTURAL APPLICATIONS

D. P. WILHEM

*Northrop Corporation
Hawthorne, California*

TECHNICAL REPORT AFFDL-TR-69-111

FEBRUARY 1970

This document has been approved for public release and sale;
its distribution is unlimited.

**AIR FORCE FLIGHT DYNAMICS LABORATORY
AIR FORCE SYSTEMS COMMAND
WRIGHT-PATTERSON AIR FORCE BASE, OHIO**

NOTICE

When Government drawings, specifications, or other data are used for any purpose other than in connection with a definitely related Government procurement operation, the United States Government thereby incurs no responsibility nor any obligation whatsoever; and the fact that the government may have formulated, furnished, or in any way supplied the said drawings, specifications, or other data, is not to be regarded by implication or otherwise as in any manner licensing the holder or any other person or corporation, or conveying any rights or permission to manufacture, use, or sell any patented invention that may in any way be related thereto.

Copies of this report should not be returned unless return is required by security considerations, contractual obligations, or notice on a specific document.

AD-702528

FRACTURE MECHANICS GUIDELINES FOR AIRCRAFT STRUCTURAL APPLICATIONS

D. P. WILHEM

*Northrop Corporation
Hawthorne, California*

This document has been approved for public release and sale;
its distribution is unlimited.

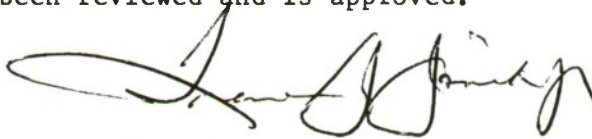
FOREWORD

This report was prepared by Northrop Corporation, Aircraft Division, Hawthorne, California, under Air Force Contract AF 33615-69-C-1313. The project was initiated under Project Number 1467, "Structural Analysis Methods;" the Task, 146704, is entitled "Structural Fatigue Analysis Methods." The work reported herein was administered under the direction of the Air Force Flight Dynamics Laboratory, Air Force Systems Command, Wright-Patterson Air Force Base, Ohio, by Mr. Howard A. Wood, FDTR, project engineer.

The research reported herein was conducted between January 1969 and November 1969. This report was submitted by the author 13 November 1969, for AFFDL review. The report has been assigned NOR 69-142 for internal control at Northrop Corporation.

The author wishes to express his appreciation to Messrs. W. E. Anderson (Battelle Northwest) and F. C. Allen (Douglas Aircraft Division) for their technical review and constructive criticisms of particular sections of the report, and to the many Northrop personnel who helped in contributing to the program. In addition, the illustrative and secretarial assistance of Mr. D. J. Nichols, Dalene Reed, and Cathy Nichols are acknowledged. The aforementioned program was under the technical direction of Messrs. J. E. Wieder and C. Rosenkranz of the Structures Research and Technology Department.

This technical report has been reviewed and is approved.



FRANCIS J. JANIK, JR.
Chief, Solid Mechanics Branch
Structures Division
Air Force Flight Dynamics Laboratory

AD-

ABSTRACT

This document provides the guidelines, limitations, and modifications required to perform a structural, fracture analysis using Griffith-Irwin fracture mechanics principles. It serves as an introduction to fracture mechanics for those personnel who are concerned with fracture strength estimates for aerospace structural applications. Illustrations and hypothetical examples are included which show how engineering solutions for critical crack size and fracture stress may be made. The critical stress intensity (fracture toughness) concept is used as a basic factor for the fracture analysis of materials. For most crack situations, a stress intensity factor can be computed which can be related to critical conditions and estimates made of critical crack lengths, stresses, and crack propagation behaviors. To provide a complete and accurate fracture analysis, the user is encouraged to become familiar with all aspects of the analysis and its limitations.

This document has been approved for public release and sale; its distribution is unlimited.

TABLE OF CONTENTS

SECTION		PAGE
I	INTRODUCTION	1
II	HISTORY OF FRACTURE MECHANICS	2
	II.1 The Griffith/Irwin Era	2
	II.2 ASTM Task Force	7
	II.3 Specimens	7
III	DESIGN PHILOSOPHIES	8
	III.1 Fail Safe	8
	III.2 Safe Life	9
IV	PLANE STRAIN VS. PLANE STRESS IN FRACTURE ANALYSIS	10
	IV.1 "Elastic or Brittle" Fracture	10
	IV.2 Plane Strain	10
	IV.3 Plane Stress	10
	IV.4 Fracture Appearance	13
V	LINEAR ELASTIC STRESS ANALYSIS OF CRACKED PLATES	15
	V.1 Modes of Crack Surface Displacement	15
	V.2 Stress Intensity Factor	15
	V.3 The Westergaard Method (Stress)	18
	V.3(a) Mode I	21
	V.4 The Westergaard Method (Displacement)	22
	V.5 Dimensional Considerations	23
	V.6 Stress Intensity - Stress Concentration	25
	V.7 The Relationship Between Strain Energy Release Rate (\dot{G}) and Stress Intensity	25
	V.8 Superposition of K Solutions	26
	V.9 Critical K Concept	26
	V.10 Summary	28
VI	CRACK TIP PLASTICITY	29
	VI.1 Estimates of Plastic Zone Size	29
	VI.2 Limitations on Plastic Zone Dimensions	31
	VI.3 Influence of Work Hardening on the Plastic Zone	31

SECTION		PAGE
	VI.4 Thickness Effects on Fracture	33
	VI.5 Inclusion of Plasticity and Geometric Corrections in K Solution	37
	VI.6 Summary	38
VII	BASIC STRESS INTENSITY FACTORS	39
	VII.1 Uniform Loading	39
	VII.2 Concentrated Forces	45
	VII.3 Thermal Induced Stresses	47
	VII.4 Stress Intensities for Known Stress Concentrations	48
	VII.5 Part-Through Crack	49
	VII.6 Finite Width Correction	50
	VII.7 Slow Tear in Cracked Structure	50
VIII	METHODS OF RESIDUAL STRENGTH ANALYSIS	55
	VIII.1 Fracture Analysis Concepts	55
	VIII.1(a) Fracture Mechanics (Critical K Concept)	55
	VIII.1(b) Empirically Derived Crack Strength Plots	55
	VIII.1(c) Method A	58
	VIII.1(d) Method B	58
	VIII.1(e) Method C	58
	VIII.1(f) Method D	58
	VIII.1(g) Method E, Notch Strength Analysis (NSA) and Crack Strength Analysis (CSA)	59
	VIII.1(h) Method F, (Part-through Cracks)	59
	VIII.2 Sample Problem Using Various Fracture Analysis Methods	59
	VIII.2(a) Fracture Mechanics Analysis	60
	VIII.2(b) Crack Strength Plot	61
	VIII.2(c) Method A Analysis	61
	VIII.2(d) Method B Analysis	62
	VIII.2(e) Method E, Crack Strength Analysis (NSA) and (CSA)	63
	VIII.2(f) Common Grounds	64

SECTION	PAGE
IX	INFLUENCE OF FRACTURE IN AIRCRAFT DESIGN 65
IX.1	Material Trade-offs 65
IX.1(a)	Material Substitutions 66
IX.1(b)	Other Methods of Material Fracture Comparison 68
IX.2	Bending Loads 68
IX.3	Other Crack Geometries 72
IX.4	Effective or Equivalent Crack Length 72
IX.4(a)	The Crack at a Hole 72
IX.4(b)	Design with Reduced Thickness 77
IX.5	Crack at Rivets 77
IX.6	Eccentrically Loaded Crack 80
IX.7	Complex Through-Cracked Structure 84
IX.7(a)	Damage Configurations 84
IX.7(b)	Geometric Corrections 84
IX.8	Geometric Combinations 88
IX.8(a)	Selection of Fracture Toughness Value 103
IX.9	Non-symmetric Crack-Integral Stringer 106
IX.9(a)	Example 106
IX.10	Summary 110
IX.11	Fracture Stress Estimates with Average Fracture Toughness Data 112
IX.11(a)	Computation of Geometric Corrections 112
IX.12	Summary 116
IX.13	Part-Through Cracks 116
IX.13(a)	Determination of Critical Discontinuity Dimensions and K_I for Part-Through Cracks 119
IX.13(b)	Arm in Bending as a Part-Through Crack Problem 119
IX.14	Application to Design - Part-Through Cracks 126
IX.15	Effect of Bulging Due to Internal Pressure 126
IX.15(a)	Example Problem 130
IX.16	Application to Reinforced Pressure Cylinders 131
IX.17	Crack Arrest 132
IX.18	Fracture of Composites 132

SECTION		PAGE
X	FATIGUE AND CRACK PROPAGATION	133
	X.1 Influence of Fatigue on Fracture	133
	X.2 Micro-mechanics	133
	X.3 Fracture Mechanics and Cyclic Crack Growth	133
	X.4 Sinusoidal Loading	135
	X.5 Random Loading	136
	X.6 Prediction of Crack Growth to Fracture in Design	136
	X.6(a) Example Problem	138
	X.7 Environmental and Load History Effects	140
	X.8 Crack Growth During Pressure Vessel Proof Testing	140
XI	ENVIRONMENTAL EFFECTS	142
	XI.1 Stress Corrosion Cracking	142
	XI.2 Environmental Fatigue Crack Growth	142
	XI.3 Temperature and Strain Rate Effects on Critical K	146
	XI.4 Summary	146
XII	FRACTURE TESTING PROCEDURES	147
	XII.1 Fracture Toughness Testing	147
	XII.2 Plane Strain Toughness Testing	147
	XII.3 Sources of Plane Strain and Plane Stress Data	151
	XII.3(a) Plane Strain (K_{IC})	151
	XII.3(b) Plane Stress (K_C)	151
	XII.4 Crack Growth Resistance (R Curve Concept)	151
REFERENCES		153
BIBLIOGRAPHY		159
	Crack Propagation-(Environmental Effects)	159
	Crack Propagation-(Theory and Correlations)	161
	Crack Propagation-(Data and Analysis)	163
	Fracture-(Environmental)	167
	Fracture Mechanics-(Theory)	169
	Fracture-(Data and Analysis)	170

LIST OF ILLUSTRATIONS

FIGURE		PAGE
1	Graphic Representation of the Fracture Process for Ideally Brittle and Other Than Brittle Behavior	5
2a	Plane Strain Behavior (Pictorial)	11
2b	Plane Stress Behavior (Pictorial)	11
3	Through-the-Thickness Views of Plane Stress and Plane Strain and Mixed Mode Fractures	12
4	Residual Strength Diagram Showing Regions of Fracture Behavior and General Trends in Fracture Appearance for Plane Strain, Plane Stress, and Mixed Modes	14
5	Modes of Crack Surface Displacement	16
6	Coordinates and Stress Components of Crack Tip Field	17
7	Geometry of Central Cracked-Infinite Plate	19
8	Example of Stress Intensity Superposition	27
9	Pictorial Representation of Through-the-Thickness Plastic Zone Development as First Visualized by Liu ⁽²⁰⁾	30
10	Experimentally Observed Surface, Plane Stress Plastic Zones ⁽¹⁷⁾	32
11	V-Slant, Plane Stress Plastic Zone as Observed by Hahn and Rosenfield ⁽¹⁷⁾	34
12	Trend in Fracture Mode Appearance vs. Crack Tip Plastic Zone Parameter	35
13	Nominal Critical Stress Intensities for Several Materials as a Function of Thickness ^(24,25)	36
14	Finite Width Correction - Center Cracks (Tension) ⁽²⁹⁾	51
15	Finite Width Correction - Double Edge Cracks (Tension) ⁽¹⁵⁾	51
16	Finite Width Correction - Single Edge Cracks (Tension) ⁽³⁰⁾	52
17	Finite Width Correction - Single Edge Crack (Bending) ⁽⁸⁾	53
18	Finite Width Correction - Eccentric Crack (Tension) ⁽²⁹⁾	54
19	Fracture Analysis Progression in Design	56

FIGURE		PAGE
20	Residual Strength as a Function of Panel Width - 0.08 Inch Gage 7075-T6 Clad	57
21	Density Normalized Plot of Plane Strain Fracture Toughness and Yield Strength for Different Materials ⁽²⁵⁾	69
22	Simply Supported Bar of Example Problem, In Bending	70
23	Feed-Through Arm with Welded Support Base	73
24	Equivalent Crack Length for Cracks at a 1-inch Diameter Hole	75
25	Crack at Rivet in a Riveted Skin-Stringer Panel (No Crack Buckling)	78
26	Superposition of Stress Intensities for Uniform Tension and Concentrated Force	79
27	Trends in Stress Intensity for Loading of Figure 26	81
28	Edge Cracked Panel Geometry for Example Problem (No Crack Buckling)	82
29	Critical Fracture Stress for Panel Geometry of Figure 28 (No Crack Buckling)	85
30	Symmetric Crack Configuration in Uniaxial Tension	86
31	Nonsymmetric Crack in Riveted Panel - Uniaxial Loading	87
32	Correction Factors for Symmetric Crack Midway Between Rivets - Riveted Stringer - Stringer Intact ⁽⁴⁷⁾	89
33	Correction Factors for Symmetric Crack Through Rivet Hole - Riveted Stringer - Stringer Intact ⁽⁴⁷⁾	90
34	Correction Factors for Nonsymmetric Conditions - Center Cracked Panel for $S' = 0.5$ and 1.0 ⁽⁴⁷⁾	91
35	Correction Factors for Nonsymmetric Conditions - Center Cracked Panel for $S' = 2.0$ ⁽⁴⁷⁾	92
36	Correction Factors for Edge Stiffened, Center Cracked Plate - Bending Stiffness, $\alpha = 0$ ⁽²⁸⁾	93
37	Correction Factors for Edge Stiffened, Center Cracked Plate - Bending Stiffness, $\alpha = 0.01$ ⁽²⁸⁾	94
38	Correction Factors for Edge Stiffened, Center Cracked Plate - Bending Stiffness, $\alpha = 0.03$ ⁽²⁸⁾	95

FIGURE		PAGE
39	Correction Factors for Edge Stiffened, Center Cracked Plate - Bending Stiffness, $\alpha = 0.05$ ⁽²⁸⁾	96
40	Correction Factors for Edge Stiffened, Center Cracked Plate - Bending Stiffness, $\alpha = 0.09$ ⁽²⁸⁾	97
41	Center Cracked Panel Geometry of Example Problem	98
42	Correction Factors for Symmetric-Cracked Plate with Reinforced Edges for the Geometry of Figure 41	101
43	Composite Correction Factors and Critical Stress as a Function of Crack Length for Geometry of Figure 41 with \bar{E} Stringer Intact (No Crack Buckling)	104
44	Comparison of Predicted Fracture Stress for Crack Geometry of Figure 41 - Center Stringer Intact and Broken (No Crack Buckling)	105
45	Sample Problem Panel Geometry	107
46	Correction Factors - Nonsymmetric Crack - Integral Stringer ⁽⁴⁸⁾	109
47	Comparison of Fracture Stress for Riveted and Integral Stringer Panels of Figures 41 and 45 (No Crack Buckling)	111
48	Lower Center Wing Panel for Example Problem	113
49	Estimates of Fracture Envelopes for the Panel Geometry of Figure 48 for Two Skin Materials (No Crack Buckling)	117
50	Comparison of Fracture Stress and Crack Lengths for Panel Geometry of Figure 48 for Two Skin Materials (No Crack Buckling)	118
51	Flaw Shape Parameter Curves ⁽⁴⁵⁾	120
52	Elastic Stress Magnification Factors for Deep Surface Discontinuities - In Tension ⁽³⁰⁾	121
53	Stress Magnification Factors for Semi-Elliptical Surface Flaw in Section in Bending at $\beta = 0^\circ$ and 90° ⁽²⁵⁾	122
54	Elastic Magnification Factors at Points Pt_1 and Pt_2 for an Embedded, Eccentric Loaded Flaw in Tension ⁽⁴⁹⁾	123
55	Combined Elastic and Plastic Magnification Factors for a Deep Surface Discontinuity - In Tension ($a/2c < 0.3$) ⁽²⁵⁾	124

FIGURE		PAGE
56	Schematic of Static and Cyclic Flaw Growth for a Given Environment ⁽⁴²⁾	127
57	Crack Geometry and Stress System for Pressurized Crack with Pressure Bulging ⁽⁵⁰⁾	128
58	Electron Fractograph of Fatigue Area on 7075-T6 Aluminum Plate	134
59	Typical Crack Growth vs. Stress Intensity Factor Range Data for 7075-T6 and 2024-T3 Aluminum ⁽⁶⁵⁾	137
60	Example Problem - Corner Crack at Bolt Hole Loaded in Tension	139
61	Schematic of Delay in Crack Growth Due to Stress Overload in Aluminum Alloys ⁽⁶³⁾	141
62	Typical Behavior of Net Stress and K_I for a Wedge Force-Loaded Specimen	143
63	Delayed Failure Due to Environmental Crack Growth	144
64	The Effect of Moisture on Fatigue - Crack Growth in a Clad 2024-T3 Aluminum Alloy ⁽⁶⁹⁾	145
65	Fracture Toughness Test Specimens	148
66	Typical Calibration Curve for a Center Crack Geometry with 0.2 inch Gage Point Distance	149
67	Representation of Typical Displacement Gage-Load Record in Fracture Toughness Test	150

LIST OF TABLES

NUMBER		PAGE
I	Comparison of Fracture Data for Various Analysis Methods	64
II	Data for Material Trade-Off Study Problem	66
III	Data for Material Substitution Study	67
IV	Correction Factors for Example Problem	99
V	Correction Factors for Example Problem	100
VI	Correction Factors for Example Problem	102
VII	Composite Correction Factors From Tables IV - VI	102
VIII	Correction Factors for Example Problem	108
IX	Correction Factors for Example Problem	108
X	Composite Correction Factors From Tables VIII & IX	110
XI	Correction Factors for Example Problem Aluminum-Aluminum and Titanium-Steel Construction	114
XII	Correction Factors for Example Problem Aluminum-Aluminum and Titanium-Steel Construction	114
XIII	Correction Factors for Example Problem Aluminum-Aluminum and Titanium-Steel Construction	115
XIV	Composite Correction Factors for Example Problem Aluminum-Aluminum and Titanium-Steel Construction From Tables XI - XIII	115
XV	Flaw Shape Parameters for Example Problems	125
XVI	Values of Bulge Correction at Temperature for Various Materials (Data from Ref. 50)	130

Symbol	<u>SYMBOLS AND NORMAL UNITS*</u>	Units
a	Crack length (usually $1/2$ total length) or crack depth (part-through crack)	inch
a_o	Initial crack length (usually $1/2$ total length)	inch
$2a$	Total crack length (tip to tip)	inch
$2a_c$	Critical crack length (tip to tip)	inch
a_c	Critical crack length	inch
a_e	Equivalent Griffith crack length	inch
a_{ec}	Critical, equivalent Griffith crack length	inch
$\Delta a, da$	Incremental crack extension	inch
$\frac{2a}{W}$	Crack aspect ratio, (crack length/panel width)	
A	Area or constant	inches ²
$A_{str.}, A_{STR}$	Cross sectional area of stringer	inches ²
B	Material thickness	inch
b, c	Length from center line to point of concentrated force	inch
C	A constant	
$2c$	Crack length (part-through crack)	inch
E	Young's Modulus or Modulus of plate	psi or ksi x 10^3
$E_{str.}, E_{STR}$	Modulus of stringer	psi or ksi x 10^3
e	(See Figure 18)	inch
F	Force per unit thickness or length	lbs/inch
f	A function of	
G	Shear Modulus	psi
\mathcal{G}	Strain energy release rate	inch-lbs/inch ²
\mathcal{G}_c	Critical \mathcal{G} for instability	inch-lbs/inch ²
I_z	Moment of inertia of stiffener about its neutral axis perpendicular to the plane of the plate	inch ⁴

* Except where noted in text.

Symbols		Units
K_I, II, III	Stress intensity factors for cracking Modes of Figure 5.	$\text{ksi}\sqrt{\text{inch}}$
K_{Ic}	Critical stress intensity factor for Mode I cracks (Plane Strain Fracture Toughness)	$\text{ksi}\sqrt{\text{inch}}$
K_c	Critical stress intensity factor for an infinite sheet for Mode I cracks (Plane Stress Fracture Toughness)	$\text{ksi}\sqrt{\text{inch}}$
\bar{K}_c	Average critical value of plane stress, Mode I stress intensity	$\text{ksi}\sqrt{\text{inch}}$
K_{Isc}	Critical stress intensity for Mode I in environmental (corrosive) conditions	$\text{ksi}\sqrt{\text{inch}}$
K_b	Bulging stress intensity factor	$\text{ksi}\sqrt{\text{inch}}$
K_{Ii}	Initial value of stress intensity factor	$\text{ksi}\sqrt{\text{inch}}$
K_h	Hoop membrane stress intensity factor	$\text{ksi}\sqrt{\text{inch}}$
K_{th}	Threshold value of stress intensity factor	$\text{ksi}\sqrt{\text{inch}}$
K_Q	Tentative value of plane strain fracture toughness	$\text{ksi}\sqrt{\text{inch}}$
k	Elastic constant for plane strain or plane stress	
M	Bending moment per unit thickness	lb-inch/inch
M_k	Elastic magnification factor	
n	Strain hardening coefficient or numerical constant	
$\Delta N, dN$	Incremental cycles	cycles
P, Q	Components of force, F , per unit thickness	lbs/inch
p	Rivet pitch	inch
Q	Flaw shape parameter	
r	Radial coordinate of crack tip, radius of hole, or relative size of plastic zone	inch
r_y	Distance from apparent crack tip to elastic-plastic boundary at $\theta = 0$.	inch

Symbols		Units
R	Pressure cylinder radius	inch
R	Crack growth resistance	ksi $\sqrt{\text{inch}}$ or inch-lbs/inch ²
S or S'	Extensional stiffness	
$\left. \begin{matrix} u \\ v \\ w \end{matrix} \right\}$	Rectangular components of displacement	
U _{surface}	Solid state surface tension of material	lbs/inch
U _{plastic}	Energy of plastic deformation	lbs/inch
W	Finite width	inch
W'	(See Figure 18)	inch
$\frac{W}{2}$	Half-width	inch
W _{req.}	Work required	inch-lbs
W _{avail.}	Work available from release of stored elastic energy	inch-lbs
$\left. \begin{matrix} x \\ y \\ z \end{matrix} \right\}$	Rectangular coordinates	
z	Complex variable ($z = x + iy$)	
Z, Z _I	Westergaard stress functions	
\bar{Z}, \bar{Z}, Z, Z'	Successive derivatives of a Westergaard stress function	
α	Angle or closing segment of a crack, "material constant", coefficient of thermal expansion, or nondimensional ratio	degrees
β	Inclination angle of a crack to in-plane loading or orientation angle of crack front for part-through cracks	degrees
θ	Angular orientation from crack plane or orientation of crack	degrees
∇	Gradient $\left[\frac{\partial}{\partial x} + \frac{\partial}{\partial y} \right]$	

Symbols		Units
∇^2, ∇^4	Harmonic and biharmonic operators	
ϵ	Strain	inch/inch
ϵ	Eccentricity, $\epsilon = \frac{2e}{W}$ (See Figure 18)	
ϵ_y, ϵ_z	Strain in y or z coordinate	inch/inch
λ	Correction factor for finite specimen geometry, $f(\frac{a}{W})$ or $f(\frac{2a}{W})$	
$\lambda', \lambda'', \lambda''', \lambda^*, \lambda^{**}$	Individual or composite correction factors for finite specimen geometry	
μ	Thermal conductivity or materials constant	
ν	Poisson's ratio	
ρ	Notch or tip radius or material density	inch or lbs/cu. inch
ζ	Magnification factor	
σ	Stress remote from the crack (gross area stress at infinity)	ksi
$\left. \begin{matrix} \sigma_x \\ \sigma_y \\ \sigma_z \end{matrix} \right\}$	Rectangular stress components	ksi
σ_c	Critical (gross area) fracture stress	ksi
σ_h	Membrane hoop stress	ksi
σ_{hc}	Critical hoop tension fracture stress	ksi
σ_ℓ	Membrane longitudinal stress	ksi
σ_{LIM}	Limit design stress	ksi
σ_{net}	Stress on the uncracked section	ksi
σ_m	Maximum stress near a stress raiser	ksi
σ_u	Material ultimate strength	ksi

Symbols		Units
σ_{ys}	Material yield strength	kci
σ_{yB}	Material biaxial yield strength	kci
$\left. \begin{array}{l} \tau_{xy} \\ \tau_{xz} \\ \tau_{yz} \end{array} \right\}$	Rectangular components of shear stress	kci
τ_{in}	Maximum shear stress adjacent to crack	kci
Φ	Westergaard Airy Stress Function ($\Phi = \text{Re } \bar{Z}_1 + y \text{ Im } \bar{Z}_1$)	
$\psi_{1,2,3}$	Harmonic functions	
Re	Real part of a complex function	
Im	Imaginary part of a complex function	

I INTRODUCTION

This report contains guidelines by which fracture mechanics principles may be used in the analysis of the fracture strength of aircraft structures. It serves as an introduction to the use of this discipline in structural, fracture analysis. The data contained herein is not all inclusive, but supplementary to other information available in the field of fracture mechanics.

Fracture mechanics has been employed to evaluate material fracture behavior with a good degree of success. If materials can be ranked by their critical stress intensity factor ($K_{critical}$), the basic unit of fracture mechanics, then this unit can be applied to the analysis of aerospace structure. Such a critical parameter has been determined for thick section fracture and provides the proper trends in determination of critical fracture stress for plane strain behavior.

Thus, a critical K can be used in fracture analysis--provided the limitations of fracture mechanics are fully understood. It is the purpose of this report to show how fracture mechanics can be used during the vehicle design stages for fracture stress and critical crack length estimations as well as optimum materials selection. To provide a basis for the use of the stress intensity factor in analysis, it is necessary to review its historical evolution, derivation, terminology, and relationship to accepted design philosophies. This is reviewed in Sections II through V. In many structural applications plasticity is not limited and geometric effects predominate. These parameters must be accounted for and lead to modified solutions to the critical K concept (Sections VI and VII). Of necessity, other influencing factors may become dominant, such as environmental effects and require additional modification of the basic critical K concept (Section XI).

With these basic concepts as background, and knowledge of the limitations of fracture mechanics which require modification to these concepts, it is then possible to compare and analyze typical structural fracture problems. These solutions are presented in Sections VIII and IX and are obtained from the following basic premise that there is a K solution for the crack problem of interest which can approach critical conditions. Following this premise, it is then possible to make engineering estimates and recommendations based on fracture mechanics analysis of structure which may become cracked by any means during its development or service lifetime. The accuracy of these estimates is dependent on the choice of critical stress intensity factor.

It is the purpose of this report to make the user of fracture mechanics analysis aware of the basic concepts, limitations, and usage in design. This can only be accomplished in a step-by-step review of all sections of this document. In this manner, the user will become familiar with, and proficient in, the use of fracture mechanics analysis.

II HISTORY OF FRACTURE MECHANICS

To understand the motivating force behind the rapid rise of this new discipline, one must go back to the large number of fracture problems which have occurred over the years. In 1919, a 2-million gallon hot molasses tank failed at a rivet line with complete disaster. Recently, another such tank fractured, resulting in an estimated clean-up requiring 2-3 weeks.

Fracture mechanics, from its unimpressive beginning with an English scientist studying the failure mechanisms in glass, to its present employment in analyzing rocket motor, tankage structure, and aircraft primary structure, has come a long way. During the war and post-war era, the Liberty Ship incidents which saw 1450 welded plate failures, 19 of which were total ship losses, were a prime motivation in extending the theory of fracture of brittle solids to more realistic structural materials. Thus, the theory of Griffith, the English scientist, was modified and updated to account for semi-ductile behavior. There have been other fracture problems, of course, such as rashes of steam generator turbine and motor failures, Polaris motor cases, the 260-inch solid rocket engine case, to name a few, which also helped to establish fracture mechanics as an analysis method, as well as a material evaluation parameter. The cost of replacement, loss of hardware, etc., have dictated the necessity of utilizing the tools of fracture mechanics. This fact is even more important now as the use of higher strength steels, titanium alloys, and exotic materials become more evident in high speed structures.

II.1 THE GRIFFITH/IRWIN ERA

The first in-depth research of sharp-crack fracture was performed by A. A. Griffith⁽¹⁾ of the Royal Aircraft Establishment, England. In 1920 he published his results on the effect of surface scratches on the mechanical strength of solids. His work was truly the initial step in the foundation of fracture science. Working with brittle material (glass), Griffith postulated that an existing crack or flaw will propagate if the total system energy is lowered in the presence of a crack or flaw. Therefore, Griffith provided a means of estimating the theoretical strength of solids and gave the correct relationship between fracture strength and defect size for brittle material.

Based on G. R. Irwin's research at the Naval Research Laboratory, the Griffith theory of fracture was ultimately shown to be not only strain and surface energy dependent, as shown by Griffith, but also highly dependent on the work of plastic deformation⁽²⁾. This led to the conclusion, supported independently by E. Orowan⁽³⁾, that for relatively ductile materials the work of plastic deformation is much larger than that of surface tension for engineering materials. Subsequent papers by Irwin indicated that the energy approach to fracture is equivalent to a critical stress distribution. From this he developed the concept of fracture toughness.

A quantitative relationship could now be placed on the fracture process which included the dimensions of the crack or flaw, the nominal stress field near the crack, and a property of the material which governed the energy balance of the material in the presence of a crack under stress or the so-called fracture toughness. Thus, for the first time, a characterization of

the fracture process for materials of limited ductility was available to the stress engineer and a new method of analysis was developed called fracture mechanics.

The Griffith/Irwin fracture mechanics approach involves an energy balance; that is, the energy required for crack growth and available system energy (stored elastic energy released by the material when the crack grows). When the energy from the elastically strained material surrounding the crack is equal to or exceeds the energy required to support crack growth, crack extension will occur without additional increase in load or stored elastic energy. Griffith's research in brittle glass⁽¹⁾ indicated that for a homogeneous, isotropic material containing a crack of length $2a$, having a thickness B undergoing a uniform tensile stress perpendicular to the crack, the crack would extend an incremental distance (da) on either end. The energy required for this incremental crack extension, which created new fracture surfaces $2B da$, was the energy required to overcome the solid state surface tension of the material, U_{surface} . (Due to symmetry, only one half of the crack is being analyzed.)

$$dW_{\text{req.}} = U_{\text{surface}} \cdot 2B da *$$

Thus, the surface energy required per incremental crack extension is

$$\frac{1}{B} \cdot \frac{dW_{\text{req.}}}{da} = \frac{dW_{\text{req.}}}{dA} = 2U_{\text{surface}} \quad (\text{II-1})$$

where $\frac{1}{B da}$ or $\frac{1}{dA}$ is the crack surface area. Therefore, Griffith indicated that the surface energy is a constant for brittle material.

Griffith then showed that the energy available ($dW_{\text{avail.}}$) from the release of stored elastic energy as the crack grew was

$$dW_{\text{avail.}} = (\text{Stored Elastic Energy}) \times (\text{Affected Volume})$$

or

$$dW_{\text{avail.}} = \frac{1}{2} \frac{\sigma^2}{E} \cdot [2 \pi Ba da]$$

This equation, written in the form of energy available per incremental crack extension, is

$$\frac{1}{B} \frac{dW_{\text{avail.}}}{da} = \frac{dW_{\text{avail.}}}{dA} = \frac{\pi \sigma^2 a}{E} \quad (\text{II-2})$$

where E is the elastic modulus of the material. Griffith then formulated the critical energy balance equation which states

$$dW_{\text{avail.}} = 2U_{\text{surface}}$$

or from Eqs. II-1 and II-2

$$\frac{1}{B} \left(\frac{dW_{\text{avail.}}}{da} \right) = \frac{1}{B} \left(\frac{dW_{\text{req.}}}{da} \right)$$

*The symbol B in fracture mechanics is standard terminology for thickness.

and

$$2U_{\text{surface}} = \frac{\pi \sigma^2 a}{E} \quad (\text{II-3})$$

or written in the familiar Griffith form, equation II-3 is

$$\sigma_{\text{critical}} = \sqrt{\frac{2E U_{\text{surface}}}{\pi a}} \quad (\text{II-4})$$

for the critical energy case.

σ_{critical} is the critical stress for unstable crack propagation (usually written σ_c). The concept stated by equation II-4 is that the critical stress is inversely proportional to the square root of the crack length and directly proportional to the square root of the surface tension. This equation forms the basis for most of the modern theories of fracture of solids.

Orowan in the early 1950's and Irwin, during the same period, showed the influence of local plastic deformation near the crack tip on the fracture control process. Orowan⁽³⁾ stated that for local plasticity, the work of plastic deformation can be treated in a manner similar to Griffith's. He also postulated that if the region of crack tip plasticity was dimensionally small compared to other body dimensions, elastic-stress analysis could be used successfully. Thus, Orowan's modified Griffith equation accounting for plasticity effects was

$$\sigma_c = \sqrt{\frac{2E (U_{\text{surface}} + U_{\text{plastic}})}{\pi a}} \quad (\text{II-5})$$

Orowan also estimated that the work or energy of plastic deformation (U_{plastic}) was 1000 times as large as U_{surface} ; therefore, the latter term could be neglected in the analysis of materials of slight ductility. In this case, equation II-5 becomes

$$\sigma_c \approx \sqrt{\frac{2E U_{\text{plastic}}}{\pi a}}$$

or

$$U_{\text{plastic}} \approx \frac{\pi \sigma_c^2 a}{2E} \quad (\text{II-6})$$

This analysis, independently supported by the work of G. R. Irwin, was the first recognition of the role of plasticity in fracture.

It became apparent with additional research by Irwin⁽²⁾ and his associates, that the energy of plastic deformation (U_{plastic}) was not, however, a constant, but a variable dependent on length of crack; i.e., the larger the crack the greater the plastic energy. To illustrate this finding, refer to Figure 1. A crack of original half length a_0 under increasing load will grow slowly and shows an increase in plastic energy dissipation, $2U_{\text{plastic}}$ (dashed curve). The shape of this curve will be dependent on specimen geometry (width, thickness, etc.) and crack speed. During the rising portion of the plastic energy dissipation curve (crack growth resistance, or R curve is the now accepted terminology), resistance to crack growth occurs with

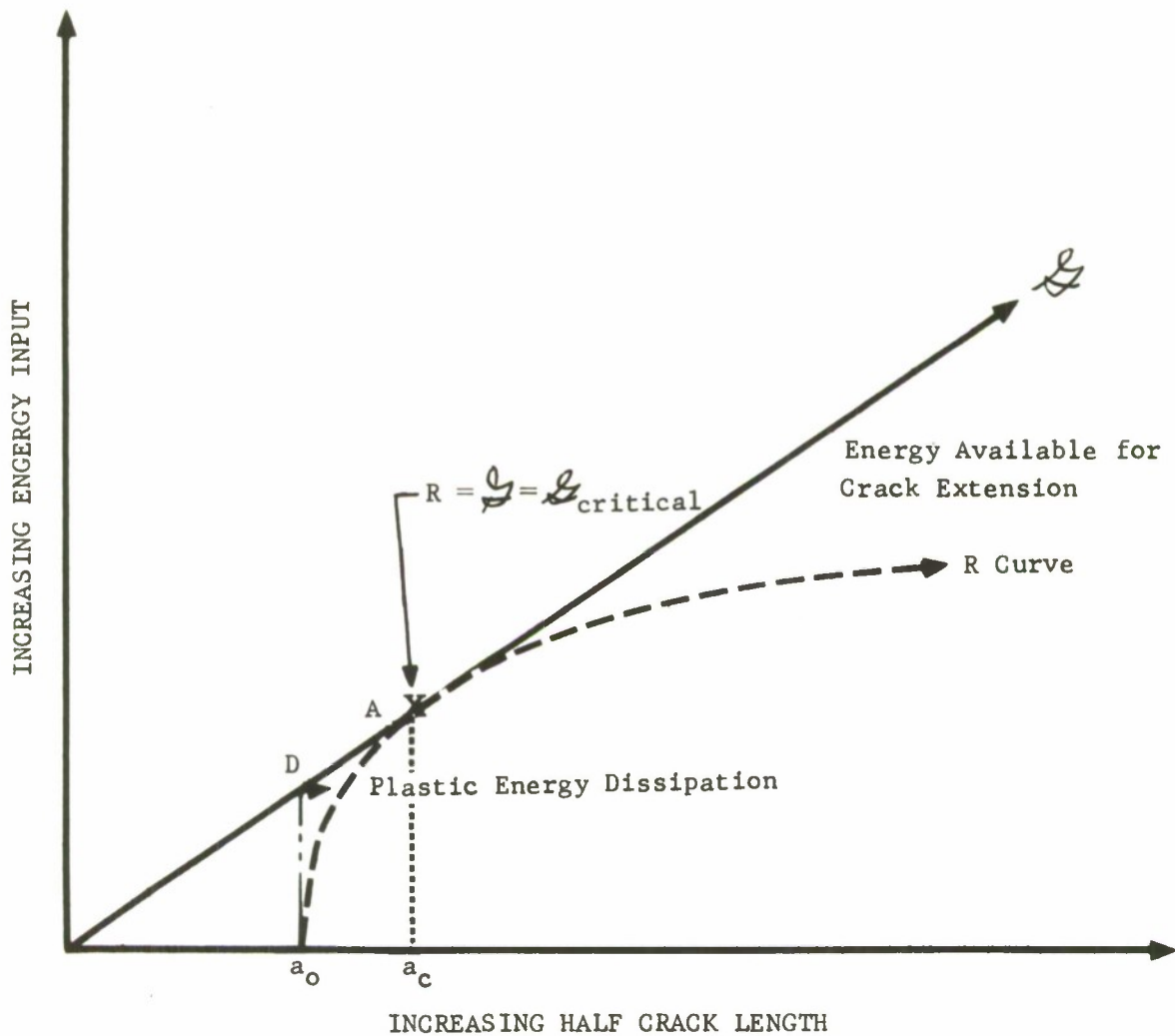


FIGURE 1. GRAPHIC REPRESENTATION OF THE FRACTURE PROCESS FOR IDEALLY BRITTLE AND OTHER THAN BRITTLE BEHAVIOR

increased plastic deformation. Additional input energy is required (increase in external load) until the point of tangency of the R curve and the available energy curve is reached (see point A, Figure 1). At this point, unstable crack growth occurs, i.e., the energy available for crack extension is greater than the dissipated plastic energy. Therefore, the crack growth process is now unlimited with no further increase in load (input energy) for crack extension, and the crack grows catastrophically. One can visualize this process by mentally walking up the R curve. Extra energy is needed to get up the hill, but once the crest is reached (point A) momentum will prevail and less effort is required to proceed.

Point D and its associated resistance curve represents typical behavior of an ideal, brittle material. It will be noted that negligible crack extension occurs prior to instability.

As shown by Irwin, the energy available per crack extension is really the elastic strain-energy release rate (\mathcal{G}) associated with increasing load. Thus, at the point of tangency, (A, Figure 1) the following conditions prevail:

$$R = \mathcal{G} = \mathcal{G}_{\text{critical}}$$

and

$$\frac{d\mathcal{G}}{dR} = \frac{dR}{da}$$

From these relationships, it follows

$$\mathcal{G}_{\text{critical}} = 2U_{\text{plastic}} f(a)$$

or from Eq. II-6

$$\mathcal{G}_c = \frac{\pi \sigma_c^2 a_c}{E} \quad (\text{II-7})$$

A quantitative relationship between critical half crack size (a_c), stress (σ_c), and fracture toughness is shown by equation II-7. The fracture toughness is represented by the critical material strain-energy release rate (\mathcal{G}_c). This equation indicates material fracture behavior on a gross scale. The control of fracture toughness will not be a constant, but dependent on crack length, (a). To date, an analytical means is not available to determine the plastic work associated with the Griffith/Irwin instability equation. However, the problem was solved experimentally by Irwin and his co-workers. The parameters needed to determine a critical strain-energy release rate in equation II-7 are the load and crack length associated with critical crack extension. The load, and hence, critical stress can be determined directly from any universal testing machine. The question remained: how could the associated critical crack length (a_c or $2a_c$) be determined accurately? This problem was solved by Irwin⁽⁴⁾ using an ink stain technique. Using a centrally slotted panel, he placed a small quantity of staining ink at the notch roots. The specimen was then uniaxially loaded perpendicular to the slot. During the rising portion of the R curve (see Figure 1), the ink could slowly follow the crack extension by capillary action. Once the critical point of crack extension was reached, the ink could not keep up with the rapidly advancing crack;

therefore, an indication of critical crack length would be outlined by the distance the ink traveled during slow crack extension. However, consistent calculations of K_{Ic} could not be made. The ink stain method, due to interpretation and experimental difficulties, has since been replaced by more sophisticated techniques, which will be discussed later in this report.

Thus, for the past 50 years, fracture research has shown the evolution of "a new discipline termed 'fracture mechanics', which provides a rational basis for analysis and control of flaw related fracturing of structures." (6)

II.2 ASTM TASK FORCE

In 1958, the Department of Defense initiated a study effort within the American Society for Testing and Materials (ASTM) motivated by several fracture problems in rocket propellant tanks. As the result of this contact, a special ASTM committee was established on Fracture Testing of High-Strength Sheet Materials. (5) The importance of the structures fracture problem can be seen by the appointment of 6 representatives from the aerospace industry and government to this special 10-man committee. Much will be said later in this report about the contributions of this committee to the standardization of fracture testing methods, terminology, and analysis.

The relationship of the analysis by fracture mechanics of aircraft and aerospace structures in preventing fracture in areas which must be fracture or damage tolerant will become evident during the development of this report.

II.3 SPECIMENS

One condition which must prevail in order to determine a valid fracture toughness value is that limited plasticity accompany the fracture process. It will be recalled that the solution of Griffith, Orowan, and Irwin are based on linear elastic approximations; therefore, the crack tip plasticity must be confined to a small zone compared to other specimen dimensions. For this reason, many different specimen designs have been introduced and evaluated since the first fracture toughness specimen. As more specimen types were introduced (notched rounds, edge notch, etc.), it became obvious that standardization of test specimens and methods was required to provide valid fracture toughness measurements. The efforts of experimentalists and analysts within The American Society for Testing and Materials have been instrumental in evaluating these design and test methods. The primary contributors to this effort have been associated with the Naval Research Laboratory (G. R. Irwin, J. M. Krafft, A. M. Sullivan, J. A. Kies, R. W. Boyle, and their co-workers) and NASA Lewis Research Center (J. E. Srawley and W. F. Brown, Jr., and their co-workers). (See, for example, Ref. 7 and 8.) Illustration of the various test specimens in use today will be shown later in Section XII of this report.

III DESIGN PHILOSOPHIES

Fatigue or structural damage can be expected during the operational life of aircraft or spacecraft structures. To account for this in modern aerospace vehicle structural design, two philosophies are frequently considered to ensure attainment of a satisfactory operational life. One of these is the "fail safe" philosophy, which is also associated with the damage tolerant concept. The other is the "safe life" concept, which is really a given life or specified lifetime philosophy. In the following, these two philosophies will be further defined and their applications explored.

III.1 FAIL SAFE

The fail safe concept has been applied to everything from electronic hardware to load-carrying structure in aircraft systems. In structural design, its philosophy states that during the service life of a structure, fatigue cracks or damage will not progress to a catastrophic condition prior to detection during regular inspection periods. Therefore, the fail safe philosophy assumes that readily detectable damage due to fatigue or accidental occurrence will remain in a somewhat stable condition upon subsequent service load history. In aircraft, this concept covers all of the primary structure, so that loss of one component does not reduce the total strength of an assembly to dangerous levels. Most of these components consist of two or more separate segments constructed in a manner that a crack can propagate completely through one section without propagating into a second area; or perhaps a structure is designed or materials selected to take advantage of slower crack growth rates, thus effectively increasing the probability of crack detection during inspection.

FAA certification for transport aircraft necessitates the fail safe concept and dictates that particular structural areas be analyzed and tested to meet fail safe requirements. In commercial design, concern is for the undetected crack, or puncture removing a structural panel between stringers or frames. It also applies to the fatigue or damage of frames and stringers. However, this concept cannot be overlooked in military aircraft, either. In military aircraft, similar damage can be caused by projectiles or shrapnel, and fail safe concepts apply.

The fail safe or damage tolerant philosophy often utilizes stringers as built-in crack or tear stoppers. Tear straps are now an integral part of almost all new commercial designs. The function of these straps as crack stoppers will be discussed further in other sections of this report. Using existing fracture mechanics principles, a fail safe analysis can be made in which critical stresses can be determined for planned designs. Because the ultimate substantiation of these assemblies requires proof testing, a good comparison can be made with the fracture analysis. However, no indication is usually provided as to structural fatigue resistance. Improvements in design are usually made by varying testing parameters and relying on fracture mechanics principles for estimating fail safe stresses.

III.2 SAFE LIFE

The safe life concept assumes that a given structure will not develop fatigue cracks during its service life. Once cracks do occur in the safe life structure, its life is assumed complete.

It is the aim of this concept that during the design phase, materials, stress raisers, and other fatigue-affecting parameters be thoroughly considered to prevent the development of catastrophic cracks under service loading conditions. To achieve this goal, fatigue-sensitive structure is subjected to simulated service testing during the aircraft development stage. Thus, a conservative or realistic test program provides an estimate of service life and establishes inspection and maintenance schedules.

It can be seen that in many cases this concept can lead to costly retrofitting when thoroughly analyzed safe life structure develops fatigue damage during a testing phase. It is quite possible that this may take place some time after production items have been delivered. Problems also arise when service loads are not accurately simulated, or a particular design is pressed into a different service load history than that for which it had been safe life designed.

Thus, the principles of safe life design depends on a fairly accurate estimate of service loading, usually involving a random spectrum. All designs must then be analyzed for fatigue, keeping in mind the starting points for damage such as stress raisers (welds, cutouts, rivet holes, notches, etc.), and the material selection should be optimized for suppression of fatigue.

It can now be seen that both philosophies of structural design have certain limitations. However, both concepts can and should be used in aircraft design to provide the optimum "safe" structure with fracture mechanics as an analysis tool and proof testing as a back-up requirement for critical structure.

IV PLANE STRAIN VS. PLANE STRESS IN FRACTURE ANALYSIS

IV.1 "ELASTIC OR BRITTLE" FRACTURE

The terms brittle or elastic fracture, in general, refer to an elastically stressed body, excluding that region surrounding the crack as the crack grows during the tearing process. Through the terms plane strain and stress, we can tie together the fracture process with fracture mechanics.

IV.2 PLANE STRAIN

In a cracked body, a zone of plasticity (see Section VI) occurs at the crack tip during increase of a remotely applied force. In a thick body, this plastic action is suppressed by interior constraint due to thickness. This is analogous to the definition of plane strain as given in Reference 9; that is, if the z dimension of a stressed body (thickness) is large, then all z direction strains and displacements are zero. This definition could well describe the behavior of a thick section fracture, except for that region near where the crack meets the free surface faces. In that region the z direction strains and displacements are not zero, and lead to the development of shear deformation or "shear lips" near the free surfaces. Therefore, in a thick section, plane strain conditions are governed by the material thickness.

One may visualize an analogous situation with a common tensile test. Shown in Figure 2a is a representative fracture for a material of limited ductility, elastic, except for the region surrounding the fracture. A negligible amount of local plasticity occurs, though the thickness and fracture occurs as indicated by the load deformation curve.

IV.3 PLANE STRESS

In a thin, cracked body subjected to in-plane loads, there is essentially no constraint in the z (thickness) direction (3-dimensional strain state), and plane stress conditions prevail. This lack of constraint is contrasted with the plane strain condition and leads to relatively large plane stress yield zones which are on the order of the material thickness itself.

Using the tensile test analogy once again, Figure 2b indicates a fracture in a ductile material which is elastic, except for the fracture region. Gross cross section deformation has taken place and typical shear failure predominates. At this point it must be realized that the tensile test analogy of Figure 2 is for illustrative purposes only and does not depict plane strain or stress (fracture mechanics) behavior.

The material thickness enters into the modes of failure and is the controlling factor. Thus, for a given material, plane strain, plane stress, or mixtures of the two can be encountered by changing the material thickness, and, therefore, the amount of plastic constraint. Examples of the usual fracture appearance of a material with plane strain, plane stress, and mixed mode type failures are shown in Figure 3.

*The general cross-sectional shape is material and thickness dependent.

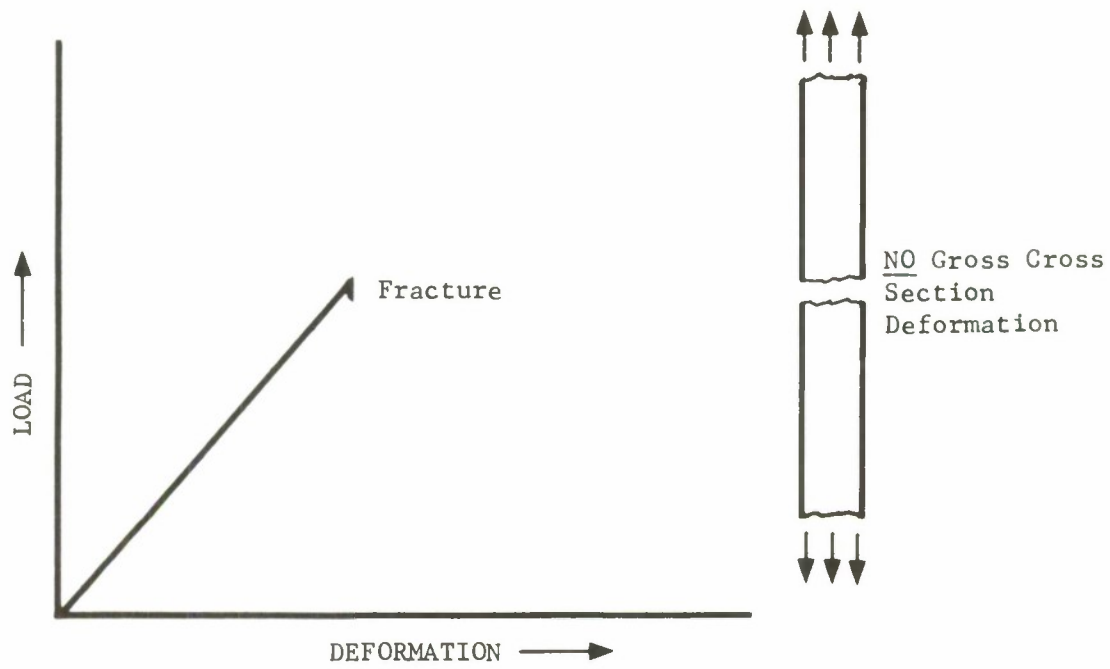


FIGURE 2a. PLANE STRAIN BEHAVIOR (PICTORIAL)

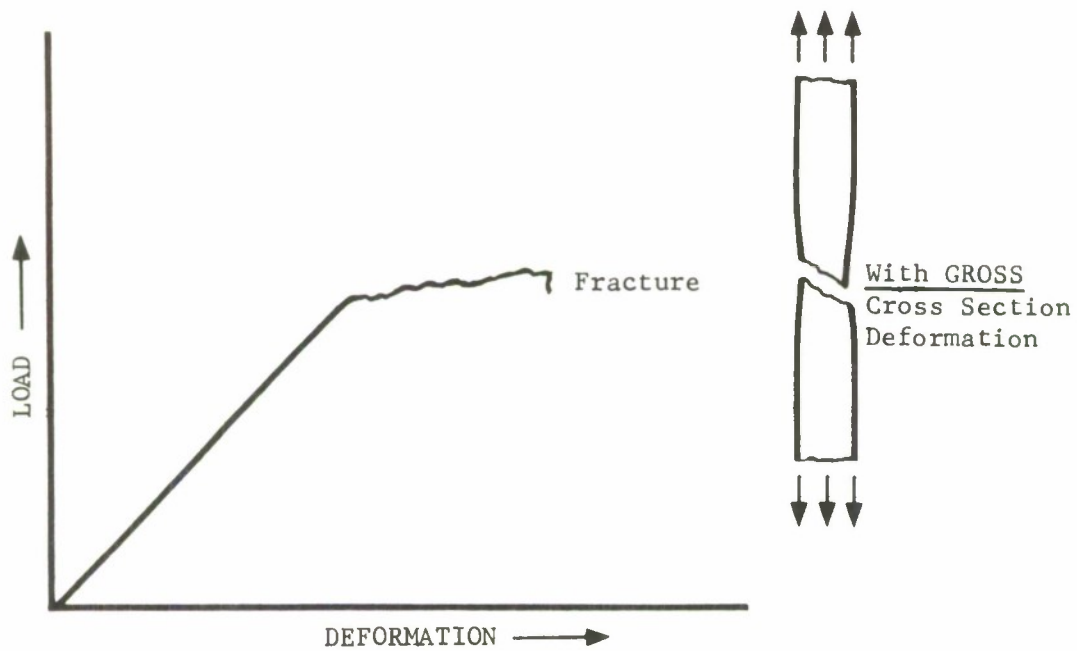
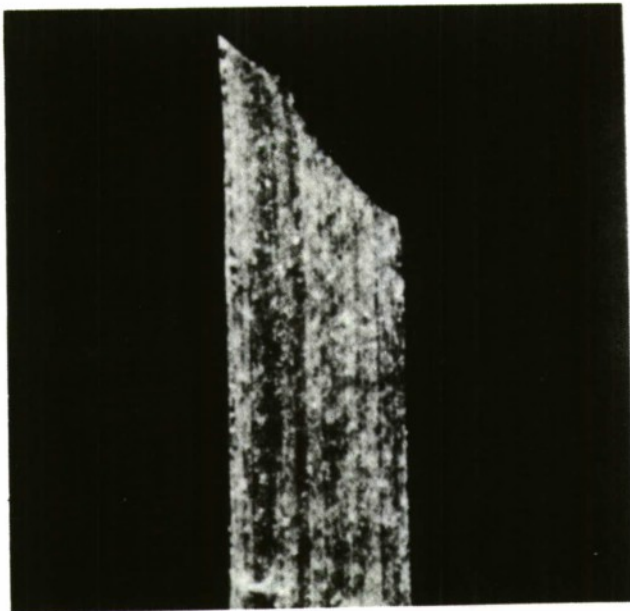
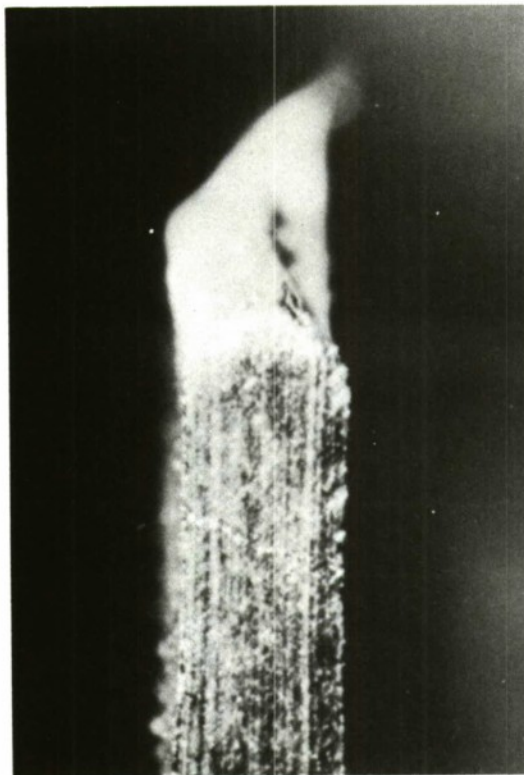


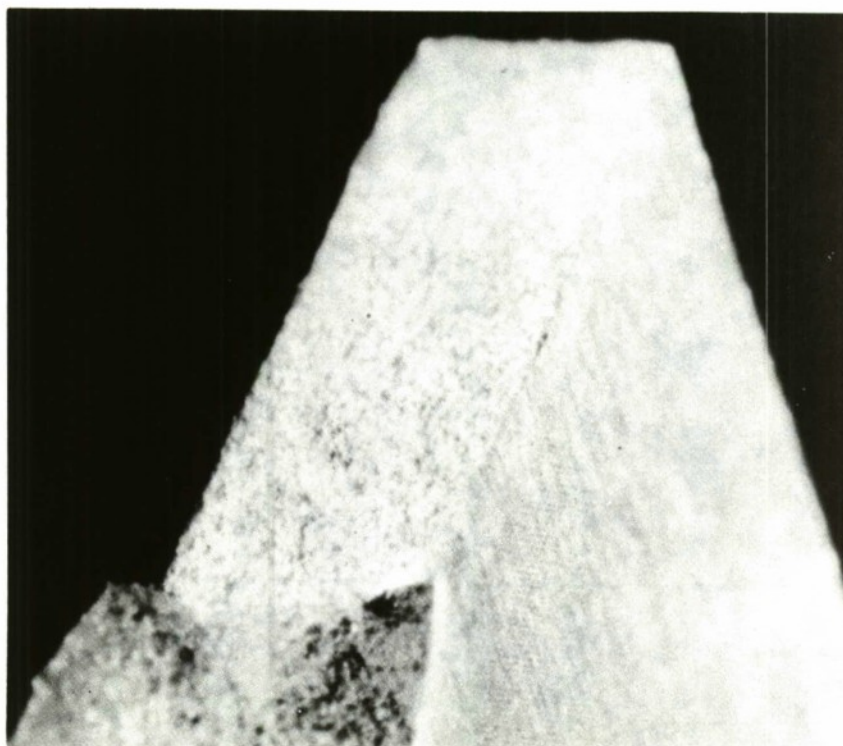
FIGURE 2b. PLANE STRESS BEHAVIOR (PICTORIAL)



PLANE STRESS (SLANT) FRACTURE



PLANE STRESS (V-SLANT) FRACTURE



PLANE STRAIN (FLAT) AND MIXED MODE FRACTURE

FIGURE 3. THROUGH-THE-THICKNESS VIEWS OF PLANE STRESS
& PLANE STRAIN & MIXED MODE FRACTURES

A familiar residual strength diagram is shown in Figure 4. These fracture envelopes would be representative of an aluminum alloy containing central cracks which were small compared to specimen width. For long cracks, plane strain behavior predominates where the nominal stress is small compared to the material yield, and thickness is sufficient to suppress gross crack tip plastic action. In this region, the fracture criterion follows that proposed by Griffith (see Eq. II-4). As the crack length or thickness decreases, a region of mixed mode failure (plane stress and plane strain) predominates due to increased plastic deformation until a condition of plane stress predominates. The elastic based theory of fracture must then be modified to account for increased plastic action.

IV.4 FRACTURE APPEARANCE

A post mortem investigation of a fracture face can tell much about the nature of the stress state, as well as identify the possible failure mechanisms. In fatigue, the appearance of the fracture surface can provide clues to the investigator as to the prior stress history. In fracture, a macroscopic view of the fracture surface can supply information as to the prior state of stress also. In this way, a decision can then be made as to the type of fracture analysis which is applicable--plane stress or plane strain. If a through-the-thickness crack has developed, the preference for crack progression during fracture can be associated with the plane stress, plane strain, or mixed mode regions of Figure 4, as shown with representative fracture surfaces of each region. Therefore, fractures under plane stress conditions usually lead to through-the-thickness, 45-degree, slant or V-slant cross sections. The development of the slant fractures at the fracture faces are referred to as "shear lips" and provide one of the many indications as to the validity of plane strain fracture toughness tests. The significance of the shear lip development will be discussed in Section VI of this report in more detail.

The square appearance of flat fracture indicative of plane strain fracture is also shown in Figure 4. In this case, plastic deformation (through-the-thickness) at the crack tip is minimized and shear lip development negligible. It is within this region that fracture mechanics works with a high degree of confidence, because the equations of fracture are based on elastic analysis.

The plane stress and mixed mode regions, although under intensive study, require modification to the elastic-analysis based theory in order to use fracture mechanics effectively. At the present time, it is these modifications, many of which are empirically based, which produce the greatest limitations on the use of fracture mechanics in design of aircraft structures. However, the basic concepts are sound, and, through an understanding of the limitations of fracture mechanics, a working knowledge of the extension of the analysis to more ductile behavior can be used with confidence.

With this background in theory, history, and basic failure modes of fracture, we can now approach the analysis of the stress state in the presence of cracks and then a major concept of fracture mechanics--the stress intensity factor.

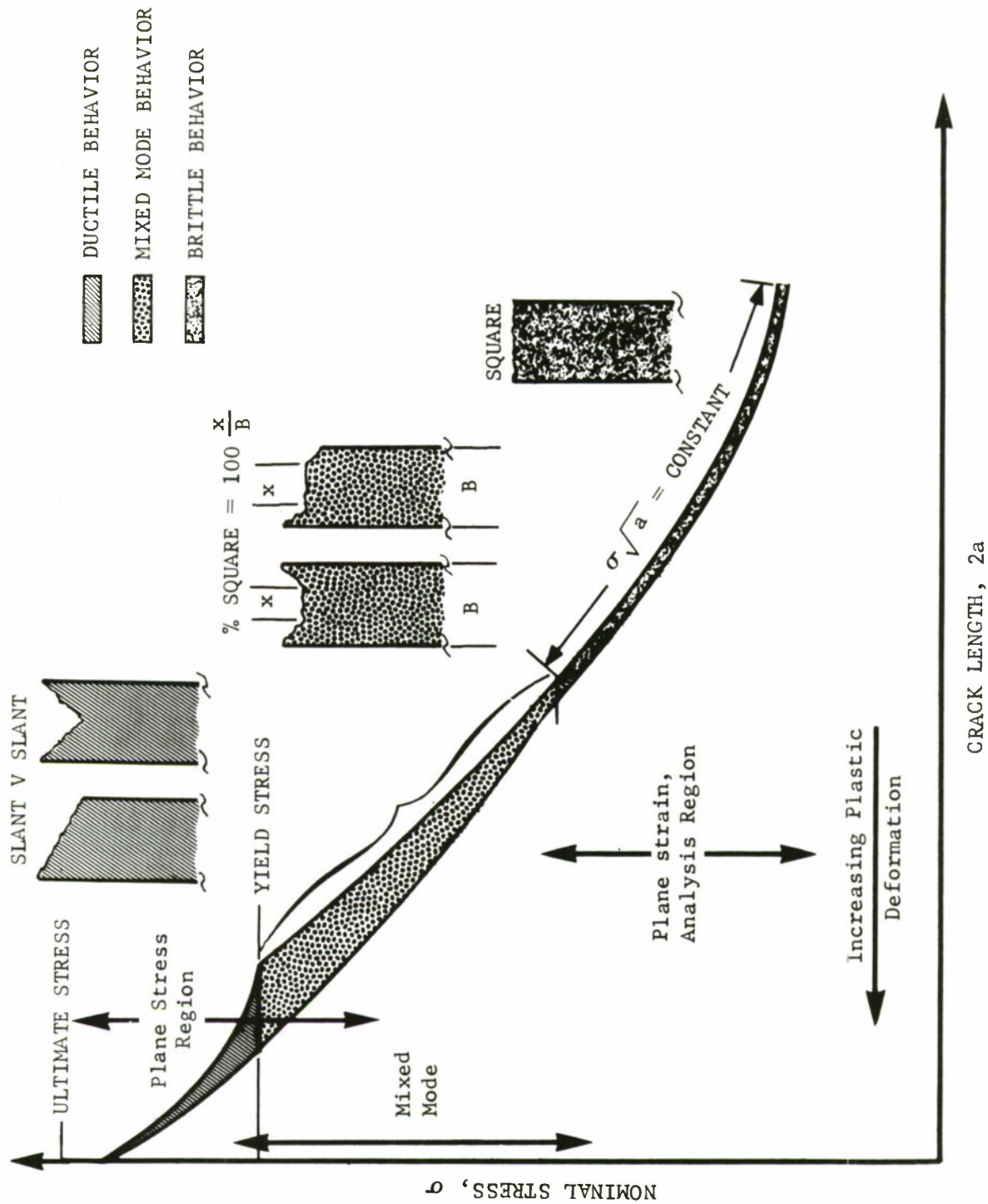


FIGURE 4. RESIDUAL STRENGTH DIAGRAM SHOWING REGIONS OF FRACTURE BEHAVIOR AND GENERAL TRENDS IN FRACTURE APPEARANCE FOR PLANE STRAIN, PLANE STRESS, AND MIXED MODES

V LINEAR ELASTIC STRESS ANALYSIS OF CRACKED PLATES

Through the use of linear elasticity, information can be gained as to the effect of cracks on the stress distribution of an essentially elastic solid. Griffith⁽¹⁾ made use of the Inglis stress solution⁽¹⁰⁾ for an elliptical hole in a uniform tension field. He then degenerated the elliptical hole into a crack solution on which his energy rate theory is based. Sneddon⁽¹¹⁾ in 1946 gave the first solution for stress field expansion near the crack tip. However, it was not until ten years later that Irwin⁽¹²⁾ and M. L. Williams⁽¹³⁾ observed the general applicability of these solutions and provided the extensions which made it possible to apply them to a cracked isotropic elastic body.

V.1 MODES OF CRACK SURFACE DISPLACEMENT

In fracture mechanics, three displacement modes of the crack surfaces are considered. These modes are shown in Figure 5. Indicated are the opening (I), sliding (II), and tearing modes (III). The sliding mode may also be referred to as the edge-sliding mode. It can be seen from Figure 5 that any crack loading problem could be solved by including combinations of two or three modes for various loading situations.

V.2 STRESS INTENSITY FACTOR

Since the crack surfaces are stress free boundaries, that portion near the tip of the crack predominantly influences the local stress field. Therefore, remote forces and boundaries only affect the intensity of this local stress field. This intensity is defined as the crack tip stress intensity factor, K_I , which will be developed in succeeding paragraphs.*

Consider the opening mode (I) crack displacement of Figure 5. Near the leading edge of the crack, the free body diagram would appear as shown in Figure 6. The stress and displacement field can be analyzed as a plane strain (extensional) problem in elasticity. Irwin⁽¹²⁾, using the method of Westergaard⁽¹⁴⁾, analyzed this problem and indicated the following stress fields and displacements for Mode I at a distance, r , close to the crack tip.

Stress Equations (Mode I)

$$\left. \begin{aligned} \sigma_x &= \frac{K_I}{\sqrt{2\pi r}} \cos \frac{\theta}{2} \begin{bmatrix} 1 - \sin \frac{\theta}{2} & \sin \frac{3\theta}{2} \end{bmatrix} \\ \sigma_y &= \frac{K_I}{\sqrt{2\pi r}} \cos \frac{\theta}{2} \begin{bmatrix} 1 + \sin \frac{\theta}{2} & \sin \frac{3\theta}{2} \end{bmatrix} \\ \tau_{xy} &= \frac{K_I}{\sqrt{2\pi r}} \sin \frac{\theta}{2} \begin{bmatrix} \cos \frac{\theta}{2} & \cos \frac{3\theta}{2} \end{bmatrix} \end{aligned} \right\} \dots \dots \dots (V-1)$$

*A physical interpretation of the stress intensity factor is a parameter which reflects the redistribution of stress in an elastic body due to the introduction of a crack and which reflects mode and magnitude of force transmission through the tip region.

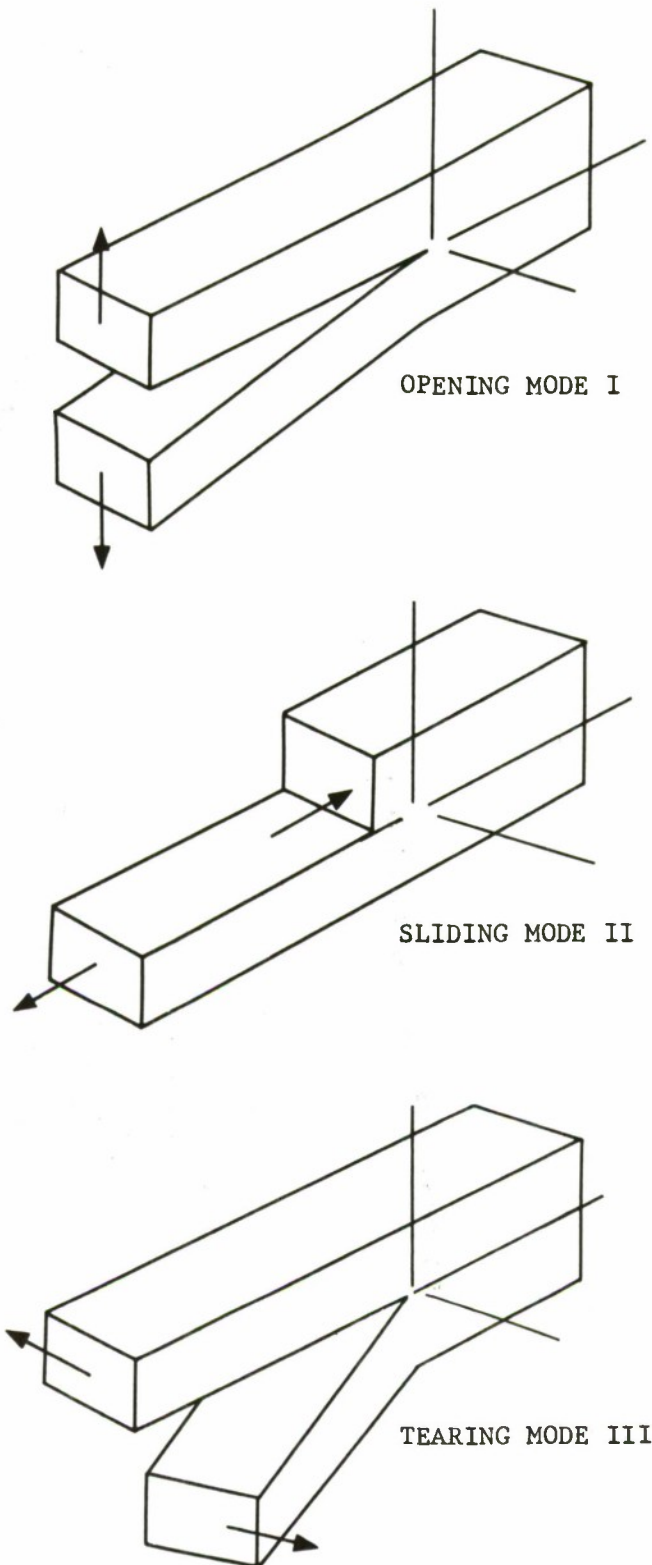


FIGURE 5. MODES OF CRACK SURFACE DISPLACEMENT

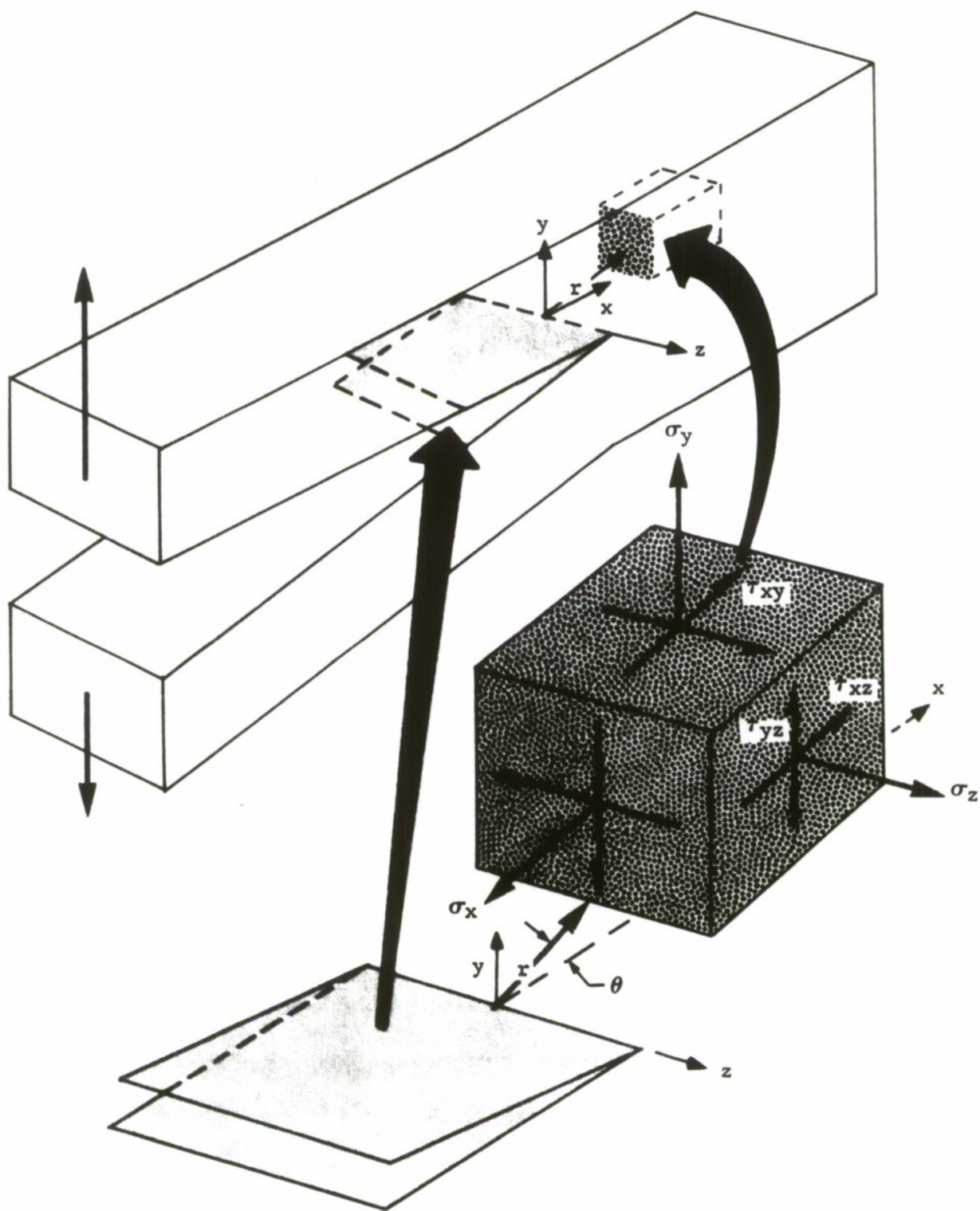


FIGURE 6. COORDINATES AND STRESS COMPONENTS OF CRACK TIP FIELD

$$\tau_{xz} = \tau_{yz} = 0$$

$$\sigma_z = 0 \text{ for plane stress conditions}$$

$$\text{or } \sigma_z = \nu(\sigma_x + \sigma_y) \text{ for plane strain conditions}$$

$$\text{and } \epsilon_z = 0$$

Displacement Equations (Mode I)

$$\left. \begin{aligned} u &= \frac{K_I}{G} \sqrt{\frac{r}{2\pi}} \cos \frac{\theta}{2} \left[1 - 2\nu + \sin^2 \frac{\theta}{2} \right] \\ v &= \frac{K_I}{G} \sqrt{\frac{r}{2\pi}} \sin \frac{\theta}{2} \left[2 - 2\nu - \cos^2 \frac{\theta}{2} \right] \end{aligned} \right\} \dots \dots \dots (V-2)$$

$$\text{and } w = 0 \text{ for plane strain conditions.}$$

V.3 THE WESTERGAARD METHOD (STRESS)

One of the several methods of analyzing cracked plates to obtain stress intensity solutions will be presented here. As mentioned previously, there are several methods available, and a good review is contained in Reference 15. The Westergaard method will be summarized for Mode I cracks of geometry similar to Figure 7. Using the Westergaard method, K can be computed from the (Westergaard) stress function Z. Obtaining the stress function involves guessing for any particular configuration; however, for those well versed in elasticity, it is not difficult. For the Griffith crack configuration of Figure 7, with the coordinates of Figure 6 and elastic material, the plane extension, elastic equilibrium equations are given as:

$$\left. \begin{aligned} \frac{\partial \sigma_x}{\partial x} + \frac{\partial \tau_{xy}}{\partial y} &= 0 \\ \frac{\partial \tau_{xy}}{\partial x} + \frac{\partial \sigma_y}{\partial y} &= 0 \\ \tau_{xy} &= \tau_{yx} \end{aligned} \right\} \dots \dots \dots (V-3)$$

and the strain/displacement relationships and Hookean conditions lead to the compatibility equation,

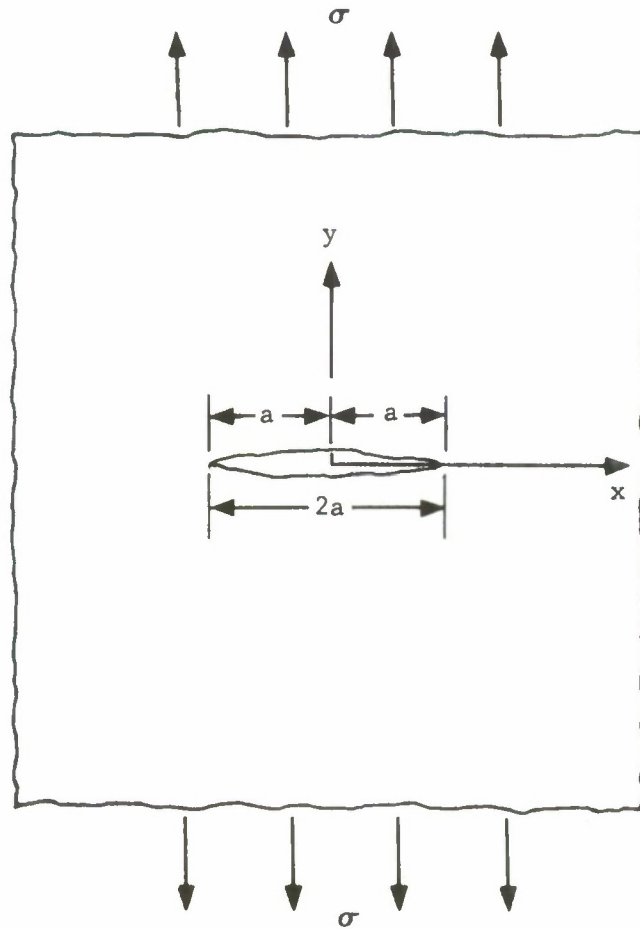


FIGURE 7 GEOMETRY OF CENTRAL CRACKED-INFINITE PLATE

$$\nabla^2(\sigma_x + \sigma_y) = \left(\frac{\partial^2}{\partial x^2} + \frac{\partial^2}{\partial y^2} \right) (\sigma_x + \sigma_y) = 0 \quad (V-4)$$

By defining an Airy stress function, Φ , the equilibrium equations V-3 are satisfied in terms of stresses

$$\left. \begin{aligned} \sigma_x &= \frac{\partial^2 \Phi}{\partial y^2} \\ \sigma_y &= \frac{\partial^2 \Phi}{\partial x^2} \\ \tau_{xy} &= - \frac{\partial^2 \Phi}{\partial x \partial y} \end{aligned} \right\} \dots \dots \dots (V-5)$$

Substitute equations V-5 into V-4

$$\nabla^4 \Phi = \nabla^2 (\nabla^2 \Phi) = 0 \quad (V-6)$$

To solve the crack problem, the stress function, Φ , must satisfy equation V-6 and its boundary conditions. The stress function, Φ , is chosen as,

$$\Phi = \psi_1 + x \psi_2 + y \psi_3 \quad (V-7)$$

which will satisfy equation V-6 if ψ 's are each harmonic, i.e., $\nabla^2 \psi_i = 0$.

Define a complex variable z as $z = x + iy$ and then functions of this variable will be $\bar{Z}(z)$, and its derivatives are

$$\left. \begin{aligned} \bar{Z} &= \frac{d\bar{Z}}{dz} \\ Z &= \frac{dZ}{dz} \\ Z' &= \frac{dZ}{dz} \end{aligned} \right\} \dots \dots \dots (V-8)$$

which have harmonic real and imaginary parts if the function is analytic, i.e., $\bar{Z} = \text{Real } \bar{Z} + i \text{ Imaginary } \bar{Z}$. Hence,

$$\nabla^2(\text{Re } \bar{Z}) = \nabla^2(\text{Im } \bar{Z}) = 0 \quad (V-9)$$

This solution is the result of Cauchy-Riemann conditions which specify,

$$\left. \begin{aligned} \frac{\partial \operatorname{Re} \bar{Z}}{\partial x} &= \frac{\partial \operatorname{Im} \bar{Z}}{\partial y} = \operatorname{Re} Z \\ \frac{\partial \operatorname{Im} \bar{Z}}{\partial x} &= -\frac{\partial \operatorname{Re} \bar{Z}}{\partial y} = \operatorname{Im} Z \end{aligned} \right\} \dots \dots \dots (V-10)$$

By using equations V-10, the functions \bar{Z} through Z can be differentiated.

V.3(a) Mode I

It is convenient to use a specific form of the Westergaard⁽¹⁴⁾ stress function for Mode I cracks. Westergaard defined an Airy stress function, Φ

$$\Phi = \operatorname{Re} \bar{Z}_I + y \operatorname{Im} \bar{Z}_I \quad (V-11)$$

where \bar{Z}_I and Z_I are related through equations V-8. (This is true for the Mode I crack except at singular points, i.e., at concentrated load points.) Using equation V-10 to differentiate equation V-11 to form the stresses according to equations V-5, we have,

$$\left. \begin{aligned} \sigma_x &= \operatorname{Re} Z_I - y \operatorname{Im} Z_I' \\ \sigma_y &= \operatorname{Re} Z_I + y \operatorname{Im} Z_I' \\ \tau_{xy} &= -y \operatorname{Re} Z_I' \end{aligned} \right\} \dots \dots \dots (V-12)$$

At this point in the analysis, any function $Z(z)$, which is analytic will give stresses, by equations V-12, which automatically satisfy the equations of elasticity. It only remains to find those functions of $Z(z)$ which will solve the crack problems, and satisfy boundary conditions.

Near the crack tip the stress free crack surfaces are the boundaries which dictate $Z(z)$. With the coordinates taken at the right hand end of a crack parallel to the x-axis, Z has the form

$$Z = \frac{f(z)}{\sqrt{z}} \quad (V-13)$$

where $f(z)$ is a well-behaved function and approaches a real constant at the origin. This results in τ_{xy} and σ_y approaching zero at the crack surfaces because the surfaces are stress free. The character of $f(z)$ away from the crack tip is then unspecified and can be adjusted to solve many Mode I crack configurations (symmetrical extension).

Close to the crack tip region, or when $|z| \rightarrow 0$, $f(z)$ may be replaced by a real constant K_I , and equation V-13 becomes

$$z \Big|_{|z| \rightarrow 0} = \frac{K_I}{\sqrt{2\pi z}} \quad (V-14)$$

The constant K_I may be thought of as representing the constant term in the series of the MacLaurin expansion of $f(z)$. By taking polar coordinates at the origin (see Figure 6)

$$z = r e^{i\theta} \quad (V-15)$$

and using equations V-14 and V-15, the stresses can be computed according to equations V-12 as

$$\left. \begin{aligned} \sigma_x &= \frac{K_I}{\sqrt{2\pi r}} \cos \frac{\theta}{2} \left[1 - \sin \frac{\theta}{2} \sin \frac{3\theta}{2} \right] \\ \sigma_y &= \frac{K_I}{\sqrt{2\pi r}} \cos \frac{\theta}{2} \left[1 + \sin \frac{\theta}{2} \sin \frac{3\theta}{2} \right] \\ \tau_{xy} &= \frac{K_I}{\sqrt{2\pi r}} \sin \frac{\theta}{2} \cos \frac{\theta}{2} \cos \frac{3\theta}{2} \end{aligned} \right\} \dots \dots \dots (V-16)$$

which are the "exact" elastic crack tip stress field equations as $r \rightarrow 0$, and in that general vicinity (see also equations V-1). Equations V-16 neglect only the higher order terms in r (beyond the constant terms in MacLaurin's expansion of $f(z)$). The factor K_I is called the crack tip stress intensity factor and has a constant value in the vicinity of the crack tip through the unspecified character of $f(z)$. K_I is seen to depend on the mode of loading.

V.4 THE WESTERGAARD METHOD (DISPLACEMENT)

The y direction strain, by Hooke's law, is

$$\epsilon_y = \frac{\partial v}{\partial y} = \frac{\sigma_y}{E} - \frac{\nu}{E} (\sigma_x + \sigma_z) \quad (V-17)$$

For plane strain ($\epsilon_z = 0$) conditions, Hooke's law states

$$\sigma_z = \nu (\sigma_x + \sigma_y) \quad (V-18)$$

Substituting equations V-12 and V-18 into equation V-17, and integrating, gives

$$v = \frac{1+\nu}{E} \left[2(1-\nu) \operatorname{Im} \bar{Z}_I - y \operatorname{Re} Z_I \right] \quad (V-19)$$

and

$$u = \frac{1 + \nu}{E} \left[(1 - 2\nu) \operatorname{Re} \bar{Z}_I - y \operatorname{Im} Z_I \right] \quad (V-20)$$

Noting that $E = 2G(1 + \nu)$ and substituting equation V-14 in its polar form into the general displacement equations V-19 and V-20, u and v become,

$$\left. \begin{aligned} u &= \frac{K_I}{G} \sqrt{r/2\pi} \cos \frac{\theta}{2} \left[1 - 2\nu + \sin^2 \frac{\theta}{2} \right] \\ v &= \frac{K_I}{G} \sqrt{r/2\pi} \sin \frac{\theta}{2} \left[2 - 2\nu - \cos^2 \frac{\theta}{2} \right] \end{aligned} \right\} \dots (V-21)$$

and $w = 0$ for plane strain conditions. Equations V-16 and V-21 are the same as the stress and displacement solutions for Mode I through cracks developed by Irwin⁽¹²⁾ using the Westergaard (stress) method (see equations V-1 and V-2. Similar solutions can be obtained for Modes II and III, and are given in Ref. 15.

It must be remembered that this is by no means the only method to obtain stress solutions for crack problems. However, it presents one of the simplest means to analyze cracks.

This two dimensional analysis of Mode I cracks indicates that the magnitude or intensity of this distribution is dependent on K_I . Thus, the relative intensity of the stress field at any point, obtained by basic stress analysis of the crack tip region, is the crack tip stress intensity factor, K_I .*

V.5 DIMENSIONAL CONSIDERATIONS

It now becomes necessary to discuss the influence of crack size, geometry, or applied load on the overall fracture problem. Consider the geometry and stress conditions of Figure 7. A crack of half length "a" under a uniform gross tensile stress, σ , is introduced into an infinite plate. Mode I displacement is evident, and two parameters are known, σ , and "a". Due to crack symmetry, only one crack tip stress intensity need be considered. Using dimensional analysis, P. C. Paris⁽¹⁶⁾ solved this problem through the use of equations V-1 and found

* When the subscript I does not accompany the stress intensity factor, opening mode is assumed. The units are normally $\text{ksi} \sqrt{\text{inch}}$, but may be seen as $\text{lbs-inches}^{-3/2}$.

$$\text{where} \quad \left. \begin{array}{l} K_I = \text{Const. } \sigma \sqrt{a} \\ K_{II} = K_{III} = 0 \end{array} \right\} \dots \text{Mode I} \dots \dots \dots (V-22)$$

Similarly, Modes II and III may be analyzed by dimensional analysis.

$$\text{where} \quad \left. \begin{array}{l} K_{II} = \text{Const. } \tau \sqrt{a} \\ K_I = K_{III} = 0 \end{array} \right\} \dots \text{Mode II} \dots \dots \dots (V-23)$$

for uniform in-plane shear, and

$$\text{where} \quad \left. \begin{array}{l} K_{III} = \text{Const. } \tau \sqrt{a} \\ K_I = K_{II} = 0 \end{array} \right\} \dots \text{Mode III} \dots \dots \dots (V-24)$$

for out-of-plane shear at infinity.

The value of the constant (Const.) is found as $\sqrt{\pi}$ for all three modes. Therefore, the stress intensity factors for an infinite plate with the crack geometry of Figure 7 are

$$\left. \begin{array}{l} K_I = \sigma \sqrt{\pi a} \\ K_{II} = \tau \sqrt{\pi a} \\ K_{III} = \tau \sqrt{\pi a} \end{array} \right\} \dots \dots \dots (V-25)$$

using both dimensional and elastic stress solutions.

The stresses in linear elasticity depend linearly upon applied load, hence Equations V-16 imply that the stress intensity factors contain load as a linear factor. Dimensional examination of the same equations show that K must also contain a characteristic length parameter (lineal dimension, etc.) for a particular body configuration, including crack length. In the Griffith crack configuration (see Section II) the only characteristic length is, a, the crack length. The similarity between Equations V-25 and the Griffith energy criteria for crack stability (see Equation II-7) indicate that instability occur at a constant value of K.

There are many other means of determining stress intensity factors (i.e., complex stress functions, numerical collocation, inner-outer expansion) which will not be included here, but lead to the same dependency on crack length and stress as eqs. V-25. An excellent summary of stress intensity factor solutions is contained in Reference 15.

V.6 STRESS INTENSITY - STRESS CONCENTRATION

Similar terms and symbols--dissimilar parameters but, the stress intensity factor (K) may be obtained as a limiting case of the stress concentration factor (K_t), i.e., when the notch radius, ρ , approaches zero.

For a crack of finite tip radius, ρ , the surrounding stress state is governed by the stress intensity factor. A proportionality then exists between K_I and σ_m , where σ_m is the maximum stress near the crack tip due to the presence of the stress raiser (crack). In order to make this proportionality dimensionally correct, the notch radius must be introduced; hence, the complete solution is:

$$K_I = \text{Const. } \sigma_m \sqrt{\rho} \quad (\text{V-26})$$

It can be recognized that this stress intensity solution is the same as that for a Mode I crack (see equations V-25) where "a" is replaced by the characteristic crack tip or notch radius, ρ . The K_t for an elliptical notch (half crack conditions) can be used as the limiting case for a crack, or when the ellipse collapses, i.e., flattened and approaches a crack shape.

$$K_t(\text{for elliptical notch}) = \frac{\sigma_m}{\sigma} = \left[1 + 2\sqrt{\frac{a}{\rho}} \right] \quad (\text{V-27})$$

Solving equation V-27 for σ_m and substituting into the equated K_I solutions of equations V-26 and V-25, when ρ approaches zero (crack situation), equation V-26 becomes

$$K_I = \lim_{\rho \rightarrow 0} \sigma_m \frac{\sqrt{\pi}}{2} \sqrt{\rho} \quad (\text{V-28})$$

and the constant (Const.) is found to be $\frac{\sqrt{\pi}}{2}$ for $\rho = 0$. By this procedure, the stress concentration analysis may be used to determine K_I mode stress intensities for various shaped flaws in finite structure as long as the stress concentration factors are available in a form similar to Equation V-27.

Another interesting feature of this analysis is that the constant (Const.) was found to be $\frac{\sqrt{\pi}}{2}$. This factor, when combined with the finite width correction (usually signified by the symbol Y^*) is dependent on both specimen and crack geometry. The finite geometry corrections will be discussed later for various crack geometries.

V.7 THE RELATIONSHIP BETWEEN STRAIN ENERGY RELEASE RATE (\mathcal{G}) AND STRESS INTENSITY

It can be observed that the relationship between strain energy release rate (\mathcal{G}) and stress intensity (K) as given by Equations II-7 and V-25 are quite similar. Both are measures of the elastic stress field effects near the crack tip. It has been shown⁽¹⁵⁾ that the relationship for displacement Modes I, II, and III is

*The correction factor (Y) usually includes the $\sqrt{\pi}$ term in its calculation. In this report, (λ) will be used to denote finite width correction which does not include the $\sqrt{\pi}$.

$$\left. \begin{aligned} G_I &= \frac{(1 - \nu^2)}{E} K_I^2 \quad (\text{Plane Strain}) \\ G_{II} &= \frac{(1 - \nu^2)}{E} K_{II}^2 \quad (\text{Plane Strain}) \\ G_{III} &= \frac{(1 + \nu)}{E} K_{III}^2 \end{aligned} \right\} \dots\dots\dots (V-29)$$

and for plane stress conditions

$$\left. \begin{aligned} G_I &= \frac{K_I^2}{E} \\ G_{II} &= \frac{K_{II}^2}{E} \end{aligned} \right\} \begin{matrix} \\ (\text{Plane Stress}) \end{matrix} \dots\dots\dots (V-30)$$

where ν and E are Poisson's ratio and modulus of elasticity, respectively. Although most of the modern terminology of fracture mechanics uses the stress intensity terminology, the relationships of equations V-29 and V-30 can be used to convert strain energy release rate data to K values directly.

V.8 SUPERPOSITION OF K SOLUTIONS

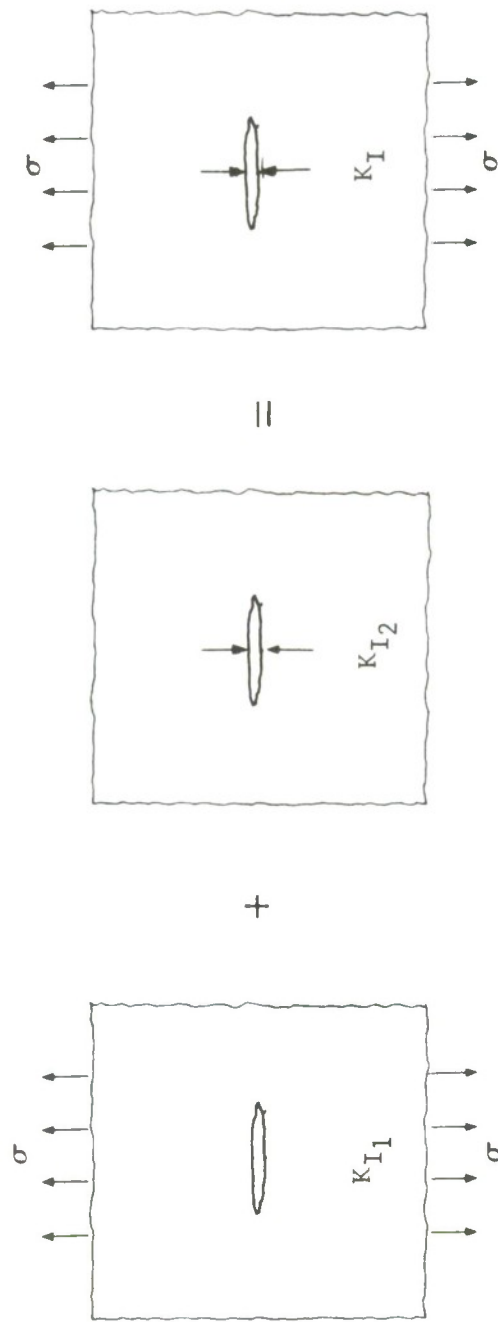
In many cases for complicated loading problems, it may be expedient to add the stress intensity solutions in Mode I only, to solve for a combined loading problem. For example, in linear elasticity the effects of two or more loads may be superimposed by adding stresses and displacements (not energy) at each point. In fracture mechanics, a problem may arise such as shown in Figure 8, which might represent a crack in a structure under uniaxial stress with superimposed compressive rivet forces.* The stress intensity factor for the total problem is then the algebraic summation of the two simpler problems.

Superposition principles also apply to the geometric corrections (λ 's) and the principles involved will be developed in later sections of this report.

V.9 CRITICAL K CONCEPT

The stress equations of eq. V-1 indicate that the stress conditions near the crack tip are of similar distributions ($1/\sqrt{r}$) and vary only in stress intensity from one case to another. Therefore, it follows that unstable crack extension will take place when the stress intensity factor, K_I , reaches a value which is critical, that is when any combination of load, crack geometry, and configuration becomes critical. This situation occurs when K_I approaches K_{Ic} , where the subscript (c) denotes a critical value in fracture mechanics terminology. This critical value, K_{Ic} , is the plane strain fracture toughness. For plane stress fracture, the symbol K_c is used.

*Since Mode II and III distribution are entirely different from Mode I, K factors cannot be added for different modes (i.e., $K_I + K_{II} \neq K_{TOTAL}$).



$$K_I = K_{I1} + K_{I2}$$

FIGURE 8 EXAMPLE OF STRESS INTENSITY SUPERPOSITION

In the case of plane strain fracture toughness (K_{Ic}), the following assumptions apply:

1. A small zone of plasticity occurs at the crack tip.
2. Griffith conditions (brittle behavior) predominate.

However, in a given material the elastic stress field is always changed due to the non-linearity at the crack tip; but always in the same way. Therefore, fracture will occur at what is termed an apparent stress intensity, K_{Ic} . Critical conditions still apply, however, ($K_I \rightarrow K_{Ic}$) for materials which show limited ductile behavior.

V.10 SUMMARY

In this section the general forms of the stress and displacement fields surrounding a crack were considered. An introduction to the form of the stress intensity factor K for the various crack displacement modes and the formulation of K factors from stress concentration factors was also presented.

Up to now, all crack and fracture criterion have been based on linear elastic theory; that is, plastic constraint confined to a small area near the crack tip. With these fundamentals, we can now approach the real life, ductile material situation where plasticity takes place and requires modification to the elastic solutions.

VI CRACK TIP PLASTICITY

VI.1 ESTIMATES OF PLASTIC ZONE SIZE

In most real engineering materials, there exists near the crack tip, under increasing load, a zone of plasticity (plastic zone) which varies in size and shape for states of stress. The distribution and size of this zone has been studied by several investigators.(17-20) Due to the highly complex analysis required to solve the plasticity equations in Modes I and II, a solution has only been obtained for Mode III.(21) An estimate can be made, however, for Mode I cracks if it is assumed that the elastic stress field equations V-1 approach yield conditions as the elastic-plastic boundary is reached.* Using Octahedral Shear theory, the relative size of the plane stress and plane strain plastic zone (r) is found to be

$$\frac{r}{r_y} = \cos^2 \frac{\theta}{2} \left(1 + 3 \sin^2 \frac{\theta}{2} \right) \quad (\text{Plane Stress}) \quad (\text{VI-1})$$
$$\frac{r}{r_y} = \cos^2 \frac{\theta}{2} \left[(1 - 2\nu)^2 + 3 \sin^2 \frac{\theta}{2} \right] \quad (\text{Plane Strain})$$

where the plastic zone radius, r_y , is given by

$$r_y = \frac{1}{2\pi} \left(\frac{K_I}{\sigma_{ys}} \right)^2 \quad (\text{Plane Stress}) \quad (\text{VI-2})$$

and the actual plastic zone diameter is $2r_y$.

The plane stress equation VI-1 indicates the following:

1. The distance r_y is the apparent crack tip location directly ahead of the actual crack tip and prescribes the elastic-plastic boundary (plane stress plastic zone radius).
2. The plastic zone is larger than that given for plane strain.

Liu,(20) in 1961, proposed a model of the plastic zone which is depicted in Figure 9. Experimental evidence has shown that this model is a good representation of the zones for plane stress and plane strain. The relative sizes of the plastic zones are as indicated.

Dugdale(22) analytically described the shape of the plastic zone on the surface as "wedge" shaped or strip model, and these types of zones have been observed experimentally(17,19); others propose a "dumb-bell" shape during the early stages of deformation. Many feel that the Dugdale equation estimates the plastic zone size more accurately for certain materials than

* This method becomes "exact" as the material stress-strain curve becomes linear.

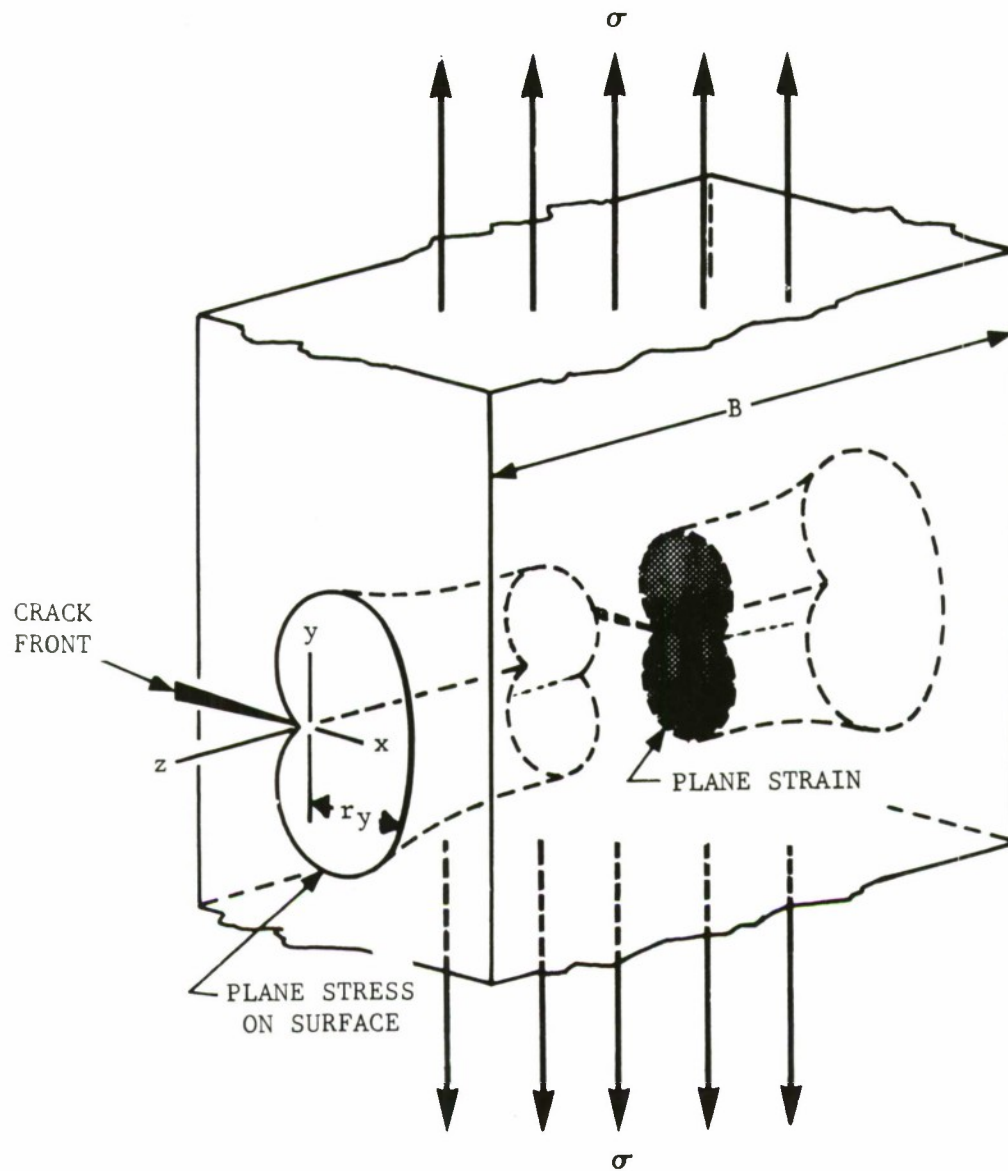


FIGURE 9 PICTORIAL REPRESENTATION OF THROUGH-THE-THICKNESS PLASTIC ZONE DEVELOPMENT AS FIRST VISUALIZED BY LIU (Ref. 20)

that given by equation VI-2. This equation assumes a wedge shaped zone whose length can be described mathematically as

$$2r_y = a \left[\sec \frac{\pi \sigma}{2 \sigma_{ys}} - 1 \right] \quad (\text{VI-3})$$

which in terms of the stress intensity factor is (when $r_y < a$)

$$2r_y = \frac{1}{2} \left(\frac{\pi K_I}{2 \sigma_{ys}} \right)^2 \quad (\text{VI-4})$$

The reason for these models will be discussed in the next section. However, what is important is that at the crack tip a plastic zone develops under increasing stress and affects the stress intensity solution.

VI.2 LIMITATIONS ON PLASTIC ZONE DIMENSIONS

The plastic zone must remain small compared to other dimensions of the material (i.e., crack length, width), or elastic fracture mechanics is invalidated.

If equation VI-2 is combined with the stress intensity equation for Mode I (see eqs. V-25), the plastic zone size can be seen as a function of the applied gross stress and crack length. (Also see equation VI-3.)

$$r_y = \frac{1}{2} a \left(\frac{\sigma}{\sigma_{ys}} \right)^2 \quad (\text{VI-5})$$

The plastic zone size given by equations VI-5 or VI-3 will be small compared to half-crack length, "a", as long as the gross stress is well below the material yield strength. This relationship places some limitation on the ratio of σ/σ_{ys} , which was reported in the fifth ASTM Special Committee Report⁽²³⁾ as

$$\frac{\sigma_{net}}{\sigma_{ys}} \leq 0.8 \quad (\text{VI-6})$$

where σ_{net} is the stress on the uncracked section at fracture. Thus, when the size of plastic zone is a large portion of the uncracked net section, linear elasticity does not represent the stress field with adequate accuracy. The relationship of equation VI-6 was determined empirically, and its validity in the high stress (small crack size) range must be verified by testing experience. This involves a computation directly from equation VI-2 to insure that the plastic zone size is small compared to other specimen dimensions.

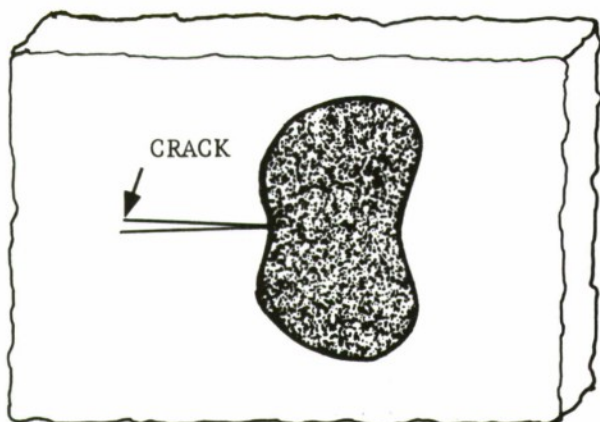
VI.3 INFLUENCE OF WORK HARDENING ON THE PLASTIC ZONE

Work hardening affects the crack tip plasticity in the following manner:

Large Work Hardening -- Equations VI-1 apply and "dumbell" or circular zones are formed (see Figure 9).

Small Work Hardening -- Concentration of slip ahead of the crack forms shear bands and the Dugdale⁽²²⁾ "wedge" model applies (see Figure 10 and equation VI-4).

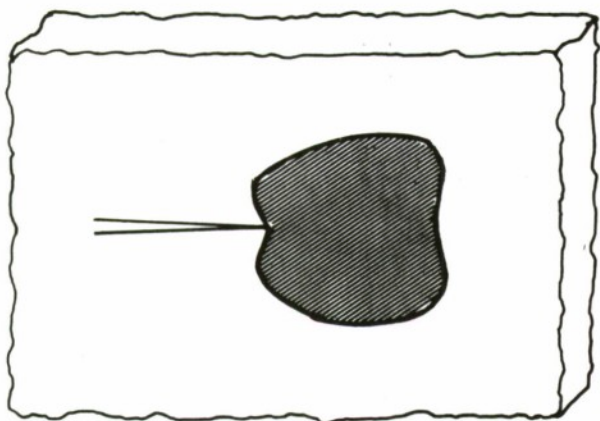
Figure 10 shows the shapes of experimentally observed plane stress plastic zones for several materials of various work hardening coefficients, n , as summarized by Hahn and Rosenfield⁽¹⁷⁾. Reference 17 contains an excellent summary of the influence of strain hardening on fracture.



2024-0 Aluminum

$$\sigma_{ys} = 15 \text{ ksi}$$

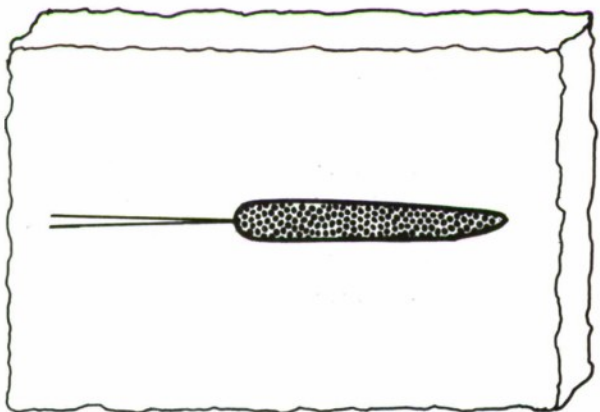
$$n = 0.250$$



4340 Steel (Annealed)

$$\sigma_{ys} = 60 \text{ ksi}$$

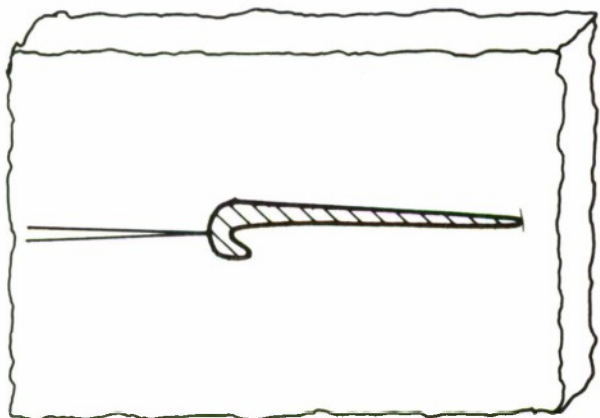
$$n = 0.145$$



1010 Steel (Cold Rolled)

$$\sigma_{ys} = 105 \text{ ksi}$$

$$n \approx 0.01-0.05$$



Mild Steel (Annealed)

$$\sigma_{ys} = 40 \text{ ksi}$$

$$n \approx 0$$

FIGURE 10. EXPERIMENTALLY OBSERVED SURFACE, PLANE STRESS PLASTIC ZONES⁽¹⁷⁾

Another illustration of the plane stress plastic zone is shown in Figure 11. It can be observed that the so-called V-slant fracture surface will occur due to this type of plastic zone. Slip within the plastic zone (at 45° to crack tip plane) is one of the causes of this type of fracture. It will be remembered that the state of plane stress or plane strain also influences the formation of slant, V-slant, and flat fracture (see Figure 3).

VI.4 THICKNESS EFFECTS ON FRACTURE

To differentiate between the terms thick and thin, the radius of the plane stress plastic zone (eq. VI-2) can provide a relative measure when compared to material thickness, B. Test results have indicated that the fracture appearance (through the thickness) is related to a normalized plastic zone size, as shown in Figure 12. This behavior is typical and indicates the transition zones as a function of the crack tip parameter, $\frac{r_y}{B}$. The shape of this curve will depend on many parameters, and the fracture mode transition on the interplay between material properties, geometry, and force. However, as a general rule, the cut-offs of 0.2 for plane strain and 1.0 for plane stress are generally accepted. However, there is one material, beryllium, which does not show a transition from flat to shear.

This brings us to the effect of material thickness (B) on the critical stress intensity factor, K_{Ic} . Figure 13 shows these trends for titanium, steel, and aluminum alloys. The form is similar in many cases to the curve of Figure 12. For example, the nominal* value of stress intensity for 7075-T6 has a minimum at 36 ksi√inch for ≥ 0.8 inch thick material. This limiting value represents the plane strain fracture toughness, K_{Ic} , for 7075-T6. A mixed mode region occurs for $0.5 > B > 0.15$ inches, and the plane stress region occurs when $B < 0.15$ inches and $K_{Ic} \approx 85$ ksi√inch. The other curves of Figure 13 show similar trends, some more gradual (Ti-6Al-4V) and others more drastic (Ti-B120VCA).

There have been several indexes proposed to measure the tendency toward plane strain or plane stress behavior. In a plate, the plastic zone radius at the surface is given by the plane stress equation VI-2 or VI-4; and in the center of the plate by the plane strain equation VI-7, which is $1/(2\sqrt{2})$ or approximately 1/3 the size of the plane stress zone equation.

$$r_y = \frac{1}{4\pi\sqrt{2}} \left(\frac{K_I}{\sigma_{ys}} \right)^2 \quad \text{Plane Strain} \quad (\text{VI-7})$$

The critical conditions for plane strain and plane stress can be estimated by comparing the surface plastic zone radius, eq. VI-2, with thickness, or when

$$B > \approx 2 \left(\frac{K_{Ic}}{\sigma_{ys}} \right)^2$$

plane strain conditions prevail. And when

*CAUTION--The critical stress intensity values shown in Figure 13 must be considered as average.

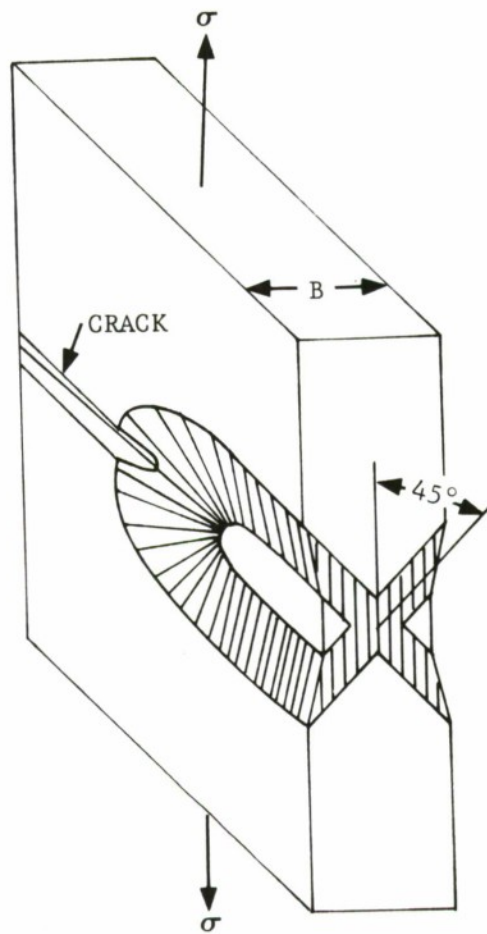


FIGURE 11. V-SLANT, PLANE STRESS PLASTIC ZONE AS OBSERVED BY
HAHN & ROSENFELD(17)

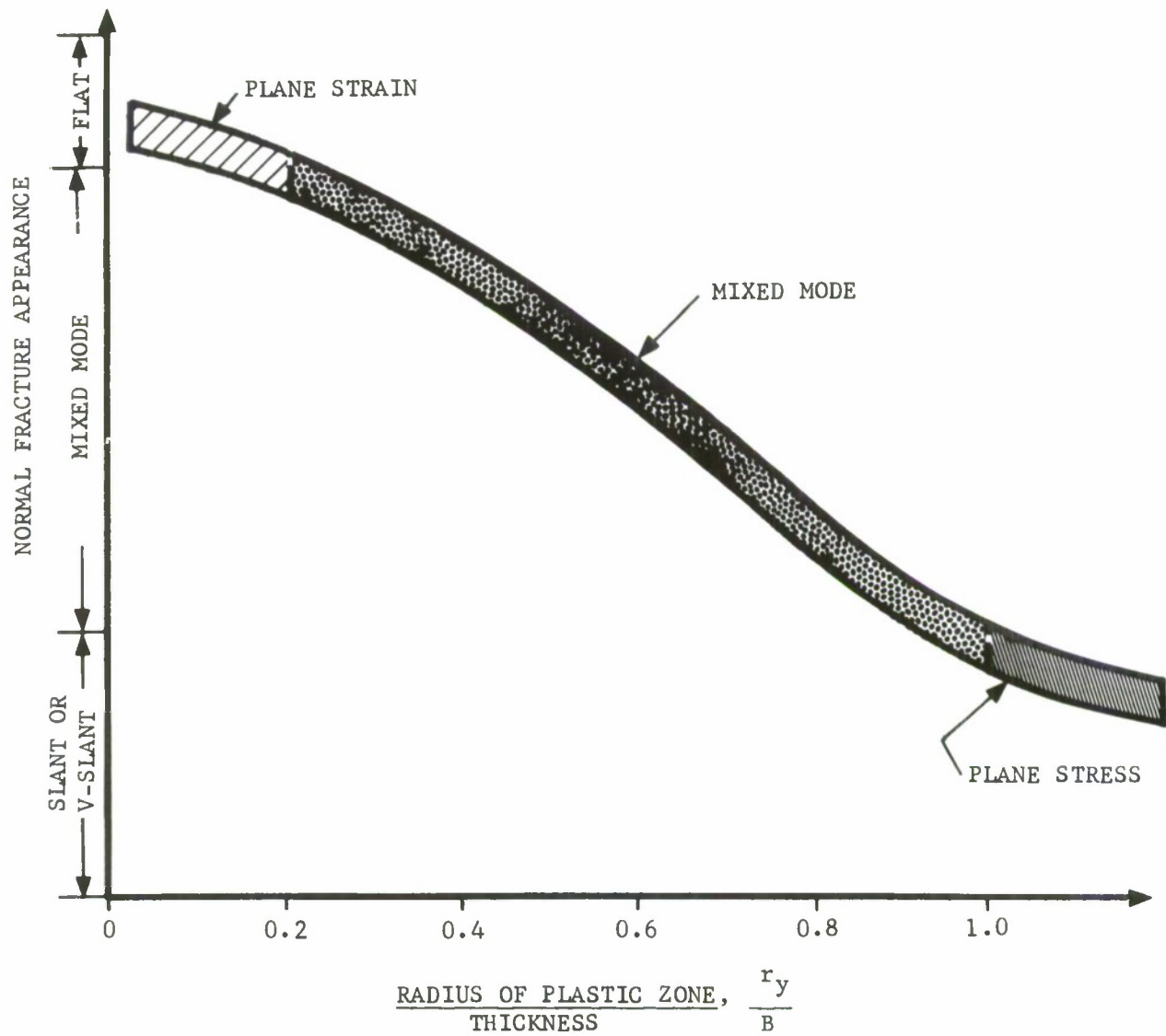


FIGURE 12. TREND IN FRACTURE MODE APPEARANCE VS. CRACK TIP PLASTIC ZONE PARAMETER

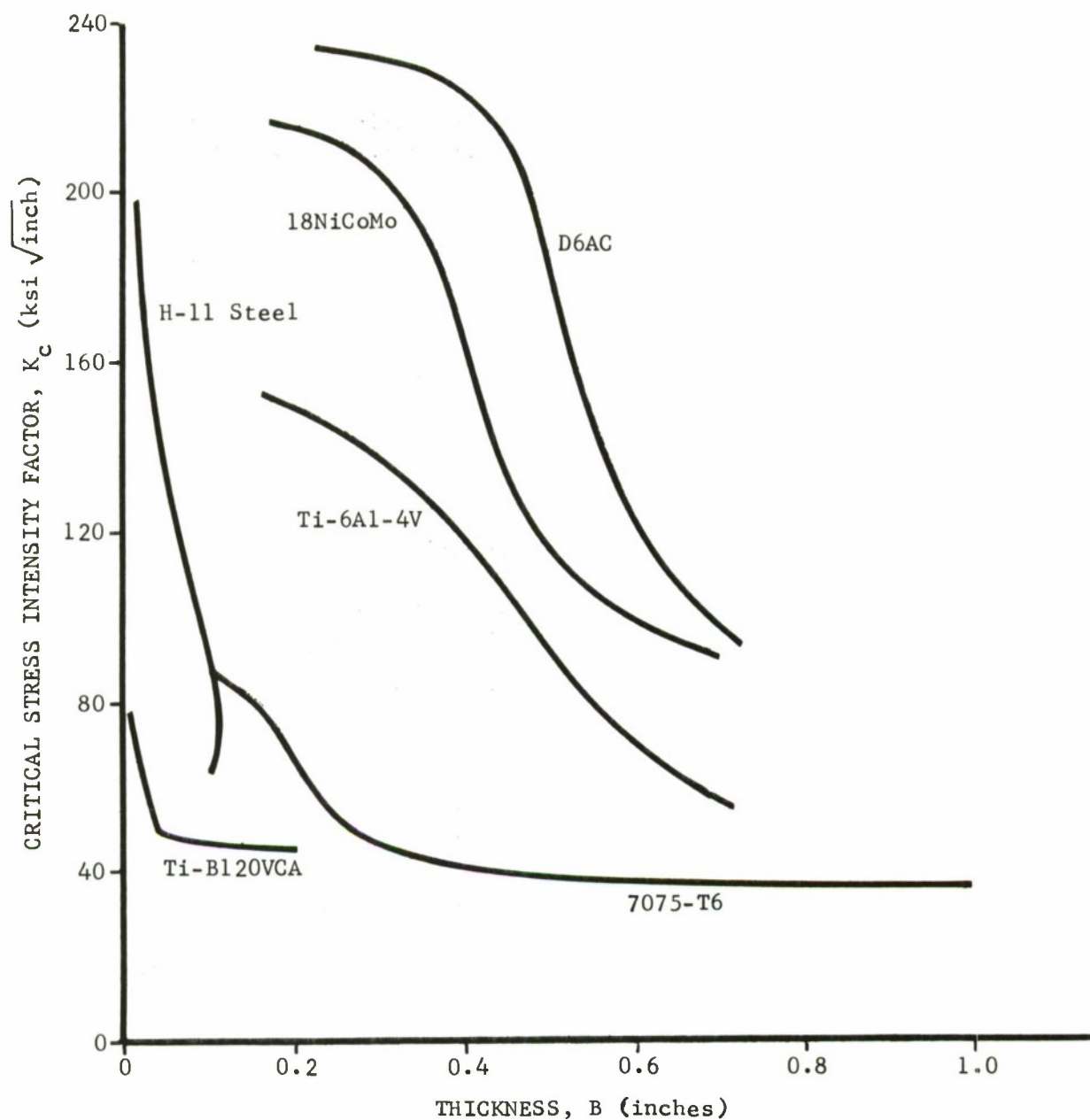


FIGURE 13. NOMINAL* CRITICAL STRESS INTENSITIES FOR SEVERAL MATERIALS AS A FUNCTION OF THICKNESS (Data from Refs. 24 and 25.)

*CAUTION - Values should be considered as average.

$$B < \approx 2 \left(\frac{K_{Ic}}{\sigma_{ys}} \right)^2$$

plane stress conditions predominate.

Relationships such as the above can be useful in setting a limit on specimen size for determining K_{Ic} . The American Society for Testing and Materials⁽⁸⁾ has set a requirement that

$$B \text{ and } a \geq 2.5 \left(\frac{K_{Ic}}{\sigma_{ys}} \right)^2 \quad (\text{VI-8})$$

in order to obtain valid plane strain fracture toughness values, under current accepted practice. However, since these are empirical estimates, the exact method of determining K_{Ic} for a particular material is to increase specimen thickness until critical K values reach a limiting value (see, e.g., 7075-T6, Figure 13).

VI.5 INCLUSION OF PLASTICITY AND GEOMETRIC CORRECTIONS IN K SOLUTION

It was shown that the radius of plastic zone, r_y , affects the material critical stress intensity factor. Therefore, it must be accounted for in some manner in the basic K equations V-22, 23, and 24. It may be thought of as adding an incremental length to the existing crack. For example, equation V-22 becomes

$$K_I = \lambda \sigma \sqrt{a + f(r_y)} \quad (\text{VI-9})$$

where the plastic zone radius, r_y , is a function of $\left(\frac{K_I}{\sigma_{ys}} \right)^2$ from eq. VI-2 or 7, and λ is the correction for finite geometry.

In a previous section, equations V-25 gave the K solutions for an infinite panel containing a central crack of half-length "a". For centrally cracked finite panels, Irwin⁽⁴⁾ suggested the following equation for stress intensity from the work of Westergaard, including geometric correction, to account for finite specimen widths, (W) and crack geometry.

$$K_I = \sigma \sqrt{W \tan \frac{\pi a}{W}} \quad (\text{VI-10})$$

This is the so-called "Irwin Tangent Formula" where the factor $\sqrt{W \tan \frac{\pi a}{W}}$ includes the geometric correction factor (λ) discussed previously. The form of equation V-25 accounting both for plasticity and finite geometry using the "Irwin Tangent Formula" becomes

$$K_I = \sigma \sqrt{W \tan \left(\frac{\pi a}{W} + f(r_y) \right)} \quad (\text{VI-11})$$

where the plastic zone size is determined from equations VI-2, 3, or 7 depending on stress state and expected zone shape.

The normal form of the opening mode stress intensity, including finite width correction is usually written as

$$K_I = \sigma \sqrt{\pi a} \ f\left(\frac{2a}{W}\right)^*$$

or

$$K_I = \sigma \sqrt{a} \ f\left(\frac{\sqrt{\pi} 2a}{W}\right)^* \quad (VI-12)$$

for centrally cracked panels. It has been determined that the "Irwin Tangent Correction" factor has an estimated accuracy of $\pm 5\%$ for crack length to panel width ratios $\left(\frac{2a}{W}\right)^{**}$ less than 0.4. Other correction factors have been developed for the center $\frac{W}{2}$ crack geometry (26-28). The expression in use today is by Isida, which has an accuracy of $\pm 0.5\%$ for $\frac{2a}{W} < 0.7$. The forms of the various correction factors which account for relative size of specimen to crack dimensions, will be discussed fully in Section VII.6.

VI.6 SUMMARY

The plastic zone at the crack tip has been shown to affect the state of stress, fracture mode appearance, and most importantly, critical stress intensity factor. It is itself, in turn, a function of thickness and material properties. Estimates can be made of the plastic zone size and result in an apparent crack length which can be used to determine stress intensities for semi-ductile fracture. The complete form of stress intensity equation will include corrections for plate/crack geometry and for plastic zone.

In the following section, the stress intensity solutions will be presented for various crack loading situations.

* Plastic zone correction not included.

**Also referred to as "crack aspect ratio", $\left(\frac{\text{TOTAL CRACK LENGTH}}{\text{PANEL WIDTH}}\right)$.

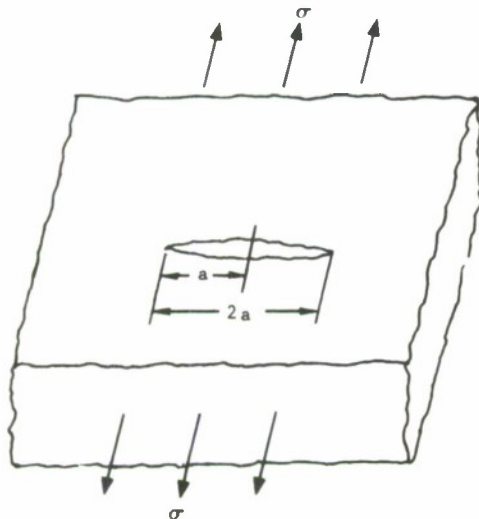
VII BASIC STRESS INTENSITY FACTORS

This section presents solutions of the basic stress intensity factor K for crack geometries and loading modes most encountered in aircraft applications. These expressions have been abstracted from Reference 15 which contains an excellent review of available K solutions. The original sources are also given in Reference 15. Using superposition principles, it will be possible to combine many of the results. In most cases the opening, Mode I, tensile stress intensity will be emphasized since this is the most common case for aircraft application.

NOTE: ALL K EQUATIONS IN THIS SECTION ARE BASED ON ELASTIC SOLUTIONS AND ARE FOR INFINITE AND SEMI-INFINITE GEOMETRY (i.e., without geometric (finite width) corrections).*

VII.1 UNIFORM LOADING

Uniform, Tensile Stress (Normal to Crack)

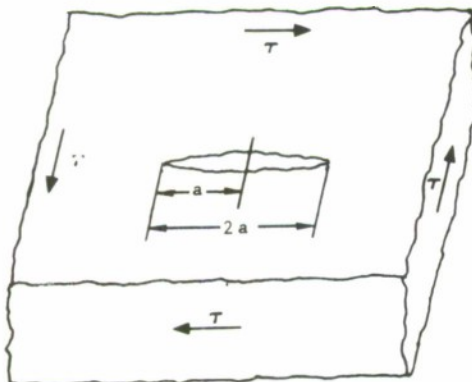


(Mode I)

$$K_I = \sigma \sqrt{\pi a} \quad (\text{VII-1})$$

with $K_{II} = K_{III} = 0$

Uniform Shear Stress



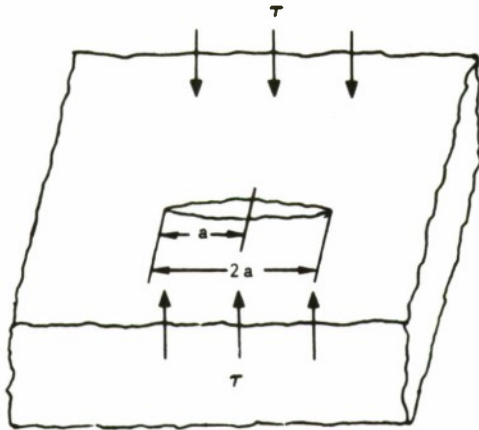
(Mode II)

$$K_{II} = \tau \sqrt{\pi a} \quad (\text{VII-1A})$$

with $K_I = K_{III} = 0$

*Except Where Noted.

Uniform, Transverse Shear Stress (Parallel to Crack)

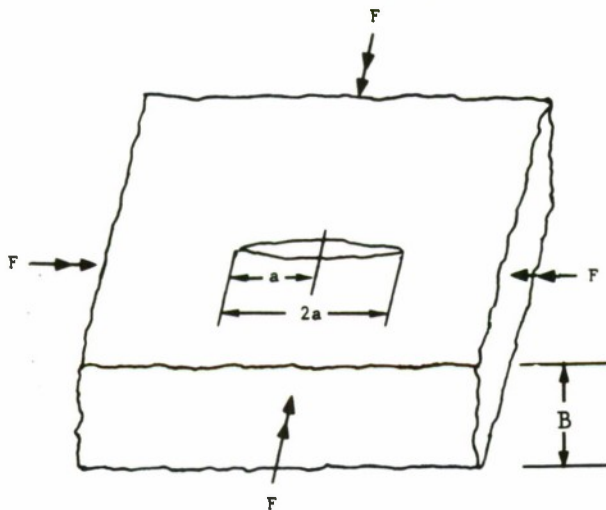


(Mode III)

$$K_{III} = \tau \sqrt{\pi a} \quad (VII-1B)$$

with $K_I = K_{II} = 0$

Uniform, Twisting Moments



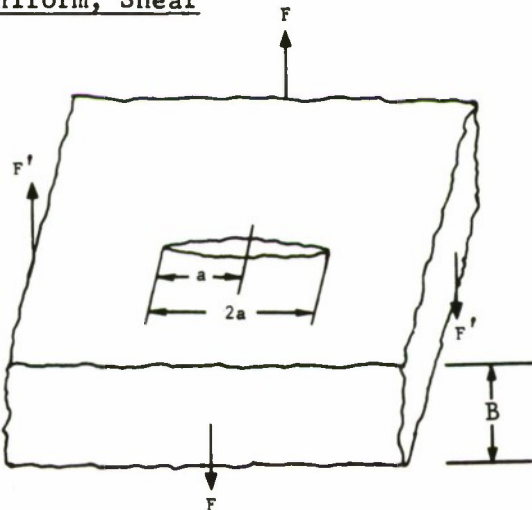
(Although the K solutions are consistent with K_I , K_{II} the standard notation is K_{shear} , K_{bending} for flexure.)

F = Pure Twisting Moment, (per unit length)

$$K_{\text{shear}} = \frac{6 F \sqrt{\pi a}}{B^2} \quad (VII-2)$$

with $K_{\text{bending}} = 0$

Uniform, Shear



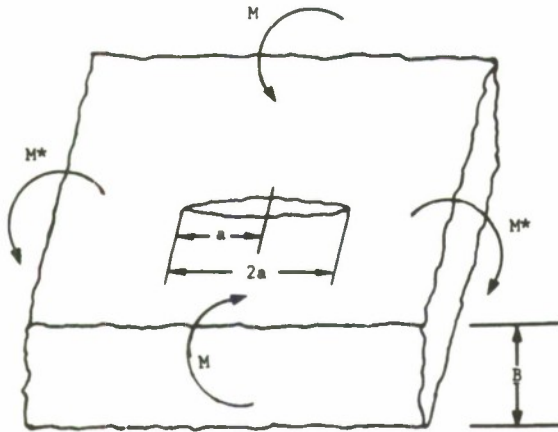
F = Uniform Shear (per unit length)

NOTE: Results are independent of F'

$$K_{\text{shear}} = \frac{8 F \sqrt{\pi a^3}}{B^2} \quad (VII-3)$$

with $K_{\text{bending}} = 0$

Uniform, Bending



M = Uniform Bending Moment

NOTE: Results are independent of M*
(Equilibrium Moments)

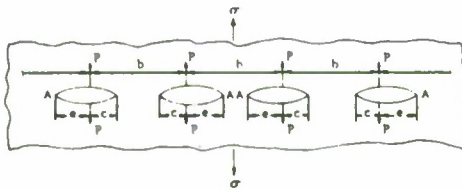
$$K_{\text{bending}} = \frac{6 M \sqrt{\pi a}}{B^2} \quad (\text{VII-4})$$

with $K_{\text{shear}} = 0$

Uniform Tensile Stress - Crack Arrays

(Mode I)

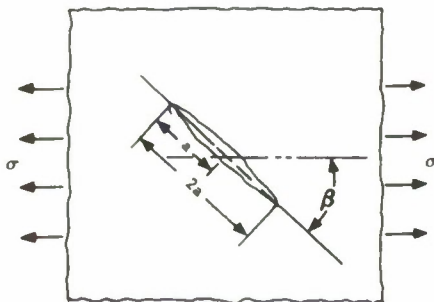
P = Force per unit thickness

$$K_I \text{ @ points A =}$$


$$\frac{\sigma \sqrt{4b} \sin \frac{\pi c}{2b}}{\sqrt{\cos \frac{\pi e}{2b} \left(\sin \frac{\pi e}{2b} + \sin \frac{\pi c}{2b} \right)}} + \frac{P \sqrt{\sin \frac{\pi c}{2b}}}{\sqrt{b \sin \frac{\pi e}{2b} \cos \frac{\pi e}{2b} \left(\sin \frac{\pi e}{2b} + \sin \frac{\pi c}{2b} \right)}} \quad (\text{VII-5})$$

with $K_{II} = 0$

Uniform, In Plane Tensile Stress - Inclined Crack



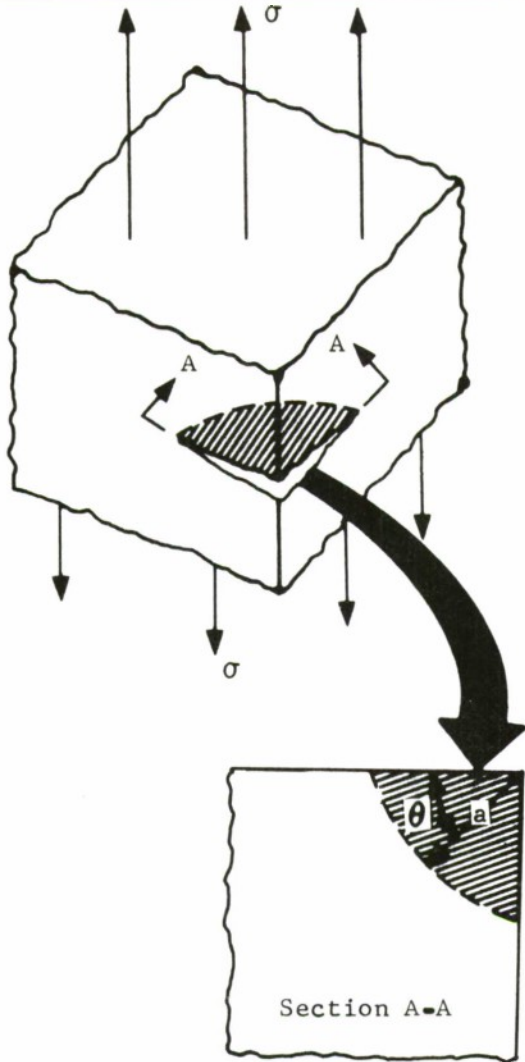
(Mode I)

$$K_I = \sigma \sin^2 \beta \sqrt{\pi a} \quad (\text{VII-6})$$

(Mode II)

$$K_{II} = \sigma \sin \beta \cos \beta \sqrt{\pi a}$$

Uniform Tensile Stress - Corner Crack



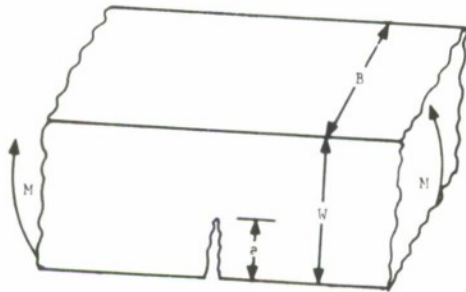
(Mode I)

$$K_I = M_k \sigma \sqrt{\pi a} \quad (\text{VII-7})$$

$\frac{\theta}{90^\circ}$	M_k
0	0.705
0.2	0.650
0.4	0.625
0.5	0.620
0.6	0.625
0.8	0.650
1.0	0.705

where values of the elastic magnification factor M_k for values of angular orientation $\frac{\theta}{90^\circ}$ are as above (Reference 25, see also Section IX).

In-Plane Bending



(Mode I)

$$K_I = \frac{6M \sqrt{\pi a}}{BW^2}$$

(VII-8)

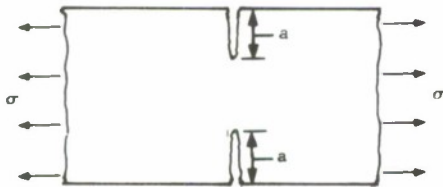
$$\text{or } K_I = \sigma_{\text{NOM}} \sqrt{\pi a}$$

M = bending moment

σ_{NOM} = nominal stress

with $K_{II} = K_{III} = 0$

Axial Tension (Double Crack)



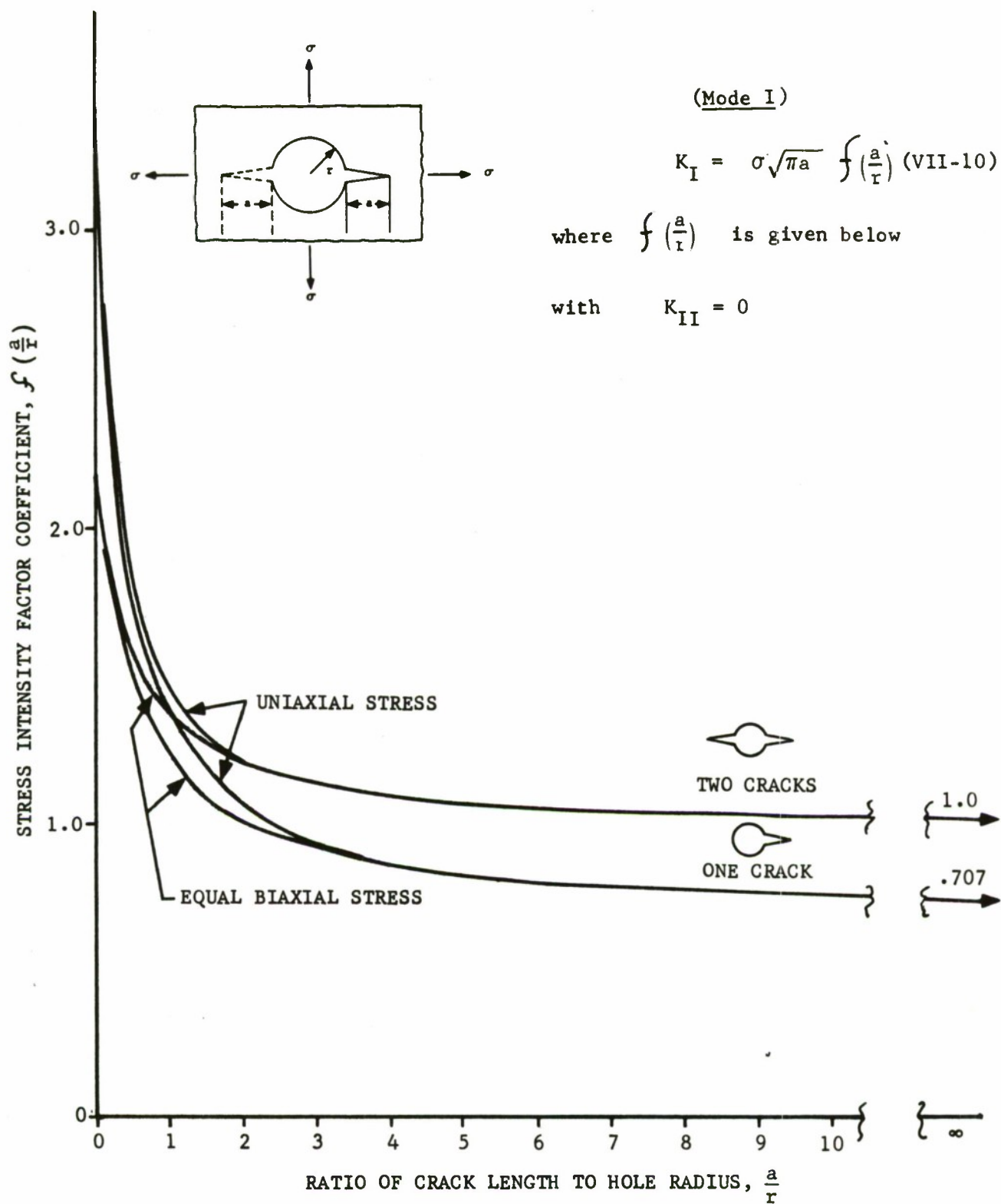
(Mode I)

$$K_I = \sigma \sqrt{\pi a}$$

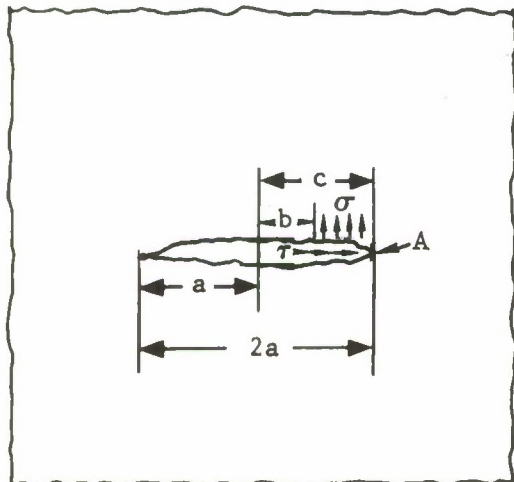
(VII-9)

with $K_{II} = K_{III} = 0$

Uniaxial or Biaxial Stressed - Cracks at Holes



Uniform Stresses on Part of Crack Surface



(Mode I)

σ = Uniform stress on one surface

τ = Uniform Shear on crack faces

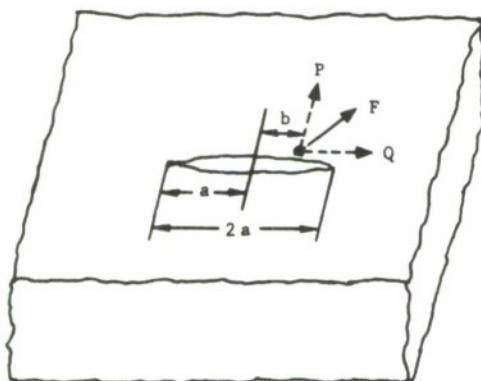
$$K_I @ A = \frac{\sigma}{2} \sqrt{\frac{a}{\pi}} \left[\sin^{-1} \frac{c}{a} - \sin^{-1} \frac{b}{a} - \sqrt{1 - \left(\frac{c}{a}\right)^2} + \sqrt{1 - \left(\frac{b}{a}\right)^2} \right] + \frac{\tau (c-b)}{2 \sqrt{\pi a}} \left(\frac{k-1}{k+1} \right) \quad (\text{VII-11})$$

$$k = 3 - 4\nu \quad (\text{Plane Strain})$$

$$k = \frac{3 - \nu}{1 + \nu} \quad (\text{Plane Stress})$$

VII.2 CONCENTRATED FORCES

Concentrated Force (F), on a Crack Surface with Arbitrary Inclination



(Mode I)

F = Force per unit thickness

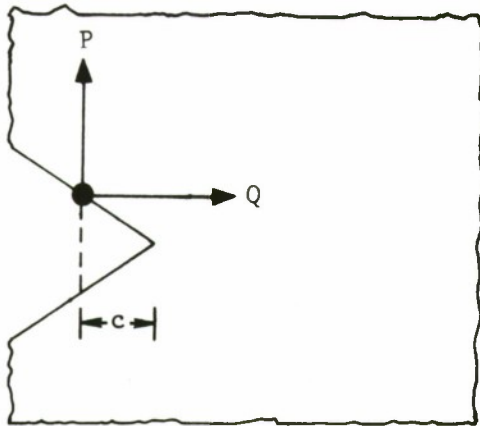
$$K_I = \frac{P}{2 \sqrt{\pi a}} \sqrt{\frac{a+b}{a-b}} + \frac{Q}{2 \sqrt{\pi a}} \left(\frac{k-1}{k+1} \right) \quad (\text{Mode II}) \quad (\text{VII-12})$$

$$K_{II} = \frac{-P}{2 \sqrt{\pi a}} \left(\frac{k-1}{k+1} \right) + \frac{Q}{2 \sqrt{\pi a}} \sqrt{\frac{a+b}{a-b}}$$

$$k = 3 - 4\nu \quad (\text{Plane Strain})$$

$$k = \frac{3 - \nu}{1 + \nu} \quad (\text{Plane Stress})$$

Concentrated Forces on Crack Surface



(Mode I)

P = Force per unit thickness

Q = Force per unit thickness

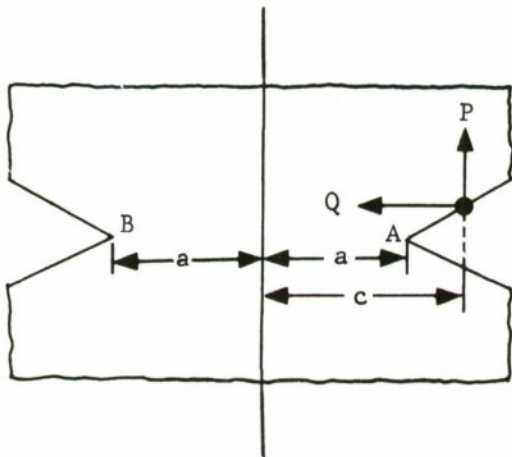
$$K_I = \frac{P}{\sqrt{2\pi c}}$$

(VII-13)

(Mode II)

$$K_{II} = \frac{Q}{\sqrt{2\pi c}}$$

Concentrated Forces on Crack Surface (Colinear Cracks)



(Mode I)

P = Force per unit thickness

Q = Force per unit thickness

(Mode I)

$$K_I @ A = \frac{P \sqrt{c^2 - a^2}}{2 \sqrt{\pi a} (c - a)}$$

(Mode II)

$$K_{II} @ A = \frac{Q \sqrt{c^2 - a^2}}{2 \sqrt{\pi a} (c - a)}$$

@ A (VII-14)

(Mode I)

$$K_I @ B = \frac{P \sqrt{c^2 - a^2}}{2 \sqrt{\pi a} (c + a)}$$

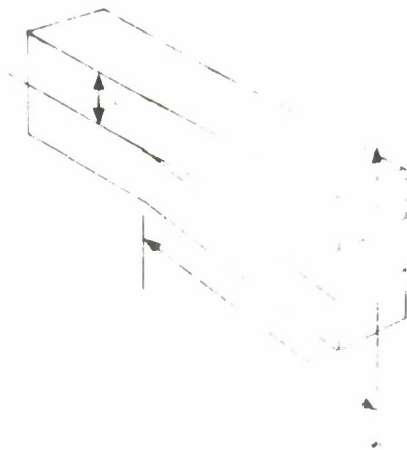
(Mode II)

$$K_{II} @ B = \frac{Q \sqrt{c^2 - a^2}}{2 \sqrt{\pi a} (c + a)}$$

@ B (VII-15)

Splitting Force Blister - Rectangular Section ($a \gg 2c$)

(Mode I)



P = Concentrated Force per unit thickness

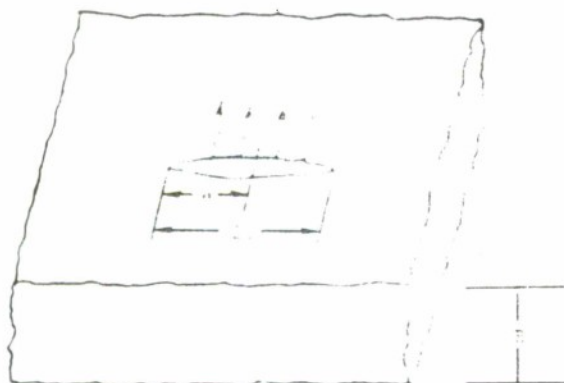
$$K_I = \frac{3.464 P a}{\sqrt{c^3}} \quad (\text{VII-16})$$

with $K_{II} = 0$

VII.3 THERMAL INDUCED STRESSES

Thermal Load on Crack Surface (Upper & Lower Crack Surfaces at Same Temperature)

(Mode I)



$$K_I = - \frac{E \alpha q \sqrt{a}}{\sqrt{\pi} (1 + k) \mu} \quad (\text{VII-17})$$

with $K_{II} = 0$

where

$k = 3 - 4\nu$ (Plane Stress)

$k = \frac{(3 - \nu)}{(1 + \nu)}$ (Plane Strain)

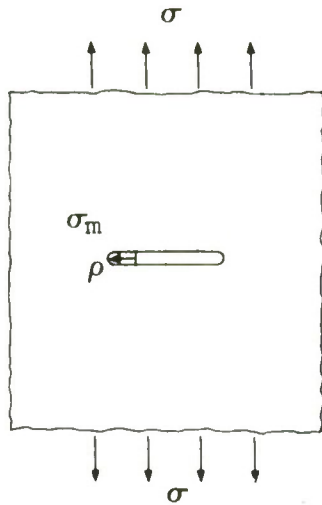
α = Coefficient of Expansion

μ = Thermal Conductivity

q = Equivalent Heat Flow Required to Produce Constant Temperature on the Crack Surfaces

E = Young's Modulus

VII.4 STRESS INTENSITIES FOR KNOWN STRESS CONCENTRATIONS

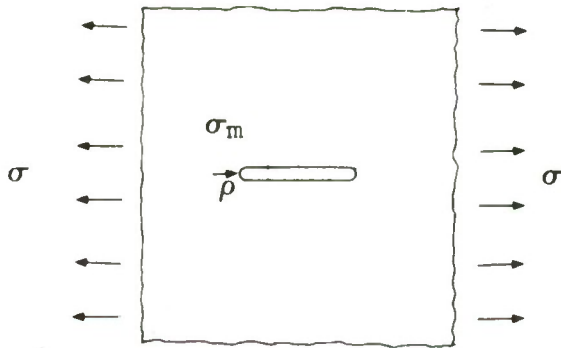


(Mode I)

$$K_I = \lim_{\rho \rightarrow 0} \sigma_m \frac{\sqrt{\pi}}{2} \sqrt{\rho} \quad (\text{from Eq. V-28})$$

(VII-18)

$$\text{with } K_{II} = K_{III} = 0$$

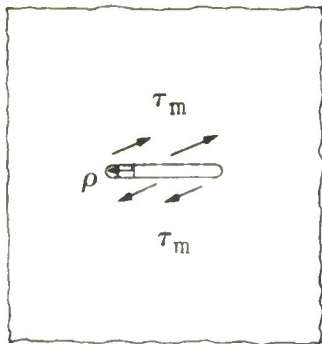


(Mode II)

$$K_{II} = \lim_{\rho \rightarrow 0} \sigma_m \sqrt{\pi} \sqrt{\rho}$$

(VII-18A)

$$\text{with } K_I = K_{III} = 0$$



(Mode III)

$$K_{III} = \lim_{\rho \rightarrow 0} \tau_m \sqrt{\pi} \sqrt{\rho}$$

(VII-18B)

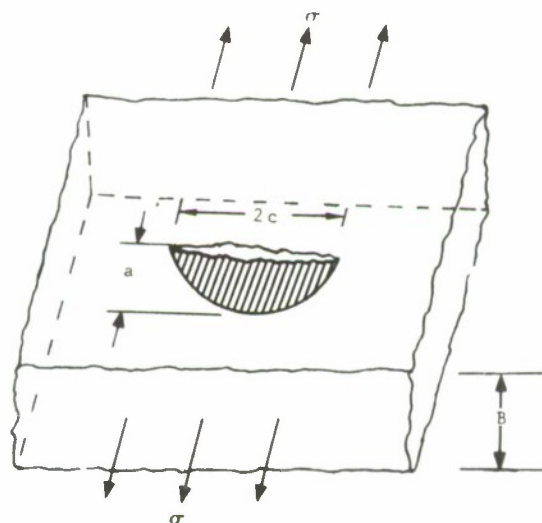
$$\text{with } K_I = K_{II} = 0$$

where σ_m is the maximum normal stress at the root of the notch caused by axial tensile stress, σ , and τ_m is the maximum shear stress adjacent to the notch.

(See above for loading conditions.)

VII.5 PART THROUGH CRACK

Uniform Tensile Stress - Semielliptical



(Mode I)

$$K_I = \left[1 + 0.12 \left(1 - \frac{a}{c} \right) \right] \frac{\sigma \sqrt{\pi a}}{\int_0^{\pi/2} \sqrt{1 - \left(\frac{c^2 - a^2}{c^2} \right) \sin^2 \theta} d\theta} \sqrt{\frac{2B}{\pi a} \tan \frac{\pi a}{2B}} \quad (\text{VII-19})$$

with $K_{II} = 0$

Other examples of part through cracks will be presented in Section IX.

VII.6 FINITE WIDTH CORRECTION

Since the stress intensity solutions previously presented in this section were based on infinite geometry, their usage for finite panel problems must be modified by finite width correction factors (see, e.g., eq. VI-9 to VI-12). With the use of these factors, fracture toughness values can be used to provide design criteria.

The width correction factor will be signified by the symbol λ (see Section V). For a center cracked sheet, seven solutions have been in use throughout the years. The ones we will concern ourselves with will be those currently in accepted usage. Finite width correction factors being analytic, lend themselves to graphic presentations. Presented in Figures 14 through 18 are the λ solutions for various crack geometries as a function of crack length to panel width ratio (crack aspect ratio). NOTE: These corrections have been proven accurate as long as the stress σ is remotely applied, i.e., panel length $\gg W$. In a center cracked panel, length $> 3W$.

Geometric corrections (or K calibrations) for current, standard fracture mechanics specimens are presented in polynomial form in Reference 8. These may be used to supplement the graphical presentations for greater accuracy for various crack loading situations.

VII.7 SLOW TEAR IN CRACKED STRUCTURE

During static stressing of cracked, ductile materials, the crack length increases from an initial length a_o , until a critical length a_c is reached (see Figure 1). Many times in design problems it is necessary to deal with the initial crack size and estimates must be made of critical crack lengths. Several empirical estimates of slow crack growth to a critical value, a_c , have been presented (Ref. 31, 32) which have the form

$$a_c = (1 + \text{const.}) a_o \quad (\text{VII-20})$$

where the constant (const.) provides the best data fit. Newman⁽³³⁾ proposed that, as a best data fit, the following equation applies:

$$a_c = \left[1 + (\text{const.})_1 \left(\frac{W}{2a_o} - 1 \right)^{(\text{const.})_2} \right] a_o \quad (\text{VII-21})$$

where the two constants were determined from experimental data. One shortcoming of equation VII-20 is that when $a_o \rightarrow 0$, or for very small crack lengths, $a_c \rightarrow 0$. In ductile materials one would expect some slow tear to occur from even the smallest discontinuity. For long initial crack lengths ($\frac{2a_o}{W} > 0.2$), equations VII-20 or VII-21 can be used with confidence in predicting the critical crack lengths. It is recommended that equation VII-21 be used for greater accuracy for predicting critical cracks of engineering size.

The slow tear behavior of thin gage material, where the plane stress fracture mode prevails is currently under study by a special task force of the American Society for Testing and Materials (Committee E-24) on Fracture Testing of Metals.

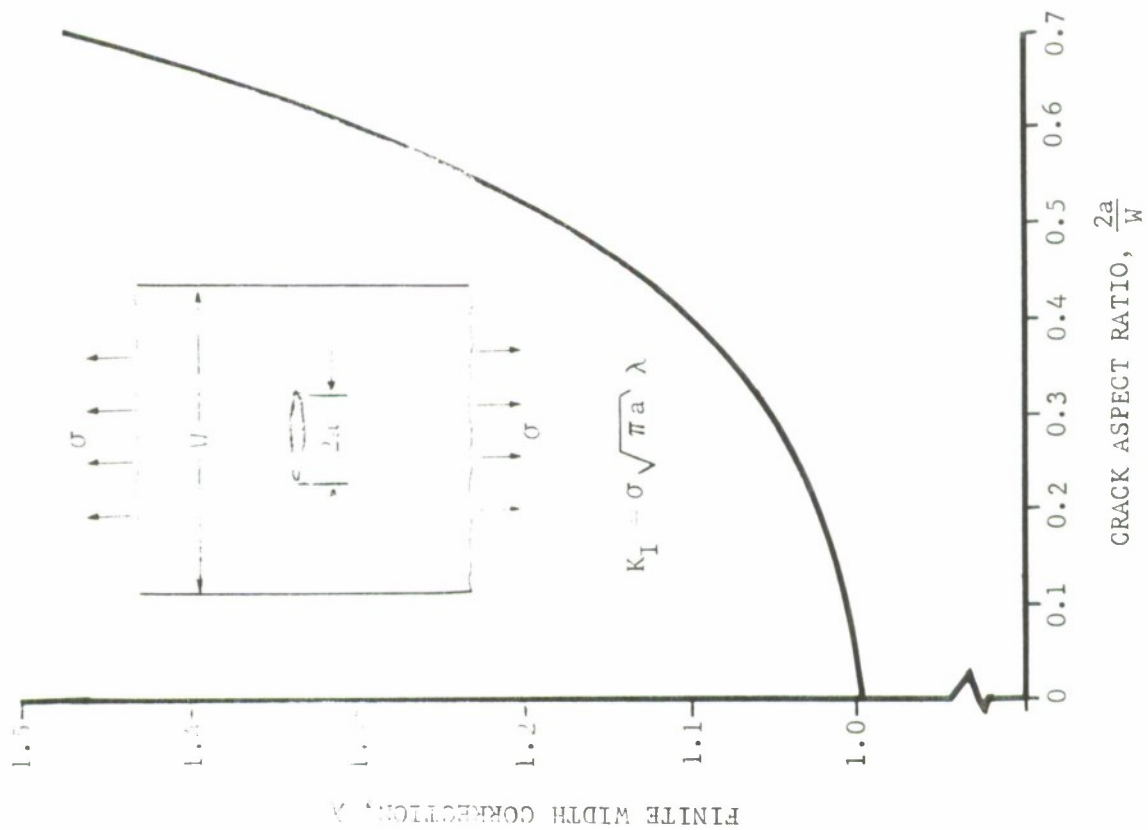


FIGURE 14. FINITE WIDTH CORRECTION-CENTER CRACKS (TENSION) (REF. 29)

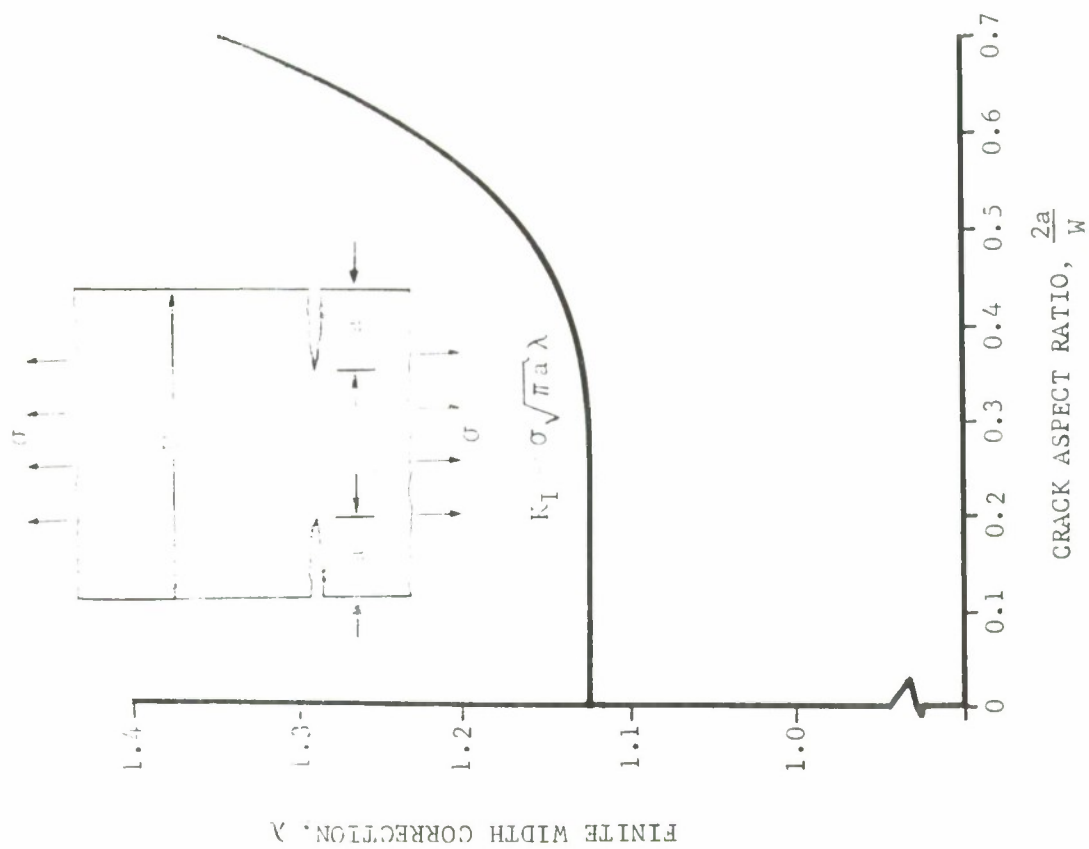


FIGURE 15. FINITE WIDTH CORRECTION-DOUBLE EDGE CRACKS (TENSION) (REF. 15)

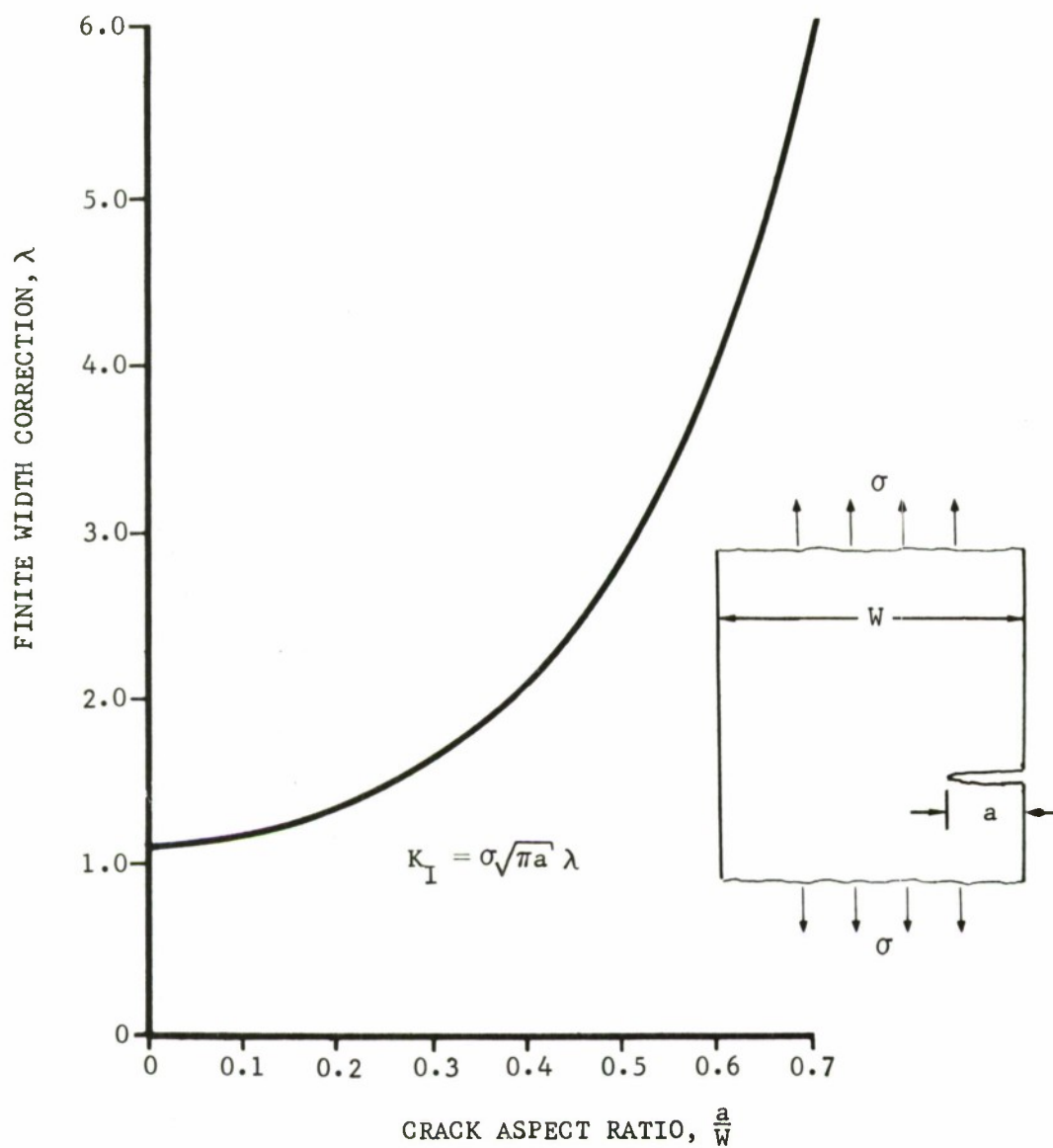


FIGURE 16. FINITE WIDTH CORRECTION-SINGLE EDGE CRACKS (TENSION) (REF. 30)

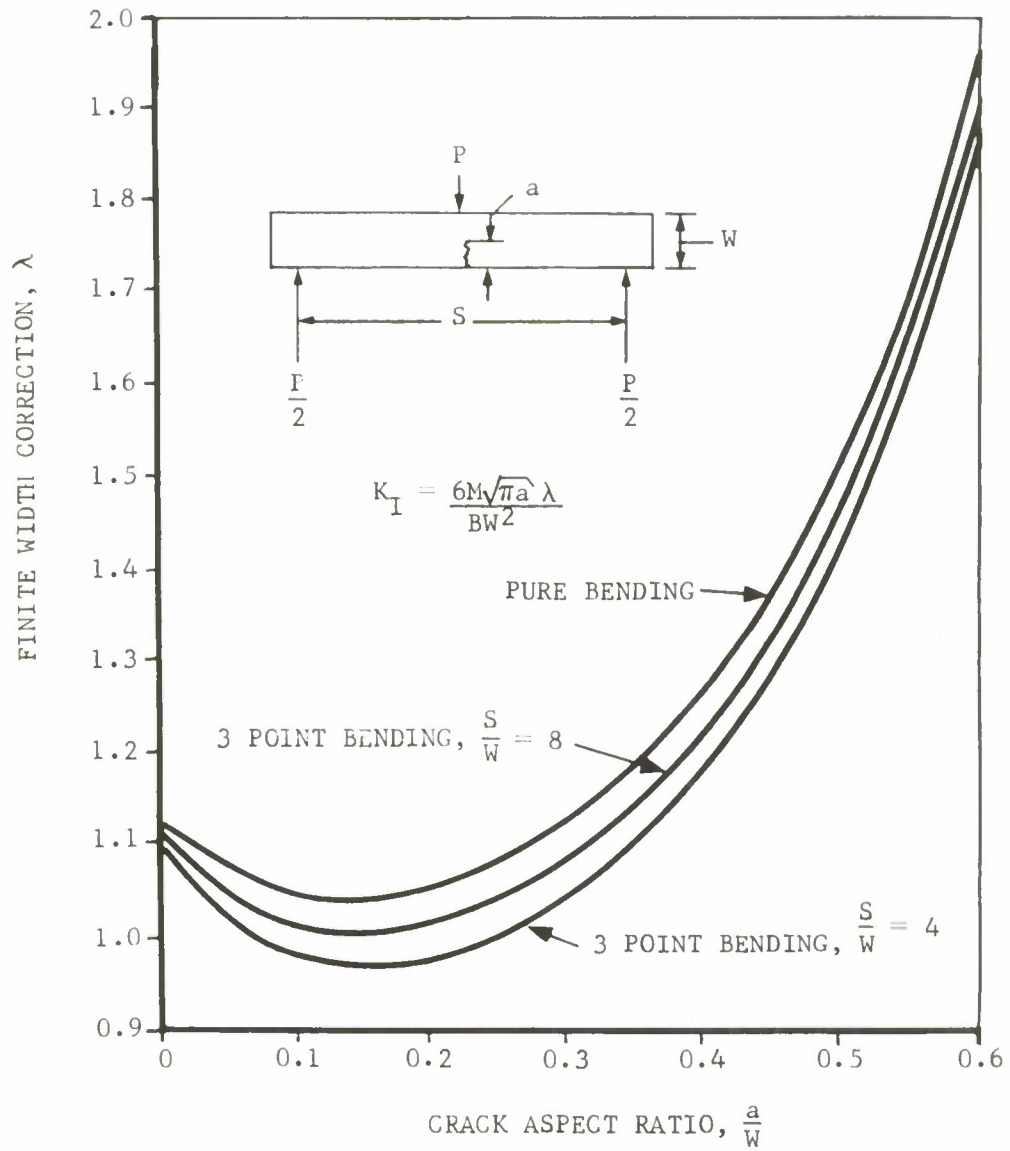


FIGURE 17. FINITE WIDTH CORRECTION-SINGLE EDGE CRACK (BENDING) (REF. 8)

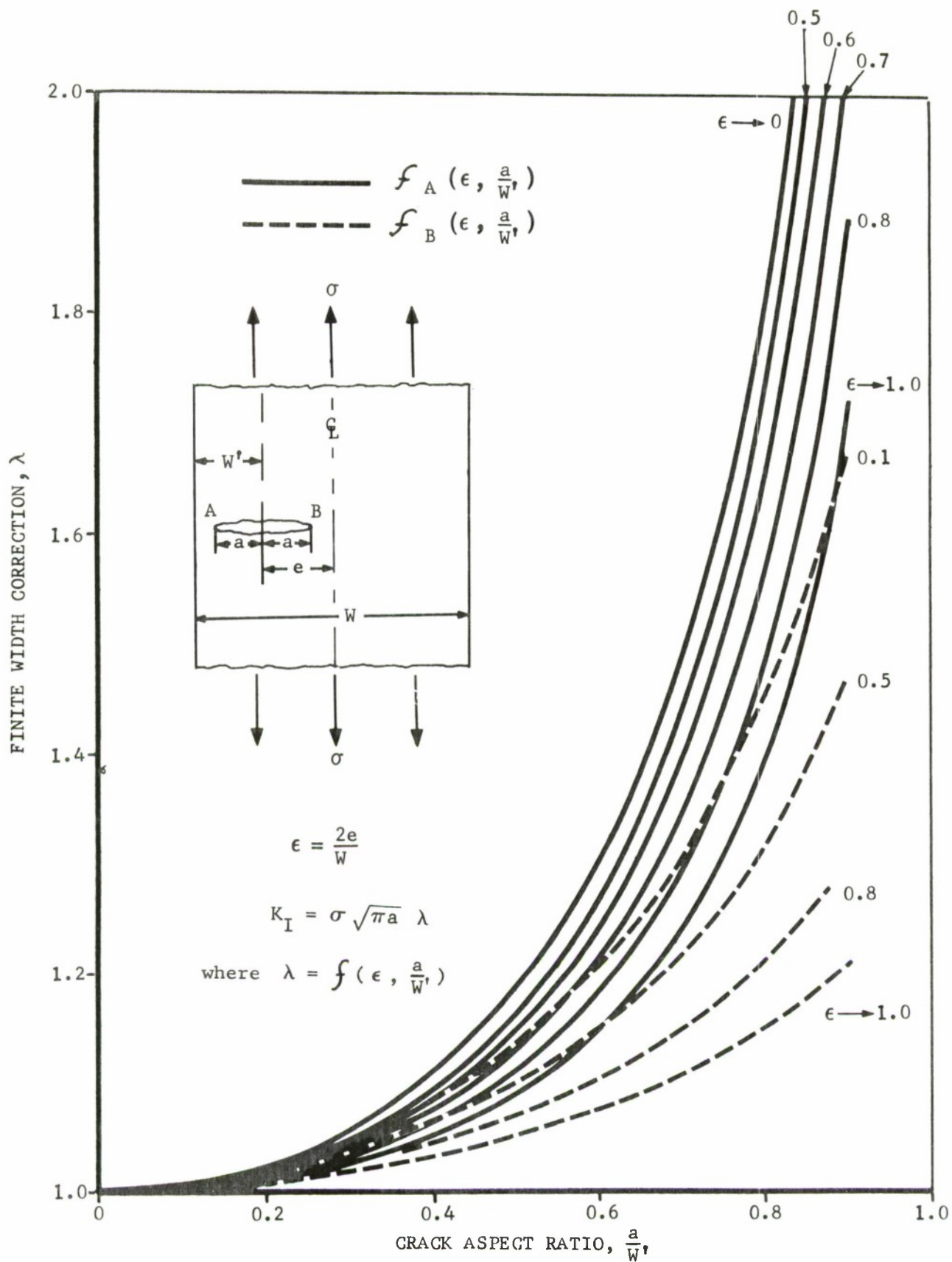


FIGURE 18 FINITE WIDTH CORRECTION-ECCENTRIC CRACK (TENSION) (REF. 29)

VIII METHODS OF RESIDUAL STRENGTH ANALYSIS

In the overall view of structural analysis for fracture prevention, initial efforts should be made to analyze fracture or fatigue-sensitive areas at an early stage of design. Figure 19 shows a logical progression from conceptual design to fracture analysis. The interplay between material and fracture parameters can be seen by the discussion thus far.

Many methods of residual strength determination are available. Through-cracked, uniaxial loaded sheet specimens and structure can be analyzed using what are essentially modifications of notch analysis. All analytical methods require determination of a "material constant" as a basic parameter. In this regard, they are in basic agreement with the fracture mechanics approach. The degree to which these methods agree for the through-crack, thin sheet, residual strength problem will be investigated in this section.

In fracture analysis there are several choices of available concepts. In fail safe design it will be remembered that concern is for the remaining strength in the presence of an existing crack or defect. Residual strength methods are based on the occurrence or presence of such cracks. Therefore, in the early part of this section, the nature of the overall problem will be given which will be solved by fracture analysis methods. The methods of analysis for the simple case of a center cracked sheet will then be presented and finally a detailed problem will be solved which will encompass and compare all pertinent fracture analysis methods. In this manner, the applicability and simplicity of the fracture mechanics approach will become evident.

VIII.1 FRACTURE ANALYSIS CONCEPTS

VIII.1(a) Fracture Mechanics (Critical K Concepts)

As we have seen so far, fracture mechanics is based on the stress analysis in the presence of an existing flaw or crack. To analyze a center cracked panel, the basic equation (VI-12) gives the interrelationship between stress, crack length, and toughness, which can be solved for critical conditions; i.e., when the stress intensity factor K reaches a critical value, the operating stress $\sigma \rightarrow \sigma_c$ and the crack length $a \rightarrow a_c$. If the material fracture toughness is known, then an analysis can be made to determine fracture stress (σ_c) for a tolerable crack size (a_c).

VIII.1(b) Emperically Derived Crack Strength Plots

In many design applications, it may suffice to use what are termed residual strength comparison plots. Fracture data from many tests on panels of various widths are plotted in Figure 20 for center cracked 7075-T6 clad aluminum panels of a given thickness. One fact evident from such plots is the change in fracture stress with panel width. One drawback to using this type of data in analysis is the expense encountered in obtaining such data. This method is usually employed in material comparisons and does not lend itself to design application.

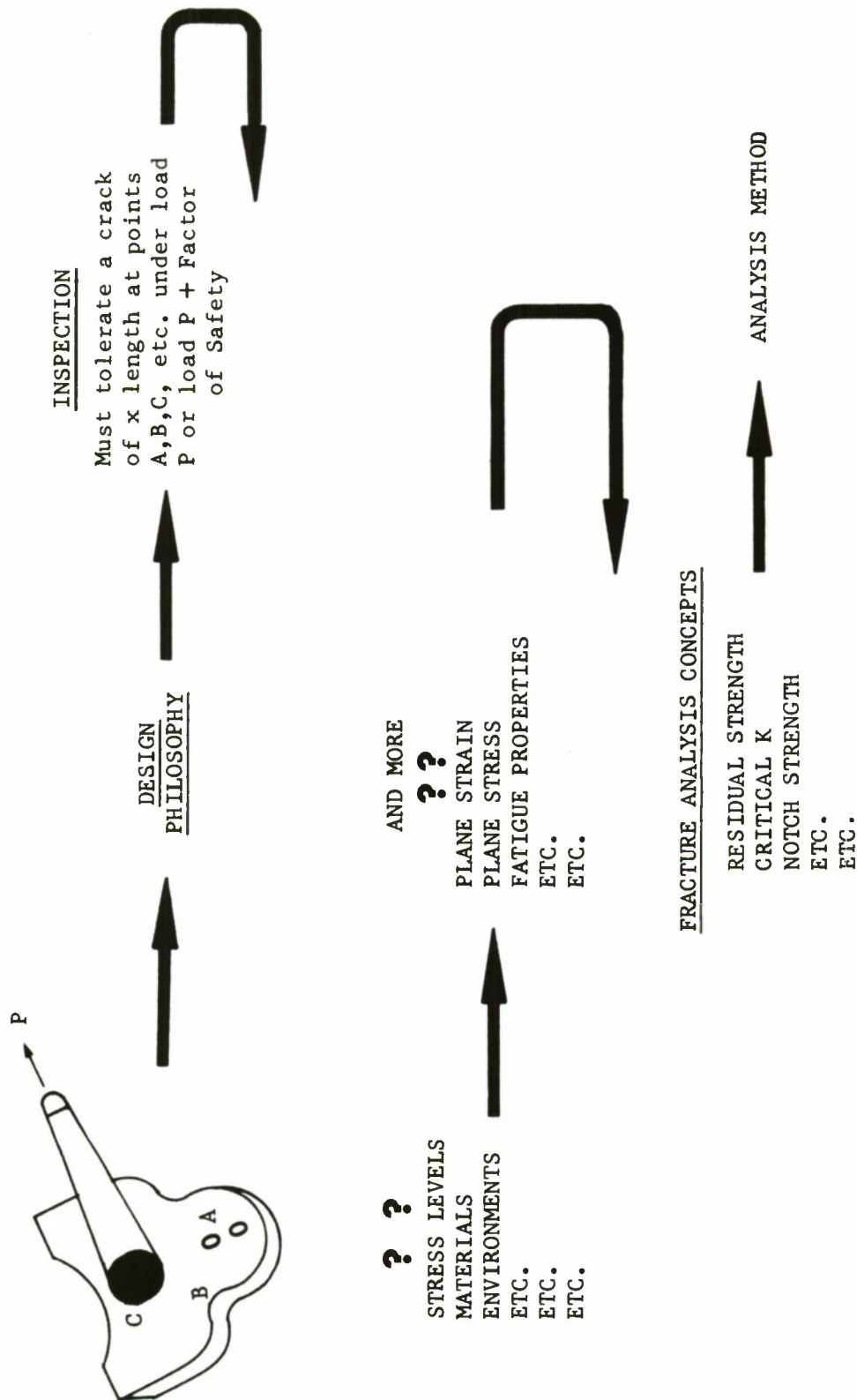
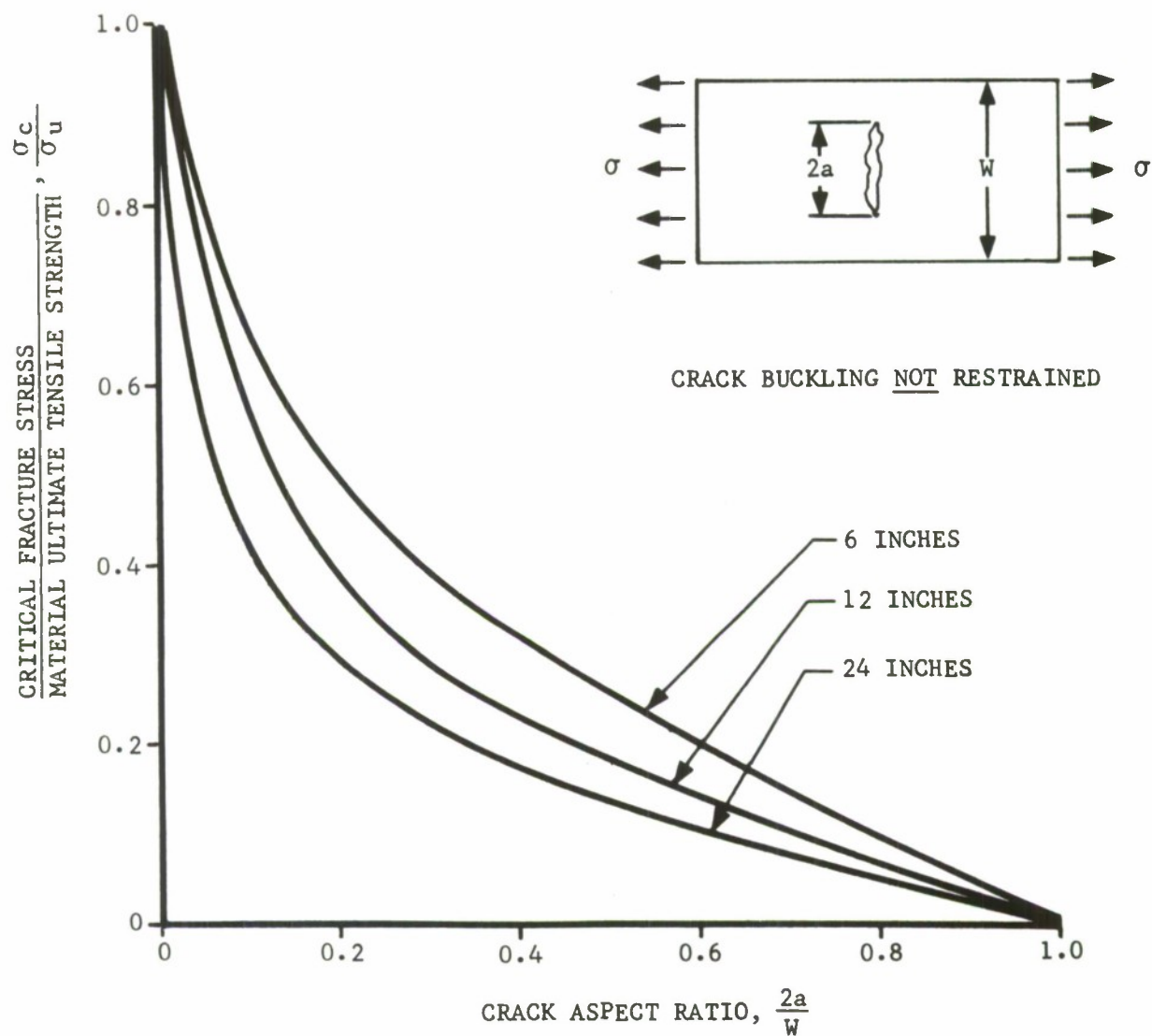


FIGURE 19. FRACTURE ANALYSIS PROGRESSION IN DESIGN



(DATA ABSTRACTED FROM "THE EFFECT OF FINITE SPECIMEN WIDTH ON THE RESIDUAL STRENGTH OF LIGHT ALLOY SHEET," BY D. BROEK, NLR-TR M.2152 NATIONAL AEROSPACE LABORATORY, NETHERLANDS, SEPT. 1965.)

FIGURE 20. RESIDUAL STRENGTH AS A FUNCTION OF PANEL WIDTH - 0.08 INCH GAGE 7075-T6 CLAD

Also, care must be exercised in using these data in analysis, since crack buckling can occur (out of plane of panel) due to compressive stresses parallel to the crack induced by Poisson's ratio effects and the longitudinal tension loading. These compressive stresses with subsequent buckling can cause a 20% to 30% reduction in fracture stress from those panels where buckling was restrained. Caution must be exercised as many times this testing parameter is neglected in the reported data.

VIII.1(c) Method A

In 1961, Crichlow⁽³⁴⁾ first presented an analysis method for cracked panels which included an effective width parameter that empirically corrected for crack buckling. Crichlow⁽³⁵⁾ has since employed the Notch Strength Analysis (NSA) parameter of Neuber⁽³⁶⁾, modified for his analysis. It will be seen later that several of the residual strength analysis methods employ a modification of the NSA. As with the fracture mechanics concept, a "material constant" (Neuber constant) must be found from these; and with knowledge of this constant, critical fracture stress can be determined.

VIII.1(d) Method B

In an effort to improve on the effective width concept of Crichlow, Christensen-Denke⁽³⁷⁾ have proposed that the stress distribution in a uni-axially loaded, cracked sheet is equal to the tensile ultimate strength in the effective width region and is a Westergaard⁽¹⁴⁾ distribution beyond this region. By integration and correction for finite width, the formula for gross area stress is

$$\sigma = \sigma_u \left[\frac{1 - \frac{2a_c}{W}}{1 + 2a_c \left(\frac{1}{\alpha^2} - 1 \right)} \right]$$

where α is an empirically determined "material constant" which is a function of the material plastic zone size.

VIII.1(e) Method C

Since this method⁽³⁸⁾ is the basis for Royal Aeronautical Society Data Sheets, it will not be repeated here. It is essentially based on material property (stress-strain derived) and effective fatigue crack tip radius parameters, and predicts crack strengths based on these properties.

VIII.1(f) Method D

This method⁽³⁹⁾, which also employs an effective crack radius, is the predecessor to the Notch Strength Analysis proposed by Kuhn, which is outlined below.

VIII.1(g) Method E, Notch Strength (NSA) and Crack Strength Analysis (CSA)

These methods utilize a modified form of the Neuber theoretical stress concentration factor. The CSA method⁽⁴⁰⁾, first introduced by Kuhn, uses this modified stress concentration factor at fracture to calculate the net area stress. A "material constant" is employed in the basic stress concentration equation and can be determined from a single fracture test. Also, the effects of crack buckling can be handled by the introduction of a correction factor. In the NSA method, the "material constant" is determined from stress-strain data which are needed as a basis for making crack strength predictions.

VIII.1(h) Method F (Part-through Cracks)

The stress intensity factor for a crack which is part way through the thickness is given by Irwin⁽⁴¹⁾ as

$$K_I = 1.1 \sigma \sqrt{\pi \frac{a}{Q}}$$

which is reasonable accurate for crack depths $\leq 50\%$ of the material thickness. The flaw shape parameter, Q , is a function of both crack or flaw depth to length ratio and operating stress to material yield stress ratio. Assumptions are made that an elliptical crack front is formed, which usually occurs in service. Tiffany, et al.,⁽⁴²⁾ have presented an analysis which can be used for thinner gage designs with deeper cracks in both crack propagation and fracture. These are presented later in a special sub-section of Section IX devoted to the part-through crack problem.

VIII.2 SAMPLE PROBLEM USING VARIOUS FRACTURE ANALYSIS METHODS

MATERIAL DATA

Material: 7075-T6 Aluminum
Panel width: $W = 20$ inches
Thickness: $B = 0.100$ inch
Material yield strength: $\sigma_{ys} = 77$ ksi
Material ultimate strength: $\sigma_u = 84$ ksi

Based on an established routine inspection schedule, it is assumed that a simple rectangular aluminum panel, uniformly loaded in tension across the width, will develop a central through-the-thickness crack (normal to loading) 4 inches long before detection.

Question: Will the panel fail at the given 45 ksi operating stress level before the crack is detected at the routine inspection interval?

NOTE: At this point a decision is made to analyze the panel using a plane stress toughness value. This decision is predicated on the material gage (0.100 inch) which should produce a plane stress slant fracture in this alloy. Increased proficiency and familiarization with fracture mechanics will make this decision easier. For those materials which have been investigated thoroughly, this is a simple task; however, other materials may require searching for valid fracture toughness values.

VIII.2(a) Fracture Mechanics Analysis

From fracture toughness data such as Figure 13, it can be seen that the plane stress fracture toughness, K_{IC} , is approximately 85 ksi $\sqrt{\text{inch}}$ for 7075-T6 of this thickness. The 20-inch width also dictates that valid K_{IC} values would probably be obtained for this crack geometry, (i.e., infinite panel behavior and $\sigma_{net} < \sigma_{ys}$).

The infinite plate solution for stress intensity, equation VII-1, is

$$K_I = \sigma \sqrt{\pi a}$$

The finite width corrected form from equation VI-12 is

$$K_I = \sigma \sqrt{a} f\left(\sqrt{\pi} \frac{2a}{W}\right) \text{ or } K_I = \sigma \sqrt{\pi a} \lambda$$

Step 1. Solve equation VI-12 for gross stress,

$$\sigma = \frac{K_I}{\sqrt{\pi a} \lambda}$$

and let critical conditions apply; i.e., $K_I \rightarrow K_{IC}$, $\sigma \rightarrow \sigma_c$, and $a \rightarrow a_c$. Therefore,

$$\sigma_c = \frac{K_{IC}}{\sqrt{\pi a_c} \lambda} \quad (\text{VIII-1})$$

Step 2. Determine the finite width correction factor, λ . For the center crack geometry the crack aspect ratio, $\frac{2a}{W} = \frac{\text{total crack length}}{\text{specimen width}}$ is

$$\frac{2a}{W} = \frac{4 \text{ inches}}{20 \text{ inches}} = 0.20$$

and from Figure 14, λ for this center crack aspect ratio is 1.03.

Step 3. Solve equation VIII-1 for the given conditions, assuming that a 4-inch crack is the critical condition.

$$\sigma_c = \frac{K_{IC}}{\sqrt{\pi a_c} \lambda} = \frac{85 \text{ ksi}\sqrt{\text{inch}}}{\sqrt{\pi (2 \text{ inch})} 1.03} = 33 \text{ ksi}$$

NOTE: The critical stress value can be reduced by 20% to 30% if crack buckling takes place. The K_{IC} value reported here assumes an unbuckled panel configuration.

Thus for specified conditions, the sheet can sustain a gross area stress which is less than 33 ksi in the presence of a 4 inch long crack. As this is 27% below the required operating stress (45 ksi), the requirements are not met.

From this illustration, a change in inspection schedule to detect a crack smaller than 4 inches or a reduction of operating stress level or both is indicated.

VIII.2(b) Crack Strength Plot

For comparison, the crack strength plot of Figure 20 can be used to obtain a very rough estimate of critical failure stress for this sample panel geometry. A critical stress of $0.3 \sigma_u$ or 25 ksi, which is 44% lower than the anticipated operating stress, would be predicted using these plots. The data of Figure 20 are for crack-buckled sheet; hence, a 20% reduction in fracture stress over that obtained by fracture mechanics analysis would be expected when no crack buckling effects are considered.

VIII.2(c) Method A Analysis

The equation given in Ref. 35 will be used to analyze the sample problem,

$$\sigma_c = \frac{\sigma_u \left(1 - \frac{2a}{W} \right)}{1 + \frac{\sqrt{2} \lambda' \sqrt{2a}}{\sqrt{\rho'} \left(1 + \frac{0.8eE}{\sigma_u} \right)}} \quad (\text{VII-2})$$

where λ' is the Dixon⁽²⁶⁾ finite width correction factor
 $\sqrt{\rho'}$ the empirically determined Neuber "material constant"
 e ultimate tensile elongation
 and E the Young's Modulus in ksi x 10^3 .

Step 1. Find the finite width correction factor:⁽²⁶⁾

$$\lambda' = \sqrt{\frac{1 - \frac{2a}{W}}{1 + \frac{2a}{W}}} = \sqrt{\frac{1 - 0.2}{1 + 0.2}} = 0.82$$

NOTE: The critical stress value can be reduced by 20% to 30% if crack buckling takes place. The K_c value reported here assumes an unbuckled panel configuration.

Step 2. Given the modulus, ultimate elongation, and Neuber constant for 7075-T6 of this thickness and rolling direction, solve equation VIII-2 for gross fracture stress:

$$E = 10.3 \text{ ksi} \times 10^3$$

$$e = 13\% = 0.13$$

and $\sqrt{\rho'}$ from published data(43) = $0.125\sqrt{\text{inch}}$

$$\sigma_c = \frac{84 \text{ ksi} \sqrt{1 - \frac{4 \text{ inch}}{20 \text{ inch}}}}{1 + \frac{\sqrt{2} \cdot 0.82 \sqrt{4 \text{ inch}}}{0.125 \sqrt{\text{inch}} \left(1 + \frac{0.8 \left[(0.13)(10.3 \text{ ksi} \times 10^3) \right]}{84 \text{ ksi}} \right)}}$$

$$\sigma_c = 32 \text{ ksi}$$

The value of critical fracture stress predicted by this method is approximately 29% below the operating stress level. If crack buckling is expected to take place, this value of critical stress is reduced in the Method A analysis by the empirical factor developed by Kuhn and Figge:(44) $1 - \gamma \frac{2a}{B}$, where γ is another material constant which has been found to be 0.001 for aluminum alloys.(35) This reduces the unbuckled critical stress value (32 ksi) by 4% and predicts a crack buckled critical stress of 30.7 ksi, which is 32% below the operating stress level.

VIII.2(d) Method B Analysis

In using this method the "material constant", α , must be determined from a fracture test,

$$\alpha = \frac{1}{\sqrt{\frac{1}{2a_c} \left[\left(\frac{1 - \frac{2a_c}{W}}{\sigma_c / \sigma_u} \right)^2 - 1 \right] + 1}} \quad (\text{VIII-3})$$

For 7075-T6, where $\alpha = 0.75 \text{ inch}$, σ_c is (Ref. 37):

$$\sigma_c = \frac{\sigma_u \left(1 - \frac{2a_c}{W} \right)}{\sqrt{1 + 2a_c \left(\frac{1}{\alpha^2} - 1 \right)}} = \frac{84 \text{ ksi} \left(1 - \frac{4 \text{ inch}}{20 \text{ inch}} \right)}{\sqrt{1 + 4 \text{ inch} \left[\frac{1}{(0.75 \text{ inch})^2} - 1 \right]}}$$

$$\sigma_c = 32.4 \text{ ksi}$$

for an unbuckled crack of the geometry of the sample problem, or 28% below the expected operating stress level.

VIII.2(e) Method E, Crack Strength Analysis (NSA) & (CSA) ⁽⁴⁰⁾

The net section stress at fracture is given in the NSA⁽⁴⁰⁾ method as

$$\sigma_{\text{net}} = \frac{\sigma_u}{1 + \alpha \lambda' \sqrt{a}} ; \quad (\text{VIII-4})$$

and in the CSA method⁽⁴⁰⁾ as

$$\sigma_{\text{net}} = \frac{\sigma_u'}{1 + \alpha' \lambda' \sqrt{a}} . \quad (\text{VIII-5})$$

The α term in equation VIII-4 is a material constant which assumes no notch strengthening. To obtain a better correlating equation, equation VIII-5 was introduced. It contains a modified "materials constant" (α') and ultimate strength (σ_u'), determined from material on which a crack strength test has been run. We will utilize equation VIII-4 to determine the net failure stress. The value of α for 7075-T6 is $1.4\sqrt{\text{inch}}^{-1}$ from published data⁽⁴⁰⁾ for this thickness, and λ' is the Dixon finite width correction term as utilized in the Crichlow analysis. From equation VIII-4,

$$\sigma_{\text{net}} = \frac{84 \text{ ksi}}{1 + 1.4 \sqrt{\text{inch}}^{-1} (0.82) \sqrt{2 \text{ inch}}} ,$$

$$\sigma_{\text{net}} = 32 \text{ ksi} .$$

The critical gross stress, σ_c , for a 4 inch crack would be 25.6 ksi or 43% lower than the operating stress for an unbuckled central crack. The buckled crack geometry reduces this value again by 4% for a critical stress of 24.6 ksi.

A comparison of the results from these various analyses is provided in Table I. The predicted fracture stress for both the buckled and unbuckled crack condition in the sample geometry is indicated as a percentage of the original assumed operating stress, 45 ksi. This comparison shows that the agreement between methods is quite good in the unrestrained condition. The NSA analysis with buckling restrained would imply lower fracture stress. In any case, the answer to the question posed in this sample problem is that the 7075-T6 panel will not be able to withstand an operating stress of 45 ksi for the crack geometry in question.

TABLE I
COMPARISON OF FRACTURE DATA FOR VARIOUS ANALYSIS METHODS

ANALYSIS METHOD	Critical Stress and Percent of Operating Stress (45 ksi)			
	With Crack Buckling		No Crack Buckling	
	(ksi)	(%)	(ksi)	(%)
Fracture Mechanics	26.4-23.1	(50-58)	33	(73)
Strength Plot	25	(56)	--	--
Method A Analysis	30.7	(68)	32	(71)
Method B Analysis	--	--	32.4	(72)
Notch Strength Analysis (NSA)	24.6	(55)	25.6	(57)

VIII.2(f) Common Grounds

In analyzing this simple case of a cracked plate in tension, it becomes apparent that the following conditions are common for all the available thin sheet analysis methods:

1. A "constant" or "constants" related to some material property must be known or determined.
2. Finite width corrections apply.
3. In-plane buckling of the sheet at the crack tip reduces the critical fracture stress.
4. All methods except the fracture mechanics analysis are based on stress reduction from the material ultimate tensile strength.

It should be remembered that the calculations of fracture stress are fundamentally based on the "material constant", be it fracture toughness or notch factor; hence, the accuracy will depend on how this parameter is determined. In fracture mechanics, it has been shown to be both width and thickness dependent in the plane stress fracture mode. However, as more K_{IC} data becomes available, and as a better understanding of the factors involved in general yielding ($\sigma_c > \sigma_{ys}$) becomes known, a better base of confidence in the fracture mechanics analysis of thin sections will be provided. Similar statements apply to the other analysis methods, which have resulted in new or modified "material constants" to better fit the available data. The introduction of tougher new materials have dictated changes in the fracture analysis and more modifications are inevitable.

IX INFLUENCE OF FRACTURE IN AIRCRAFT DESIGN

In conventional aircraft structural design, the terms "limit load" (stress), "ultimate load" (stress), and "factor of safety" are extensively employed. For purposes of this report, the terms may be briefly defined as follows:

Limit load (stress) is the maximum load (stress) expected in operational service (usually set by or derived from structural design criteria specifications, and represents that value for which the probability of exceeding that load is very small).

Ultimate load (stress) is the limit load times the factor of safety (specifications usually require that the structure be capable of sustaining ultimate load, as defined; structure collapse just beyond ultimate is accepted).

Factor of safety is the multiplying factor (usually set by specifications) to convert limit load (stress) to ultimate load (stress). Customary USAF practice is to employ a factor of safety (ultimate of 1.5).

The examples presented in this section assume that the factor of safety is 1.5 and that the tension stress encountered at limit load (limit design stress) is $2/3$ of the ultimate tensile strength of the material ($2/3 \sigma_u$). (This simplification is for illustrative purposes herein only; it is recognized that other requirements, e.g., fatigue, stiffness, etc., often dictate lower values of stress at limit and ultimate loads.)

NOTE: The examples presented in this section are for illustrative purposes only. In practice each problem will have its unique solution.

IX.1 MATERIAL TRADE-OFFS

Quality control dictates that cracks must be detectable within certain limits. As an example, in a center cracked panel*, a $1/2$ -inch long crack can be detected in routine inspections. The material thickness is planned to be 0.100 inch. There is a choice of three materials which possess approximately the same ultimate tensile strength properties. The design stresses, mechanical properties, and fracture toughness are listed in Table IX-II. Infinite panel behavior is assumed in this design ($\frac{2a}{W} < 0.1$) and the finite width correction, λ , from Figure 14, is 1.00.

From the tabular data, the 2024-T3 alloy appears to be the most suitable material based on average plane stress fracture toughness (\bar{K}_C). The critical gross fracture stress, σ_c , is:

$$\sigma_c = \frac{\bar{K}_C}{\sqrt{\pi a \lambda}} = \frac{95 \text{ ksi} \sqrt{\text{inch}}}{\sqrt{\pi} 0.25 \text{ inch} (1.00)}$$
$$\sigma_c = 107 \text{ ksi}$$

The predicted critical fracture stress is 2.3 times the guaranteed minimum yield for this material. This indicates that fracture will occur with gross plastic deformation and yielding on the net section rather than directly

*Although this crack geometry occurs rather infrequently in service, it provides a good illustrative basis for material fracture evaluation. As such, it will be used here for just such a comparison.

from the influence of the 1/2-inch crack. It would be acceptable under these circumstances to choose a less fracture-tough, but stronger alloy with a higher limit design stress.

TABLE II
DATA FOR MATERIAL TRADE-OFF STUDY PROBLEM

Alloy Designation	$\sigma_u^{(1)}$ (ksi)	$\sigma_{ys}^{(1)}$ (ksi)	$\bar{K}_c^{(2,3,4)}$ (ksi $\sqrt{\text{inch}}$)	$\sigma_{LIM.}^{(5)}$ Limit Design Stress (ksi)	σ_c (ksi)	$\frac{\sigma_c}{\sigma_u}$	$\frac{\sigma_c}{\sigma_{ys}}$	$\frac{\sigma_c}{\sigma_{LIM.}}$
2024-T81 CLAD	67	59	65	45	73	1.1	1.2	1.6
7075-T6 CLAD	73	64	85	49	96	1.3	1.5	2.0
2024-T3 CLAD	63	46	95	42	107	1.7	2.3	2.5

- NOTES: (1) MINIMUM VALUES FROM MIL-HDBK-5
 (2) AVERAGE TEST VALUES - PARTICULAR DESIGN WOULD CALL FOR FRACTURE TOUGHNESS VALUES FOR 0.100-INCH MATERIAL IN THE WIDTH OF INTEREST.
 (3) PLASTIC ZONE ADJUSTMENTS HAVE BEEN INCLUDED IN THESE VALUES, AND NO CRACK BUCKLING IS ASSUMED.
 (4) ENVIRONMENTAL EFFECTS HAVE BEEN NEGLECTED.
 (5) BASED ON A F.S. OF 1.5.

The other possibilities listed in Table II are 2024-T81 and 7075-T6. The critical fracture stresses were computed as for the 2024-T3 alloy. The ratios of critical stress to yield and ultimate are similar, with 7075-T6 having slightly higher values. Therefore, since the limit design stress is 10 percent higher for the 7075 alloy and the densities are comparable, the 7075-T6 material would be chosen over the 2024-T81 alloy. It would also provide higher strength to weight capability as well as sufficient fracture toughness to cope with the inspectible crack.*

IX.1(a) Material Substitutions

If, during the material selection phase, or perhaps the design stage, it may be desirable to consider evaluating different materials, how can this be handled? For example, it may be planned to substitute steel sheet in place of the 7075-T6 alloy for possible weight savings and higher allowable stresses. Mechanical property and fracture data are listed in Table III for a 4340 (0.035-inch gage) steel.

To determine the smallest possible crack which can be tolerated in the structure at the limit design stress, we have, when $K_I \rightarrow K_c$, $2a/W \rightarrow 0$, $\lambda \rightarrow 1.00$, and

$$a = \frac{1}{\pi} \left[\frac{K_I}{\sigma \lambda} \right]^2$$

and for critical conditions,

* Environmental effects have not been considered. If they are present, 7075-T6 could be a poor choice (see Section XI).

$$2a_c = 2 \left[\frac{\bar{K}_c}{\sigma_{LIM} \lambda} \right]^2 \frac{1}{\pi} = 2 \left[\frac{85 \text{ ksi} \sqrt{\text{inch}}}{49 \text{ ksi} (1.00)} \right]^2 \frac{1}{\pi} = 1.92 \text{ inches}$$

for the 7075-T6 alloy, and 0.77 inches for the 4340 steel.*

NOTE: These estimated values of critical crack length include crack tip plastic zone, r_y length due to the use of plasticity corrected \bar{K}_c values; i.e., $2a_c \neq 2a_c$ by visual inspection, but $2a_c = 2(a_c + r_y)$ (see Equa. VI-9, Section VI).

With limit strength-density ratios about equal and the greater crack tolerance of the aluminum alloy at the design stress, the 7075 alloy remains a better choice. Other operational considerations such as inspection for small cracks and stress-corrosion cracking lead to lower threshold K_c values which should, for completeness, be considered in this substitution study.

It has been determined that environmental heating of the structure due to performance changes in the prototype design makes the choice in aluminum marginal. Titanium alloy Ti-6Al-4V sheet is being considered as a replacement material. Pertinent material and fracture data for the Ti-6Al-4V alloys are shown in Table III.

TABLE III
DATA FOR MATERIAL SUBSTITUTION STUDY

Alloy Designation	σ_u (1,4) (ksi)	σ_y (1,4) (ksi)	Density ρ (lb/cu.in.)	\bar{K}_c (2,3,4) (ksi $\sqrt{\text{inch}}$)	$\sigma_{LIM.}$ (5) Limit Design Stress (ksi)	$\frac{\sigma_{LIM.}}{\rho}$ (in $\times 10^3$)	Critical Crack Length $2a_c$ (Inches)
7075-T6 CLAD	73	64	0.101	85	49	485	1.92
4340	200	176	0.283	154	140	495	0.77
Ti-6Al-4V	134	126	0.160	160	89	555	2.06

- NOTES: (1) MINIMUM VALUES FROM MIL-HDBK-5.
(2) AVERAGE TEST VALUES - PARTICULAR DESIGN WOULD CALL FOR FRACTURE TOUGHNESS VALUES FOR THE THICKNESS AND WIDTH OF INTEREST.
(3) PLASTIC ZONE ADJUSTMENTS HAVE BEEN INCLUDED IN THESE VALUES AND NO CRACK BUCKLING IS ASSUMED.
(4) ENVIRONMENTAL EFFECTS HAVE BEEN NEGLECTED.
(5) BASED ON A F.S. OF 1.5.

* Although the embrittlement of 4340 alloy at the high σ_u is such that this choice would be for comparison purposes only.

The gross fracture stress (σ_c) for the 1/2-inch crack in the titanium alloy is 181 ksi. A calculated critical crack length at the maximum limit design stress (89 ksi) of 2.06 inches can be tolerated prior to fracture, or a 10 percent increase in critical crack length over the 7075-T6 alloy. In addition, the strength-density ratio at the maximum allowable operating stress is 14 percent greater for the titanium alloy than for either 7075-T6 or 4340. Therefore, the Ti-6Al-4V would be a good fracture resistance choice for a substitute material for this application (see Note below).

IX.1(b) Other Methods of Material Fracture Comparison

In materials trade-off studies, it would be helpful if a comparison based on weight could be made. For example, a trade-off between weight, yield strength, and fracture toughness (plane strain), first presented in Reference 25, appears as shown in Figure 21(a). Normalization has been done with respect to a materials density. An upper bound curve has been indicated, setting the upper data limit.

On a linear plot of K_{Ic} versus σ_{ys} or σ_u , an indication can be obtained of the trade-offs between strength and toughness (see, for example, Reference 45). If this type of plot is density normalized (as in Figure 21 (a)), a straight line drawn from the origin to the upper bound curve at a particular strength level has a slope of K_{Ic}/σ_{ys} (see Figure 21 (b)). The square of this slope defines a test specimen of suitable dimension for fracture toughness determinations. These relationships were discussed in Section VI. It also provides an indication of the plastic zone size (see, e.g., Equation VI-7).

Any valid fracture toughness data which plot below the upper bound curve indicate that the material is not as crack resistant as another material at the same strength level. In this manner, the density normalized plot can be used to compare the fracture toughness of new materials with other materials at a given strength level.

IX.2 BENDING LOADS

An arm in bending is shown in Figure 22. It has developed cracks at C, or it is suspected that cracks will develop at C. A force of 2,000 or 3,000 lbs. is supplied through a hydraulic cylinder at point B and the bar ends are simply supported.

Question: Which material would be a better fracture resistant choice if a 1/4-inch deep through-the-thickness crack can be detected at C; 7075-T6 or 2219-T851?

This geometry has significance in plane strain toughness testing, which will be discussed in Section XII.

NOTE: Caution: The values normally reported for plane stress fracture toughness do not include the effects of environments or other than uniaxial loading. Where doubt exists as to the component stress or environment, simulated tests must be conducted to determine K_c or fracture stress values.

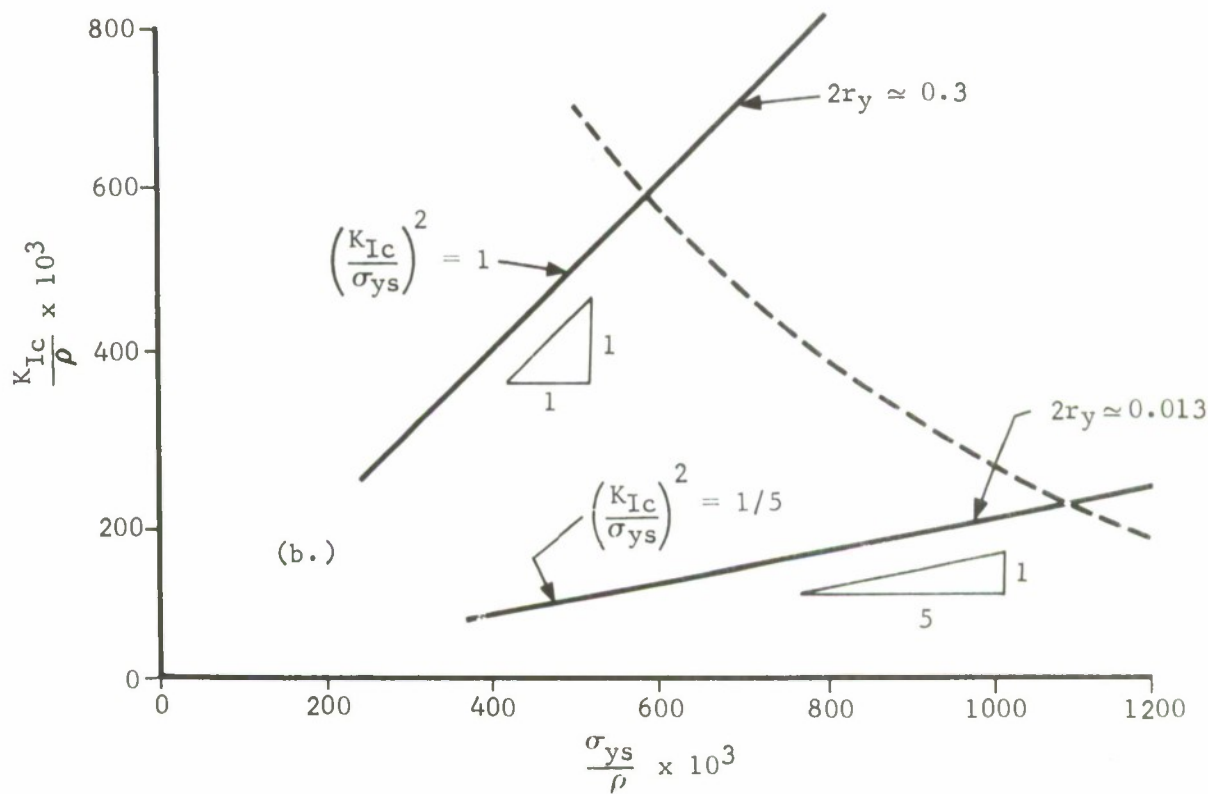
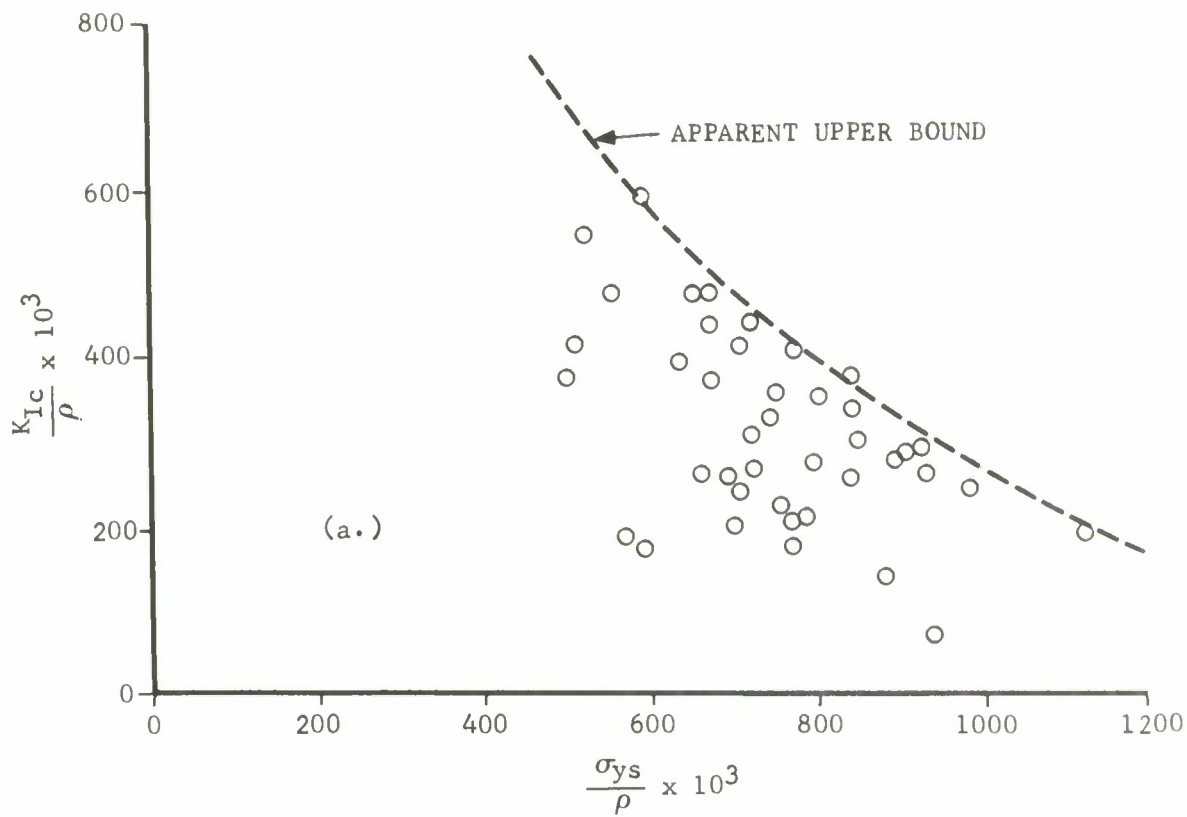


FIGURE 21 DENSITY NORMALIZED PLOT OF PLANE STRAIN FRACTURE TOUGHNESS AND YIELD STRENGTH FOR DIFFERENT MATERIALS (REF. 25)

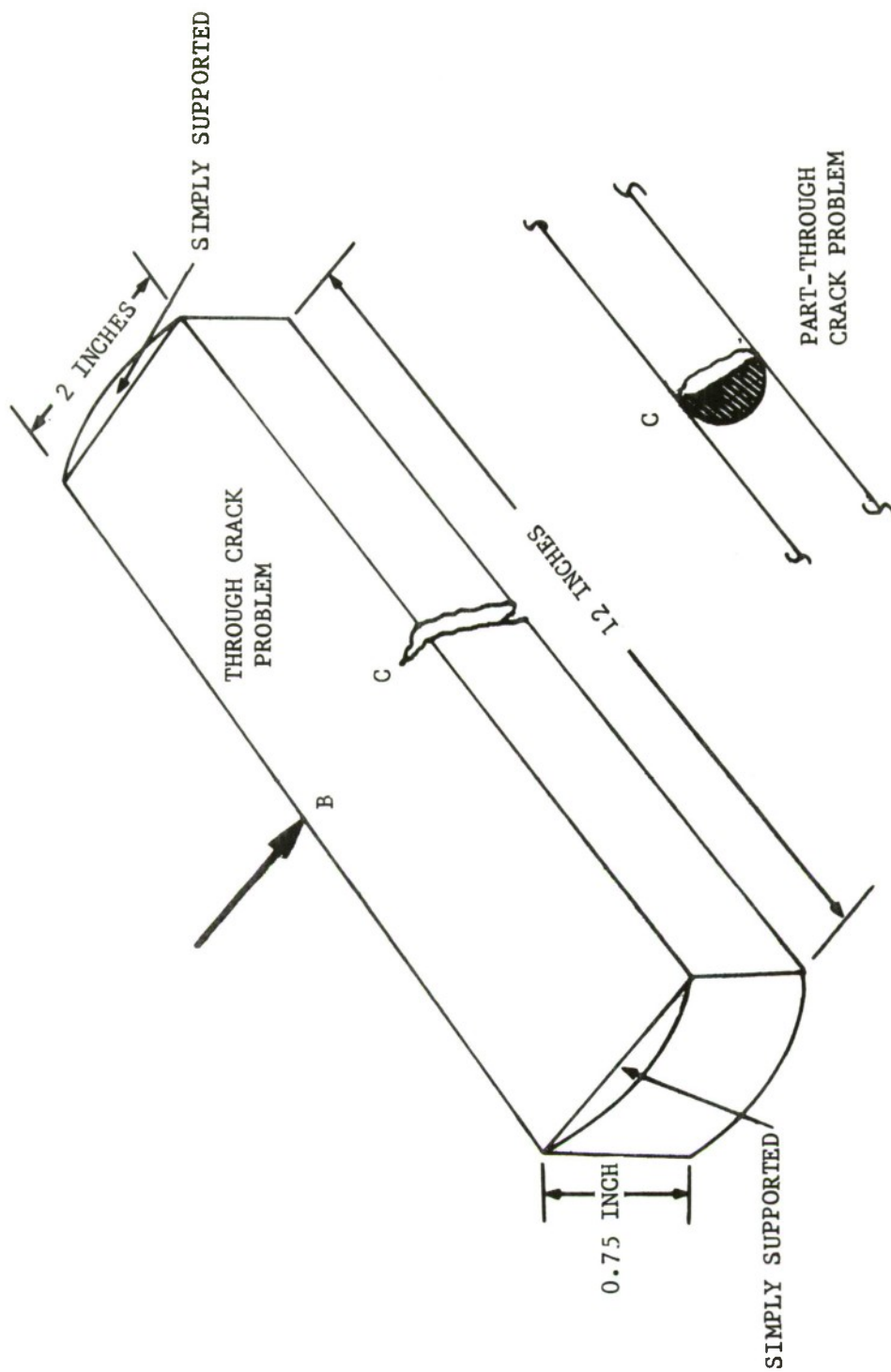


FIGURE 22 SIMPLY SUPPORTED BAR OF EXAMPLE PROBLEM, IN BENDING

STEP 1. Equation VII-8 gives the stress intensity factor for the crack geometry with in-plane bending. Compute the stress intensity factor for a $\frac{1}{4}$ -inch deep crack. For a 2,000 lb. force,

$$M = 2,000 \text{ lbs.} \times \frac{12 \text{ inches}}{4} = 6,000 \text{ lb.-in.}$$

$$K_I = \frac{6M\sqrt{\pi a}}{BW^2} = \frac{6(6,000 \text{ lb.-in.})\sqrt{\pi(0.25 \text{ inch})}}{(0.75 \text{ inch})(2 \text{ inch})^2} = 10.6 \text{ ksi}\sqrt{\text{inch}}$$

for a 3,000 lb. force,

$$M = 3,000 \text{ lbs.} \times \frac{12 \text{ inches}}{4} = 9,000 \text{ lb.-in.}$$

$$K_I = \frac{6M\sqrt{\pi a}}{BW^2} = \frac{6(9,000 \text{ lb.-in.})\sqrt{\pi(0.25 \text{ inch})}}{(0.75 \text{ inch})(2 \text{ inch})^2} = 16.0 \text{ ksi}\sqrt{\text{inch}}$$

STEP 2. Compute the stress intensity factors with geometric correction using Figure 17 with an a/W of 0.125, $\lambda = 1.05$ for pure bending. For a 2,000 lb. force at B

$$\begin{aligned} K_I &= 10.6 \text{ ksi}\sqrt{\text{inch}} (1.05) \\ &= 11.1 \text{ ksi}\sqrt{\text{inch}} \end{aligned}$$

For a 3,000 lb. force at B

$$\begin{aligned} K_I &= 16.0 \text{ ksi}\sqrt{\text{inch}} (1.05) \\ &= 16.8 \text{ ksi}\sqrt{\text{inch}} \end{aligned}$$

STEP 3. Compare these values of stress intensity factor to the plane strain fracture toughness values.

MATERIAL	K_{Ic} (ksi $\sqrt{\text{inch}}$)	$\frac{K_I}{K_{Ic}}$ (2,000 lbs.)	$\frac{K_I}{K_{Ic}}$ (3,000 lbs.)
7075-T6	40	0.28	0.42
2219-T851	32.6	0.34	0.52

For the 2,000 lb. force, either material would be suitable for this design--the 7075 alloy being a slightly better choice. The 2219 alloy could be considered as the poorer choice for the 3,000 lb. force and 1/4-inch crack depth condition, if environmental considerations are not a factor.

IX.3 OTHER CRACK GEOMETRIES

In service, an aircraft can, and usually does, sustain cracks other than the center crack configuration. There are cases where cracks start at sheet edges, on the surface, or at angles to the loading path. Fracture mechanics can handle these problems with reasonable confidence and accuracy for areas where plane strain mode fracture prevails and with fair success for the mixed mode and/or plane stress situations at this time.

To become familiar with the usage of the fracture mechanics analysis, simple crack geometries will be considered as they may occur in typical designs. In this manner, one can become familiar with the steps involved and the limitations of the current state-of-the-art of fracture analysis.

IX.4 EFFECTIVE OR EQUIVALENT CRACK LENGTH

In cases where there may be a crack traversing from the edge of a hole or at angles to the loading direction, it becomes necessary to introduce an equivalent or effective "Griffith" crack length rather than the absolute measure of the crack length. In most cases, the equivalent crack length is the same as the absolute crack length plus the discontinuity, for the crack and hole situation. However, for particular applications, estimates should be made of effective length magnitude, and compared with the absolute crack length. The requirements for calculating equivalent crack length will be indicated in the following sections.

IX.4(a) The Crack at a Hole

A design for a proposed feed-through arm is shown in Figure 23. In its center is a hole with a tubular insert welded at the top and bottom surface. Fatigue is a consideration, particularly if a brittle weld condition occurs. Inspection dictates that a $\frac{1}{2}$ -inch crack can be detected at regular inspection periods (we will assume a through-the-thickness crack). The arm material is $\frac{3}{4}$ inches thick 2219-T851 aluminum with a yield of 51.2 ksi, a plane strain* fracture toughness of $32.6 \text{ ksi}\sqrt{\text{inch}}$, and an operating stress environment of 35 ksi prevails.

Question: Can this design be considered safe in the presence of an inspectable crack, at a 25% overload condition due to pressure pulses at P? What design modifications would be recommended?

STEP 1. Assuming the worst fatigue crack condition, i.e., the tube has split along the crack axis, it can be seen that this situation then becomes the Bowie crack solution (see Section VII - Eq. VII-10) as indicated at the bottom of Figure 23.

In this case, to solve the stress intensity equation, an equivalent crack length should be introduced. In other words, an equivalent "Griffith" crack length must be found for the geometry in question.

* The plane strain (K_{IC}) fracture toughness value is applicable in this case with $\frac{3}{4}$ " thick plate material. It would be a safe assumption that plane strain fracture behavior predominates.

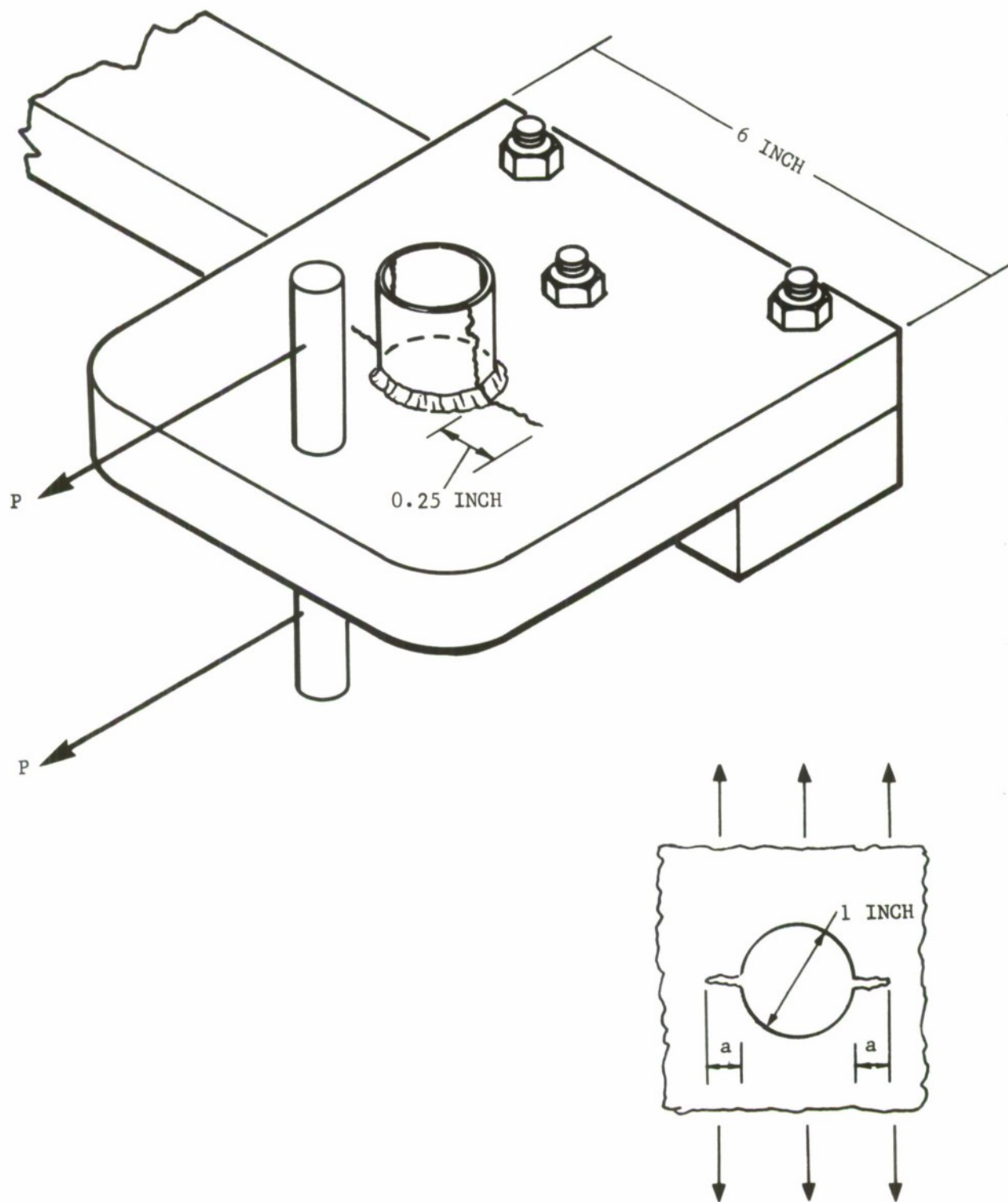


FIGURE 23 FEED THROUGH ARM WITH WELDED SUPPORT BASE

As the importance of the effective or equivalent crack length has many implications in fracture analysis, we will present this typical example which will have direct bearing on our problem.

The stress intensity for a crack or cracks at a hole in an infinite plate in uniform tension is from Equation VII-10,

$$K_I = \sigma \sqrt{\pi a} \quad f\left(\frac{a}{r}\right)$$

and the stress intensity for a central crack in an infinite plate in uniform tension is from Equation VII-1,

$$K = \sigma \sqrt{\pi a_e}$$

where a_e is the equivalent "Griffith" crack. By equating these two solutions, the equivalent crack length is determined by

$$a_e = a \left[f\left(\frac{a}{r}\right) \right]^2$$

and the values $f\left(\frac{a}{r}\right)$ are shown with Equation VII-10.

At this point, a comparison can be made of the effective crack length and the actual crack length of the Bowie geometry. For a 1.0 inch diameter hole, the equivalent crack lengths are shown in Figure 24. For the half-crack length of interest (0.25 inch, see Figure 23), it can be seen that the effective crack length is the hole radius plus actual crack length. Beyond a crack length of 0.12 inch, there is a little difference between the equivalent crack lengths computed by the Bowie solution or the crack length plus radius approximation.

STEP 2. The equivalent "Griffith" crack length for the feed-through arm has been found to be

$$a_e \cong a + r = 0.25 \text{ inch} + 0.50 \text{ inch}$$

or

$$a_e \cong 0.75 \text{ inch}$$

STEP 3. Compute the finite geometry correction factor for the problem using the equivalent crack length. The crack aspect ratio is (from Fig. 23)

$$\frac{2a}{W} = \frac{1.5 \text{ inches}}{6 \text{ inches}} = 0.25$$

From Figure 14, $\lambda = 1.04$ for a crack aspect ratio of 0.25.

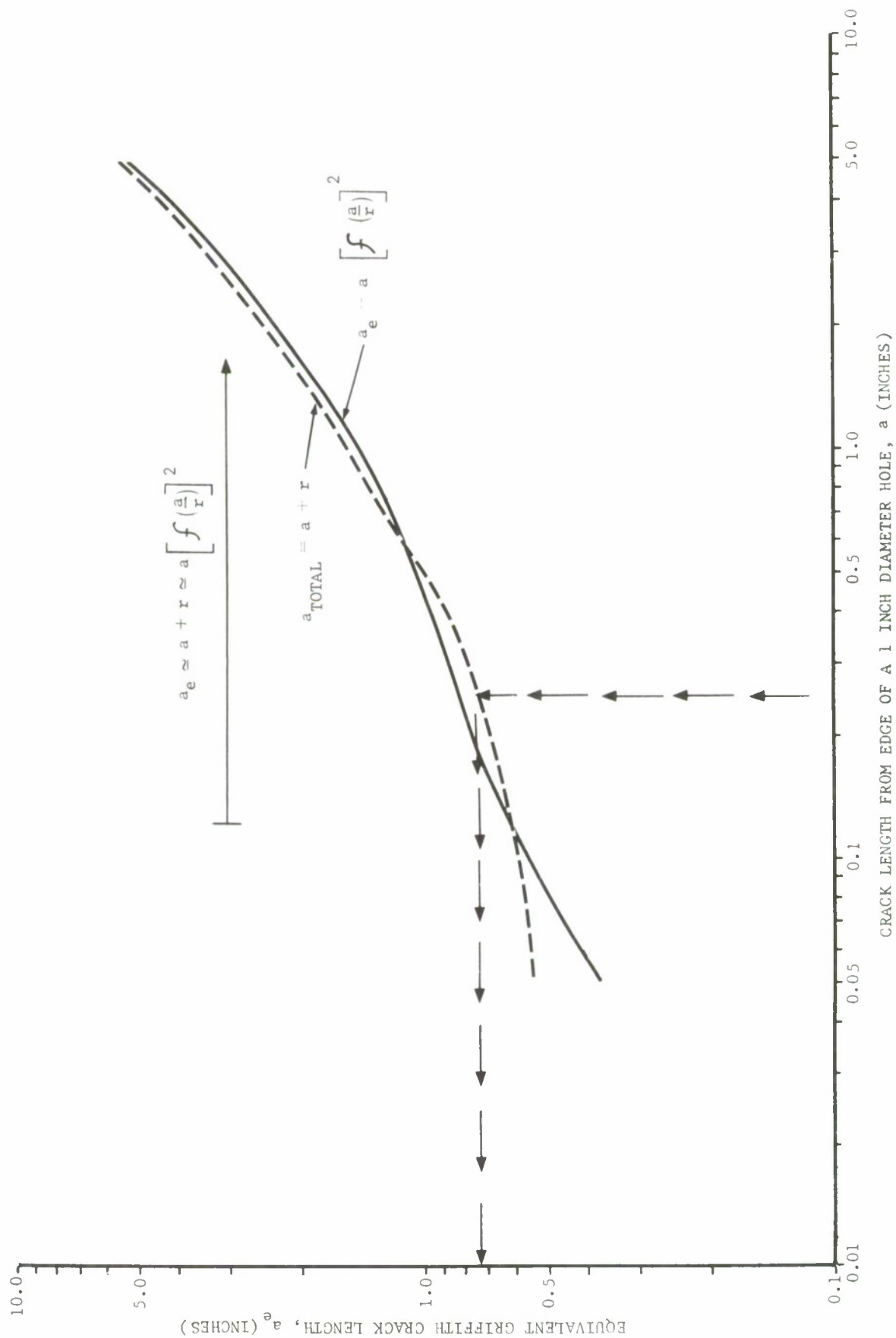


FIGURE 24 EQUIVALENT CRACK LENGTH FOR CRACKS AT A 1 INCH DIAMETER HOLE

STEP 4. Solve the basic stress intensity equation for critical conditions; i.e., $a_e \rightarrow a_{ec}$, $\sigma \rightarrow \sigma_c$, and $K \rightarrow K_{Ic}$ in plane strain. Therefore,

$$\sigma_c = \frac{K_{Ic}}{\sqrt{\pi a_{ec}} \lambda} = \frac{32.6 \text{ ksi} \sqrt{\text{inch}}}{\sqrt{\pi(0.75 \text{ inch})} (1.04)}$$

$$\sigma_c = 20.5 \text{ ksi}$$

Clearly this design will not tolerate an inspectable crack at the anticipated operating conditions.

What would be the least tolerable crack for this design? The answer to this question can be obtained through fracture mechanics by assuming bounds on the crack length parameter. For example, manipulation of the basic stress intensity equation, again assuming critical conditions at the operating stress, 35 ksi,

$$a_e = \frac{1}{\pi} \left[\frac{K_{Ic}}{\sigma_c \lambda} \right]^2$$

gives the solution for equivalent critical crack length. However, the finite width correction, λ , is also a function of crack length. For this crack geometry, an estimate can be made as $\frac{2a}{W} \rightarrow 0$, $\lambda \rightarrow 1.00$, so the smallest equivalent critical crack length will be 0.276 inch. Referring to Figure 24, an equivalent crack length of 0.276 inch would be a crack less than 0.05 inch long from the edge of the 1-inch diameter hole. This perhaps would correspond to a slight nick caused by a tool at the hole edge; therefore, a re-evaluation of the design is inevitable.

It may be possible to introduce four reasonable design modifications which, as alternatives, could assure a fracture safe part. They are:

1. Reduce allowable operating stress,
2. Reduce hole diameter,
3. Use a different material (higher K_{Ic}),
4. Reduce plate thickness and still meet stress criteria.

In many cases it is difficult to change the configuration to satisfy new operating parameters. Items 1 or 2 could satisfy the design requirement, $\sigma_c \geq 35 \text{ ksi}$, for the inspectable crack. But, we have already seen that the smallest tolerable crack for this geometry is very small ($< 0.05 \text{ inch}$), which is an undue restriction; and the operating stress level may be invariant.

This brings us to the third or fourth alternatives. Changing to a tougher material (higher K_{Ic}) will solve the problem. However, by increasing the material plane strain fracture toughness, one may gain some of the necessary fracture resistance, but not enough for the given operating stress and inspectable crack. This leaves the remaining fourth alternative as a consideration.

It will be remembered that by reducing the plate thickness, one takes advantage of the material's ability to fracture by net section yielding. In other words, a brittle fracture behavior had been assumed and by reducing the

thickness a mixed mode or possibly plane stress fracture would result. This would tend to result in higher values of fracture toughness. Plane stress (K_C) fracture toughness values of $\approx 113 \text{ ksi}\sqrt{\text{inch}}$ ⁽⁴⁶⁾ have been reported for this 2219 material in 0.10 inch thick sheet. This value reflects the influence of plastic zone size (see Eq. VI-2). In this problem we could safely assume that for a reduction in plate thickness to 3/8 inch, we would gain $\approx 50\%$ of the plane stress fracture toughness, or $56.5 \text{ ksi}\sqrt{\text{inch}}$. (This would be a conservative estimate and would imply that full plastic zone development or total plane stress behavior would not be realized.)

IX.4(b) Design with Reduced Thickness

STEP 5. Compute the new critical fracture stress based on a mixed mode type of failure with a reduced plane stress fracture toughness, $K_C \approx 57 \text{ ksi}\sqrt{\text{inch}}$.

$$\sigma_c = \frac{K_C}{\sqrt{\pi a_{ec}} \lambda} = \frac{57 \text{ ksi}\sqrt{\text{inch}}}{\sqrt{\pi(0.75 \text{ inch})} (1.04)}$$

$$\sigma_c = 36 \text{ ksi}$$

Therefore, this re-design (assuming a 35 ksi operating stress) would be considered fracture safe for the $\frac{1}{2}$ -inch crack condition, but not for the 25% overload condition. However, compensation must be made for the reduction in area caused by the reduction in thickness.

The designer and stress analyst must now decide on the basis of stress analysis of this re-design if a reduction in plate thickness will meet static strength requirements, and other stress criteria, for example. This is where the interplay between material/stress and fracture parameters enters the picture, and trade-offs are selected.

IX.5 CRACK AT RIVETS

Many times in aircraft design a part may develop cracks at rivet holes where the skin is attached to the frame or stringer. This situation is depicted in Figure 25, and will be analyzed as a simple case in which the sheet is in uniaxial tension and the rivets above and below the crack are influential in keeping the crack closed. (Tests of panels with concentrated forces superimposed on uniform tension simulate crack growth behavior in the presence of rivets.) The insert of Figure 25 shows the local parameters necessary for determining the stress intensities.

Question: Assuming that a crack grows from the rivet hole, what is the local stress intensity for this geometry?

STEP 1. This problem involves the use of stress intensity superposition principles which were discussed earlier in this report (see Section V). Closer examination of Figure 25 indicates two stress intensities as shown in Figure 26. Geometry (a) and associated stress intensity is for a center cracked sheet in tension, with the equivalent crack length approximately equal to $2a$. Geometry (b) and associated stress intensity is for a central crack subjected to concentrated forces. NOTE: This stress intensity equation is applicable only if the concentrated forces

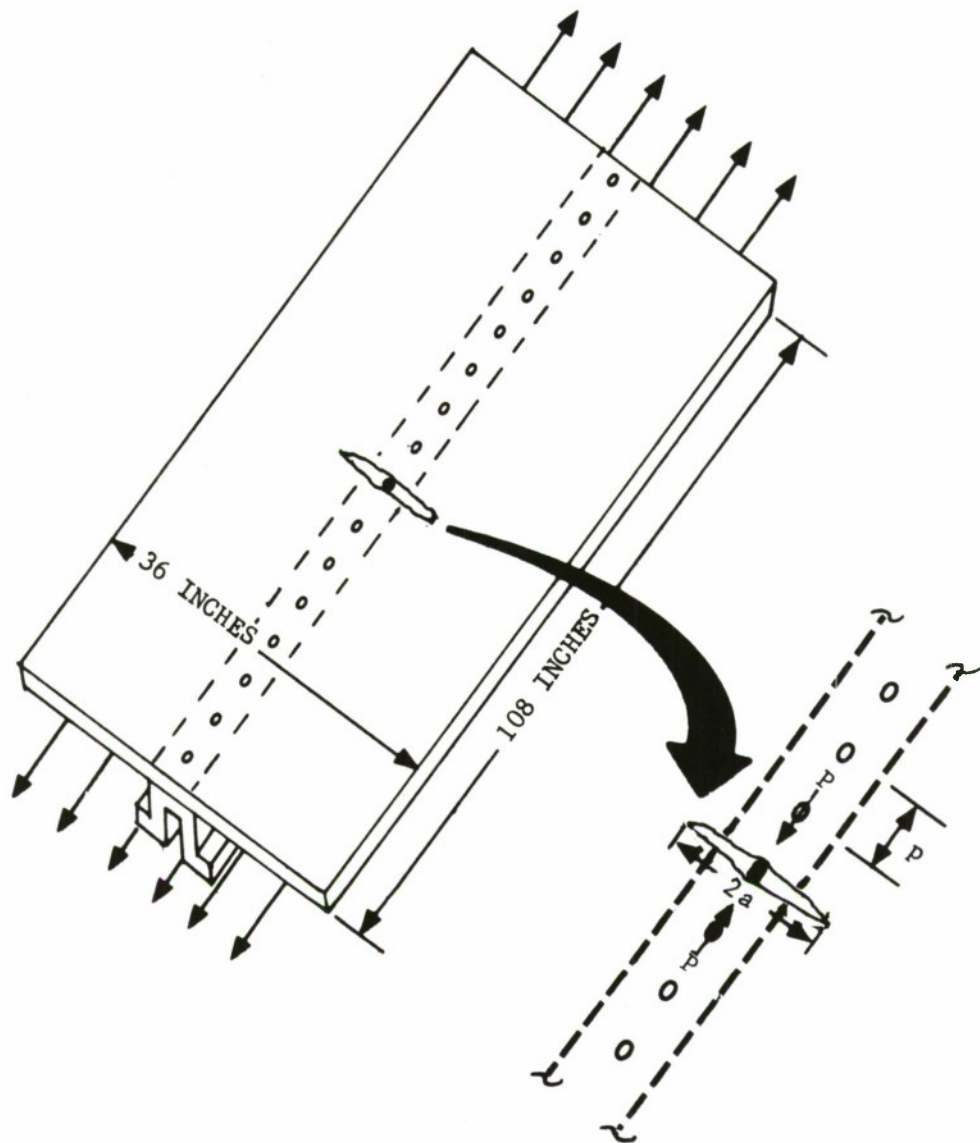


FIGURE 25 CRACK AT RIVET IN A RIVETED SKIN-STRINGER PANEL
(NO CRACK BUCKLING)

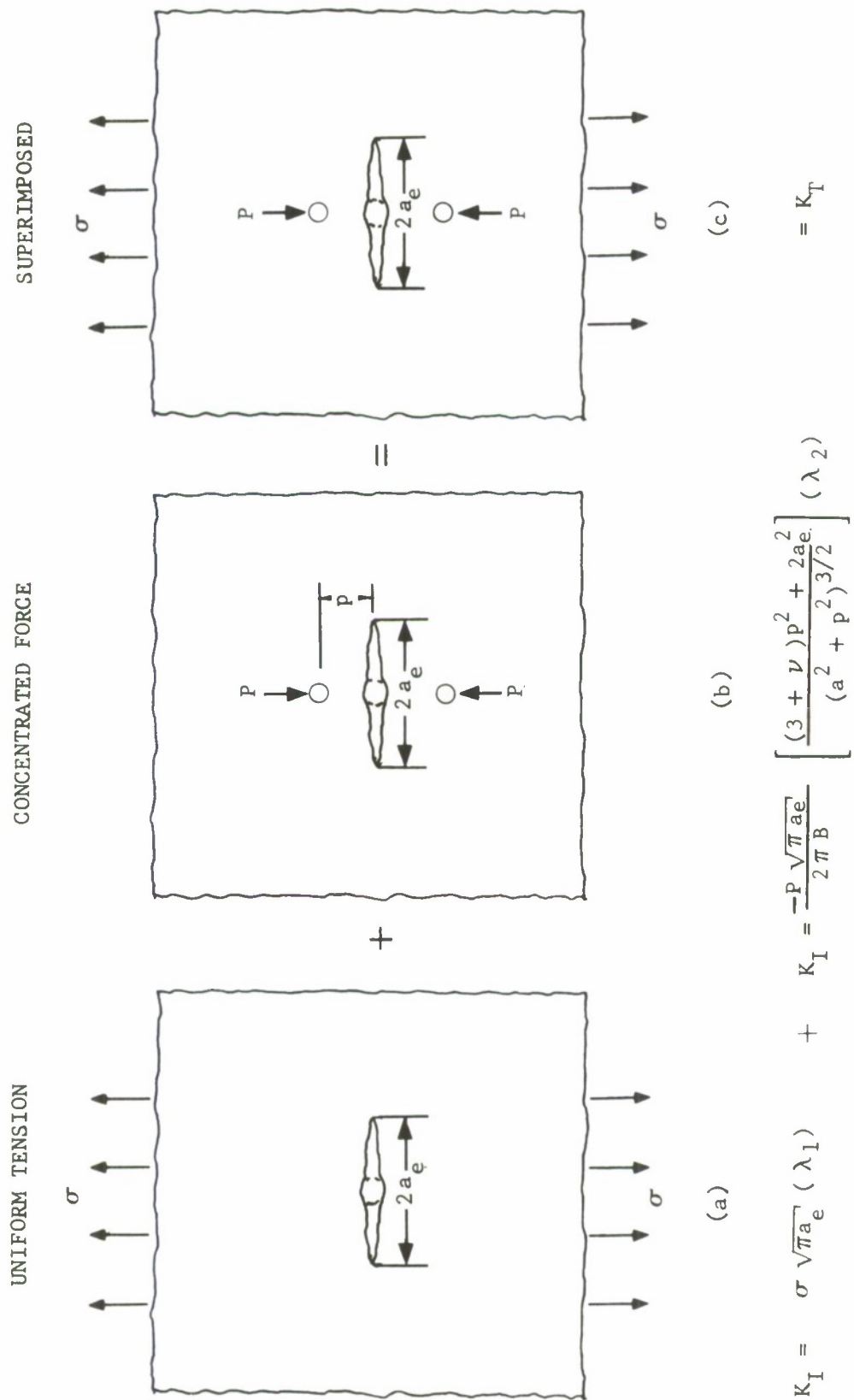


FIGURE 26 SUPERPOSITION OF STRESS INTENSITIES FOR UNIFORM TENSION AND CONCENTRATED FORCE

are applied at the center line of the sheet and at a distance greater than 3 or 4 times the hole diameter. The finite width corrections, λ , are those for a center cracked sheet (see Figure 14) and are the same in both cases.

Inasmuch as the concentrated forces are in an opposite direction to the uniform stress, and tend to close the crack, this stress intensity is subtracted from the uniform extensional stress intensity factor.

STEP 2. The individual stress intensity factors can now be superimposed to compute the total stress intensity factor for the problem geometry. To better understand the principles of superposition, a pictorial representation of the individual and superimposed stress intensities is shown in Figure 27.

With knowledge of the stress intensity solution for this geometry, it is possible to determine what effect the rivet closure forces have on the local stress field for similar problems.

Methods exist to analyze riveted, cracked structure when boundary forces are known. These will be demonstrated later in this section.

IX.6 ECCENTRICALLY LOADED CRACKS

A situation which occurs quite frequently in service is that of a crack starting at a rivet hole and progressing to a critical length by fatigue crack propagation. Analyzing this type of problem through fracture mechanics involves both equivalent crack length and combined geometric correction principles.

Take, for example, the geometry of Figure 28. In a line of rivets, a crack has started at rivet A and has progressed to a length of 3 inches from the hole edge prior to being detected. The operating stress of the panel is 30 ksi, and it is fabricated of 7075-T6 sheet with a plane stress fracture toughness of $85 \text{ ksi}\sqrt{\text{inch}}$. Overall panel width is 2 feet. (For now we will not consider the methods available to analyze riveted structure, but only analyze the local crack problem using fracture mechanics.)*

Question: What are the critical conditions for fracture for this crack geometry and loading? Should the panel be replaced?

STEP 1. In examining this problem, it can be seen that it is the crack at hole geometry shown as an insert of Figure 28. (NOTE: This is not the simple solution for a centrally stressed crack at a hole as in Equation VII-10.) This problem involves an eccentric load and determination of an equivalent crack length as in the preceeding problem.

STEP 2. Find the equivalent Griffith crack length and compare this result to the hole radius plus crack length approximation. For small diameter rivet holes, the function $f\left(\frac{a}{r}\right)$, from the corrections of Equation VII-10, for a single crack from the edge of a hole, is 0.707.

*Two opposing point rivet forces (above and below the crack) are assumed in this analysis.

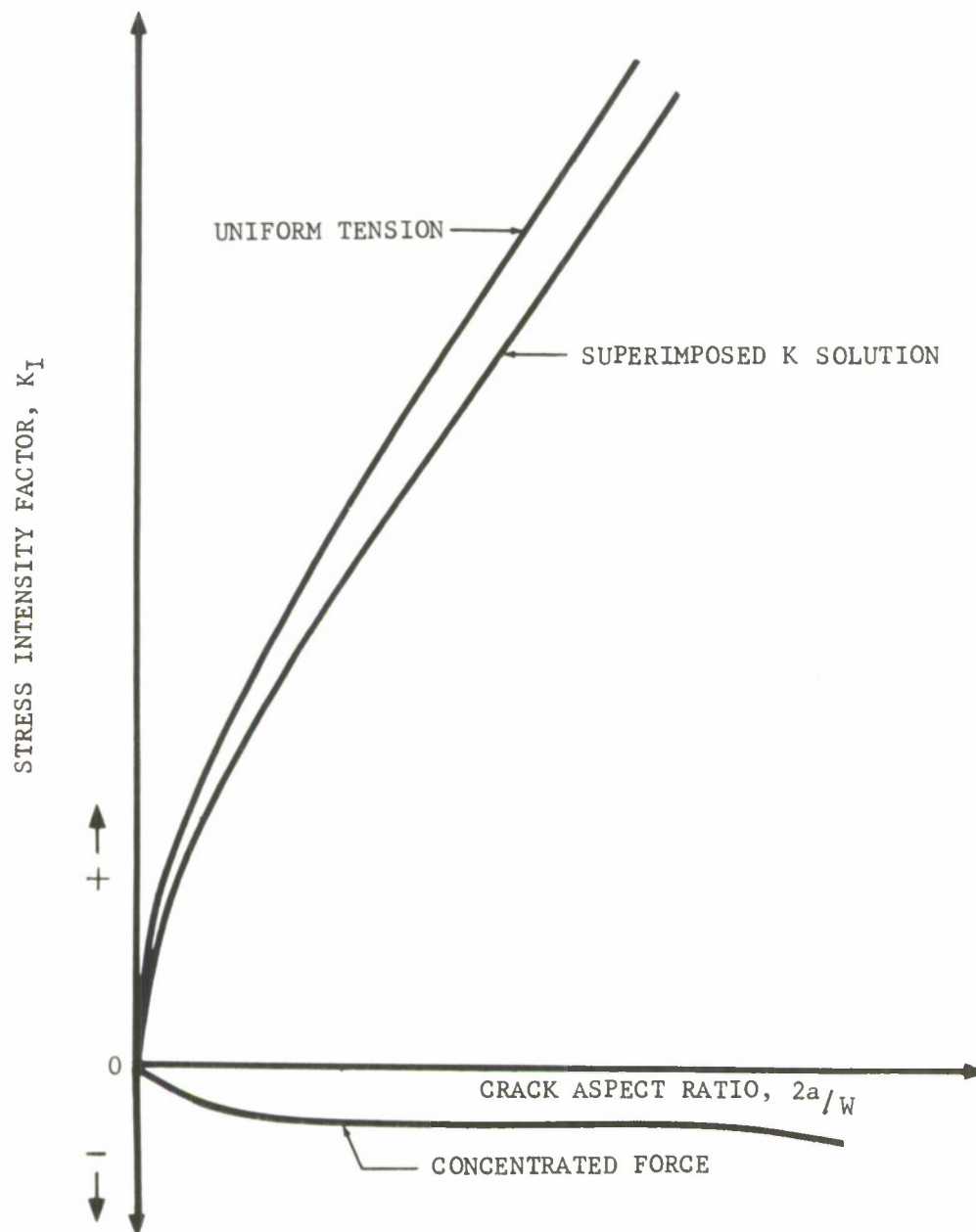


FIGURE 27 TRENDS IN STRESS INTENSITY, FOR LOADING OF FIGURE 26

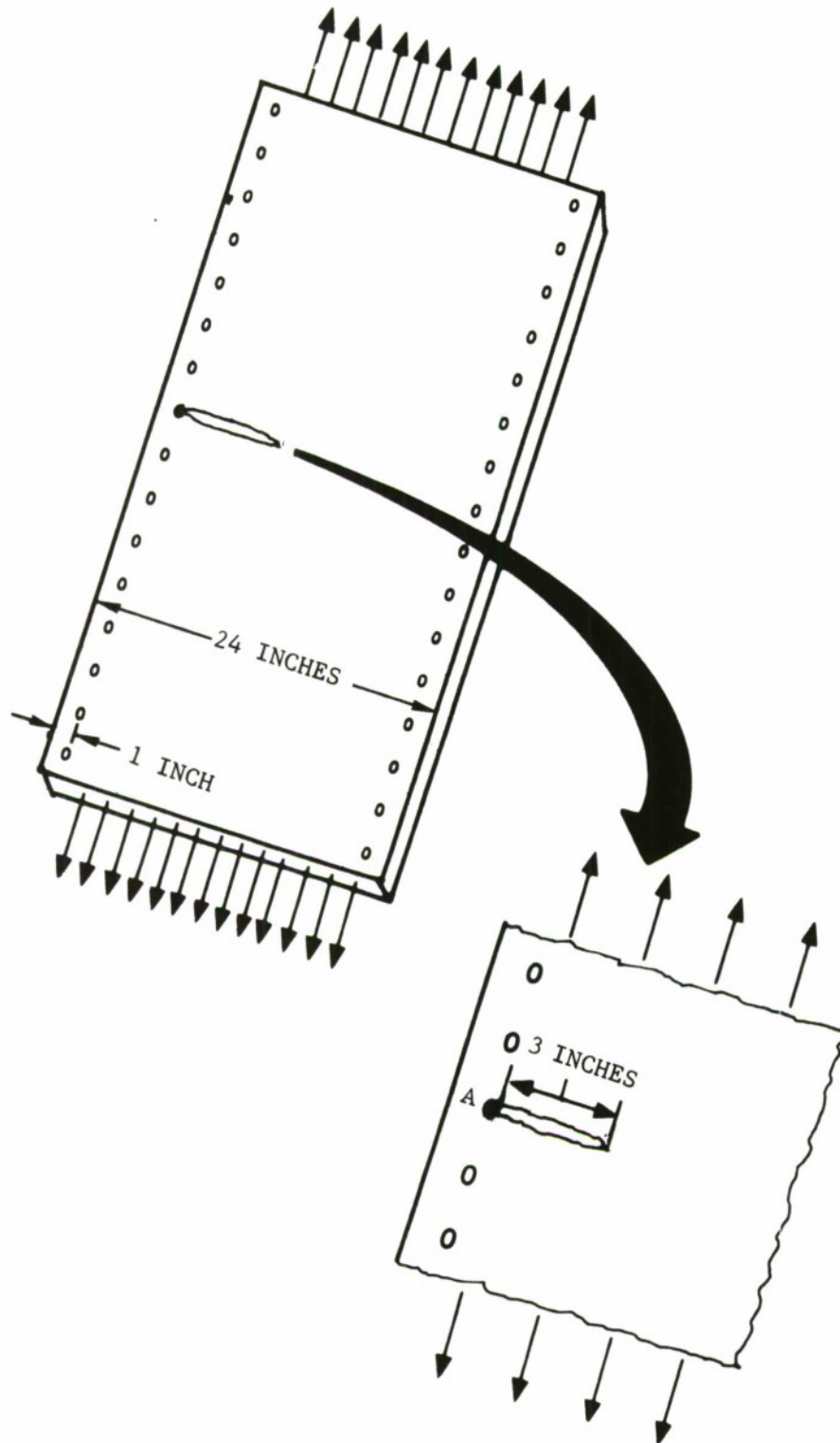


FIGURE 28 EDGE CRACKED PANEL GEOMETRY FOR EXAMPLE PROBLEM
(NO CRACK BUCKLING)

From equivalent crack length computations (hole plus absolute crack length)

$$2a_e \cong (a + r) \cong 3.1875 \text{ inches}$$

for a 3/16 inch rivet hole, edge crack configuration. This is compared to 3.0 inches for the equivalent crack length solution.

There is a stress intensity solution available for eccentric cracks in tension⁽²⁹⁾ which includes the finite width correction. The stress intensity factor for the problem is

$$K_I = \sigma \sqrt{\pi a_e} (\lambda_{1,2})$$

where $\lambda_{1,2}$ is the correction factor for eccentric loading conditions and a function of the eccentricity, e , and λ_2 is the finite width correction and a function of a/W' . (See Figure 18).

STEP 3. Determine the crack aspect ratio $\left(\frac{a}{W'}\right)$, and normalized eccentricity (ϵ) for the problem.

$$\frac{a}{W'} = \frac{1.5 \text{ inch}}{(1.5 + 1 \text{ inch})} = 0.60$$

and

$$\epsilon = \frac{2e}{W} = \frac{2(11.6 \text{ inch})}{24 \text{ inch}} = 0.799$$

The associated correction factor for eccentricity and finite width from Figure 18 is $\lambda_1, \lambda_2 = 1.10$ for the end of the 3 inch long crack tip which is nearest the panel center line.

STEP 4. Assume critical conditions for the stress intensity equation,

$$K_I \longrightarrow \bar{K}_c, \quad \sigma \longrightarrow \sigma_c, \quad \text{and} \quad a_e \longrightarrow a_c$$

and solve for critical stress.

$$\sigma_c = \frac{\bar{K}_c}{\sqrt{\pi a_c} \lambda_{1,2}} = \frac{85 \text{ ksi} \sqrt{\text{inch}}}{\sqrt{\pi(1.5 \text{ inch})} (1.10)}$$

$$\sigma_c = 35.6 \text{ ksi}$$

Hence, it can be assumed the panel analyzed as a simple plate would be fracture safe under the 30 ksi operating stress with this length crack.*

The second part of the question may be re-phrased for our purposes. When should the panel be replaced? Or, in particular, at what crack length, at the given operating stress, should the panel be replaced?

* NOTE: This is a safe assumption as long as the other end of the crack remains stopped at the rivet hole.

The easiest way to approach this problem is to plot the representative stress-crack length history of this eccentric cracked panel as shown in Figure 29. To a crack length of 4.0 inches, this panel would be fracture safe. This, of course, depends on how accurately the value used for the plane stress fracture toughness reflected the material behavior in service, and assumes that the crack remains stationary at the rivet hole. NOTE: There are additional ways to analyze crack-riveted structure using fracture mechanics principles. These will be presented in the following paragraphs.

IX.7 COMPLEX THROUGH-CRACKED STRUCTURE

In this section we will examine the analysis of built-up structure (primarily skin/stiffener construction) which contain a crack using fracture mechanics principles. Skin-stringer or frame construction poses a particular fracture analysis problem in aircraft design when a crack is caused by sudden puncture or fatigue. In addition, fail safe operation specifies load carrying requirements for particular bay sections cracked. To meet these needs, it is possible to utilize available boundary corrections in conjunction with the Griffith-Irwin fracture toughness parameters to compute critical fracture stresses.

Examples of the use of these procedures will be presented as a series of problems. In this manner, the user can become more familiar with the steps involved in the analysis.

NOTE: Examples presented herein are for illustrative and demonstrative purposes only. In practice, each case must be considered as individual problems with unique solutions.

IX.7(a) Damage Configurations

The types of damaged structure which can be analyzed are:

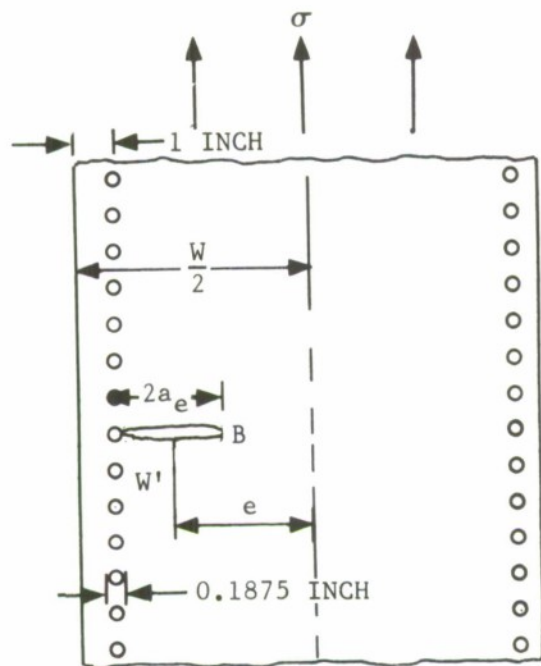
- (1) Elastic* skin with central, rivet attached stringer and cracks at stringers,
- (2) Elastic* skin with fixed edges and/or cracks between stringers,
- (3) Combinations of 1 and 2.

Figures 30 and 31 show the various combinations of damaged structure for which the analysis is valid with applicable nomenclature.

IX.7(b) Geometric Corrections

In 1964, J. Bloom presented an analysis of the boundary corrections for a cracked, riveted sheet stringer⁽⁴⁷⁾ construction under tensile loads (see Figures 30(a) and (b) and 31). The following year Grief and Sanders

* Elastic behavior is assumed in the derivation of all the analysis methods, even though elasto-plastic action is known to occur at the crack tip. If these zones are small compared to the crack length, then these assumptions are valid and fracture mechanics principles can be used to provide reasonable results.



$\frac{a_e}{W'}$	$\epsilon = \frac{2e}{W}$	$\lambda_{1,2}$
0.33	0.87	1.03
0.50	0.83	1.05
0.60	0.79	1.10
0.67	0.75	1.15
0.71	0.71	1.20
0.75	0.67	1.22
0.80	0.53	1.28
0.86	0.42	1.42
0.90	0.08	1.7

* Assuming $\bar{K}_c \cong 85 \text{ ksi}\sqrt{\text{inch}}$

$$\sigma_c^* = \frac{\bar{K}_c}{\sqrt{\pi a_c} \lambda_{1,2}}$$

$$e = \frac{W}{2} - \left[\left(\frac{2a_e - 0.1875''}{2} \right) + 1.0'' \right]$$

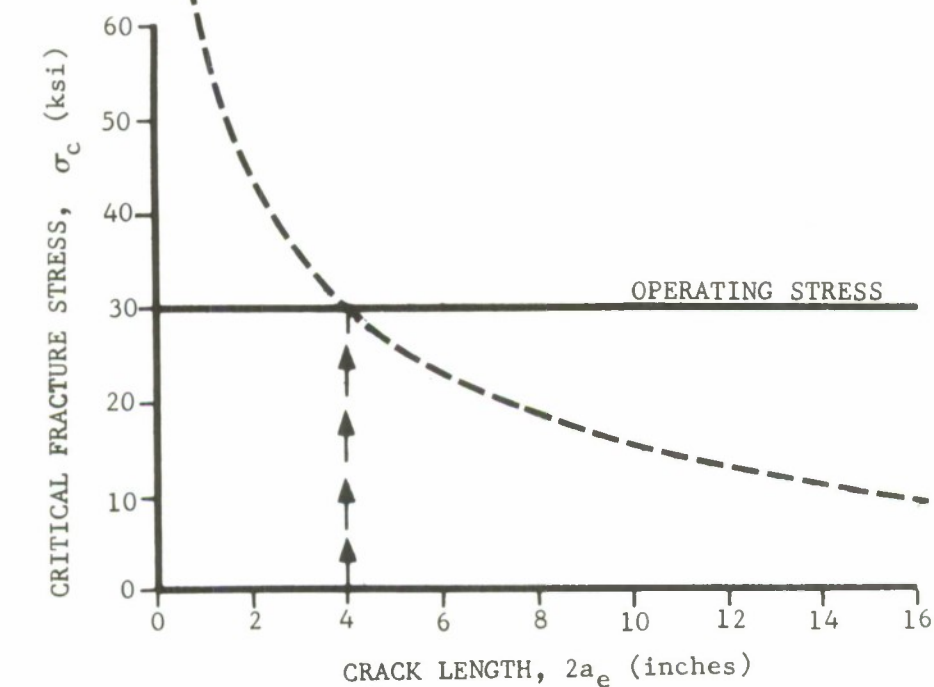
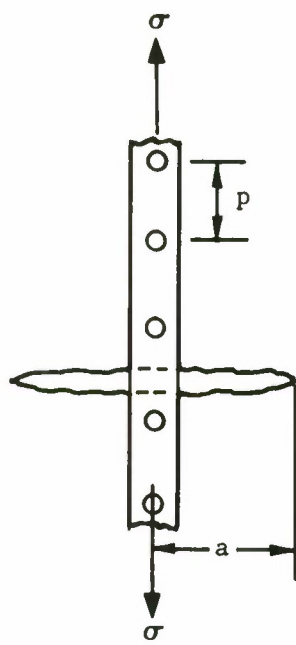
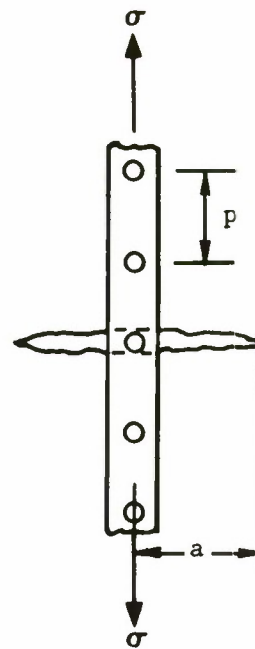


FIGURE 29 CRITICAL FRACTURE STRESS FOR PANEL GEOMETRY OF FIGURE 28 (NO CRACK BUCKLING)



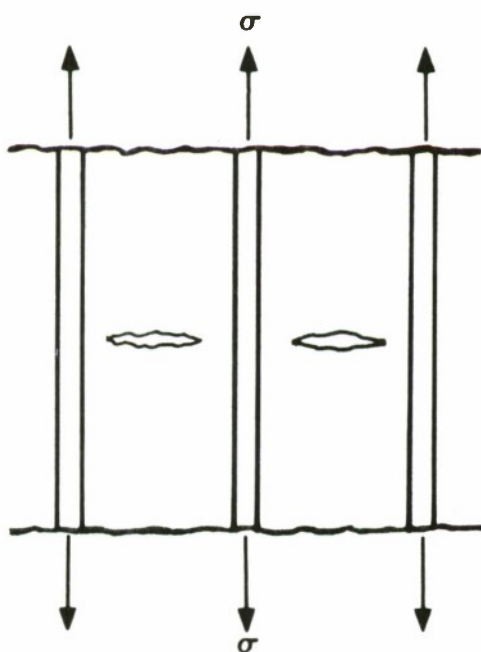
(a)

CRACK BETWEEN RIVET



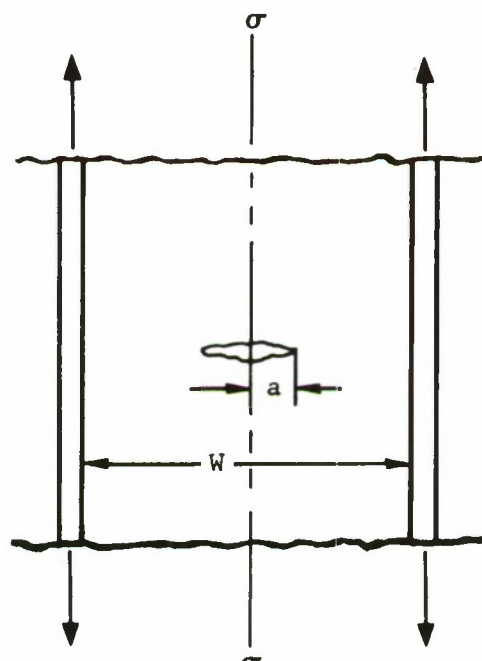
(b)

CRACK THROUGH RIVET HOLE



(c)

MULTIPLE CRACKS
(REINFORCED EDGES)



(d)

CENTER CRACK
(REINFORCED EDGES)

FIGURE 30 SYMMETRIC CRACK CONFIGURATION IN UNIAXIAL TENSION

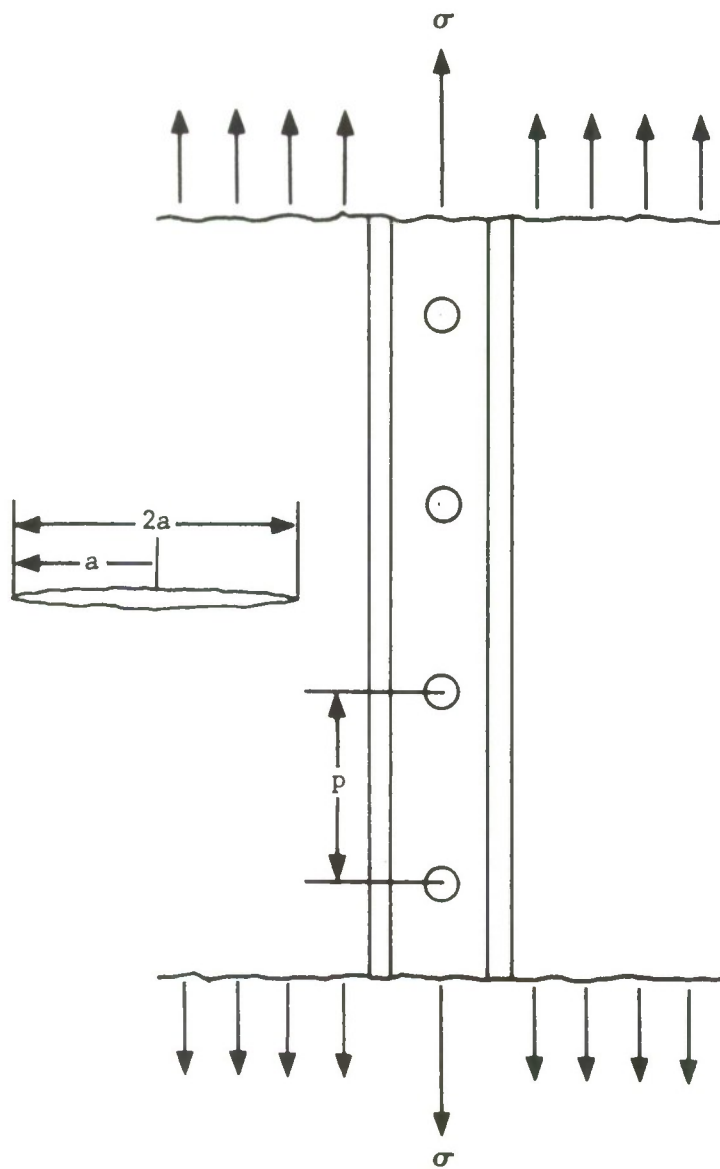


FIGURE 31 NONSYMMETRIC CRACK IN RIVETED PANEL - UNIAXIAL LOADING

presented the boundary corrections for a continuous stringer-cracked sheet combination⁽⁴⁸⁾. Isida, et al, (Reference 28) have calculated the crack tip stress intensities for various combinations of extensional and bending stiffness of the stiffeners for the crack geometry of Figures 30(c) and 30(d).

The associated correction factors for the crack geometries of Figures 30 and 31 are shown graphically in Figures 32 through 40. The crack between rivets (stringer intact) is indicated in Figure 32. For the crack through the rivet hole and stringer intact, see Figure 33.

The boundary corrections for a nonsymmetric crack near a riveted stringer for various crack aspect ratios, for values of extensional stiffness, S , equal to 0.5, 1 and 2 are shown in Figures 34 and 35. Boundary corrections for a center cracked plate in tension, with reinforced edges, as analyzed by Isida and Itagahi⁽²⁸⁾ are shown in Figures 36 through 40 for various values of extensional stiffness, S , and bending stiffness of the stringers, α . The α term is essentially a nondimensional inertia parameter. It is a function of the moment of inertia of the stiffener about its neutral axis perpendicular to the plane of the plate or sheet, I_z , divided by the product of the plate or sheet thickness, B , and the cube of the half stringer spacing or sheet width $\frac{W}{2}$. This factor is multiplied by the nondimensional ratio of stringer to plate modulus.

$$\alpha = \frac{I_z}{B\left(\frac{W}{2}\right)^3} \cdot \frac{E_{str.}}{E} \quad (IX-1)$$

The dashed portion of the correction factor curves, in all cases, reflects the limiting values obtained experimentally by Grief and Sanders⁽⁴⁸⁾ on integrally stiffened panels assuming a value of $\frac{a}{p}$ of 100.

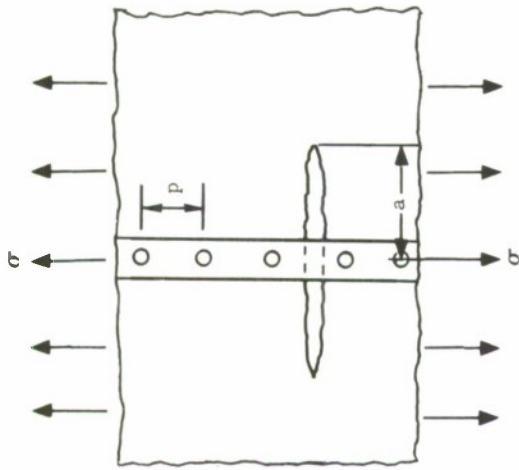
IX.8 GEOMETRIC COMBINATIONS

To analyze the panel section of Figure 41 for fracture strength, we will utilize applicable geometric corrections and fracture mechanics. The following conditions apply to the panel of Figure 41,

- . center cracked-perpendicular to loading direction
- . cracked at rivet with stringer intact
- . uniaxial loading (sheet and stringer stressed uniformly, remotely from the crack)
- . rivet pitch - 1.00 inch
- . symmetrical crack growth with respect to panel center line
- . repetitive structure (analyze only portion of structure-3 bays).

To determine the influence of the central stringer on the critical fracture stress for this geometry, we will separate the problem into parts. In this way, the influence of the center stringer will become more apparent.

Consider the problem first as a center cracked, edge stiffened sheet with center stiffener removed. The geometry of Figure 30(d) applies. In Reference 28, the edge stiffeners are considered as integral; however, it is felt that negligible error is introduced for crack aspect ratios ≤ 0.8 .⁽²⁸⁾ As the crack approaches the edges stiffeners, the influence of these stiffeners predominates and the crack geometry of Figure 31 applies.



a = half crack length
 p = rivet pitch
 E = modulus of plate
 $E_{STR.}$ = modulus of stringer
 $A_{STR.}$ = area of stringer

$$S = \frac{2(aB)E}{A_{STR} E_{STR}}$$

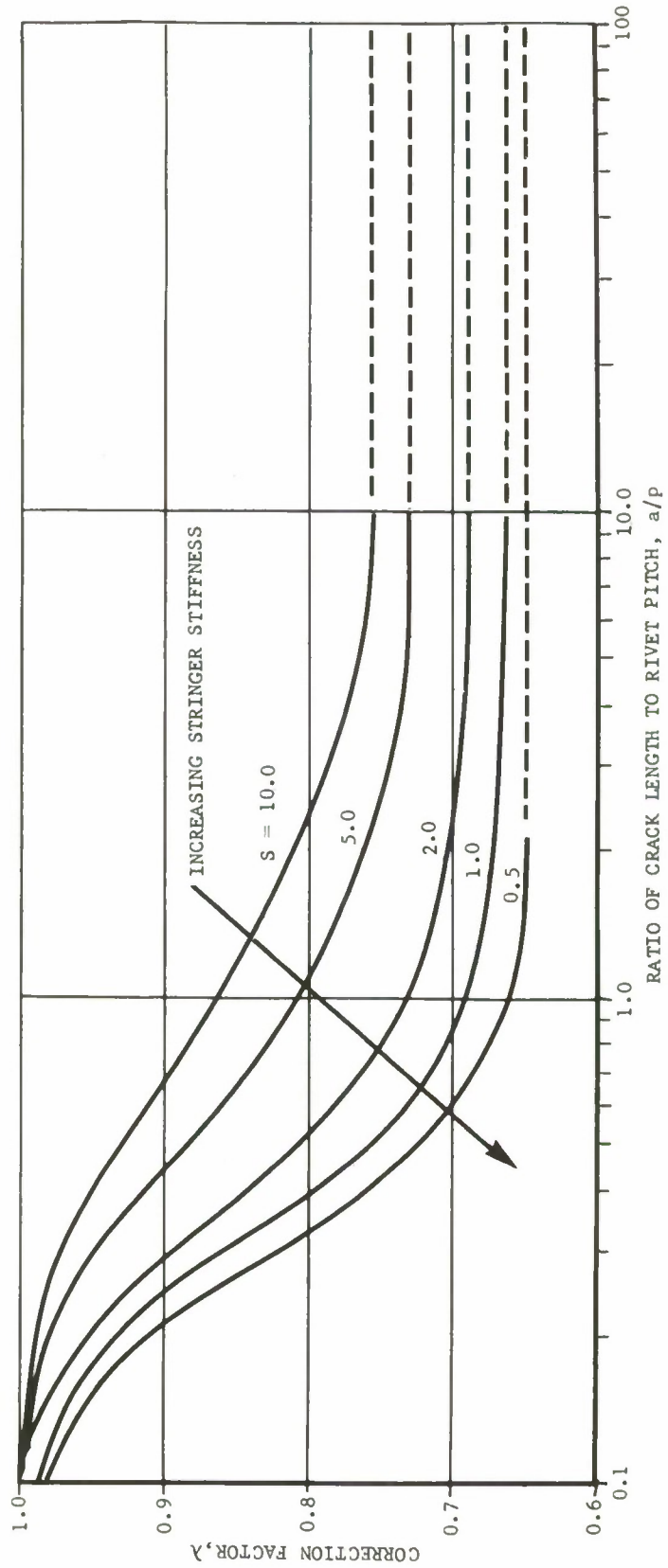


FIGURE 32 CORRECTION FACTORS FOR SYMMETRIC CRACK MIDWAY BETWEEN RIVETS - RIVETED STRINGER - STRINGER INTACT (REF. 47)

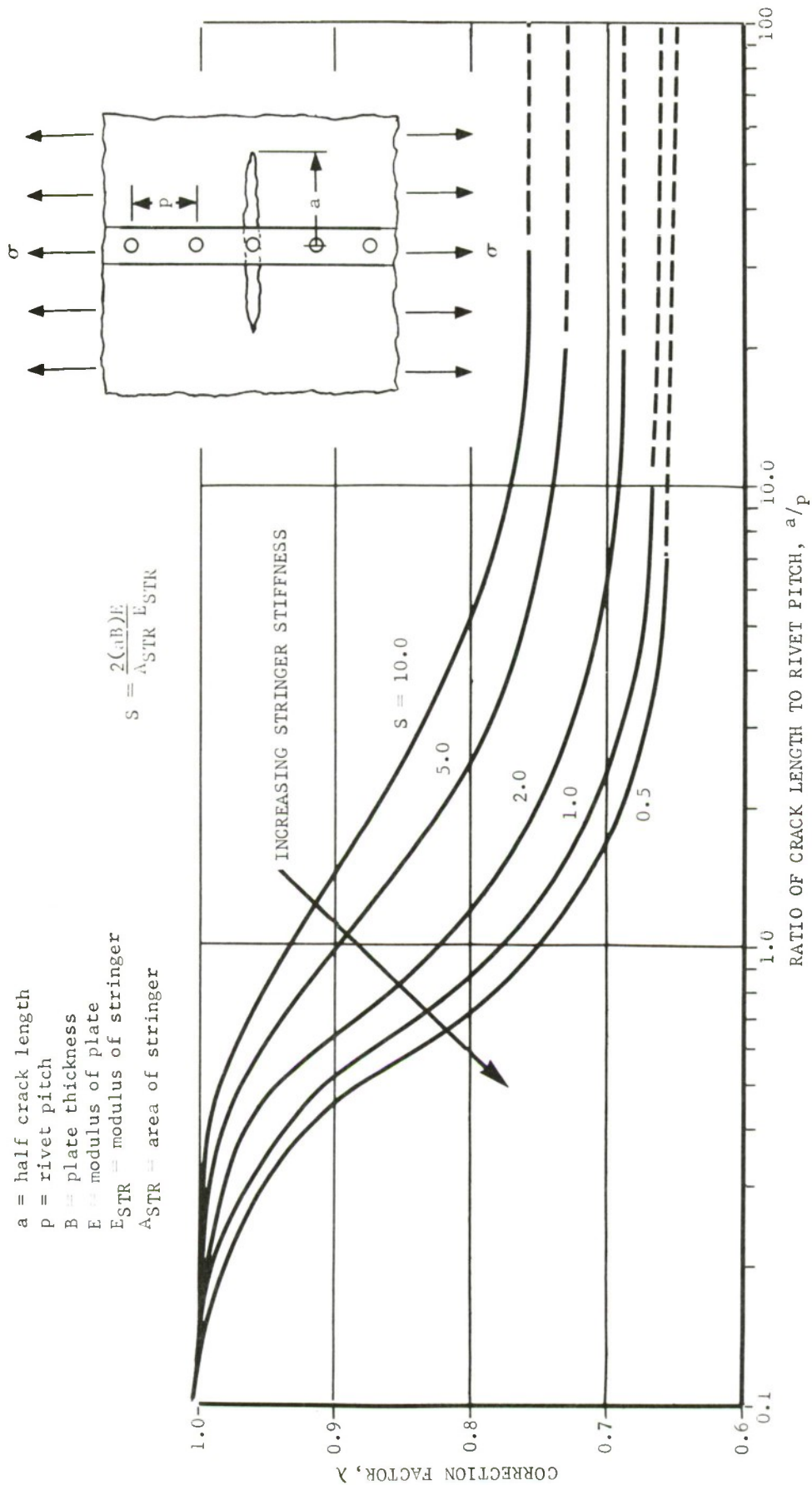


FIGURE 33 CORRECTION FACTORS FOR SYMMETRIC CRACK THROUGH RIVET HOLE - RIVETED STRINGER - STRINGER INTACT (REF. 47)

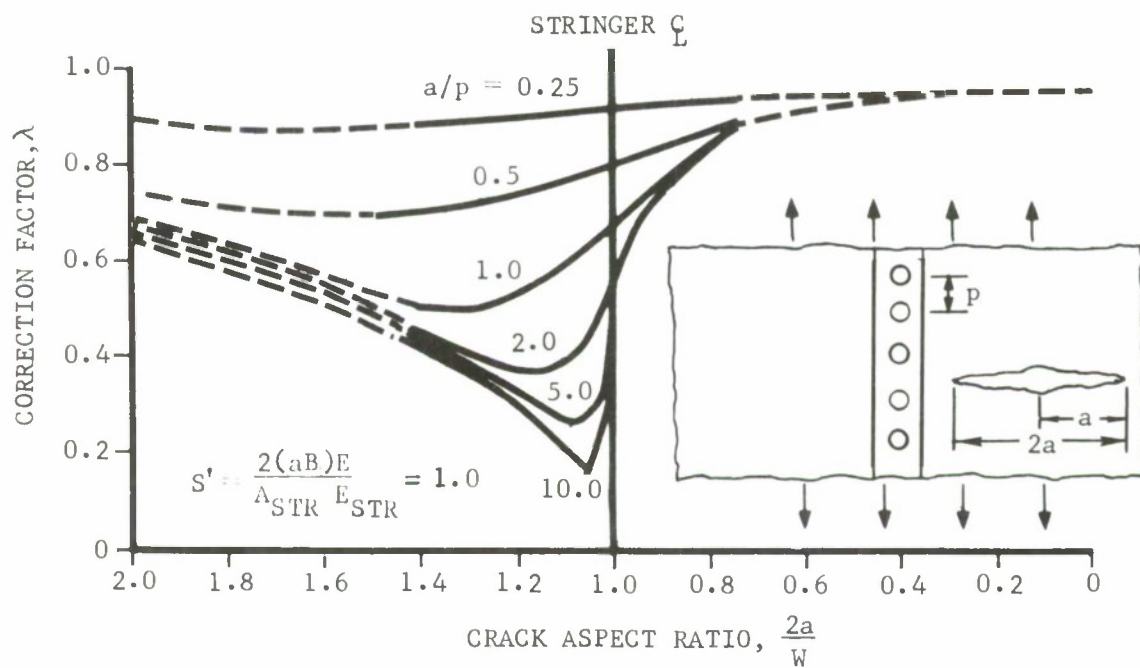
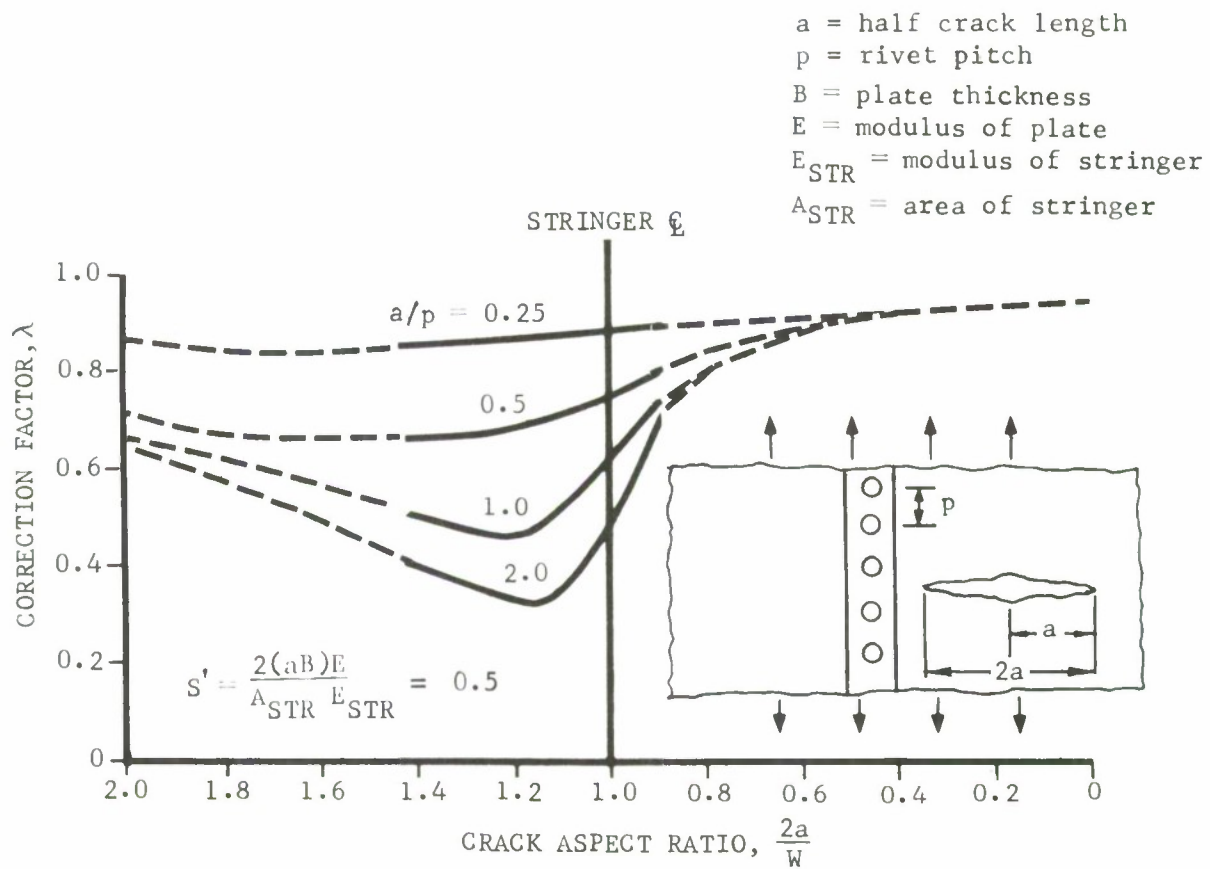


FIGURE 34 CORRECTION FACTORS FOR NONSYMMETRIC CONDITIONS - CENTER CRACKED PANEL FOR $S' = 0.5$ AND 1.0 (REF. 47)

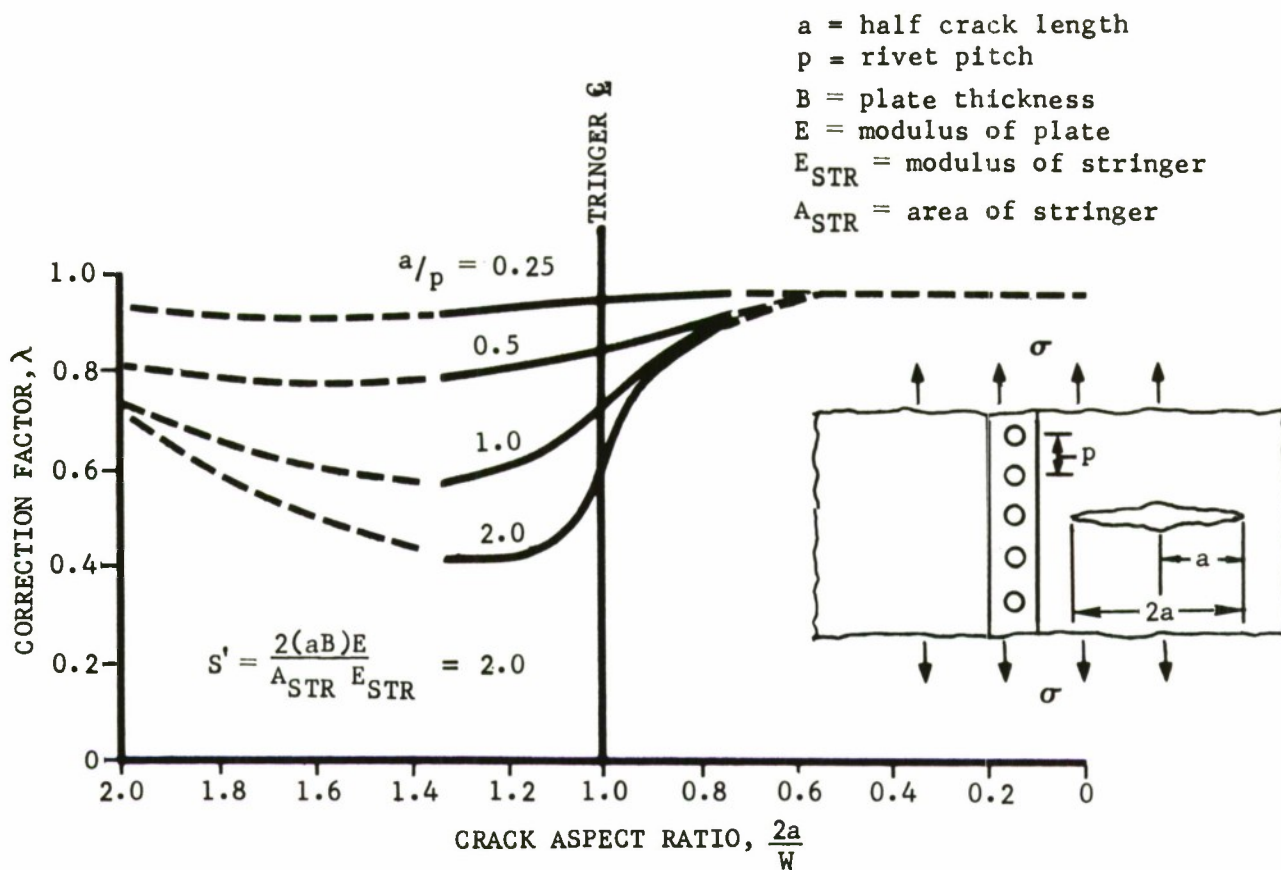


FIGURE 35 CORRECTION FACTORS FOR NONSYMMETRIC CONDITIONS - CENTER CRACKED PANEL FOR $s' = 2.0$ (REF. 47)

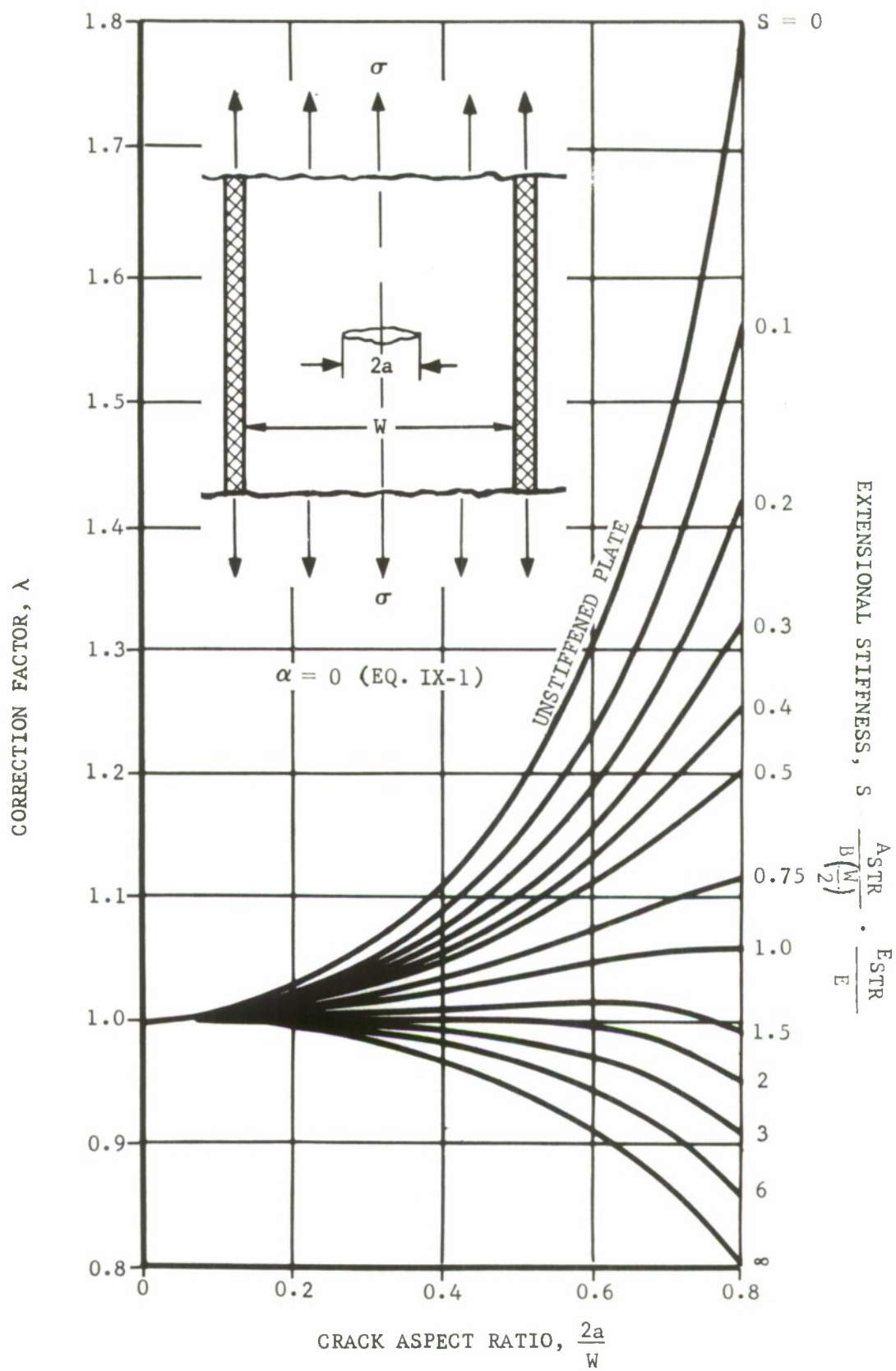


FIGURE 36 CORRECTION FACTORS FOR EDGE STIFFENED, CENTER CRACKED PLATE - BENDING STIFFNESS, $\alpha = 0$ (REF. 28)

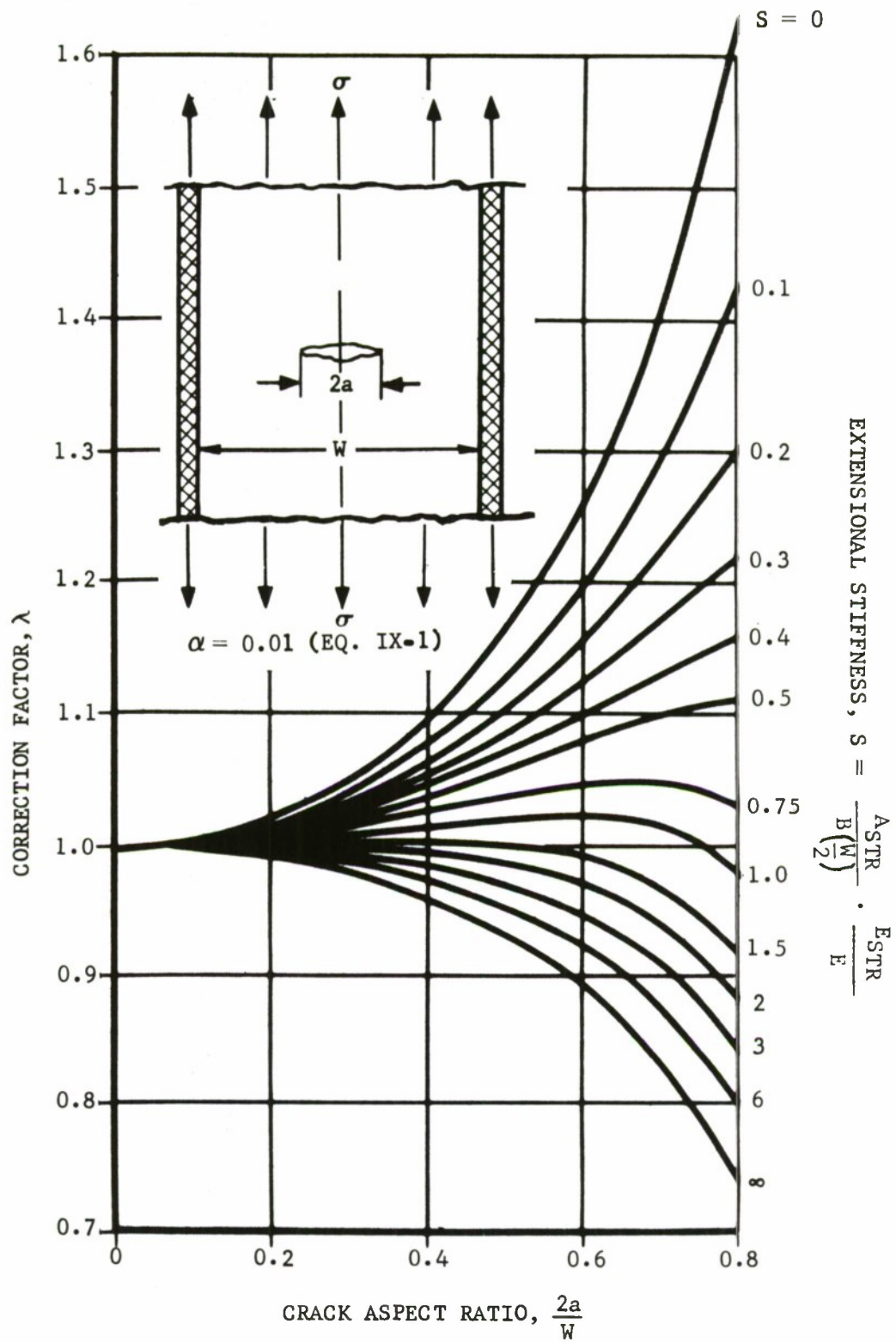


FIGURE 37 CORRECTION FACTORS FOR EDGE STIFFENED, CENTER CRACKED PLATE - BENDING STIFFNESS, $\alpha = 0.01$ (REF. 28)

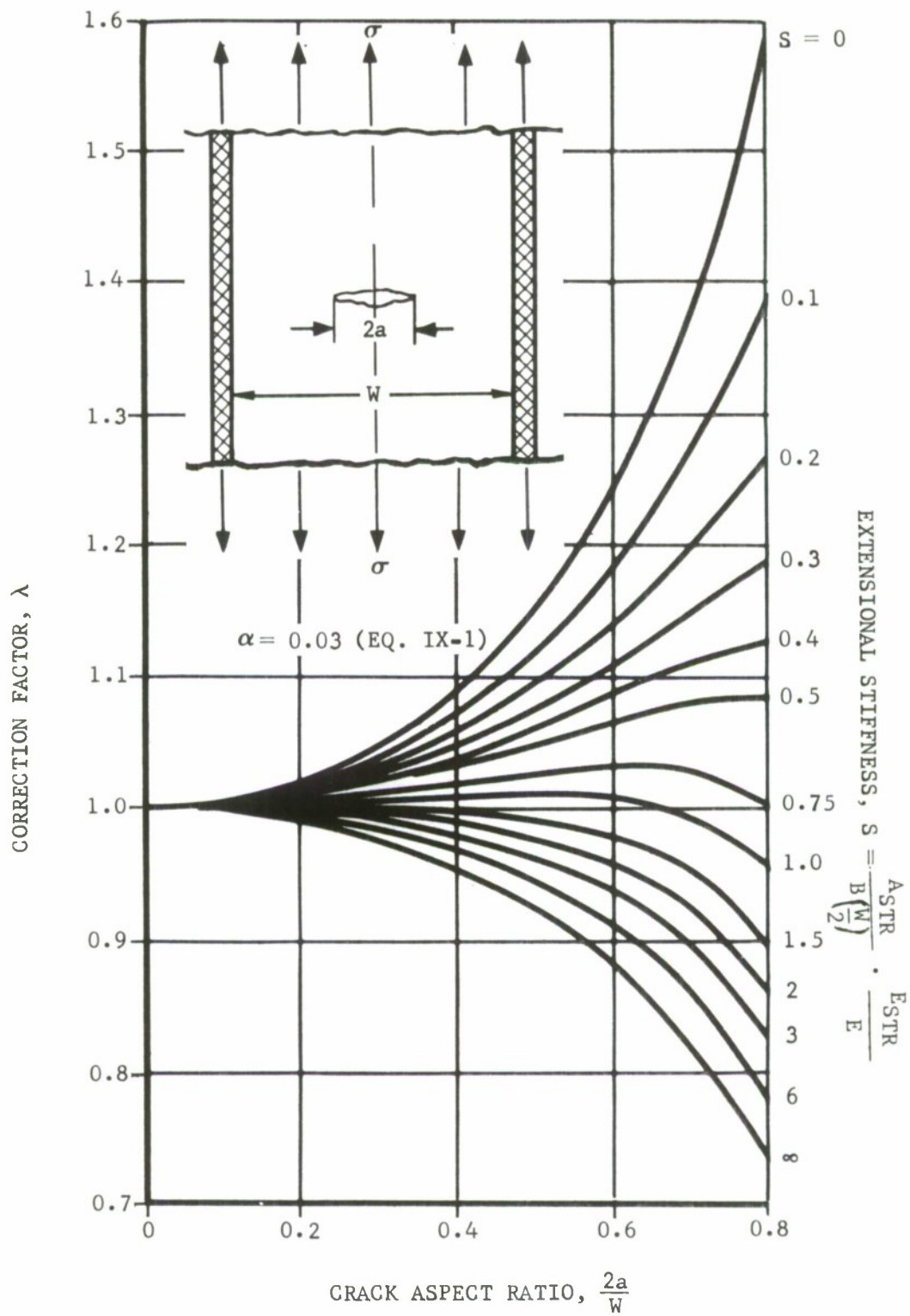


FIGURE 38 CORRECTION FACTORS FOR EDGE STIFFENED, CENTER CRACKED PLATE - BENDING STIFFNESS, $\alpha = 0.03$ (REF. 28)

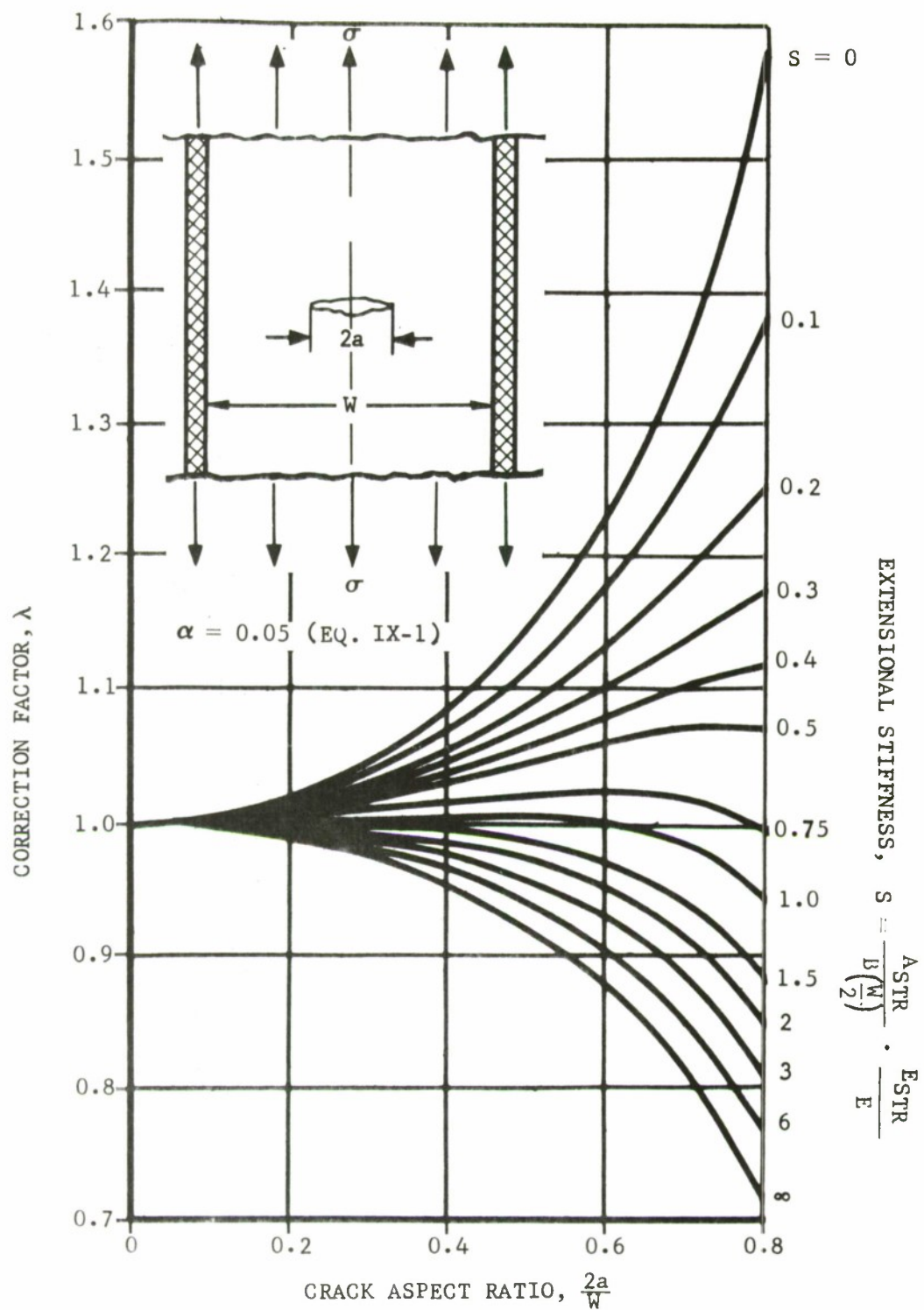


FIGURE 39 CORRECTION FACTORS FOR EDGE STIFFENED, CENTER CRACKED PLATE BENDING STIFFNESS, $\alpha = 0.05$ (REF. 28)

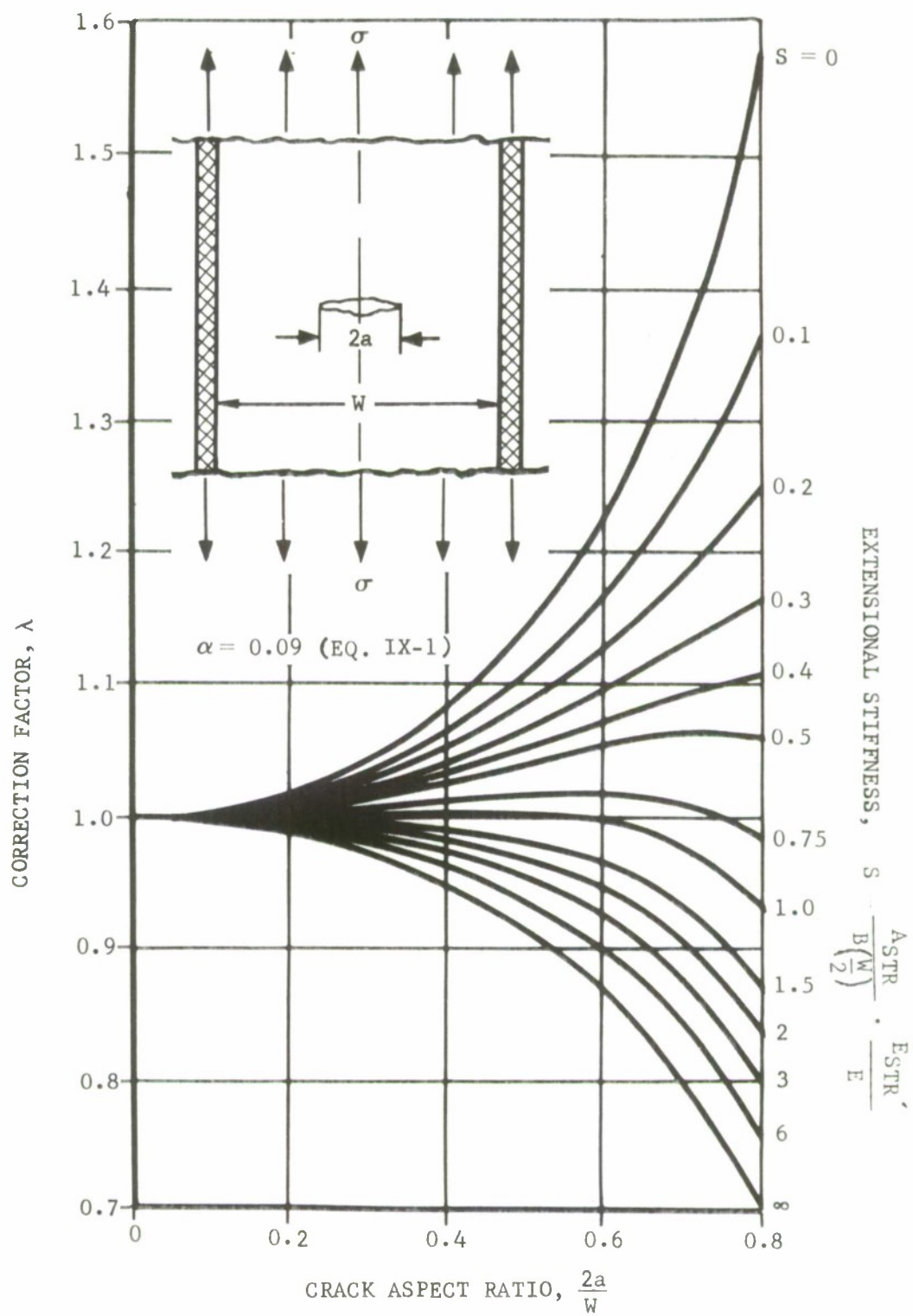


FIGURE 40 CORRECTION FACTORS FOR EDGE STIFFENED, CENTER CRACKED PLATE - BENDING STIFFNESS, $\alpha = 0.09$ (REF. 28)

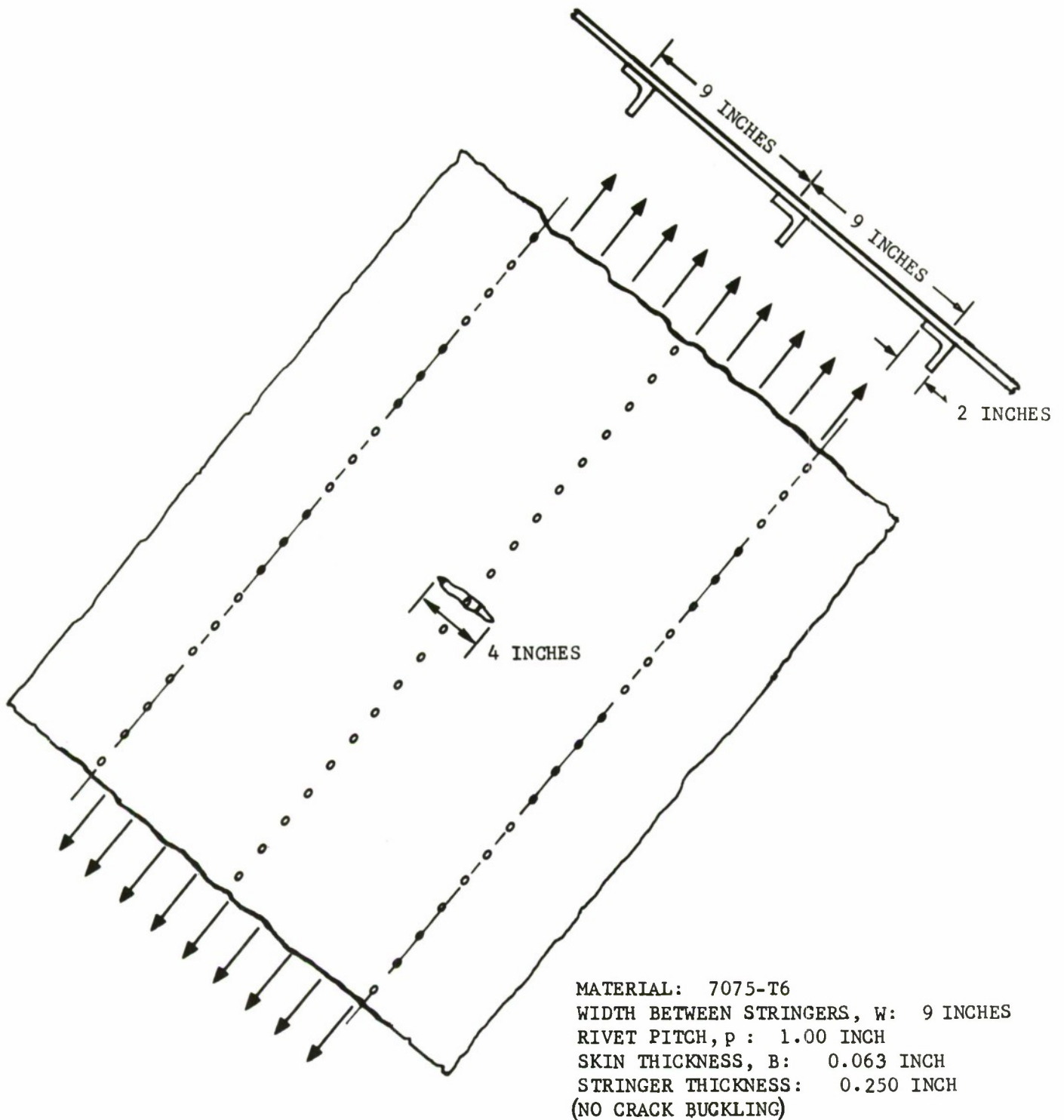


FIGURE 41 CENTER CRACKED PANEL GEOMETRY OF EXAMPLE PROBLEM

STEP 1. Determine the nondimensional inertia parameter, from Equation IX-1. In this case (I_z) the moment of inertia of the edge stiffener (angle section length 2 inch, thickness 1/4 inch) about the stringer neutral axis-perpendicular to the plane of the plate is

$$I_z = 0.322 \text{ inches}^4$$

and the ratio of stringer to sheet modulus is 1.0. Therefore, α is

$$\alpha = \frac{0.322 \text{ inches}^4}{0.063 \text{ inch} \left(\frac{18 \text{ inches}}{2} \right)^3} \cdot \frac{10^7 \text{ psi}}{10^7 \text{ psi}} \cong 0.01$$

and the correction factors of Figure 37 apply.

STEP 2. Compute the extensional stiffness, S , for the finite width, cracked strip. This is from Figure 37.

$$S = \frac{A_{\text{str.}}}{B \left(\frac{W}{2} \right)} \cdot \frac{E_{\text{str.}}}{E} \quad (\text{IX-2})$$

$$S = \frac{0.25 \text{ inch} (2 \text{ inch} + 1.75 \text{ inch})}{0.063 \text{ inch} \left(\frac{18 \text{ inches}}{2} \right)} \cdot \frac{10^7 \text{ psi}}{10^7 \text{ psi}} = 1.65$$

STEP 3. Prepare a table of correction factors (λ') for various crack aspect ratios, as shown in Table IV for $S = 1.65$ from Figure 37.

TABLE IV
CORRECTION FACTORS FOR EXAMPLE PROBLEM

TOTAL CRACK LENGTH, 2a (inches)	CRACK ASPECT RATIO, 2a/W	λ' (From Fig. 37)
1.8	0.1	1.00
3.6	0.2	
5.4	0.3	
7.2	0.4	
9.0	0.5	1.00
10.8	0.6	0.98
12.6	0.7	0.97
14.4	0.8	0.91

As the crack approaches the edge stiffeners $\frac{2a}{W} > 0.8$ the analysis of Reference 28 is not valid. However, the problem becomes one of a non-symmetric crack approaching a riveted stiffener, or the geometry of Figure 31. (With the center stiffener broken, little effect will be noticed on the correction from this stringer.)

STEP 4. Determine the correction factors as the crack goes through the edge stringer areas and beyond (see Figure 34 and 35). Compute the stiffness ratio S' and ratio of crack length to rivet pitch for crack aspect ratios > 0.8 . Where S' is

$$S' = \frac{2(aB)}{A_{str.}} \cdot \frac{E}{E_{str.}} \quad (IX-3)$$

and corresponding correction factors are shown in Table V.

TABLE V
CORRECTION FACTORS FOR EXAMPLE PROBLEM

$\frac{2a}{W}$	S'	$\left(\frac{a}{p'}\right)^*$	λ^{**}
0.9	1.09	4.05	0.70
1.0	1.21	4.50	0.45
1.1	1.33	4.95	0.28
1.2	1.45	5.40	0.32

* The crack is assumed to grow through a rivet hole, thus effectively doubling the rivet pitch, $p' = 2p$.

**From Figures 34 and 35

The correction factors λ' and λ'' for the two crack geometries are shown in Figure 42 as a function of crack aspect ratio. It is apparent that the maximum reduction in correction factor will occur when the crack tip is approaching the riveted stiffener ($0.9 > \frac{2a}{W} > 0.7$). The correction factor curves for a nonsymmetric crack (Figures 34 and 35) also indicate this trend for small to moderate rivet spacings. This reduction is caused by the remaining rivet forces, near the crack tip tending to pinch the crack together more effectively as the crack is within the riveted stringer area. Before the crack reaches this area, this effect is lost.

STEP 5. We can now examine the effect of the center stiffener on the correction factor to the stress intensity. As the crack is assumed to start in the sheet at the center stiffener and progress in a symmetric manner, the corrections of Figures 32 or 33 apply depending on where the crack starts, i.e., at or between rivets. The author of Ref. 47 has computed the correction curves of Figures 32 and 33 using a Poisson's ratio of 0.33 and a rivet diameter to rivet pitch ratio of $\frac{d}{2p} = 0.1$. However, he did indicate relative insensitivity of the correction factor to variation in this ratio. It should be noted that

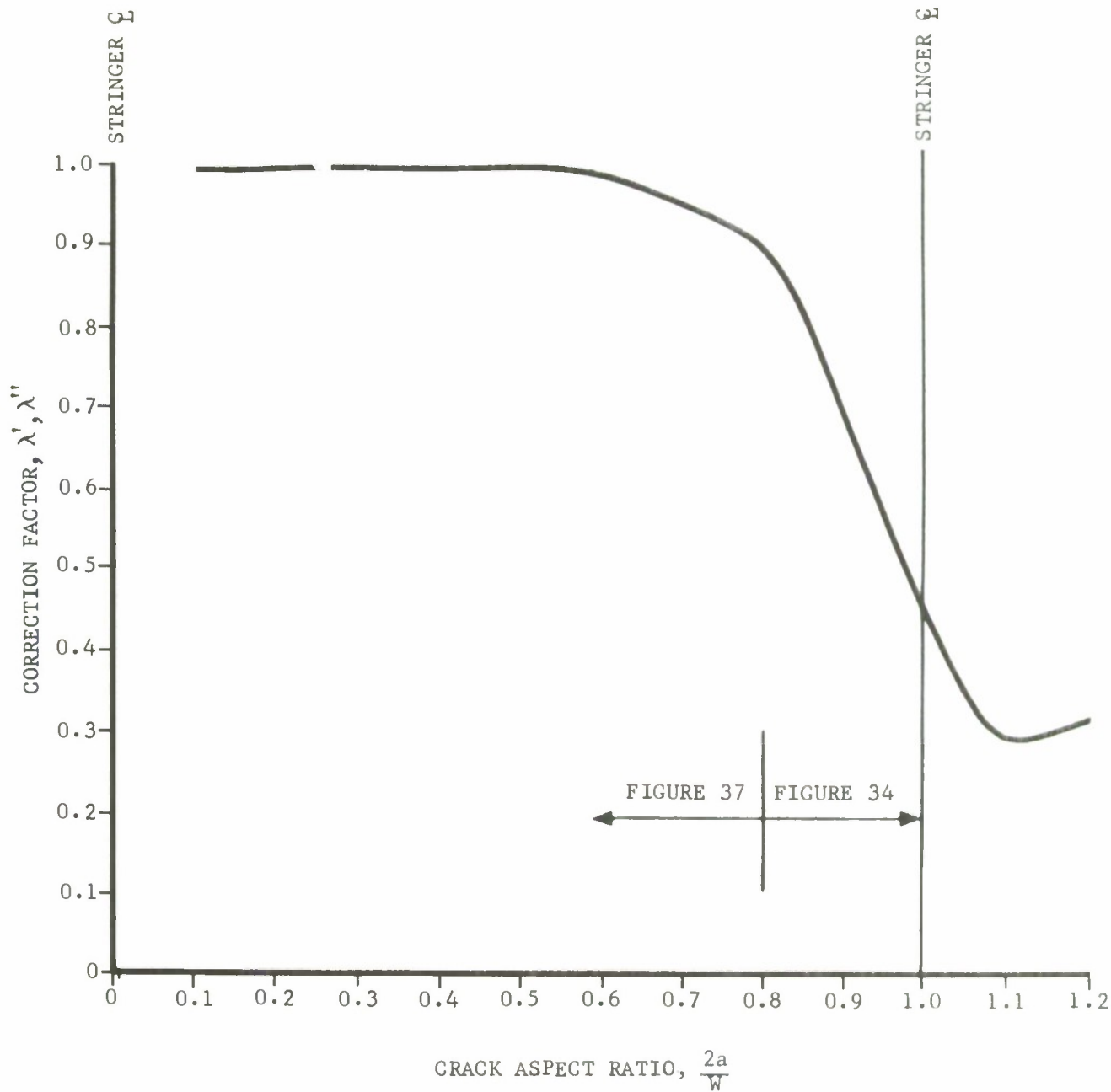


FIGURE 42 CORRECTION FACTORS FOR SYMMETRIC - CRACKED PLATE WITH REINFORCED EDGES FOR THE GEOMETRY OF FIGURE 41

the crack running through the rivet hole effectively doubles the pitch over that of a crack midway between rivets (i.e., compare Figures 32 and 33). We will first examine the most plausible situation, a crack starting at a rivet with stringer intact. In this case, the geometric corrections are shown in Table VI from Figure 33.

TABLE VI
CORRECTION FACTORS FOR EXAMPLE PROBLEM

$\frac{2a}{W}$	S	$\frac{a}{p}$	λ'' (*)
0.1	0.12	0.90	0.73*
0.2	0.24	1.80	0.68*
0.3	0.36	2.70	0.68*
0.4	0.48	3.60	0.675
0.5	0.60	4.50	0.68
0.6	0.73	5.40	0.68
0.7	0.85	6.30	0.69
0.8	0.97	7.20	0.69
0.9	1.09	8.10	0.69
1.0	1.21	9.00	0.695
1.1	1.33	9.90	0.695
1.2	1.45	10.80	0.70

* Obtained by Interpolation

**From Figure 33

STEP 6. Multiply the correction factors obtained in Table IV for an edge stiffened plate with those above to obtain a combined correction factor λ^* and λ^{**} . These factors are defined and indicated in Table VII along with the nonsymmetric case from Table V.

TABLE VII
COMPOSITE CORRECTION FACTORS FROM TABLES IV-VI

$\frac{2a}{W}$	$\lambda^* = \lambda' \times \lambda''$	$\lambda^{**} = \lambda'' \times \lambda'''$
0.1	0.73	—
0.2	0.68	—
0.3	0.68	—
0.4	0.68	—
0.5	0.68	—
0.6	0.67	—
0.7	0.66	—
0.8	0.63	—
0.9	—	0.48
1.0	—	0.31
1.1	—	0.19
1.2	—	0.22

IX.8(a) Selection of Fracture Toughness Value

With the use of fracture mechanics we can now make an estimate of critical fracture stress for each crack aspect ratio. Plane stress, K_c data*** on 0.063 inch thick 7075-T6 aluminum sheet indicated a $\bar{K}_c \approx 85 \text{ ksi}\sqrt{\text{inch}}$. This average plane stress fracture toughness value includes plastic zone correction. However, when any correction for plasticity is employed it will lead to larger values of fracture toughness, hence fracture stress. As a matter of choice, it is usually better practice to base preliminary design and fracture analysis on a fracture toughness value which does not include plasticity corrections. The reason is that any calculations of fracture stress will tend to be conservative particularly for the small crack situation (see e.g. Eq. VI-5, Section VI). For the tougher materials (e.g. 7075-T6 and 2024-T3 aluminum) this may become unduly conservative and lead to restrictive designs. In these cases it would be better to include plasticity corrections in the analysis. The examples presented herein assume plasticity corrections to the plane stress or plane strain fracture toughness.

STEP 7. Using equation VIII-1 compute the critical fracture stress for the crack aspects ratios of interest. Equation VIII-1 becomes, for this example

$$\sigma_c = \frac{\bar{K}_c}{\sqrt{\pi a_c} (\lambda^* \text{ or } \lambda^{**})} \quad (\text{IX-4})$$

for critical conditions (i.e. $K \rightarrow K_c$, $a \rightarrow a_c$, $\sigma \rightarrow \sigma_c$). The trend in fracture stress with increasing crack aspect ratio as well as the composite correction factor is shown in Figure 43.

Thus, for the geometry of Figure 41 the fracture stress decreases until the crack approaches the edge stringers ($14.5'' > 2a > 0$). The edge stringers start to pick up the load at that point and the maximum fracture stress is reached once the crack goes through the stringer area ($2a = 20$ inches). It is interesting to note that the influence of the center stringer on the correction factor remains fairly constant throughout the crack range of interest. (See Table VI.)

If this stringer is broken, however, the effect on critical stress is quite pronounced. In this case the crack geometry becomes one of Figure 30(d) until a crack aspect ratio of 0.8 is reached and the geometry of Figure 31 applies. Critical fracture stresses can be computed as before using the geometric corrections of Table IV and V. Fracture stresses are plotted in Figure 44 for the broken center line stringer case. Comparison of this analysis with that for the stringer intact (dashed curve) indicate an approximate 30% reduction in fracture stress for most values of $\left(\frac{2a}{W}\right)$ for this condition. With the center line stringer broken, there will be some $\left(\frac{2a}{W}\right)$ crack buckling resulting in lower fracture stresses at the larger crack lengths. The analysis, as presented, does not account for this effect. However, it is felt that this reduction will be minimal due to the influence of the

***Valid fracture data from the material in question must be available for the thickness of interest to solve this problem. This implies "infinite" sheet data.

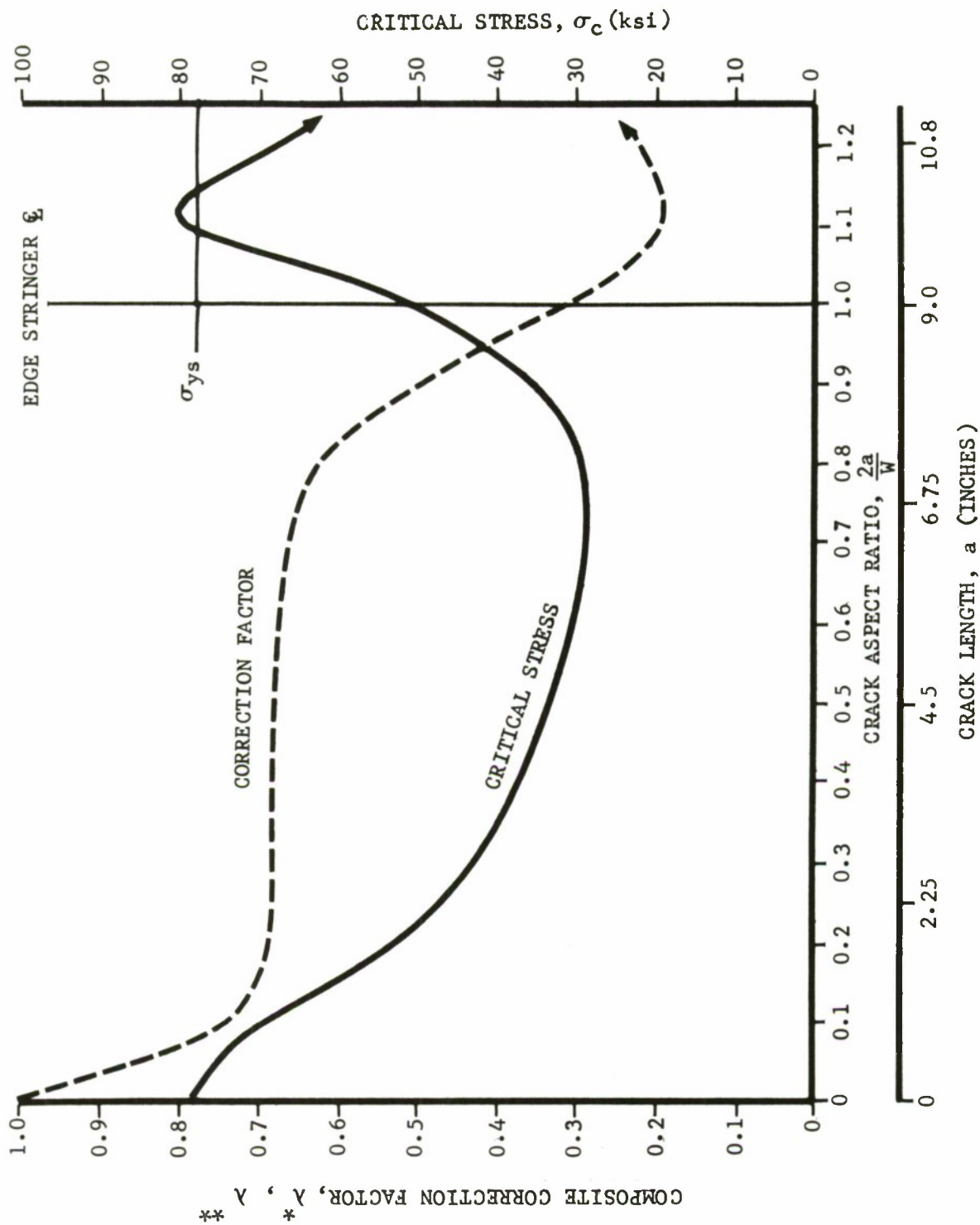


FIGURE 43 COMPOSITE CORRECTION FACTORS & CRITICAL STRESS AS A FUNCTION OF CRACK LENGTH FOR GEOMETRY OF FIGURE 41 WITH λ STRINGER INTACT (NO CRACK BUCKLING)

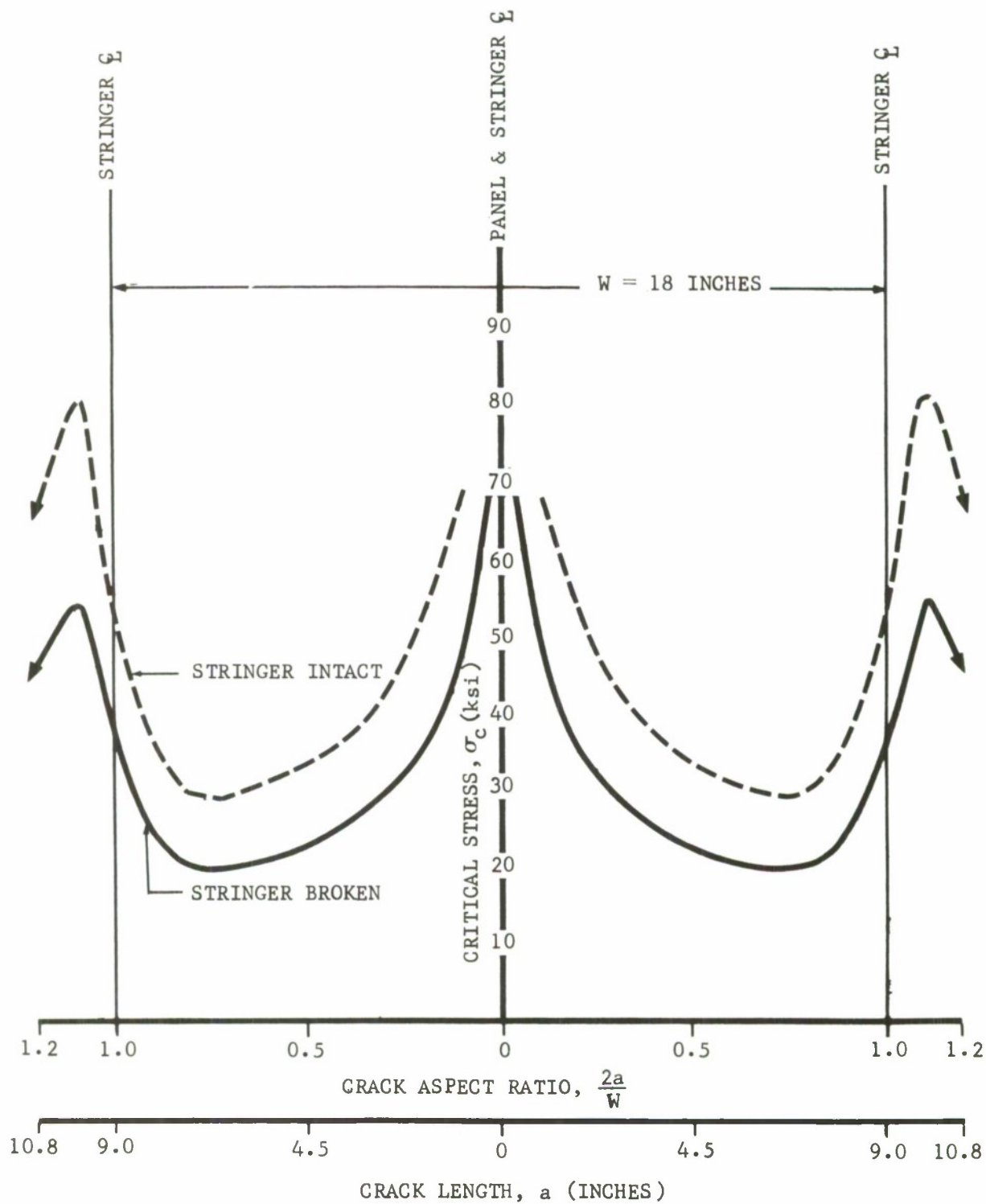


FIGURE 44 COMPARISON OF PREDICTED FRACTURE STRESS FOR CRACK GEOMETRY OF FIGURE 41 - CENTER STRINGER INTACT & BROKEN (NO CRACK BUCKLING)

edge stiffeners within the important crack aspect ratios of $0.8 > \frac{2a}{W} > 0.2$.

For cases of repetitive structure, it can be seen that this problem then becomes similar to the geometry (many skin/stringer bays) of Figure 30(c) and can be treated in the same manner.*

IX.9 NON-SYMMETRIC CRACK-INTEGRAL STRINGER

In 1965, Grief and Sanders⁽⁴⁸⁾ performed an analysis of a cracked plate with continuously attached (integral), zero width stringer. They assumed zero bending stiffness and continuous attachment (integral) of the stringer. Therefore, an analysis of an edge-stiffened sheet can be performed for the geometry of Figure 30(d) using the Isida corrections for crack aspect ratios $\frac{2a}{W} < 0.8$ and the Grief-Sanders results for $\frac{2a}{W} > 0.8$. Comparisons can then be made between critical stress for an integral stiffened and riveted stringer.**

IX.9(a) Example

In this case, we have the structure as shown in Figure 45. It is similar to that of Figure 41 with centerline stringer removed and 0.125" thick hat section stringers installed instead of angles. The hat sections are welded to the skin or could be riveted with very small pitch.

STEP 1. Compute the correction factors for crack aspect ratios, $\frac{2a}{W} < 0.8$.
In this case from equation IX-1 and $I_z = 0.385 \text{ inches}^4$,

$$\alpha = \frac{I_z}{B\left(\frac{W}{2}\right)^3} \cdot \frac{E_{\text{str.}}}{E} = \frac{0.385 \text{ inch}^4}{0.063 \text{ inch} \left(\frac{18 \text{ inches}}{2}\right)^3} \cdot \frac{10^7 \text{ psi}}{10^7 \text{ psi}}$$

$$\alpha \approx 0.01$$

As in the previous problem, the correction curves of Figure 37 apply. The extensional stiffness is (Equation IX-2),

$$S = \frac{A_{\text{str.}}}{B\left(\frac{W}{2}\right)} \cdot \frac{E_{\text{str.}}}{E} = \frac{0.594 \text{ inch}^2}{0.063 \text{ inch} \left(\frac{18 \text{ inches}}{2}\right)} \cdot \frac{10^7 \text{ psi}}{10^7 \text{ psi}}$$

$$S = 1.05$$

and the correction factors are shown in Table VIII.

*This problem has recently been analyzed by C. Poe, Jr., "The Effect of Riveted and Uniformly Spaced Stringers on the Stress Intensity Factor of a Cracked Sheet," M.S. Thesis, Va. Polytechnic, 1969.

**NOTE Based on the assumptions in this and previous analyses, satisfactory results will be obtained as long as the distance of the crack from the stringer is on the order of the rivet spacing or stringer width.

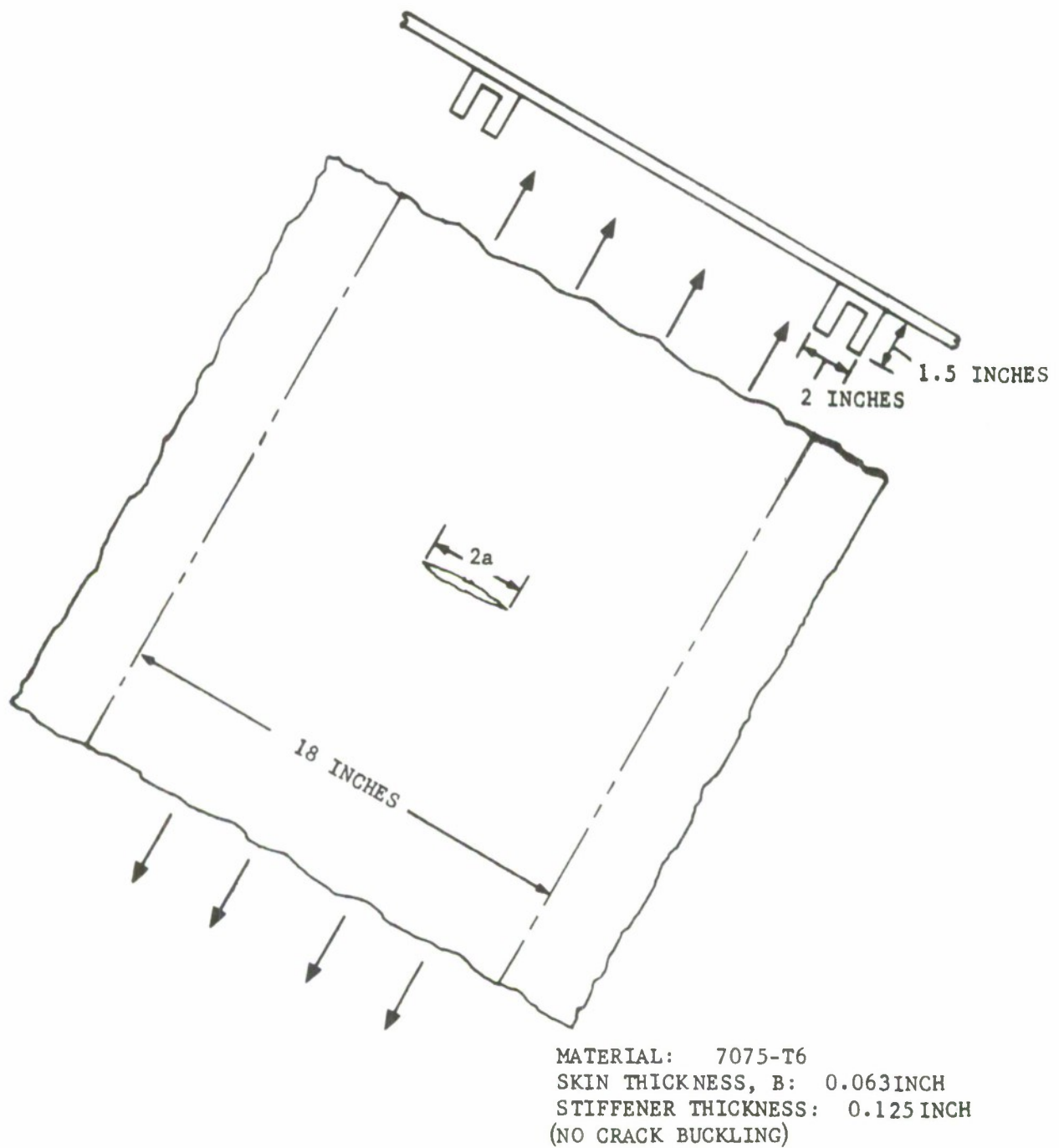


FIGURE 45 SAMPLE PROBLEM PANEL GEOMETRY

TABLE VIII
CORRECTION FACTORS FOR EXAMPLE PROBLEM

$\frac{2a}{W}$	λ (Fig. 37)
0	1.0
0.1	1.0
0.2	1.01
0.3	1.015
0.4	1.02
0.5	1.025
0.6	1.025
0.7	1.015
0.8	0.98

STEP 2. As the crack approaches the hat stiffeners, the correction factors of Figure 46 apply and the values for S and λ' are given in Table IX. S in this case is

$$S = \frac{4EB l}{A_{STR} E_{STR} (1 + \nu)(3 - \nu)}, \quad (IX-5)$$

where $l = \frac{2a + W}{2}$ for a center crack geometry.

TABLE IX
CORRECTION FACTORS FOR EXAMPLE PROBLEM

$\frac{2a}{W}$	$l, (\text{inch})$	S	λ' (Fig. 46)
0.6	14.4	1.72	0.925
0.7	15.3	1.83	0.885
0.8	16.2	1.94	0.810
0.85*	16.65	1.99	0.785
0.90*	17.1	2.04	0.690

*Analysis not valid for $l - 2a >$ stringer width.

It will be noticed that there is a small (< 0.2) difference in correction factors for crack aspect ratios, $\frac{2a}{W}$, between 0.6 and 0.8 in Tables VIII and IX. Therefore, average composite correction factors, λ^* , between Tables VIII and IX are indicated in Table X for crack aspect ratios ($\frac{2a}{W}$) of 0.6, 0.7, and 0.8 for the geometry of Figure 45.

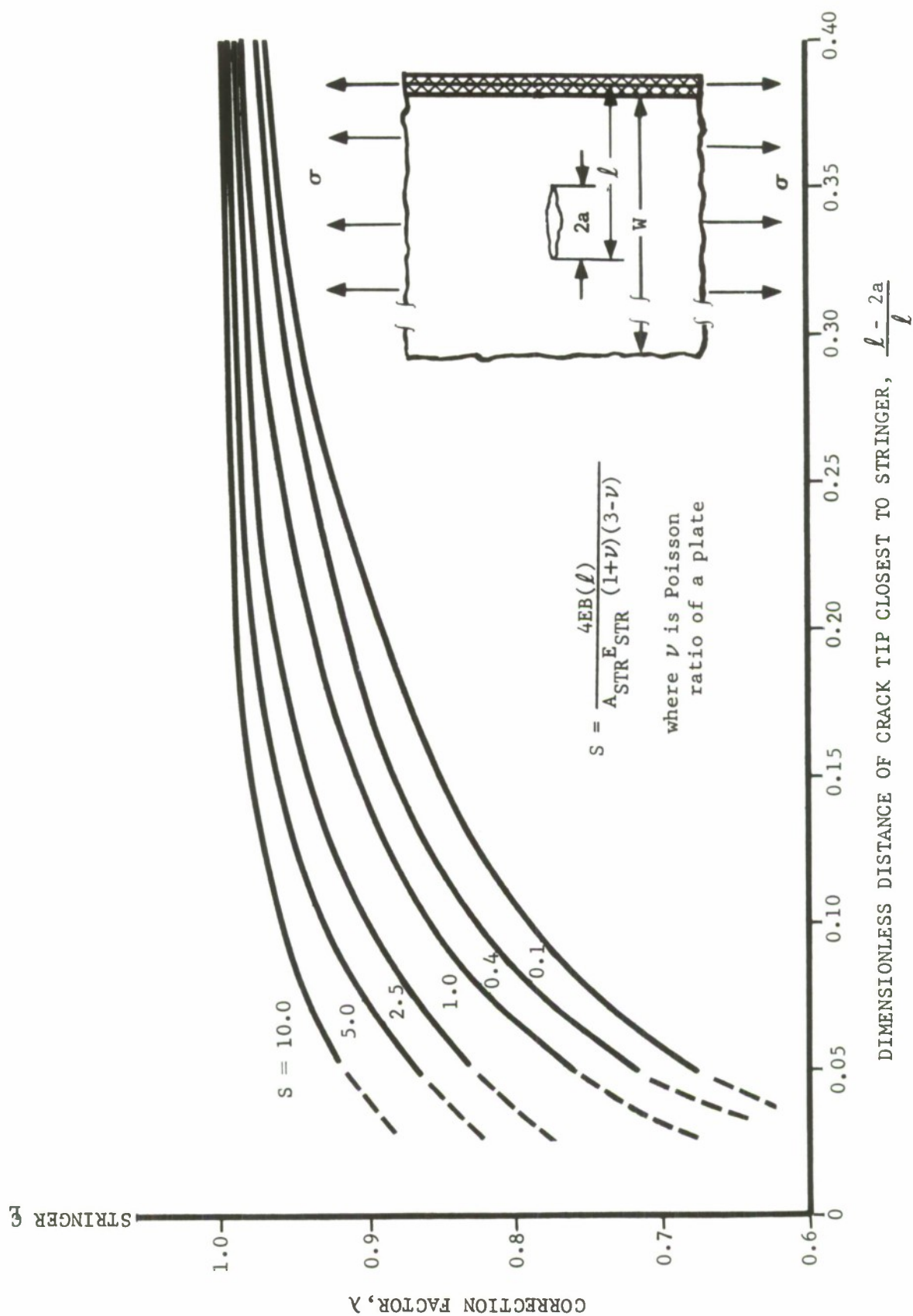


FIGURE 46 CORRECTION FACTORS - NONSYMMETRIC CRACK - INTEGRAL STRINGER (REF. 48)

TABLE X
COMPOSITE CORRECTION FACTORS FROM TABLES VIII & IX

$\frac{2a}{W}$	λ	λ'	λ^*
0	1.0	—	1.0
0.1	1.0	—	1.0
0.2	1.01	—	1.01
0.3	1.015	—	1.015
0.4	1.02	—	1.02
0.5	1.025	—	1.025
0.6	1.025	0.925	0.975
0.7	1.015	0.885	0.950
0.8	0.98	0.810	0.895
0.85	—	0.785	0.785
0.90	—	0.690	0.690

A plot of critical stress for the integral stringer of this example compared with the riveted stringer of the previous problem is shown in Figure 47, assuming a plane stress fracture toughness, $\bar{K}_C \cong 85 \text{ ksi}\sqrt{\text{inch}}$.

It will be noticed there is little difference between the riveted edge stringer and welded stringer results. In the case of the riveted stringer, the rivet pitch is small enough that it can be assumed that it will behave in a manner similar to the integral stringer. This is borne out by the results plotted in Figure 47. Also indicated in this comparison is the trend in stress pick-up by the edge stringer at a crack aspect ratio of 0.8, which corresponds to the riveted structure case.

IX.10 SUMMARY

Thus the fracture strength can be computed for riveted skin/stringer and integral stringer/skin construction using fracture mechanics as a base. It should be remembered that the analysis as presented here has included crack tip plasticity which can be quite large for tougher materials. Neglecting this plasticity can lead to overly conservative results for the higher fracture-tough alloys. Therefore, this type of analysis is limited only by the selection of the proper value of plane stress fracture toughness (K_C). When possible, this value should be obtained by test, from cracked sheets (preferably of the geometry of interest) of the thickness which is under consideration. However, lacking positive fracture toughness data for the material of interest, a conservative estimate of fracture stress can be computed. In the following section, it will be shown how fracture envelopes can be useful in this regard.

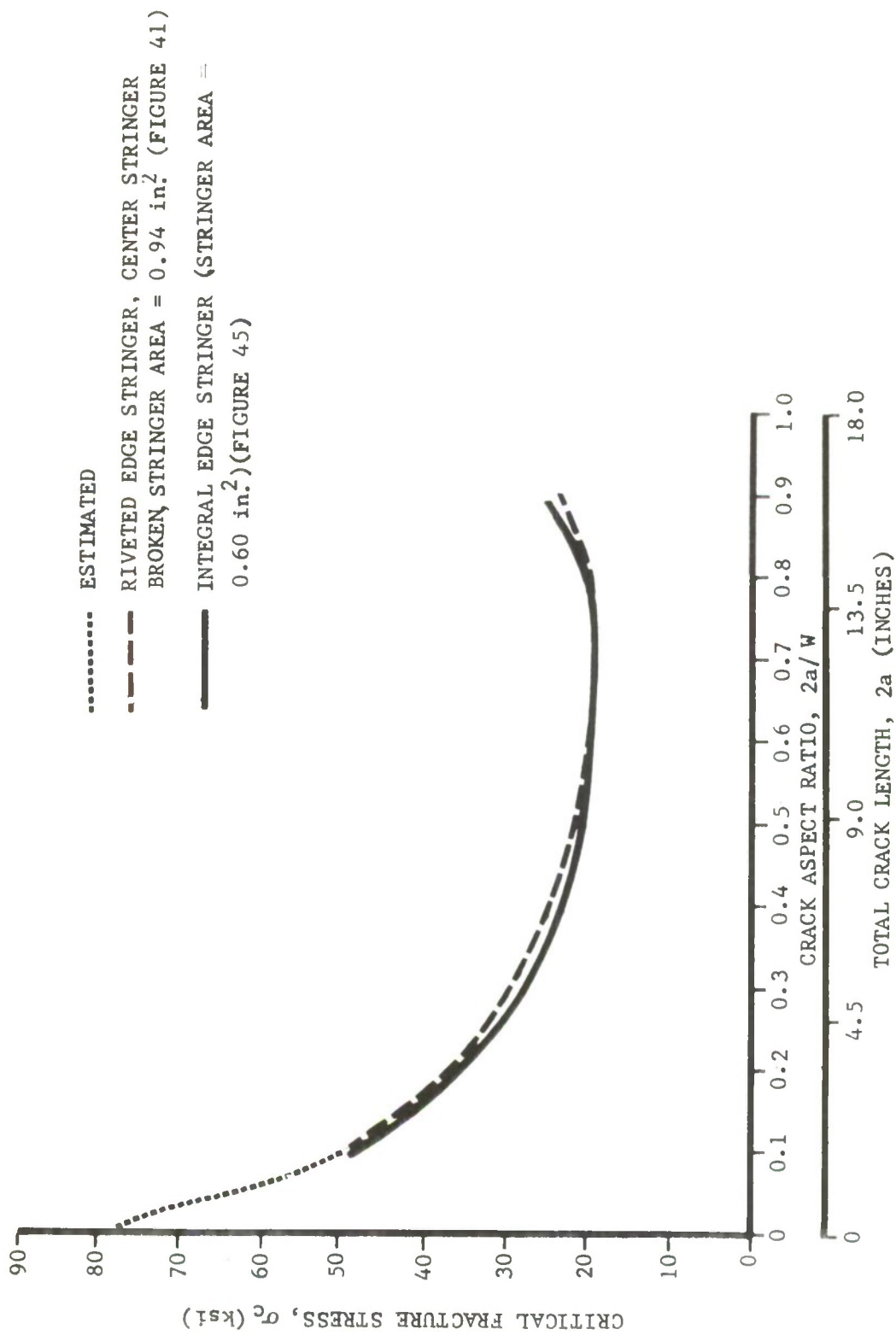


FIGURE 47 COMPARISON OF FRACTURE STRESS FOR RIVETED AND INTEGRAL STRINGER PANELS OF FIGURES 41 & 45 (NO CRACK BUCKLING)

IX.11 FRACTURE STRESS ESTIMATES WITH AVERAGE TOUGHNESS DATA

In many cases an estimate of critical stress or tolerable crack length must be made for designs for which the material's fracture data is known from only a limited number of tests. Perhaps average K_C data is not available for the thickness of interest. Or dissimilar materials may be under consideration for skin/stiffener applications in a particular design. Through the use of the composite correction principles shown thus far, it is possible to make preliminary estimates of critical fracture stress based on fracture mechanics analysis. One such problem will be analyzed to indicate the applicability of these methods.

A design shown in Figure 48 could represent a portion of a lower center wing panel which is subjected to primary tension loads. Width between the ZEE stringers is 9 inches. In this problem, consideration is being given to two skin materials, 2219-T87 and Ti-6Al-4V. If the titanium alloy is used, the ZEE stringers will be of a high strength steel alloy. For the aluminum construction, the ZEE stringers will also be aluminum. Average plane stress fracture toughness values (\bar{K}_C) for the Ti-6Al-4V skin range from 155-165 ksi $\sqrt{\text{inch}}$.* For the 2219-T87 aluminum alloy, \bar{K}_C ranges from 115-125 ksi $\sqrt{\text{inch}}$.**

To provide the maximum data, two adjacent bays should be analyzed, assuming a crack would start at a rivet hole in the sheet at the center ZEE stringer. It can be seen from Figure 48 that the wing panel is, for the crack problem, similar to the geometry of Figure 41. Therefore, the crack geometry is the composite of Figures 30 (b and d) and 31, and the procedures followed in the first reinforced panel problem of this section are applicable.

IX.11(a) Computation of Geometric Corrections

STEP 1. The moment of inertia of the ZEE stringer about the stringer neutral axis, perpendicular to the plane of the plate, I_z is 0.0511 inches⁴, and the Modulus of the steel stringer is 28×10^6 psi, and the titanium sheet 16×10^6 psi.

For the all 2219-T87 aluminum alloy construction, the inertia parameter (Eq. IX-1) is calculated as

$$\alpha_{Al/Al} = \frac{0.0511 \text{ inch}^4}{0.100 \text{ inch} \left(\frac{18 \text{ inches}}{2} \right)^3} \cdot \frac{10^7 \text{ psi}}{10^7 \text{ psi}} \cong 0.0001 \cong 0$$

Assuming the same ZEE section properties for the steel stringers (i.e., $I_z = 0.0511$ inches⁴) for simplicity, the titanium panel with alloy steel stringers gives a nondimensional inertia parameter of

$$\alpha_{Ti/St} = \frac{0.0511 \text{ inch}^4}{0.050 \text{ inch} \left(\frac{18 \text{ inches}}{2} \right)^3} \cdot \frac{2.8 \times 10^7 \text{ psi}}{1.6 \times 10^7 \text{ psi}} \cong 0.002 \cong 0$$

Therefore, the corrections of Figure 36 apply in this analysis to both skin materials.

The extensional stiffnesses are from Figure 36, again assuming equal ZEE stringer areas.

* Approximate range in values for $B = 0.100$ inch. Wide panel tests.

** Approximate range in values for $B = 0.05$ inch. Wide panel tests.

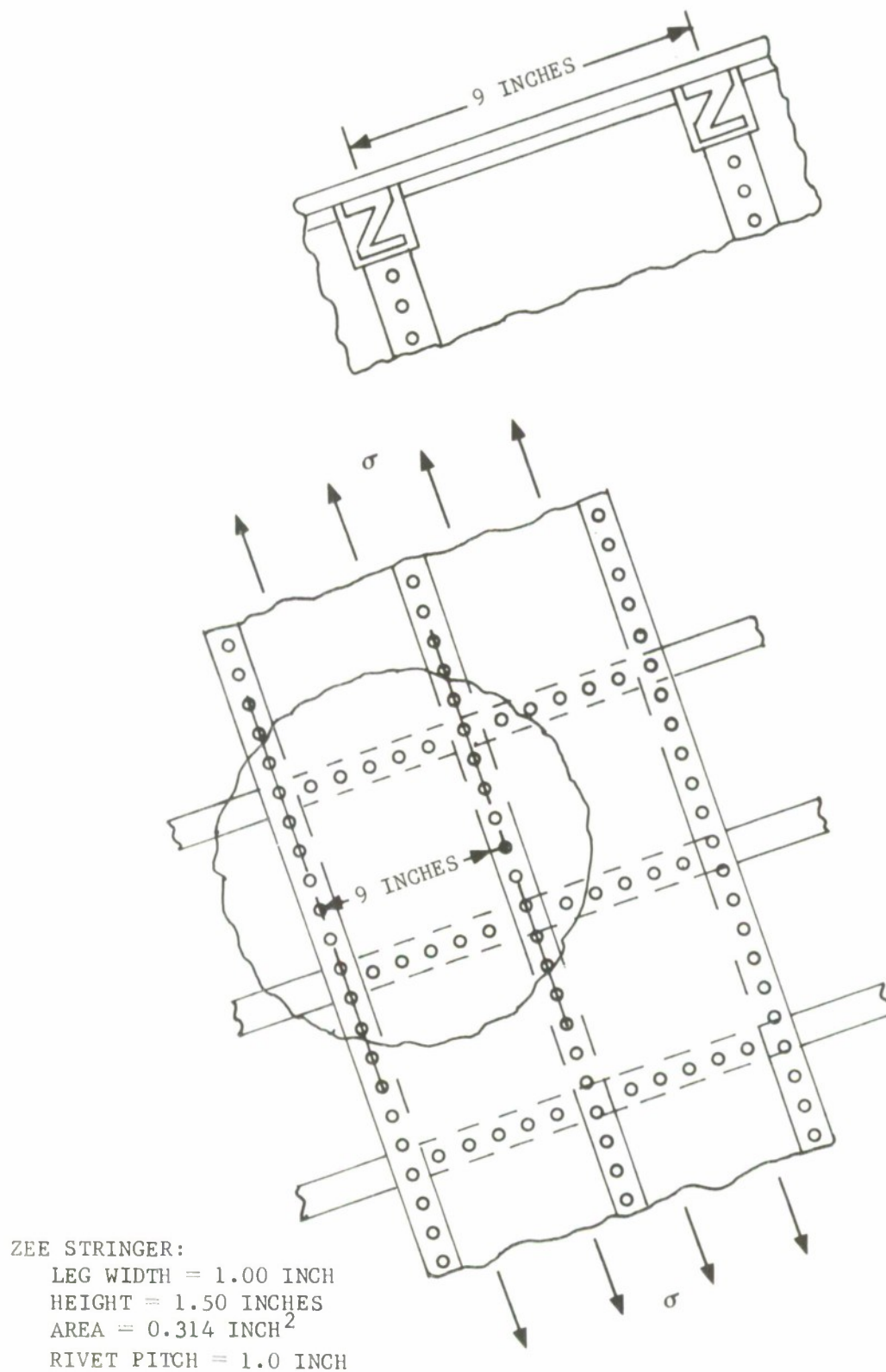


FIGURE 48 LOWER CENTER WING PANEL FOR EXAMPLE PROBLEM

$$S_{Al/Al} = \frac{0.314 \text{ inches}^2}{0.100 \text{ inch} \left(\frac{18 \text{ inches}}{2} \right)} \cdot \frac{10^7 \text{ psi}}{10^7 \text{ psi}} \cong 0.35$$

and

$$S_{Ti/St} = \frac{0.314 \text{ inches}^2}{0.050 \text{ inch} \left(\frac{18 \text{ inches}}{2} \right)} \cdot \frac{2.8 \times 10^7 \text{ psi}}{1.6 \times 10^7 \text{ psi}} \cong 1.2$$

Values of the correction factors for these material configurations are listed in Table XI.

TABLE XI
CORRECTION FACTORS FOR EXAMPLE PROBLEM
ALUMINUM-ALUMINUM AND TITANIUM-STEEL CONSTRUCTION

2a/W	2a (inches)	Aluminum-Aluminum $\lambda'_{Al/Al}^*$	Titanium-Steel $\lambda'_{Ti/St}^*$
0.1	1.8	1.01	1.01
0.2	3.6	1.015	1.01
0.3	5.4	1.03	1.015
0.4	7.2	1.06	1.02
0.5	9.0	1.10	1.025
0.6	10.8	1.15	1.03
0.7	12.6	1.20	1.025
0.8	14.4	1.28	1.02

* From Figure 36.

STEP 2. For crack aspect ratios $0.8 > \frac{2a}{W} > 0.6$, as the crack approaches the edge ZEE stiffeners, for small rivet pitch (assume crack grows through rivet and center stringer remains intact), the correction factors from Figure 46 apply. Tabular results are given in Table XII.

TABLE XII
CORRECTION FACTORS FOR EXAMPLE PROBLEM
ALUMINUM-ALUMINUM AND TITANIUM-STEEL CONSTRUCTION

2a/W	2a (inches)	Aluminum-Aluminum		Titanium-Steel	
		$S_{Al/Al}^{**}$	$\lambda''_{Al/Al}^{***}$	$S_{Ti/St}^{**}$	$\lambda''_{Ti/St}^{***}$
0.6	10.8	5.2	0.995	1.55	0.93
0.7	12.6	5.5	0.97	1.6	0.875
0.8	14.4	5.8	0.94	1.7	0.80
0.85*	15.3	6.0	0.92	1.74	0.76
0.90*	16.2	6.1	0.91	1.8	0.69
0.95*	17.1	6.3	0.80	1.83	~.6

* Analysis is invalid for $l-2a > \text{stringer width}$, however, proper trend is noted.

** From Equation IX-5.

*** From Figure 46.

STEP 3. The problem can now be analyzed for the geometry of Figure 30(b) with the crack emanating from the rivet hole of the central ZEE stringer. The correction factors from Figure 33 for the two cases are shown in Table XIII.

TABLE XIII
CORRECTION FACTORS FOR EXAMPLE PROBLEM
ALUMINUM-ALUMINUM AND TITANIUM-STEEL CONSTRUCTION

$\frac{2a}{W}$	2a (inches)	Aluminum-Aluminum		Titanium-Steel	
		$S_{Al/Al}^*$	$\lambda''_{Al/Al}^{***}$	$S_{Ti/St}$	$\lambda''_{Ti/St}^{***}$
0.1	1.8	0.57	0.75	0.16	0.71**
0.2	3.6	1.15	0.725	0.33	0.675**
0.3	5.4	1.72	0.715	0.49	0.675
0.4	7.2	2.29	0.73	0.655	0.67
0.5	9.0	2.87	0.73	0.82	0.67
0.6	10.8	3.44	0.73	0.98	0.67
0.7	12.6	4.01	0.74	1.15	0.675
0.8	14.4	4.59	0.74	1.31	0.675
0.85	15.3	4.87	0.745	1.39	0.68
0.9	16.2	5.16	0.75	1.47	0.68
0.95	17.1	5.45	0.75	1.56	0.68

* From Equation IX-3.

** Interpolated from Figure 33.

*** From Figure 33.

STEP 4. The composite correction factors for the aluminum/aluminum and titanium/steel construction can now be computed by superposition. The results for the crack history are shown in Table XIV.

TABLE XIV
COMPOSITE CORRECTION FACTORS FOR EXAMPLE PROBLEM
ALUMINUM-ALUMINUM AND TITANIUM-STEEL CONSTRUCTION FROM TABLES XI-XIII

$\frac{2a}{W}$	2a (inches)	Aluminum-Aluminum	Titanium-Steel
		$\lambda^* = \lambda' \times \lambda'' \times \lambda'''$	$\lambda^* = \lambda' \times \lambda'' \times \lambda'''$
0.1	1.8	0.77	0.72
0.2	3.6	0.74	0.68
0.3	5.4	0.74	0.685
0.4	7.2	0.77	0.68
0.5	9.0	0.80	0.69
0.6	10.8	0.835	0.629
0.7	12.6	0.861	0.596
0.8	14.4	0.890	0.548
0.85	15.3	0.685	0.517
0.9	16.2	0.682	0.469
0.95	17.1	0.60	0.408

STEP 5. Using the composite correction factors of Table XIV and the range in average K_c values for the 2219-T87 (115-125 ksi $\sqrt{\text{inch}}$) and Ti-6Al-4V (155-165 ksi $\sqrt{\text{inch}}$) and Equation VIII-1, compute the associated critical stress ranges for this panel geometry. Comparison of the two proposed panel fracture stress envelopes is shown in Figure 49.

In this comparison of fracture strength to yield strength ratio, (this is only one of the many ways of presenting fracture data comparisons) the all aluminum construction shows as the better fracture safe configuration for $\frac{2a}{W} < 0.7$. However, in Figure 50, a comparison of fracture stress alone indicates the superiority of the 2219-T87 construction for inspectable size cracks. For example, the dashed line could be the anticipated limit design stress for the 2219-T87 and the solid line the limit design stress for the Ti-6Al-4V construction. Clearly the aluminum construction will tolerate a 7.2-inch long crack at the limit design stress whereas the titanium/steel construction will permit a 4 1/2-inch long crack for a 90 percent increase in limit design stress. Both crack lengths are within inspectable limits.

IX.12 SUMMARY

Thus far we have seen how fracture mechanics can be used to make preliminary estimates of fracture stress. Composite correction factors which account for various boundary conditions for riveted and integral stringer/skin construction are used to correct for crack geometry. All of these analyses have been performed with the assumption of limited crack tip plasticity to provide conservative results. Therefore, actual material fracture data for the problem or design of interest would be required to present the total fracture envelope (i.e., same thickness, alloy and environment). In all cases the analysis deals with through-the-thickness crack situations. However, it is known that in many cases (i.e., pressure vessels, thick sections, etc.) the part through crack situation is prevalent in service. This problem will be treated in the next section.

IX.13 PART-THROUGH CRACKS*

Normally part-through cracks can occur in pressure vessels and initiate from small flaws or discontinuities which may or may not manifest themselves during proof testing. Flaw growth can occur during subsequent pressurization cycles and lead to catastrophic failure. One of the prime difficulties in analyzing for fracture is the presence of environmental factors (corrosive media) which may enter into the problem. Fortunately, fracture mechanics can be used with good success to analyze these structures. A great amount of research has been directed at this problem due to its historical permanence (see Section II).

It is necessary to show that the largest inspectable initial flaw will not become critical during its life span. The crack size requirements are dictated by nondestructive testing (NDT) and the parameters by fracture mechanics (stress levels, fracture toughness, material thickness and location and orientation of flaws).

* Although discussion of this crack problem is usually oriented towards pressure vessel applications, the part-through crack can also occur, and the same analysis applies to any structure with these crack conditions.

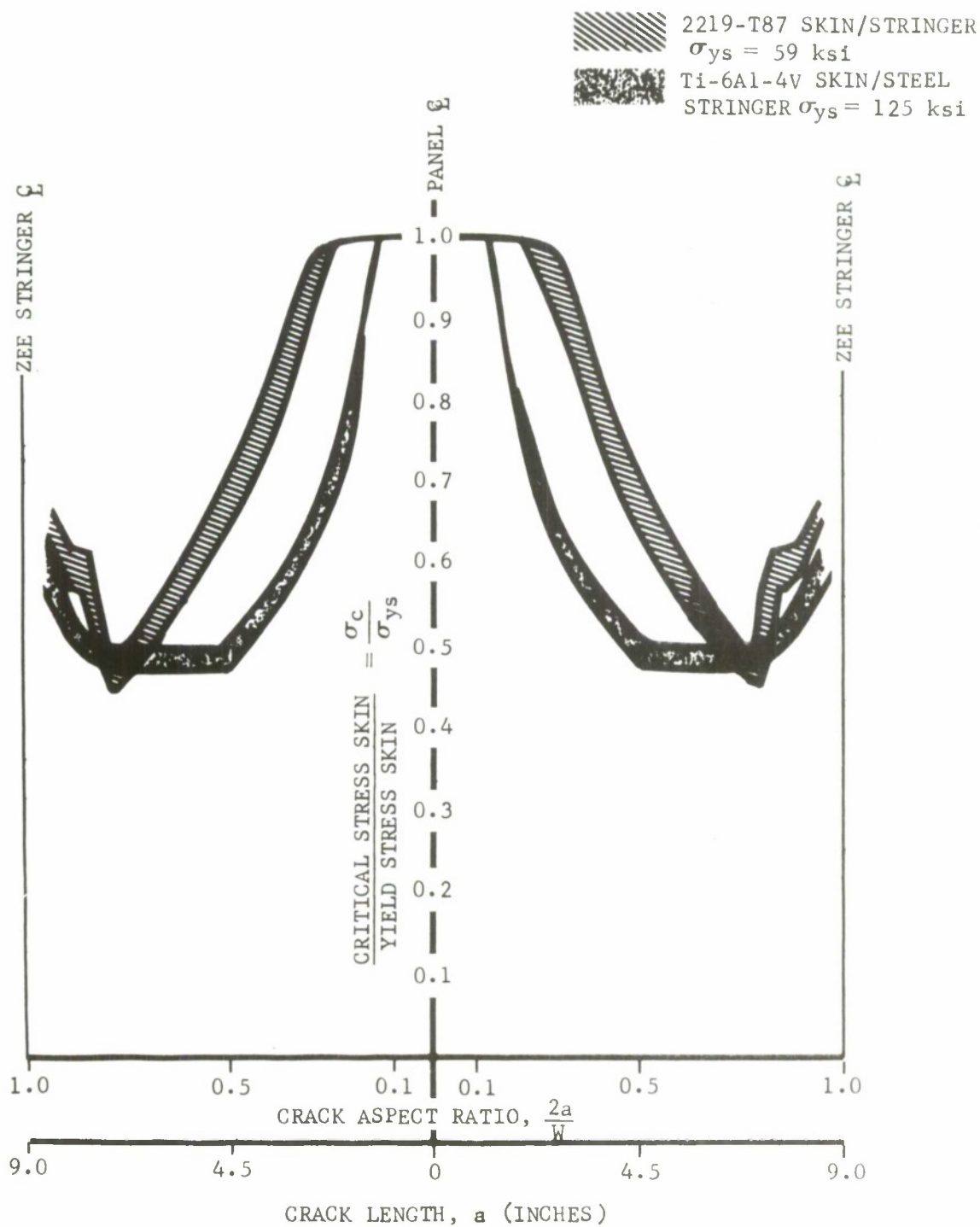


FIGURE 49 ESTIMATES OF FRACTURE ENVELOPES FOR THE PANEL GEOMETRY OF FIGURE 48 FOR TWO SKIN MATERIALS (NO CRACK BUCKLING)

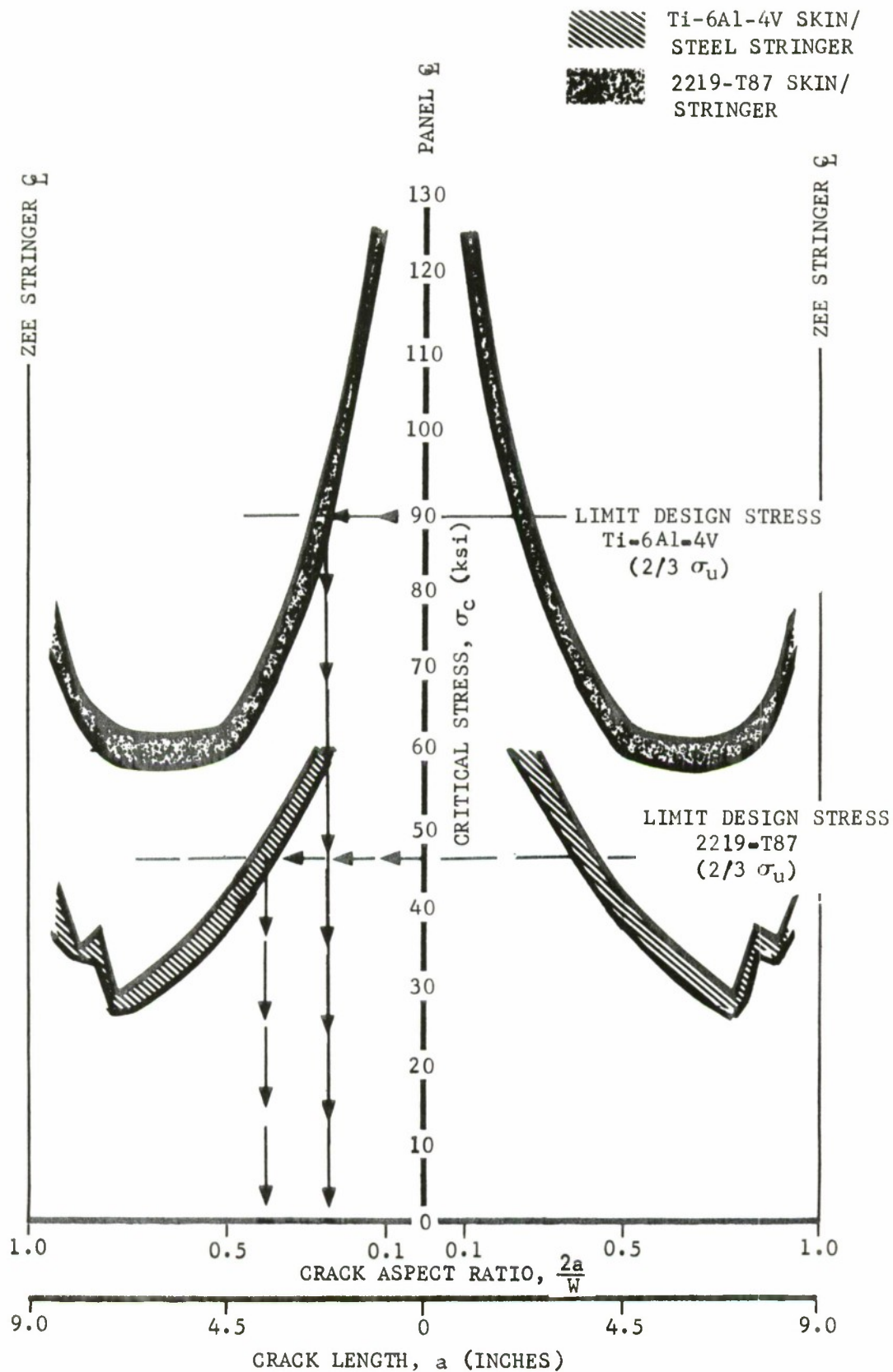


FIGURE 50 COMPARISON OF FRACTURE STRESS & CRACK LENGTHS FOR PANEL GEOMETRY OF FIGURE 48 FOR TWO SKIN MATERIALS (NO CRACK BUCKLING)

IX.13(a) Determination of Critical Discontinuity Dimensions and K_I for Part-Through Cracks

Part-through cracks usually manifest themselves as surface or embedded flaws. For thick wall structures, pressure vessels for example, with surface discontinuities or small embedded flaws, the following equation applies for critical conditions.

$$K_{Ic} = \sigma_c \sqrt{C\pi} \left(\sqrt{\frac{a_c}{Q}} \right)_c \quad (\text{IX-6})$$

Irwin (41), first described the opening mode stress intensity solution for a part-through elliptical crack as

$$K_I = A \sigma \sqrt{\pi} \sqrt{\frac{a}{Q}} \quad (\text{IX-7})$$

where $\left(\frac{a}{Q}\right)$ in both cases is used to describe the flaw size. The relationship between flaw shape (Q) and discontinuity aspect ratio (depth \div length, $\frac{a}{2c}$) is given in Figure 51. In equation IX-6, the constant $C = A^2 = 1.21$ for surface discontinuities and unity for small embedded flaws. Figure 51 shows the flaw shape relationship for various operating to yield stress ratios. Notice that the critical dimension for part-through cracks is always through-the-thickness, therefore, a , is the crack depth dimension for this class of crack situation.

Equation IX-6 has been found quite accurate for $\frac{a}{B} \leq 50\%$ (where B is material thickness); however, at greater crack depths the stress intensity solution of Equation IX-7 must be modified due to the stress intensity magnification as the flaw reaches a free surface (i.e. $\frac{a}{B} > 50\%$). Therefore, an elastic magnification factor (M_K) is applied to K which varies with a/B as shown in Figure 52 and is described functionally by Equation IX-8.

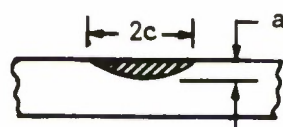
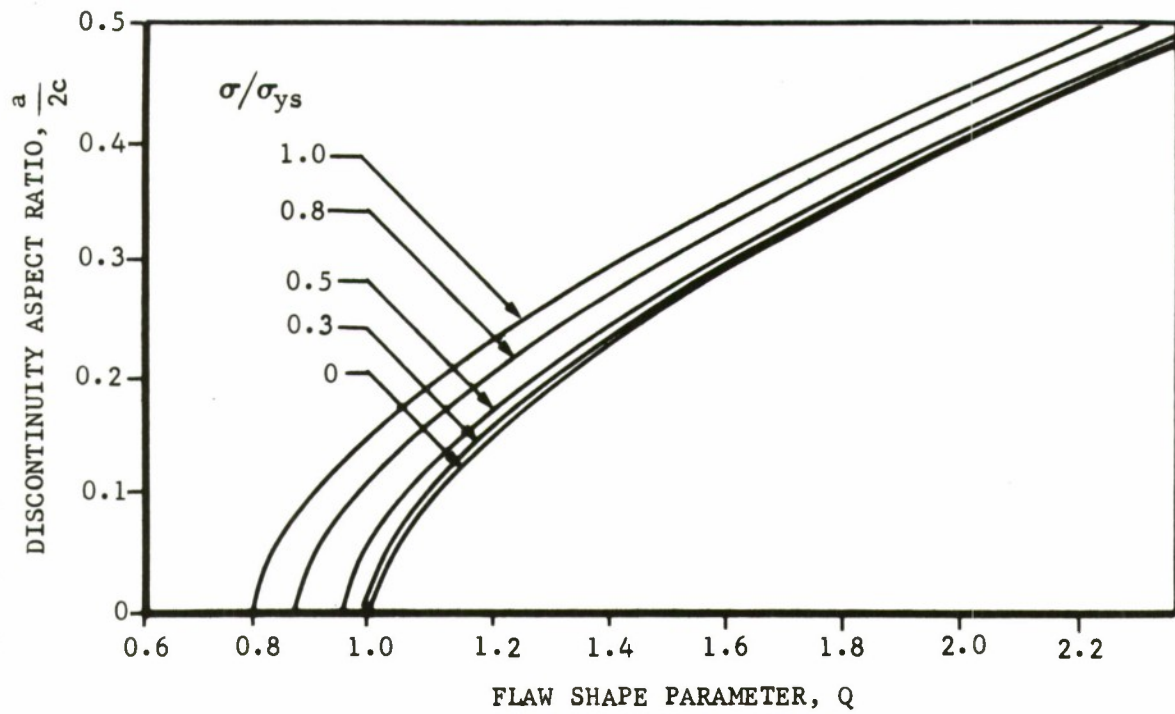
$$K_I = A \sigma \sqrt{\pi} M_K \sqrt{\frac{a}{Q}} \quad (\text{IX-8})$$

This implies, for example, that in "thin" walled pressure vessels the stress intensity becomes large (see Equation IX-8 and Figure 52) for small flaw sizes. Or $K_I \rightarrow K_{\text{critical}}$ faster for a given flaw size when $\frac{a}{B} > 0.5$.

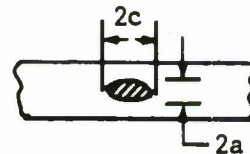
The elastic magnification factors for semi-elliptical surface flaws in a section in bending at the crack surface ($\beta = 90^\circ$) and root ($\beta = 0$) for $\frac{a}{2c} < 0.5$ are given in Figure 53. And the magnification factors for embedded flaws in finite thickness plate as a function of eccentricity and crack depth aspect ratio is shown in Figure 54. The combined elastic-plastic magnification factors for deep surface flaws are given in Figure 55, (i.e., "thin" wall cylinders).

IX.13(b) Arm In Bending as a Part-Through Crack Problem

In analyzing the arm of Figure 22, it is possible that a part-through (elliptical) crack occurs at point C (shown as insert in Figure 22). This part has been previously treated as a plane bending problem. We will now use part-through crack principles and fracture mechanics and compare these results with the through-the-thickness crack situation.



SURFACE FLAW



EMBEDDED FLAW

FIGURE 51 FLAW SHAPE PARAMETER CURVES (REF. 45)

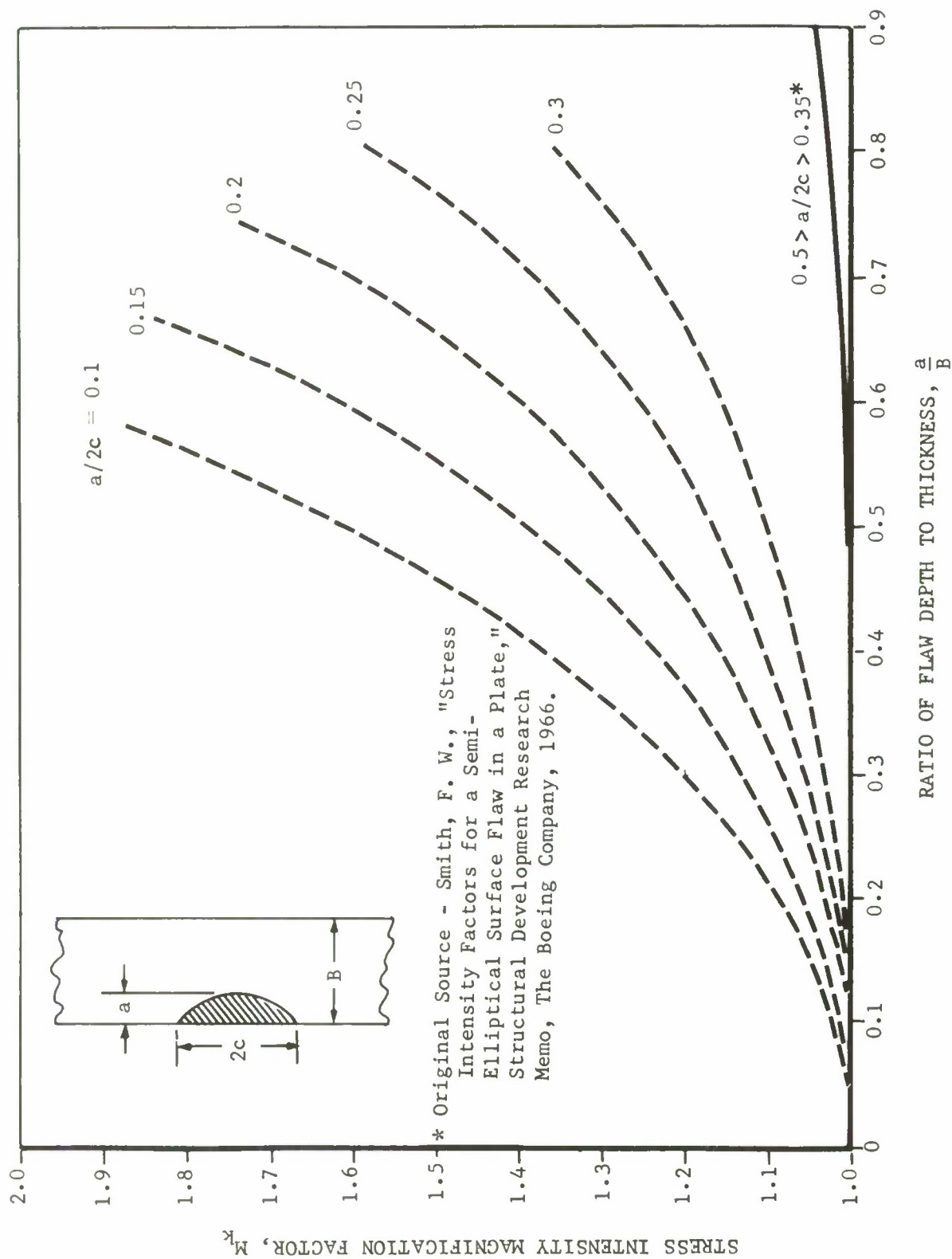
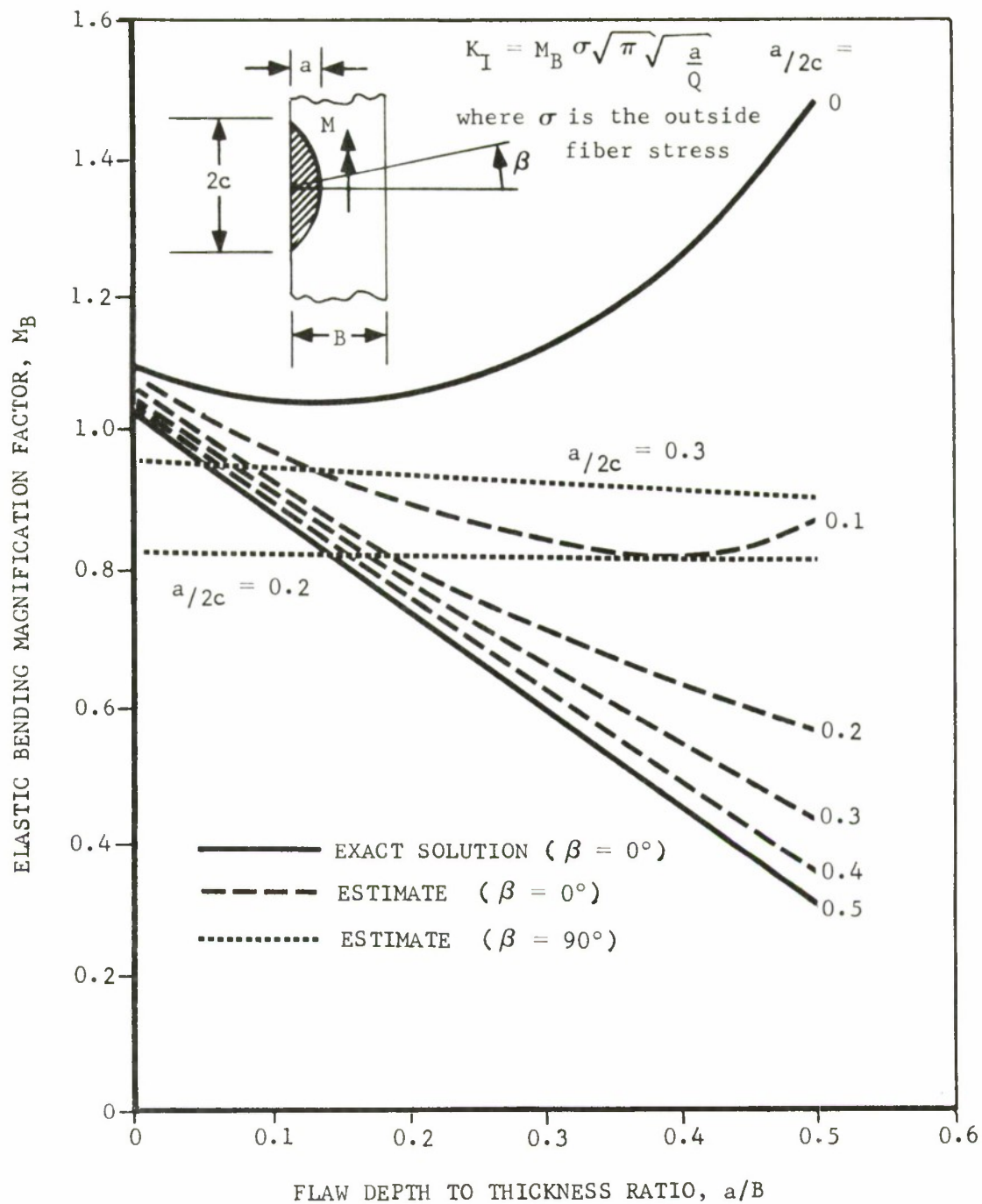


FIGURE 52 ELASTIC STRESS MAGNIFICATION FACTORS FOR DEEP SURFACE DISCONTINUITIES - IN TENSION (REF. 30)



*Original Sources - Smith, F. W., "Stresses Near Semi-Circular Edge Crack," Ph.D. Dissertation, Univ. of Washington, 1966.
 Smith, F. W., "Stress Intensity Factors for a Semi-Elliptical Surface Flaw in Plate," Structural Development Research Memo, The Boeing Company, 1966.
 Gross, B. J. & Srawley, J. E., NASA TND-2603, 1965.

FIGURE 53 STRESS MAGNIFICATION FACTORS FOR SEMI-ELLIPTICAL SURFACE FLAW IN SECTION IN BENDING AT $\beta = 0^\circ$ & 90° (REF. 25)*

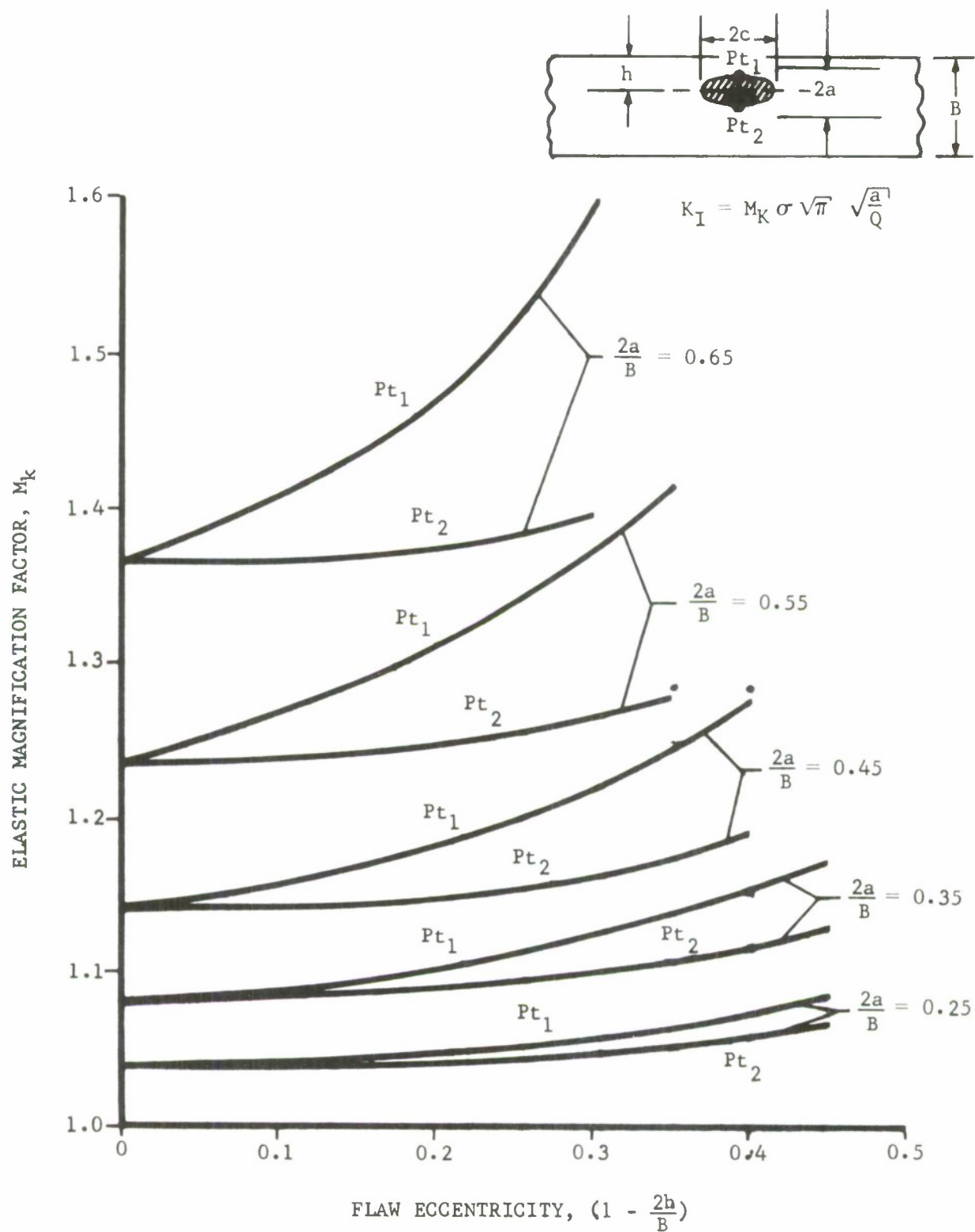


FIGURE 54 ELASTIC MAGNIFICATION FACTORS AT POINTS Pt_1 & Pt_2 , FOR AN EMBEDDED, ECCENTRIC LOADED FLAW IN TENSION (REF. 49)¹

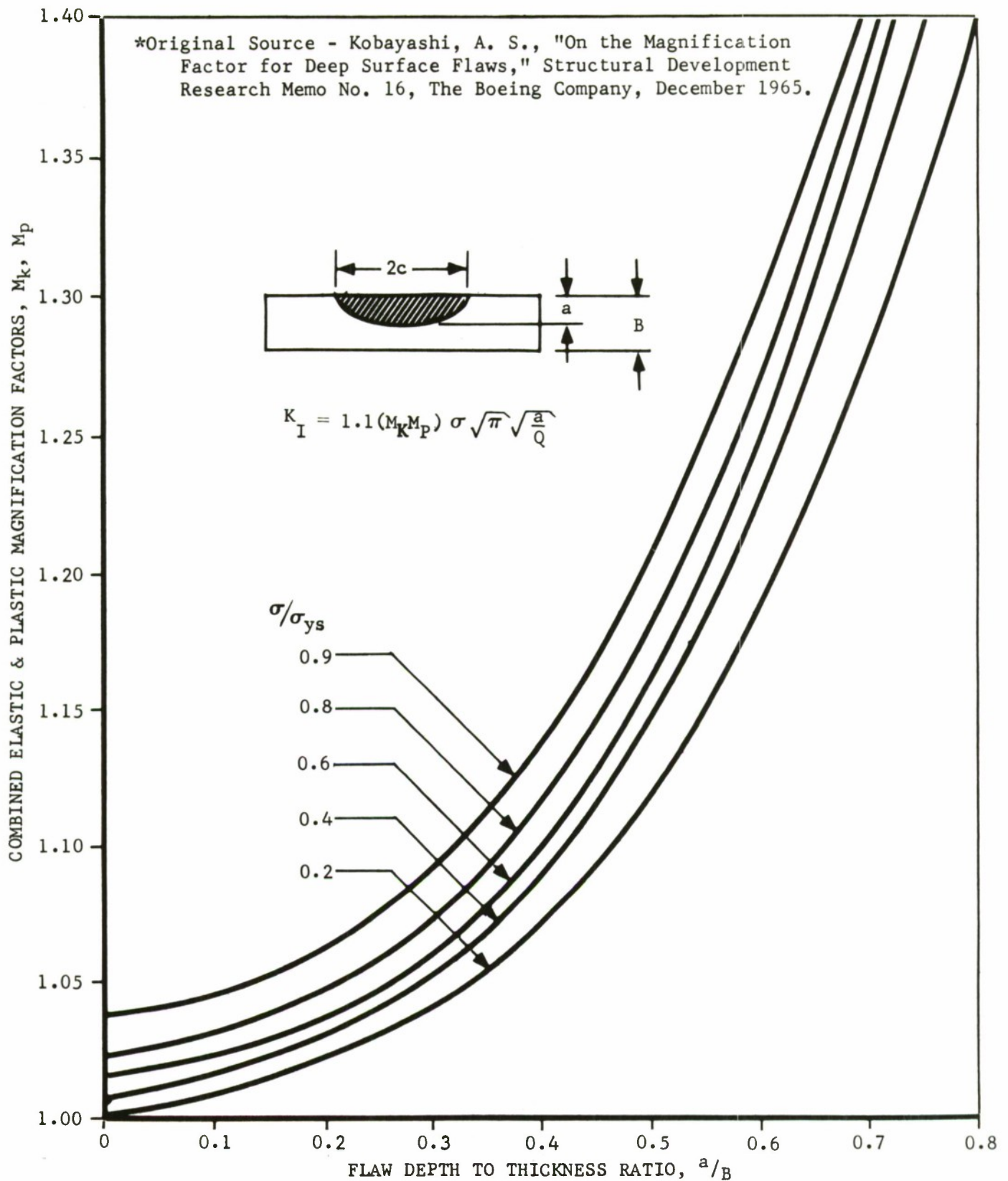


FIGURE 55 COMBINED ELASTIC & PLASTIC MAGNIFICATION FACTORS FOR A DEEP SURFACE DISCONTINUITY - IN TENSION ($a/2c < 0.3$) (REF. 25)*

Assume that a surface crack starts at point C (Figure 22), and has a semi-elliptical shape through the thickness. In this case, we will be analyzing a part-through crack situation with the shape of Figure 52 with tensile loading. Equation IX-8 applies and the ratio of crack depth to thickness, $\frac{a}{B}$ is $\frac{0.25 \text{ inch}}{2 \text{ inch}} = 0.125$. Assume that the discontinuity aspect ratio $\frac{a}{2c} \approx \frac{1/4 \text{ in.}}{3/4 \text{ in.}} \approx 0.33$, the elastic bending magnification factor, M_B , is from Figure 53 equal to 0.9. This value is not unexpected as it is approaching a through-crack geometry and the correction factor will tend toward unity.

STEP 1. Determine the flaw shape parameter, Q . The yield strength for the 7075-T6 alloy is 65 ksi and the 2219 alloy, 50 ksi. The nominal (tensile) stress for the arm at the crack position is by simple stress analysis 12 ksi and 18 ksi for the 2,000 and 3,000 lb. force, respectively. The values of the flaw shape parameters are given in Table XV for the operating to yield stress ratios and a discontinuity aspect ratio ($a/2c$) of 0.33.

TABLE XV
FLAW SHAPE PARAMETERS FOR EXAMPLE PROBLEM

MATERIAL	$\frac{\sigma}{\sigma_{ys}}$ (2000 lb force)	Q^*	$\frac{\sigma}{\sigma_{ys}}$ (3000 lb force)	Q^*
7075-T6	0.18	1.75	0.28	1.73
2219-T851	0.24	1.73	0.36	1.70

* From Figure 51.

STEP 2. From Equation IX-8, A is 1.1 for a surface crack. The value of K_I can now be determined for the 1/4" deep surface flaw. For a 2,000 lb. force and 7075-T6 material

$$K_I = 1.1 (12 \text{ ksi}) \sqrt{\pi} (0.9) \sqrt{\frac{1/4 \text{ inch}}{1.75}} = 8.0 \text{ ksi}\sqrt{\text{inch}}$$

and for a 3,000 lb. force and 7075-T6 material

$$K_I = 1.1 (18 \text{ ksi}) \sqrt{\pi} (0.9) \sqrt{\frac{1/4 \text{ inch}}{1.73}} = 12.0 \text{ ksi}\sqrt{\text{inch}}$$

The stress intensities for the 2219-T851 material are 8.0 ksi $\sqrt{\text{inch}}$ (2,000 lb. force) and 12.1 ksi $\sqrt{\text{inch}}$ (3,000 lb. force). The stress intensities for a 2,000 and 3,000 lb. force and through the thickness crack obtained previously are 11.1 ksi $\sqrt{\text{inch}}$ (2,000 lb. force) and 16.8 ksi $\sqrt{\text{inch}}$ (3,000 lb. force).

Thus, results obtained for the semi-elliptical part-through crack compared to the through crack indicate slightly lower ($< 3 \text{ ksi}\sqrt{\text{inch}}$) stress intensities. However, the geometric corrections approach unity in both cases.

IX.14 APPLICATION TO DESIGN - PART-THROUGH CRACKS

An excellent summary of the application of fracture mechanics to the design of pressure vessels is given in Reference 42. Those concerned with the analysis of part-through surface or embedded flaws should refer to that document for the limitations of the analysis as well as complete illustrative examples.

For a given environment and loading profile, the time or cycles to failure of a pressure vessel depends primarily on the initial stress intensity (K_{Ii}) for an assumed discontinuity compared to the material plane strain fracture toughness. That is the number of cycles to failure or time to failure is a function of $\frac{K_{Ii}}{K_{Ic}}$. Through the use of empirical data, curves of $\frac{K_{Ii}}{K_{Ic}}$ can be established as shown in Figure 56 for static loaded and cyclic loaded structure. For the static loaded case, it can be seen that below some threshold value $\frac{K_{Ii}}{K_{Ic}}$ or $\frac{K_{th}}{K_{Ic}}$ that the crack or flaw will not grow as load is sustained indefinitely; whereas, if the initial flaw (and corresponding K_{Ii}) is above the threshold value, the crack will grow with time as constant load (stress) is sustained and failure will ensure. For the cyclic load case, no threshold value is evident and some crack growth and eventual failure can be expected unless a non-propagating crack situation develops. Much variation in threshold value has been experimentally detected and is caused by alloy, heat treat, temperature, etc. The techniques used in employing threshold stress intensity data in design and analysis are reported in Reference 42 in detail.

IX.15 EFFECT OF BULGING DUE TO INTERNAL PRESSURE

In thin gage, pressurized cylinders it is known that the stress intensity of a through crack is influenced not only by the membrane stresses, but also by bulging of the material on either side of the crack.⁽⁵⁰⁾ The crack geometry of this problem is shown in Figure 57. This problem has been treated in Reference 50 as a stress intensity superposition. When the crack is oriented parallel to the cylinder axis, the superimposed stress intensity is the sum of the factors for hoop membrane (K_h) and bulging (K_b), or, (see also Section V.)

$$K = K_h + K_b \quad (\text{IX-9})$$

The complete solution, from Reference 50, is

$$K = \sigma_h \sqrt{\pi a} \left[1 + C \frac{B}{R} \left(\frac{a}{B} \right)^\mu \right] \quad (\text{IX-10})$$

where C and μ are empirically determined constants obtained from pressurized burst tests on precracked cylinders, and R is the cylinder radius. Equation IX-10 does not include correction for crack tip plasticity. The plasticity corrected form of Equation IX-10 is (see also Section VI).

$$K = \sigma_h \sqrt{\pi a + \frac{K^2}{2 \sigma_{yB}^2}} \left[1 + C \frac{B}{R} \left(\frac{a}{B} \right)^\mu \right] \quad (\text{IX-11})$$

In equation IX-11, σ_{yB} is the material yield strength in a 2:1 biaxial stress field. The constants C and μ for the materials tested in Reference 50 were found to be equal and can be computed from pressure cylinder fracture data.

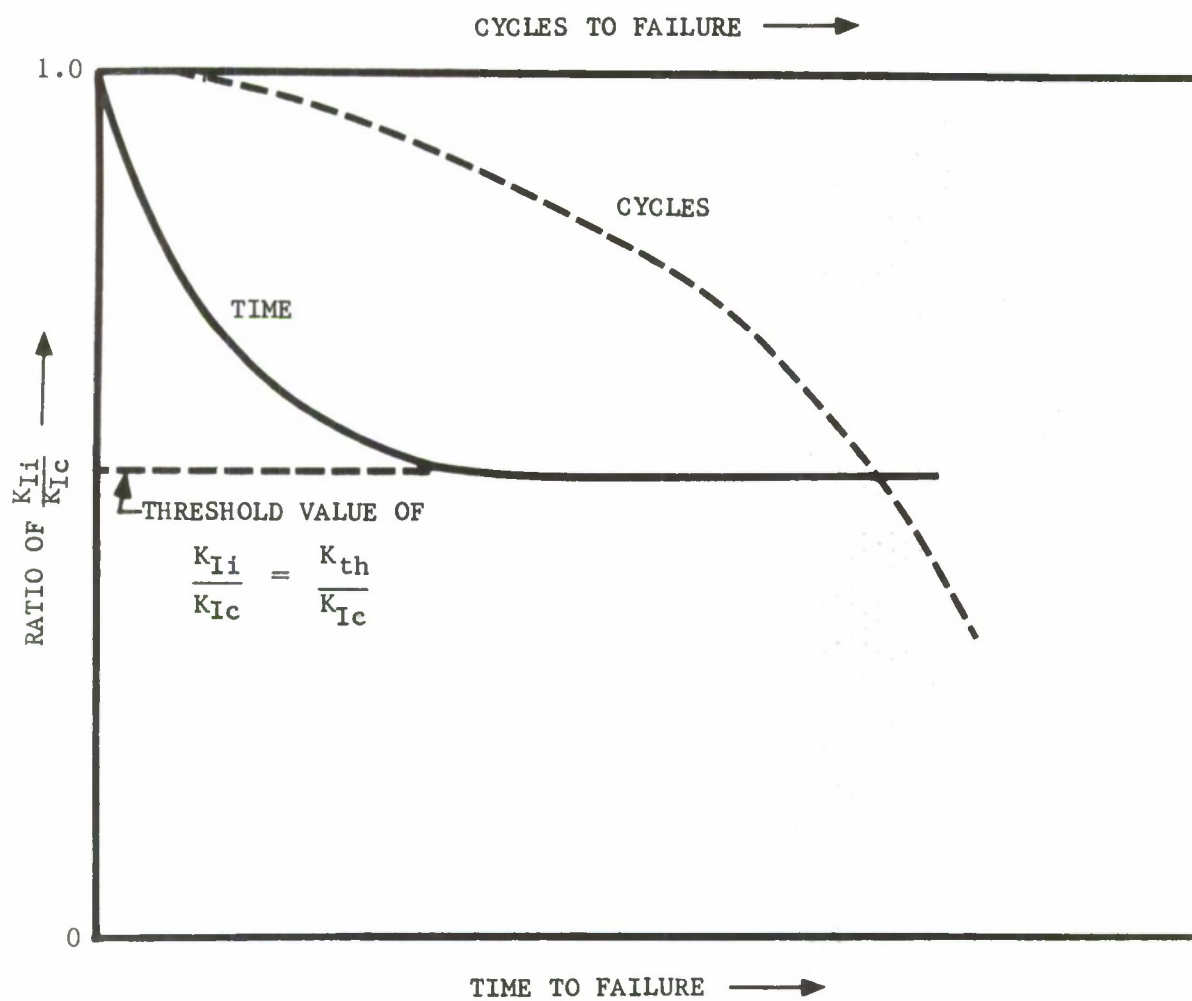


FIGURE 56 SCHEMATIC OF STATIC AND CYCLIC FLAW GROWTH FOR A GIVEN ENVIRONMENT (REF. 42)

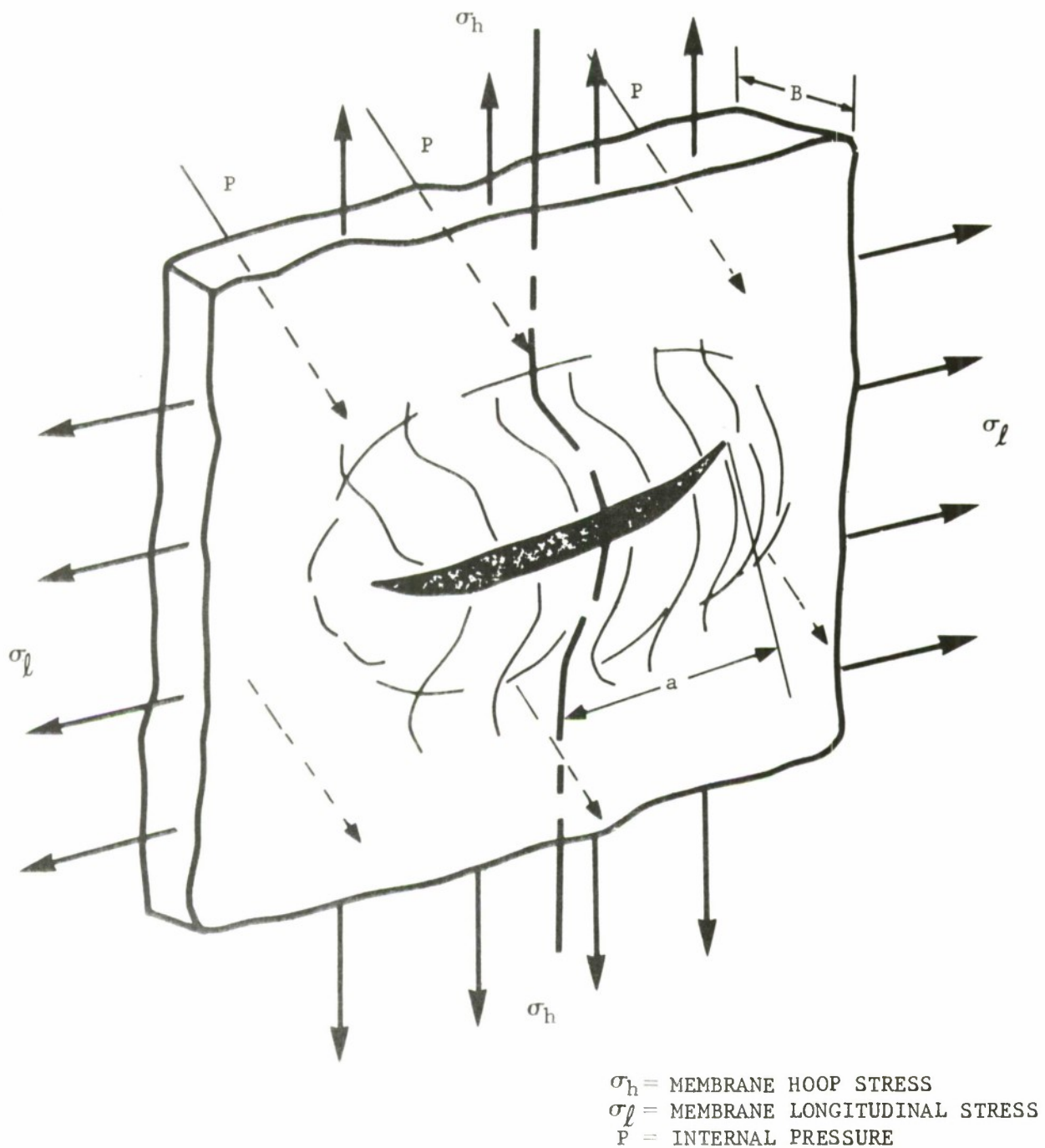


FIGURE 57 CRACK GEOMETRY & STRESS SYSTEM FOR PRESSURIZED CRACK WITH PRESSURE BULGING (REF. 50)

Thus, for critical conditions, $a \rightarrow a_c$, $K \rightarrow K_c$ and $\sigma_h \rightarrow \sigma_{hc}$ the bulge coefficient C is

$$C = \mu = \frac{R}{a_c} \left[\frac{\frac{K_c}{\sigma_{hc}}}{\pi a_c + \frac{K_c^2}{2 \sigma_{yB}^2}} - 1 \right] \quad (\text{IX-12})$$

Rearranging terms and solving for the critical hoop stress (σ_{hc}) for critical conditions

$$\sigma_{hc} = \frac{K_c}{\sqrt{\pi a_c + \frac{K_c^2}{2 \sigma_{yB}^2} \left(1 + C \frac{a_c}{R} \right)}} \quad (\text{IX-13})$$

or

$$\sigma_{hc} = \frac{K_c}{\sqrt{\pi a_o + \frac{K_c^2}{2 \sigma_{yB}^2} \left(1 + C \frac{a_o}{R} \right)}} \quad (\text{IX-14})$$

based on knowledge of the original crack length, a_o , only. In this case, K_c is the nominal plane stress fracture toughness of the material obtained from flat sheet fracture tests.

In equations IX-13 and IX-14 the geometric correction is $\lambda = (1 + C \frac{an}{R})$. Values of the bulge coefficient C , based on original crack length a_o , as given in Reference 50 are repeated in Table XVI. It should be pointed out that C was empirically determined in Reference 50 and its dependence on temperature or material is not clearly understood.

TABLE XVI
VALUES OF BULGE CORRECTION AT TEMPERATURE FOR VARIOUS MATERIALS
(DATA FROM REF. 50)

Material	Test Temperature	Bulge Correction (C)
2014-T6	Room	6.4
2014-T6	-320°F	3.5
2014-T6	-423°F	2.9
<hr/>		
Ti-5Al-2.5 Sn (ELI)	-320°F	4.3
Ti-5Al-2.5 Sn (ELI)	-423°F	1.6
<hr/>		
2024-T3	Room	9.5
<hr/>		
7075-T6	Room	9.5

IX.15(a) Example Problem

Compare the critical hoop tension fracture stress (σ_{hc}) for a 20-inch diameter pressure bottle which can withstand a 1/2-inch long crack without leaking catastrophically or bursting for two materials which are being considered, 2014-T6 ($\sigma_{ys} = 68$ ksi) and 7075-T6 ($\sigma_{ys} = 77$ ksi) aluminum. The material thickness is 0.060 inch for the 2014-T6 and 7075-T6 cylinders, with nominal \bar{K}_C of 58.4 ksi $\sqrt{\text{inch}}$ for 2014-T6 aluminum and \bar{K}_C of 85 ksi $\sqrt{\text{inch}}$ for the 7075.

Using the bulge corrections from Table XVI and Equation (IX-14), determine the critical hoop tension stresses. (The biaxial yield strength from Von Mises yield criteria can be assumed to be $\sim 1.15 \sigma_{ys}$ -- see Ref. 50.)

$$\begin{aligned}
 \text{2014-T6} \quad \sigma_{hc} &= \frac{58.4 \text{ ksi}\sqrt{\text{inch}}}{\sqrt{\pi \frac{0.5 \text{ inch}}{2} + \frac{(58.4 \text{ ksi}\sqrt{\text{inch}})^2}{2 [1.15 (68 \text{ ksi})]^2} \left(1 + 6.4 \left[\frac{0.5 \text{ in.}}{2} \right] \right)}} \\
 &= 48.8 \text{ ksi}
 \end{aligned}$$

$$\begin{aligned}
 \text{7075-T6} \quad \sigma_{hc} &= \frac{85 \text{ ksi}\sqrt{\text{inch}}}{\sqrt{\pi \frac{0.5 \text{ inch}}{2} + \frac{(85 \text{ ksi}\sqrt{\text{inch}})^2}{2 [1.15 (77 \text{ ksi})]^2} \left(1 + 9.5 \left[\frac{0.5 \text{ in.}}{2} \right] \right)}} \\
 &= 61.5 \text{ ksi}
 \end{aligned}$$

The 7075-T6 material would be a better choice on a fracture stress basis, or a fracture stress to biaxial ratio, $\frac{\sigma_{hc}}{\sigma_{yB}} \sim 0.7$ compared to 0.6 for the 2014-T6 material.

Recently, the authors of Reference 51 have compared the various methods available to fracture analyze pressurized, through-the-thickness cracks. This analysis included the data obtained in Reference 50. Better correlation was obtained if a criteria was set on the crack tip plasticity. The general form of the equation presented in Reference 51 for long cracks is,

$$\sigma_{hc} = \frac{K_c}{\sqrt{\pi a \gamma} \sqrt{\zeta}} \quad (\text{IX-15})$$

where γ is a plasticity correction and ζ is the magnification factor applied to hoop stress which provides nominal stress values so comparisons can be made with flat panel fracture behavior. In this case, the K_c value is obtained from a pressure vessel burst test. Hahn, et. al., (51) have proposed that for "thin" wall, low to intermediate toughness vessels, with relatively long cracks (i.e., rocket tankage and pressure fuselages) ζ can be expressed as

$$\zeta = \sqrt{1 + 1.61 \frac{a^2}{R^2} \left(50 \tanh \frac{R}{50B} \right)}$$

The plasticity correction γ is given by

$$\gamma = \left(\frac{\pi \sigma_{hc} \zeta}{2 \bar{\sigma}} \right) \ln \left[\sec \frac{\pi \sigma_{hc} \zeta}{2 \bar{\sigma}} \right] \quad (\text{IX-16})$$

In Equation IX-16, $\bar{\sigma}$ is the average flow stress and is not precisely defined. The upper and lower bounds are given as $\sigma_{ys} < \bar{\sigma} < \sigma_u$.

Other fracture equations for intermediate thickness vessels with long and short crack situations (e.g., steel pipe lines and pressure vessels operating at low temperatures) are presented in Reference 51.

IX.16 APPLICATION TO REINFORCED PRESSURE CYLINDERS

In pressurized fuselage structure, the analysis of References 50 and 51 which were just presented, can be seen to have direct application. The primary loads on these structures are the membrane hoop tension due to cabin pressurization, and bending loads from maneuver, gust, landing and take-off. From Equation IX-10, (Reference 50) the crack bulging correction, $\left[1 + C \frac{B}{R} \left(\frac{a}{B} \right)^\mu \right]$ is seen as a crack geometry correction, λ , which can be treated in the same manner as other geometric corrections. For example, it would be possible to

analyze riveted skin-stringer fuselage section designs where reduction due to pressure bulging would occur due to sudden puncture. Methods employed earlier in this section to obtain composite correction factors for skin-stringer designs could then be used in combination with the bulge factor. Thus, pressurization effects can be accounted for in calculating fracture stress envelopes. For large fuselage diameters (i.e., $R \gg a$), it can be seen that the bulge correction factor $(1 + C \frac{a}{R})$ approaches 1.0 or infinite plate behavior. However, in failsafe analysis, long crack lengths are common and the reduction in fracture stress due to crack bulging can be extensive (depending on material) and should enter into the overall fracture mechanics analysis.

IX.17 CRACK ARREST

A frequent objective in structural design is to provide some technique for limiting or arresting crack growth so that catastrophic failure can be prevented. Requirements for fail-safe structure necessitate the development and application of such techniques.

There are two ways in which it can be attempted to arrest a running crack; one material oriented, the other by structural design considerations. Both of these approaches have one thing in common, that is reducing the stress (and, therefore, stress intensity) near the crack tip. Material changes which lead to higher toughness materials can assist in making crack arrest easier. However, when a material's higher toughness is combined with designs which incorporate structural members in a redundant load carrying structure, the optimum possibility of crack arrest is achieved (see Section III).

There is a popular and effective concept frequently employed in commercial aircraft design, which utilizes crack stoppers or tear straps at strategic points in a load bearing structure. These straps of thin gage aluminum or titanium are normally adhesively bonded to the main structure. In principle, they act as a point of stress redistribution for an advancing crack. The increase in effective thickness due to the layering effect is accomplished with no loss in fracture toughness. In other words, the fracture toughness of the layered structure is on the order of the one layer itself and does not change with layering thickness (see, i.e., Reference 52). Geometrical boundaries (splices, etc.) also aid in arresting a running crack and are often employed as crack arrest barriers.

Reference 53 contains a description of the crack arrest problem and summarizes the research which has been performed in this area. The crack arrest problem in riveted sheet-stringers is analyzed in Reference 54. Additional sources can be located in the Bibliography of this report.

IX.18 FRACTURE OF COMPOSITES

Research into the fracture of composite materials has been limited until recently (see, for example, References 55 and 56). However, with the greater employment of these materials in aerospace structural applications, additional data will become available on both crack propagation and fracture strength which can be used in design. In general, it is known that the fracture process in fiber composites is discontinuous. The ductile matrix material tends to aid in crack branching along the fiber at the fiber/matrix interface and leads to increasing the overall fracture strength in uniaxial tension loading parallel to the fibers.

X FATIGUE AND CRACK PROPAGATION

X.1 INFLUENCE OF FATIGUE ON FRACTURE

As mentioned in earlier sections of this report, fracture mechanics assumes the preexistence of flaws, inhomogenities and discontinuities in a material. It is from these flaws that cracks often nucleate and grow under cyclic load. The prediction of crack nucleation is beyond the scope of this report; however, it must be recognized that any local geometric, physical or metallurgical feature which intensifies the stress is a prospective site for fatigue.

During stress or strain cycling of a material, there is a "shake-down" period of a few number of cycles (dependent on magnitude) during which the material will cyclic harden or soften. (57) For a period of time, the crack will nucleate and then grow by stages. (58) In fracture mechanics we are interested in the propagation of engineering cracks of detectable size. The prediction of crack growth is discussed later in this section.

X.2 MICRO-MECHANICS

It is possible, from microfractography, to determine not only the site of fatigue but the subsequent stress history as long as the plastic zone is small at the crack tip. This is usually the case in high cycle fatigue and/or brittle material which produce flat (plane strain) type fracture surfaces. An example of an electron microscope fractograph taken from an area on a 7075-T6 aluminum fracture surface where a crack has grown is shown in Figure 58. The direction of crack propagation is indicated by the arrow. The rippled appearance (striations) is the result of successive fatigue cycles, and the distance between successive striations can give a measure of the crack growth rate (per cycle). Through the use of fracture mechanics, it is then possible to determine operating stress and cycles to fracture. The Bibliography of this report lists documents which should be consulted for additional information.

X.3 FRACTURE MECHANICS AND CYCLIC CRACK GROWTH

In order to establish a method of inspection intervals for aircraft structure, it would be desirable if a means were available to predict successive crack lengths during service history. During preliminary design, it would be helpful if a method of material comparison (in addition to conventional S-N data) were used to rank material on the basis of cyclic crack growth resistance. For example, it has been shown (Refs. 59-62) that the stress intensity factor is a good correlating factor for crack propagation under fluctuating as well as static loading.

It was previously indicated that microscopic crack propagation takes place on a cyclic scale in tune with the fluctuating load or stress. On this basis, it is reasonable to assume that incremental crack extension (Δa) in a small number of cycles (ΔN) is related to the slope (derivative) of the continuous crack length (a) vs. cycle (N) curve, $\frac{\Delta a}{\Delta N} = \frac{da}{dN}$.

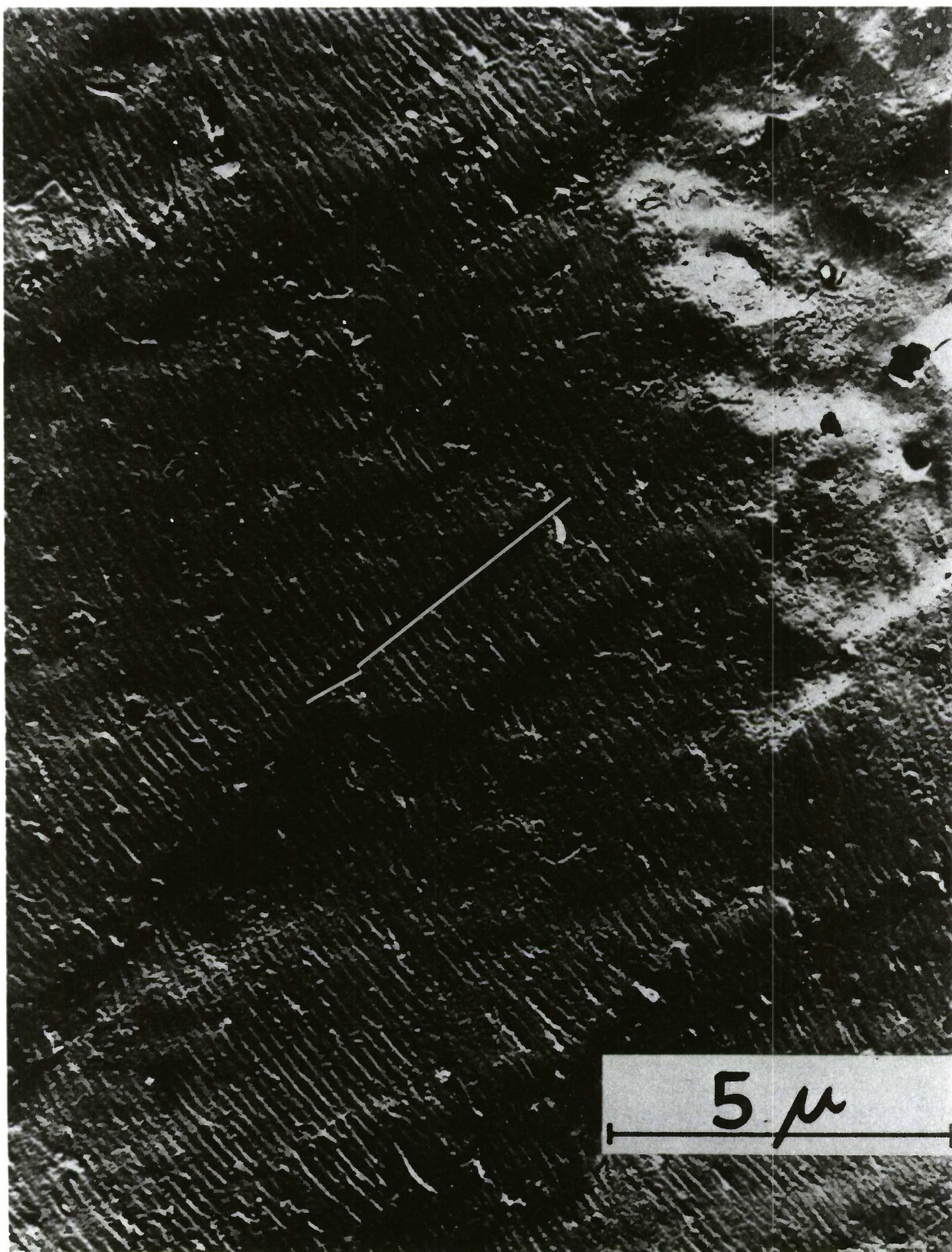


FIGURE 58 ELECTRON FRACTOGRAPHIC OF FATIGUE
AREA ON 7075-T6 ALUMINUM PLATE

The growth rate $\frac{da}{dN}$ is a function of (1) Material, (2) Environment, (3) Load-Time History, and (4) Geometry, including crack. Stress intensity can describe items 3 and 4 with a single parameter, K . The two remaining items will be discussed later. Paris⁽⁶²⁾ showed that the stress intensity factor (K) describes the effect of external load and crack geometry for cyclic crack growth. For this reason, he showed that $\frac{da}{dN} = f(K)$. Since K is a linear factor in the elastic stress equations, it depends on the load or stress magnitude and crack length in a linear fashion. If $K(t)$ and $\sigma(t)$ are time history of load (stress) and stress intensity, and if the crack length varies slowly with time (t), the local crack tip stress intensity history is $K(t) = P(t) \cdot f(a)$ ⁽⁶²⁾. In terms of stress for a center crack (infinite) plate (see Eqs. V-25), $K(t) = \sigma(t) \cdot \sqrt{\pi a}$.

Therefore, the time dependent character of fatigue crack growth can be expressed as

$$\frac{da}{dN} = K(t) \quad (X-1)$$

The reason that fracture mechanics analysis has shown greater applicability to fatigue crack propagation is due to the conditions for fatigue being less than critical. In other words, the fatigue cracking process involves stress levels and crack lengths (hence, K 's) below the static, critical values. Work hardening during cyclic loading raises local (crack tip) yield strengths and produces small yield zones (see, e.g., Equation VI-2). Therefore, elastic stress field solutions are more directly applicable due to smaller plastic zones.

X.4 SINUSOIDAL LOADING

In fatigue testing, sinusoidal loading is quite common. $K(t)$ local to the crack is then a sine wave about some mean value of K and variations in K can then be generally described by a sinusoidal amplitude, a mean, and frequency.

Many equations have been proposed for the prediction of fatigue crack growth based on fits to empirical data (Bibliography). These equations appear to be valid as long as they are applied within the test limits and conditions from which they are derived. In 1963, Paris and Erdogan⁽⁶⁰⁾ reviewed existing crack propagation equations and from a wide range of test data proposed that a best fit might be:

$$\frac{da}{dN} = \frac{1}{C} (\Delta K)^n, \quad (X-2)$$

where C is a material constant and ΔK is the stress intensity factor range ($K_{\max.} - K_{\min.}$). Equation X-2 suggests a straight line data fit, with $n = 4$ for $\log \Delta K$ vs. $\log da/dN$. With this relationship, numerous researchers attempted correlations based on Equation X-2 (see, e.g., Reference 63), but it became obvious that a single equation could not account for large differences in fatigue stress ratio. To account for this parameter, the authors of Reference 64 presented equation X-3 as a better data fit which would account for stress ratio effects and apply to the point of fracture.

$$\frac{da}{dN} = \frac{C(\Delta K)^n}{(1-R) K_c - \Delta K} \quad (X-3)$$

In 1967, Hudson⁽⁶⁵⁾ empirically compared equation X-3 with other equations for crack growth and concluded that it represented the data quite well. Some data from Reference 65 has been abstracted and is shown in Figure 59 for 7075-T6 and 2024-T3 aluminum alloy sheet tested at two cyclic stress ratios.

However, it must be pointed out that environmental, metallurgical, multi-axial stress and frequency effects appear only as lumped parameters in the material constant (C) and numerical exponent (n) of equations X-2 and X-3. (Typical values of C and n for 7075-T6 and 2024-T3 are shown in Figure 59.) The individual effect of these parameters on fatigue crack propagation have not as yet been separated.

X.5 RANDOM LOADING

Crack propagation data from random load tests have indicated that correlation on a stress intensity basis is not only feasible but adequately describes the crack growth for such loading (see, for example, Reference 62). The data of Swanson⁽⁶⁶⁾ on 7079-T6 aluminum indicates that fracture mechanics was the most effective approach to analyzing crack propagation for both constant amplitude and Rayleigh, random amplitude loading.

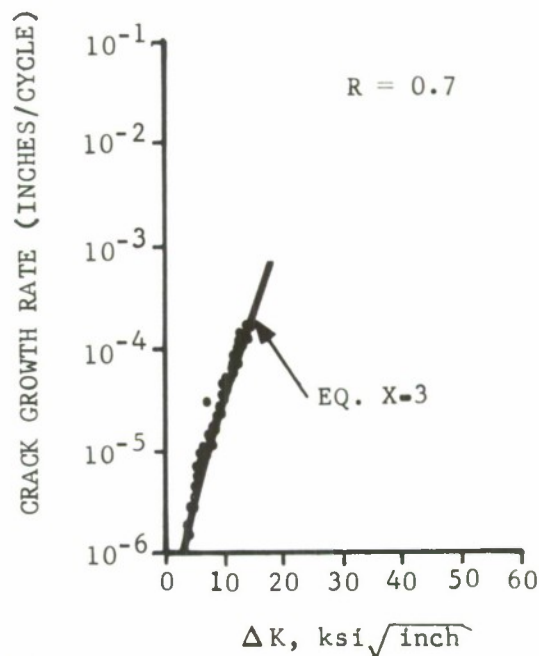
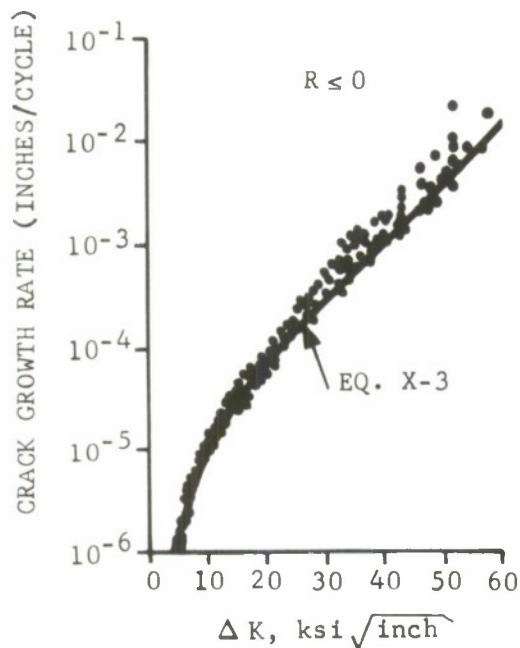
X.6 PREDICTION OF CRACK GROWTH TO FRACTURE IN DESIGN

Estimates can be made of crack growth or extension using Equation X-2 or X-3. For uniform, sinusoidal loading in a plate (small crack lengths) integration of Equation X-3 was suggested by Forman,⁽⁶⁴⁾ et. al., to compute cycles to failure for a given fatigue crack,

$$N_c - N_o = \frac{2}{\pi C (1-R)^2 \sigma^2} \left[\frac{K_c}{K_o} - 1 - \ln \frac{K_c}{K_o} \right], \quad (X-4)$$

where N_c is the critical value of cycles at crack instability, N_o is the initial value of cycles, and K_o is the initial crack tip stress intensity, i.e., $f(a_o)$.

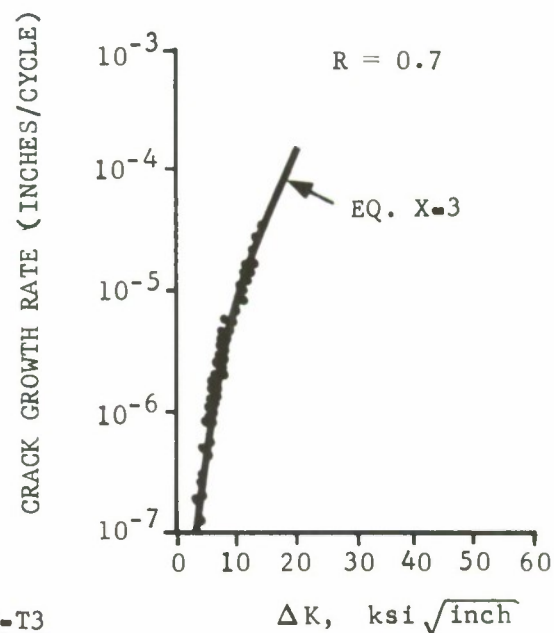
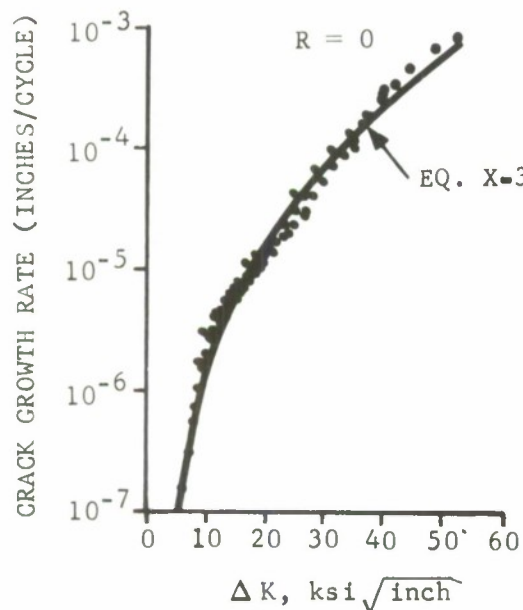
We will examine a problem in crack growth in two ways, growth to fracture and cycles to crack detection.



7075-T6

CONSTANTS FOR
EQUATION X-3

$C = 2.13 \times 10^{-13}$
 $n = 3.21$



2024-T3

CONSTANTS FOR
EQUATION X-3

$C = 3.22 \times 10^{-14}$
 $n = 3.38$

FIGURE 59 TYPICAL CRACK GROWTH VS STRESS INTENSITY FACTOR RANGE
DATA FOR 7075-T6 & 2024-T3 ALUMINUM (DATA FROM REF. 65)

X.6(a) Example Problem

A corner crack has developed at the top surface of a bolt hole in the part shown in Figure 60. The plate thickness, B, is 1 inch and the material is a 100 ksi yield strength alloy steel. The plane strain fracture toughness (K_{IC}) is assumed to be $130 \text{ ksi}\sqrt{\text{inch}}$. The operating cyclic stress of the part in question is sinusoidal with a maximum stress of 70 ksi and a minimum of 1.4 ksi (R of 0.02).

Question: Assume that a 0.3 inch deep, semi-circular crack grows under the bolt heat, how many cycles will it take for the crack to grow through to the back surface (through the plate thickness)? Also, how many cycles will be allowed before critical conditions prevail, assuming that the crack changes from a semi-circular to a straight front-through the thickness crack after penetrating the thickness.

STEP 1. To answer the first part of the question, it is necessary to assume that the crack depth (a_c) is reached when the crack grows through the plate thickness. Thus, when the crack length a_c is 1 inch, compute a critical K_I or K_Q . From Equation VII-7 when $K_I \rightarrow K_Q$ with $\frac{B}{a_c} = 0$:

$$\begin{aligned} K_Q &= 0.705 \sigma \sqrt{\pi a_c} \quad , \\ &= 0.705 (70 \text{ ksi}) \sqrt{\pi (1 \text{ inch})} = 87.5 \text{ ksi}\sqrt{\text{inch}} \end{aligned}$$

Using Equation X-4, solve for the number of cycles for the initial crack (0.3 inch) to grow through the thickness (1 inch), where K_Q is $87.5 \text{ ksi}\sqrt{\text{inch}}$. Values of the constant, C, have not been reported for this constructional steel, but we may assume that it is on the order of 10^{-13} (see, e.g., Figure 59 and Refs. 64 and 65 for aluminums).

$$\begin{aligned} N_c &= \frac{2}{\pi 10^{-13} (1-0.02)^2 (70,000 \text{ psi})^2} \left[\frac{87,500 \text{ psi}\sqrt{\text{inch}}}{0.705 (70,000 \text{ psi}) \sqrt{\pi (0.3 \text{ inch})}} - 1 \right. \\ &\quad \left. - \ln \frac{87,500 \text{ psi}\sqrt{\text{inch}}}{0.705 (70,000 \text{ psi})^2 \sqrt{\pi (0.3 \text{ inch})}} \right] \end{aligned}$$

$$N_c = 303 \text{ cycles.}$$

STEP 2. The second question can be answered by using Equation X-4 and the applicable stress intensity solution and elastic magnification factor for a through crack at hole (Equation VII-10) where $a = a_c = 1 \text{ inch}$ and $r = 0.25 \text{ inch}$. In this case, $f\left(\frac{a}{r}\right) = 0.75$ (see Equation VII-10). Compute N_c :

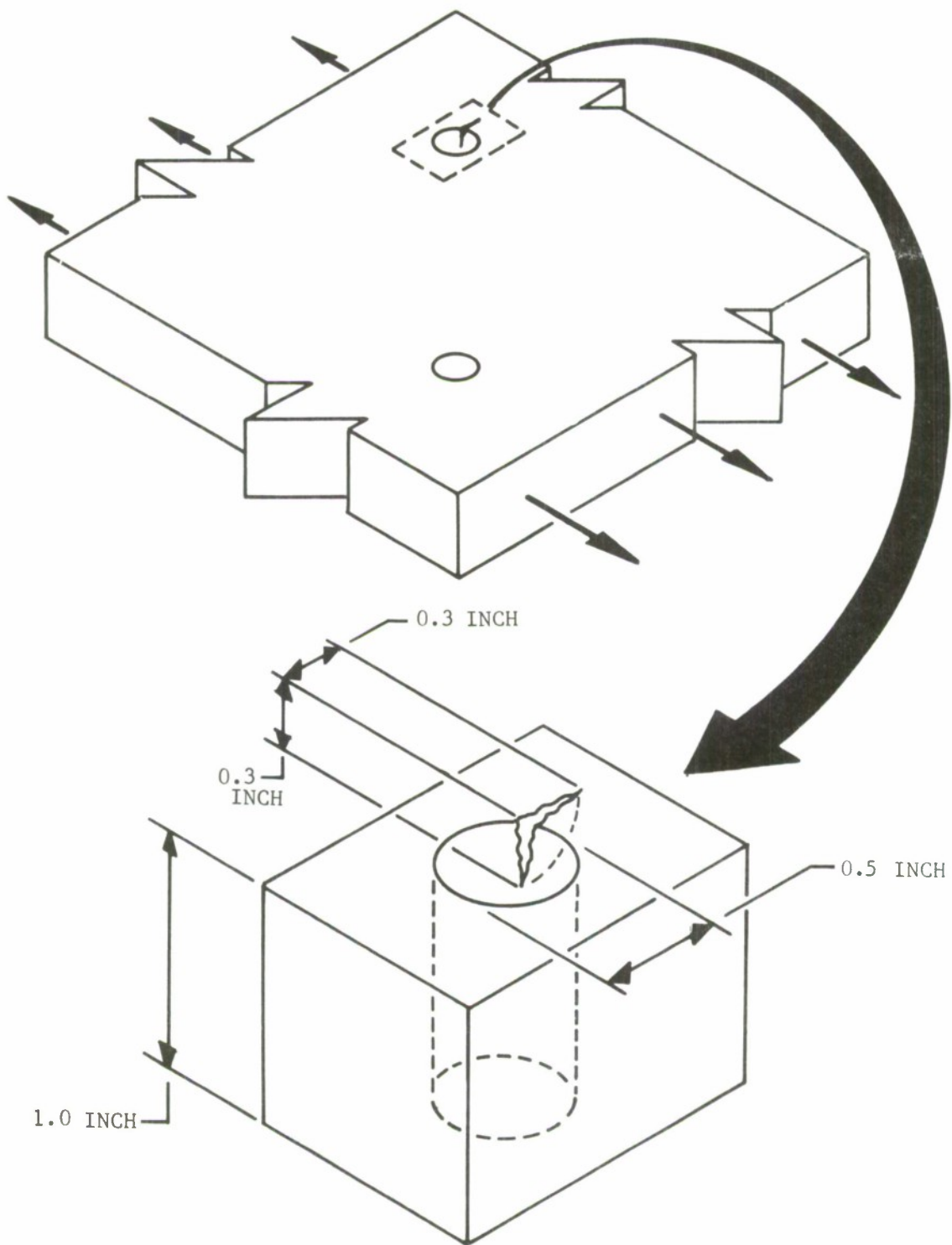


FIGURE 60 EXAMPLE PROBLEM - CORNER CRACK AT BOLT HOLE LOADED IN TENSION

$$N_c = \frac{2}{\pi 10^{-13} (1-0.02)^2 (70,000 \text{ psi})^2} \left[\frac{130,000 \text{ psi} \sqrt{1 \text{ inch}}}{0.75 (70,000 \text{ psi}) \sqrt{\pi (1.0 \text{ inch})}} - 1 \right. \\ \left. - \ln \frac{130,000 \text{ psi} \sqrt{1 \text{ inch}}}{0.75 (70,000 \text{ psi}) \sqrt{\pi (1.0 \text{ inch})}} \right]$$

$$N_c = 84.8 \text{ cycles.}^*$$

Thus, for a sinusoidal loading condition of 70 ksi maximum stress, the 0.3 inch corner crack at a bolt hole will grow through the plate in ≈ 300 cycles, and will approach critical conditions in 385 cycles. In an aircraft application, this would mean that approximately 85 cycles of life remain prior to fracture, once the crack completely penetrates the plate.

Equation X-2 can be used in conjunction with graphical integration to obtain load (stress) or K vs. crack growth curves for particular problems. A good review of this procedure is contained in Reference 67, where predictions of crack growth rate using fracture mechanics principles are outlined and compared with data from simulated tests.

X.7 ENVIRONMENTAL AND LOAD HISTORY EFFECTS

If environmental conditions prevail, it can be expected that the values of cyclic life will be reduced on the order of 20-30 percent for certain materials. There are data available on environmental crack growth which can be used to modify the predicted curves based on Equations X-2, X-3 (see Bibliography). It must be remembered that for varying load history, the order of integration is extremely important. To better illustrate the effect of load history on crack growth, refer to Figure 61. This is a typical representation of the delays in crack growth rate caused by the application of three successive cycle overloads during a sinusoidal load spectrum. Data of this type may be found in Reference 63.

Until the parameters which influence crack growth are fully understood, any estimates of service crack growth conditions must be considered as preliminary estimates only.

X.8 CRACK GROWTH DURING PRESSURE VESSEL PROOF TESTING

This special class of problems will not be explored in this report. For those who are concerned with this problem, an excellent summary of crack growth analysis for part-through cracks in pressure vessels is contained in Reference 42.

* It can be seen that critical conditions are being rapidly reached ($87.5 \text{ ksi} \sqrt{1 \text{ inch}} \rightarrow K_{IC}$), and this value is not unexpected at the high σ_m .

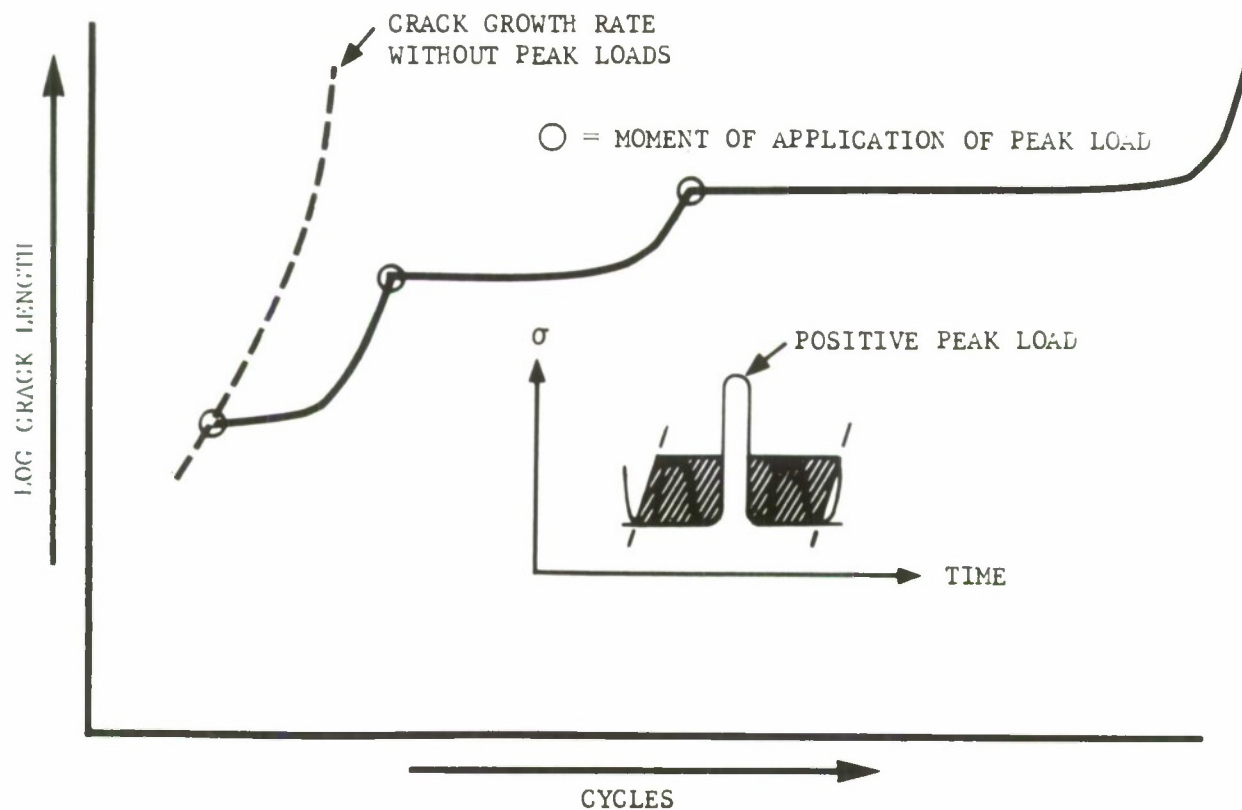


FIGURE 61 SCHEMATIC OF DELAY IN CRACK GROWTH DUE TO STRESS OVERLOAD IN ALUMINUM ALLOYS (REF. 63)

XI ENVIRONMENTAL EFFECTS

XI.1 STRESS CORROSION CRACKING

The traditional measure of stress corrosion is based on the time-to-failure of a smooth specimen at different stress levels in the environment of interest. However, the effect of environment on crack initiation (production of pitting) and the slow growth of subsequent cracks cannot be separated. In design practice, the presence of crack or crack-like defects must be considered to occur in the structure. Thus far we have touched lightly on the effect of environments on static or fatigue crack growth and the role of stress intensity as a correlating parameter.* An example of the trend of dependence of crack growth on K is shown in Figure 62 for wedge open loaded specimens (K decreases with increasing a) from the data of Smith⁽⁶⁸⁾. Such crack growth is often referred to as sub-critical crack growth or delayed failure under environmental conditions.

Experimental measurement of sub-critical stress corrosion susceptibility involves the measurement of time-to-failure for precracked specimens at various load levels. By reducing the load (stress) in steps, a threshold level of K_I is reached below which no failure should occur. This K_I level is called K_{Isc} . The relationship between this environmentally determined threshold stress intensity (K_{Isc}) and the plane strain fracture toughness in air provides a measure of material stress corrosion susceptibility which can be used in material selection and design.

Data presentation for statically loaded specimens can take one or two forms as shown in Figure 63: the applied stress intensity or normalized (to K_{Ic}) stress intensity vs. time to failure. Comparisons of a "wet" and "dry" environment can be made in this manner.

XI.2 ENVIRONMENTAL FATIGUE CRACK GROWTH

The effect of environment on fatigue crack growth is best summarized by examining data reported by Hartman⁽⁶⁹⁾ on 2024-T3 clad material. In these data, the effect of a moist environment had a 10-fold influence on crack growth at low values of K over a "dry argon" reference environment. Trends for 2024-T3 shown in Figure 64 for two values of the stress ratio are typical for 7075-T6 also. In the presence of a saline or other more corrosive media, more drastic changes can be expected. As with delayed failure, the prediction of environmental fatigue crack growth is not a simple task, due to the many parameters which influence fatigue and compounded by the presence of environmental effects.

* It bears repeating that the crack tip stress intensity will represent the driving force with reasonable accuracy in materials which exhibit limited plasticity. Actual cases must be verified by experimental results.

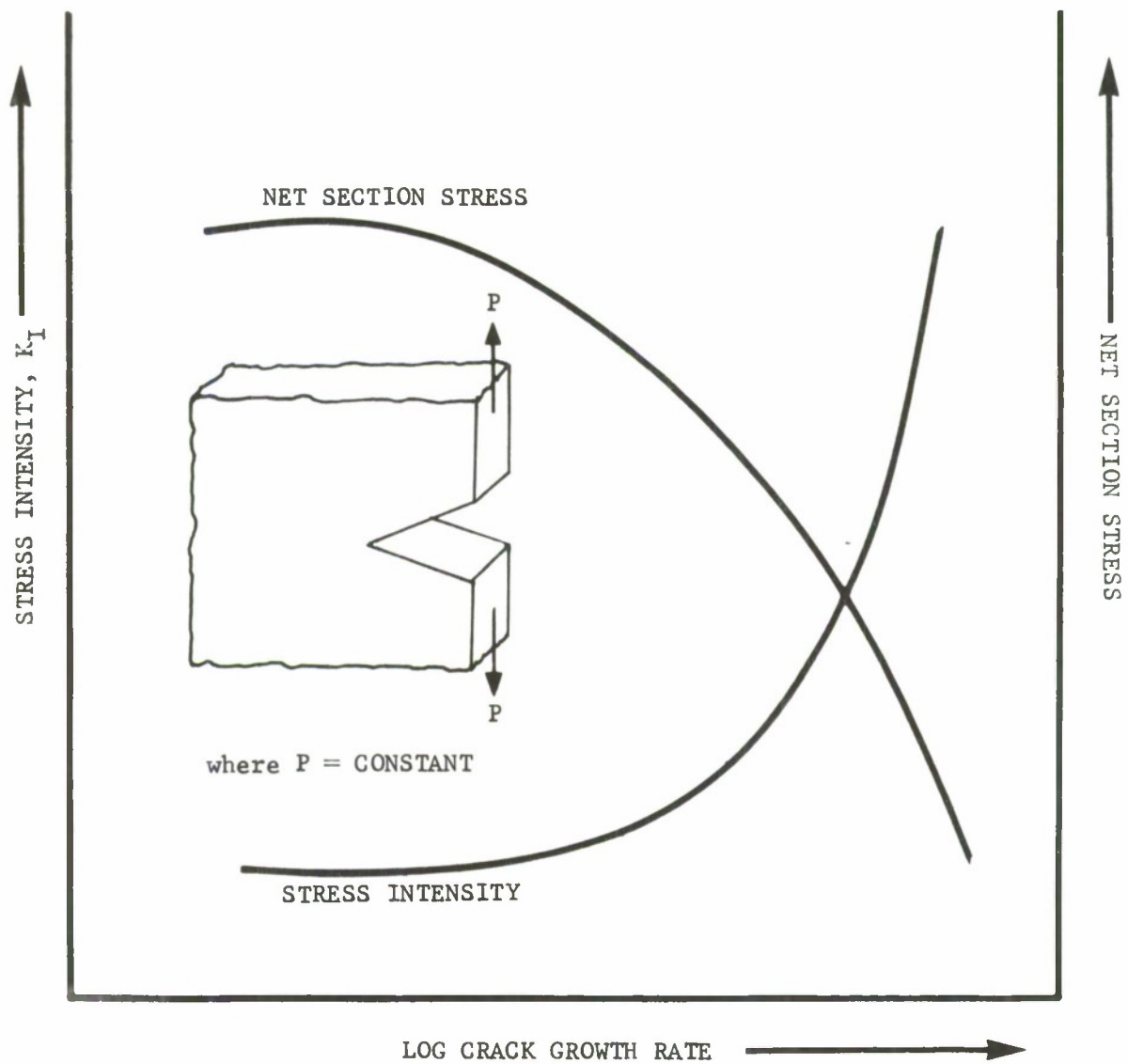


FIGURE 62 TYPICAL BEHAVIOR OF NET STRESS AND K_I FOR A WEDGE FORCE-LOADED SPECIMEN

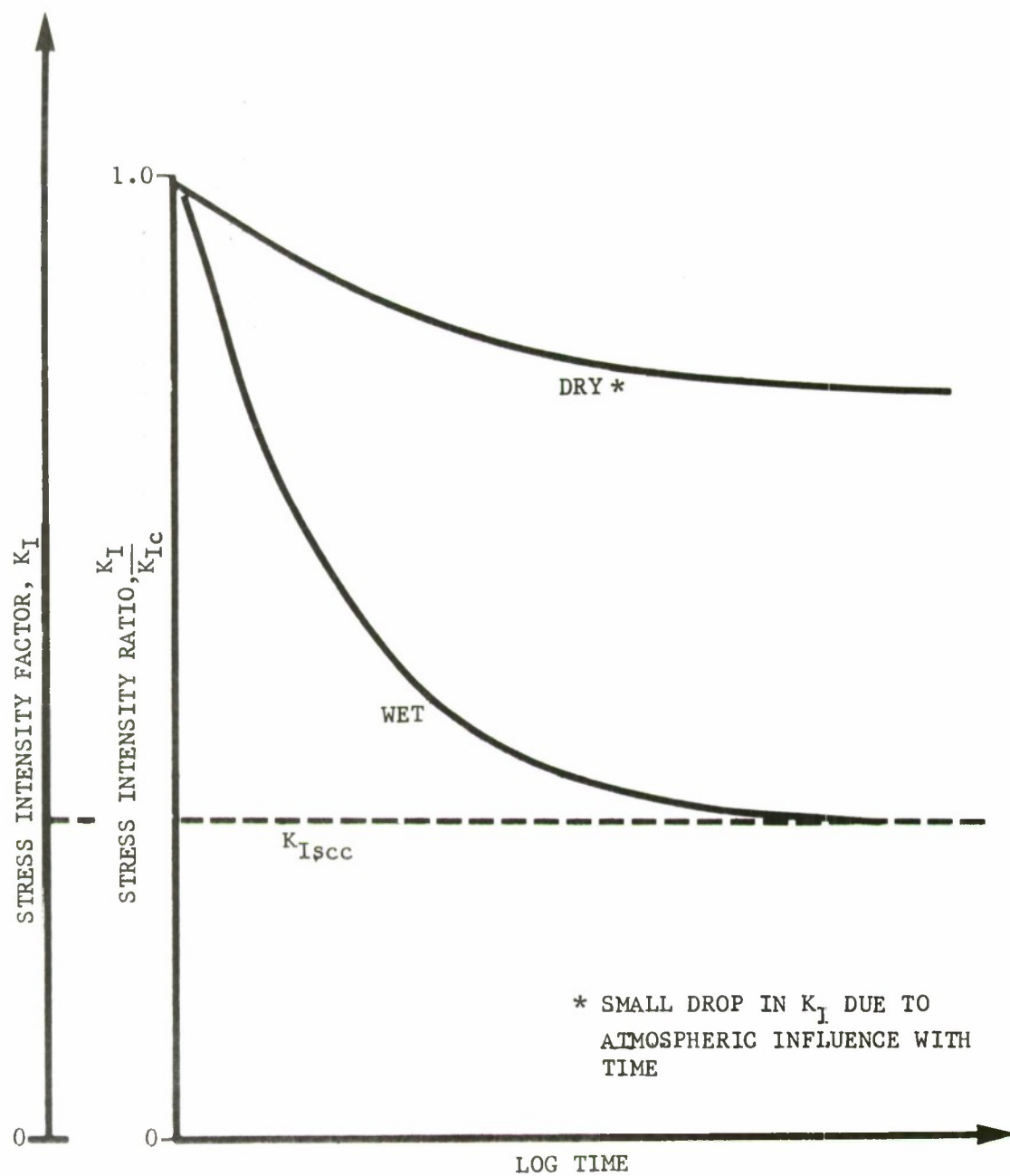


FIGURE 63 DELAYED FAILURE DUE TO ENVIRONMENTAL CRACK GROWTH

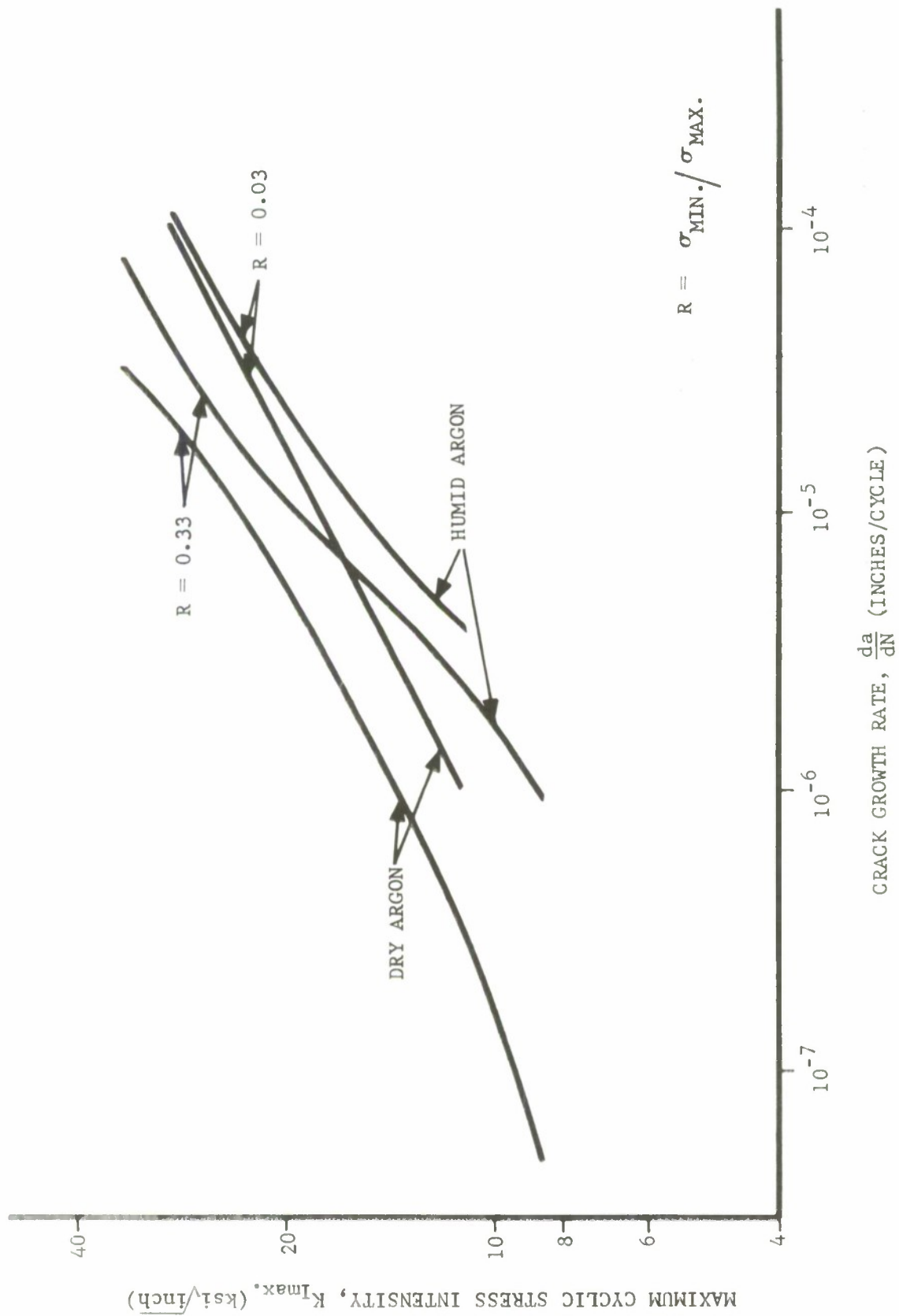


FIGURE 64 THE EFFECT OF MOISTURE ON FATIGUE-CRACK GROWTH IN A CLAD 2024-T3 ALUMINUM ALLOY (REF. 69)

XI.3 TEMPERATURE AND STRAIN RATE EFFECTS ON CRITICAL K

The available data on temperature and strain rate effects indicates in general that the lower strength materials such as structural steels can be expected to exhibit a sensitivity to these parameters. These materials have received more definitive examination due to their pronounced changes in strength and toughness with temperature and strain rate.

If it is suspected in design that temperature and/or high strain rates will be operative, it would be expedient to determine the critical stress intensities for maximum or minimum temperature and strain rates of interest.

In some applications, thermal cycling may occur during service (e.g., supersonic aircraft), which also should be considered in the evaluation of fracture criteria.

XI.4 SUMMARY

To insure satisfactory results from a fracture mechanics evaluation of a specific design, the critical stress intensity for the environment of interest should be determined. Environment enhanced crack growth can be correlated by the use of stress intensity for sub-critical crack growth and fatigue crack propagation. For those interested in the application of fracture mechanics to stress corrosion cracking and the current limitations, a good review is presented in Reference 70.

In the overall view of design against fracture, the role of environment cannot be avoided and must be represented in the analysis by modification to the critical stress intensity.

XII FRACTURE TESTING PROCEDURES

XII.1 FRACTURE TOUGHNESS TESTING

The objective of the fracture toughness test is to determine an accurate value of the critical stress intensity for the material in a given environment. Most of the historic effort has been expended in determination of the critical plane strain fracture toughness (K_{IC}). The following general comments apply to all specific types.

- . Specimen must contain a sharp fatigue induced crack.
- . Specimen must exceed minimum geometric dimensions (see e.g. Section VI).
- . Crack extension and loading must be accurately determined.

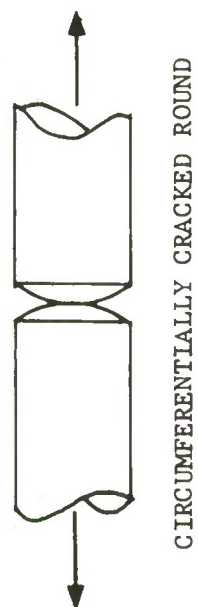
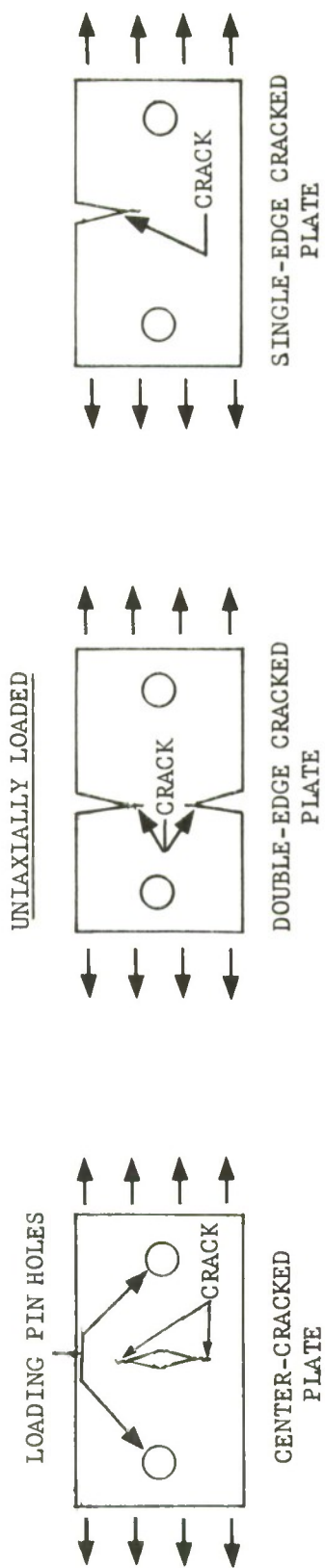
The details which are required to obtain K_{IC} data will not be covered in this report as documents are available which cover these items in great detail. (See Refs. 7, 8, and current ASTM proposed test method, Ref. 71).

At present, there is no standard test method for fracture toughness testing of thin gage materials which do not exhibit brittle like (plane strain) behavior. A special Task Force within Committee E-24 of the American Society for Testing and Materials has been established to study and eventually recommend standards for thin section fracture testing.

XII.2 PLANE STRAIN TOUGHNESS TESTING

Starting from the center cracked through the three point bend and compact tension, the evolution of plane strain fracture toughness specimens (K_{IC}) is shown in Figure 65. From this progression, two specimens, the bend and compact tension, have been proposed by ASTM (Ref. 71) as they have been shown to fulfill the requirements for valid and repeatable data.

Accurate measurements are made of both load and displacement through the use of autographic recording of test machine load and the displacement of two precisely located points above and below the crack. With the aid of suitable calibration curves of specimen displacement vs. elastic compliance established with the displacement gage in place, accurate measurements of crack extension are possible. A typical calibration curve is shown in Figure 66 in terms of relative crack extension for a center crack geometry. The specimen compliance $\left(\frac{vEB}{P}\right)$ is determined from the fracture test where v is the crack displacement, P is the load associated with displacement, and E and B are Modulus and specimen thickness, respectively. Any particular calibration applies to any other geometrically similar specimen with different Modulus or thickness. Thus, the information obtained from the autographic recording during the fracture test (see, for example, Figure 67) can be translated into stress/crack length and critical points established. With these critical points, the critical plane strain fracture toughness (K_{IC}) can be determined from the suitable stress intensity equation for the geometry and loading configuration. Many different types of load displacement curves are possible; for a further discussion see Reference 8.



PROPOSED SPECIMENS

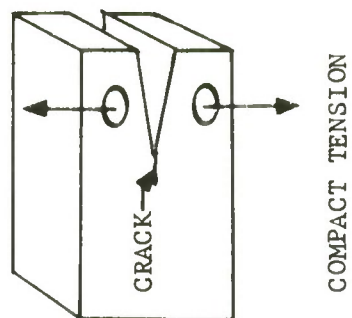
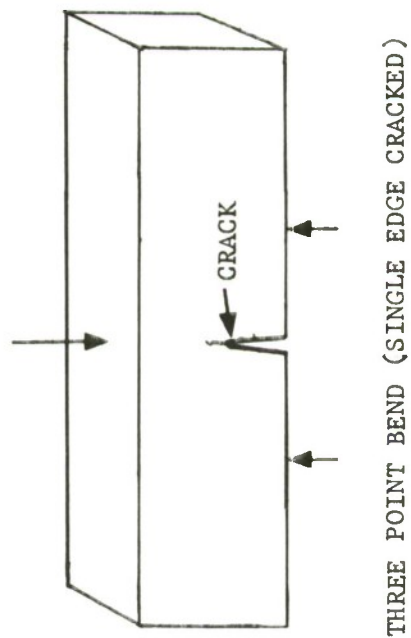


FIGURE 65 FRACTURE TOUGHNESS TEST SPECIMENS

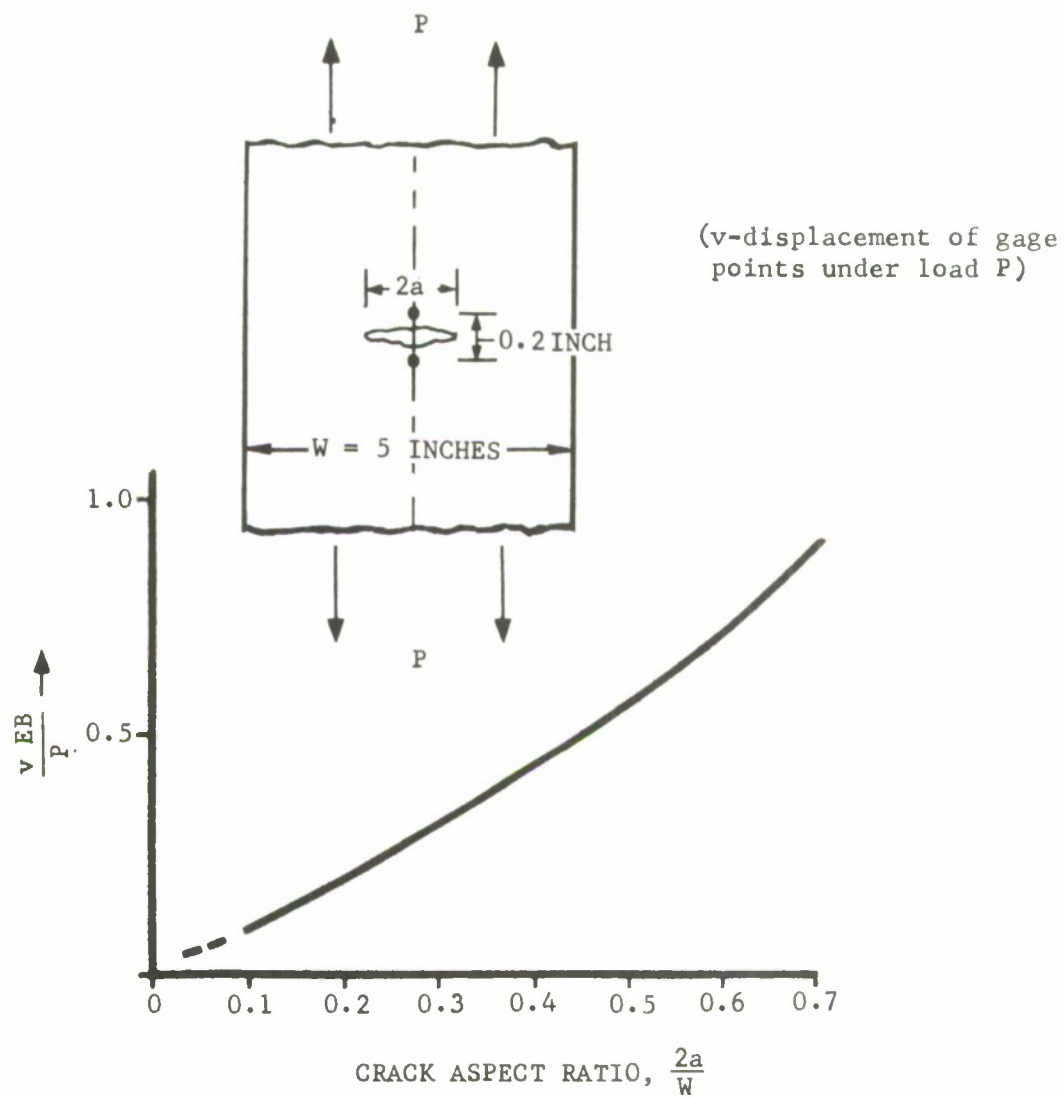


FIGURE 66 TYPICAL CALIBRATION CURVE FOR A CENTER CRACK GEOMETRY WITH 0.2 INCH GAGE POINT DISTANCE

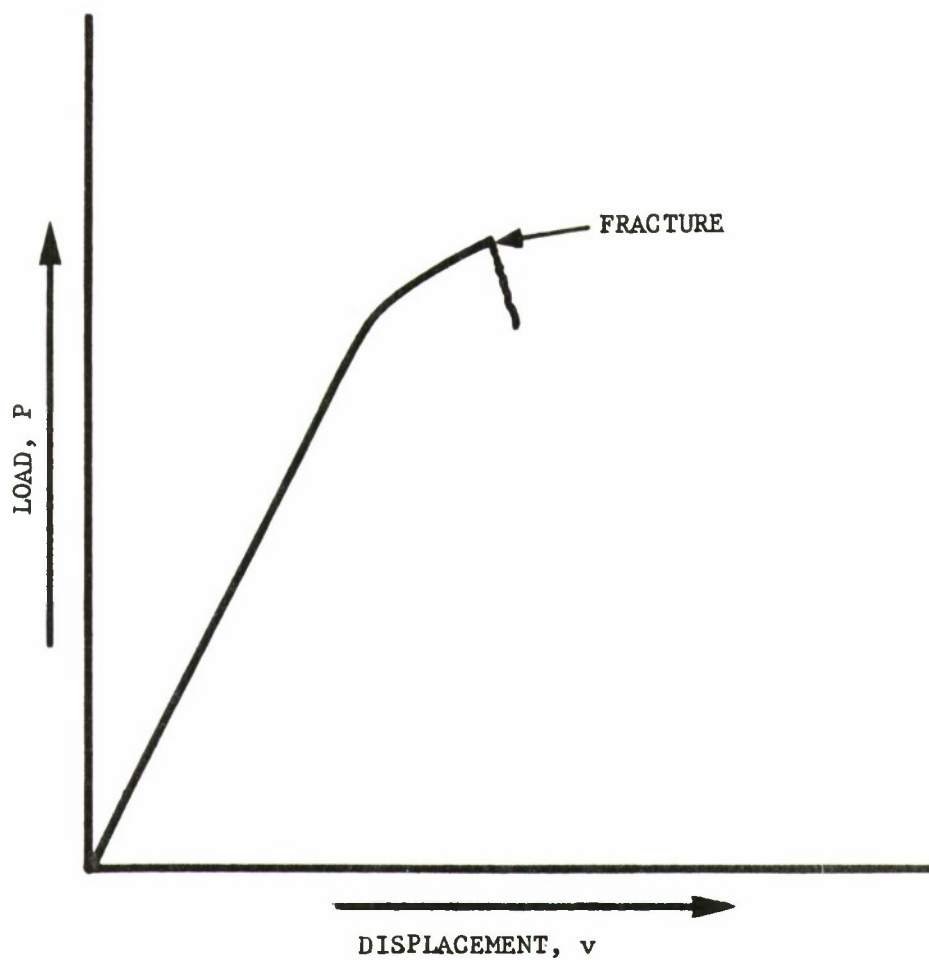


FIGURE 67 REPRESENTATION OF TYPICAL DISPLACEMENT GAGE-LOAD RECORD IN FRACTURE TOUGHNESS TEST

To obtain a valid value of plane strain fracture toughness, it is required that both the specimen thickness, B , and crack length, a , exceed 2.5 times the square of the ratio of plane strain fracture toughness to 0.2 percent offset yield strength (see equation VI-8). As shown in Section VI, this requirement sets plastic zone limits so that elastic fracture mechanics principles apply directly. One advantage of the displacement measurement of crack extension is that the value of crack length obtained includes both crack length and the increment due to plasticity. Therefore, approximate expressions for plasticity corrections need not be used.

With knowledge of the critical crack length and associated critical load, the critical stress intensity factor can be calculated for the crack geometry. This stress intensity is designated K_Q until such time as it is shown that all criteria of Reference 71 are met. Then, and only then, can this K_Q value be designated a valid plane strain fracture toughness value (K_{Ic}). Reference 71 describes the limitations, specimen design, and testing criteria required in plane strain fracture toughness testing and should be consulted for additional information.

XII.3 SOURCES OF PLANE STRAIN AND PLANE STRESS DATA

XII.3(a) Plane Strain (K_{Ic})

In evaluating reported plane strain fracture toughness data, it is imperative that a prime criterion, the relationship of Equation VI-8, be met. As a general rule, any data which has been taken using the proposed method (Ref. 71) can be considered as valid data as long as the limited plasticity of Equation VI-8 is fulfilled. Those organizations which are members of ASTM Committee E-24 or who follow the criteria of the proposed testing method can be used as sources for valid K_{Ic} data. Older data which does not meet this criteria must be considered as K_Q values and used only for the thickness and specimen geometry for the reported data.

XII.3(b) Plane Stress (K_c)

In general, data on K_c must come from specific tests employing the material, thickness, and specimen width for the intended application. The net section stress, at fracture, must not exceed 0.8 times the yield stress ($\sigma_{net} \leq 0.8 \sigma_{ys}$) and crack buckling must be restrained or accounted for in the analysis. The preceding are general criteria and must be considered as such until specific testing methods are available from ASTM Committee E-24.

It is recommended that those who are interested in further discussion of the fracture testing of metals consult References 7, 8, and 71.

XII.4 CRACK GROWTH RESISTANCE (R CURVE CONCEPT)

In Section II (Figure 1) the crack growth resistance concept of Irwin is depicted. Further discussions of this concept are contained in Reference 72 and 73. Krafft⁽⁷²⁾, et al, hypothesized that, neglecting environmental effects and with controlled testing, the crack growth resistance (resistance to crack extension) is primarily a function of absolute crack extension ($a_c - a_0$) and independent of initial crack length. This concept leads to many implications, such as uniqueness of R curves for materials, etc.

Recent research has shown that crack growth resistance offers a means of determining a critical plane stress fracture toughness, K_{IC} for (74) those thin materials whose fracture properties are highly geometric (width and original crack length) dependent. Thus, it is hoped that the crack growth resistance curve for a given material and thickness (again neglecting loading and environmental conditions) can be used to determine critical crack driving forces or stress intensities for specimens of other geometries. The results of Heyer and McCabe⁽⁷⁴⁾ are encouraging in this respect and bear further study as additional crack growth resistance data for various crack geometries becomes available.

REFERENCES

1. Griffith, A. A., "The Phenomena of Rupture and Flow in Solids," Phil. Trans. Royal Society, A221, 1920.
2. Irwin, G. R., "Fracture Dynamics," Trans. ASM 40A, 1948.
3. Orowan, E., "Fundamentals of Brittle Behavior in Metals," in Fatigue and Fracture of Metals, The Technology Press of M.I.T. and John Wiley and Sons, 1952.
4. Irwin, G. R., Fracture Testing of High-Strength Sheet Material Under Conditions Appropriate for Stress Analysis, U.S. Naval Research Laboratory Report 5486, July 1960.
5. ASTM Committee on Fracture Testing of High-Strength Metallic Materials (ASTM-FTHSMM Committee), "Fracture Testing of High-Strength Sheet Materials," ASTM Bulletin, January 1960 and February 1960.
6. Irwin, G. R., "Exploratory Aspects of Fracture Mechanics," Fracture Mechanics Workshop Notes, August 1965.
7. Fracture Toughness Testing, American Society for Testing and Materials Special Technical Publication 381, 1964.
8. Plane Strain Crack Toughness Testing of High Strength Metallic Materials, American Society for Testing and Materials Special Technical Publication 410, 1966.
9. Timoshenko, S., and Goodier, J. N., Theory of Elasticity, McGraw-Hill, Second Edition, 1951.
10. Inglis, C. E., "Stresses in a Plate Due to the Presence of Cracks and Sharp Corners," Proceedings, Institute Naval Architects, Vol. 60, 1913.
11. Sneddon, I. N., "The Distribution of Stress in the Neighborhood of a Crack in an Elastic Solid," Proceedings, Royal Society London, Vol. A-187, 1946.
12. Irwin, G. R., "Analysis of Stresses and Strains Near the End of a Crack Transversing a Plate," Transactions, American Society of Mech. Engineers, Journal of Applied Mechanics, 1957.
13. Williams, M. L., "On the Stress Distribution at the Base of a Stationary Crack," Transactions, American Society Mech. Engineers, Journal of Applied Mechanics, 1957.
14. Westergaard, H. M., "Bearing Pressures and Cracks," Transactions, American Society Mech. Engineers, Journal of Applied Mechanics, 1939.
15. Paris, P. C., and Sih, G. C., "Stress Analysis of Cracks," American Society for Testing and Materials Special Technical Publication 381, 1964

16. Paris, P. C., Stress-Intensity-Factors by Dimensional Analysis, Lehigh University, Institute of Research Report, 1961.
17. Hahn, G. T., and Rosenfield, A. R., "Sources of Fracture Toughness: The Relation Between K_{Ic} and the Ordinary Tensile Properties of Metals," paper presented to ASTM, Applications Related Phenomena in Titanium and its Alloys, April 1967.
18. McClintock, F. A., and Irwin, G. R., "Plasticity Aspects of Fracture Mechanics," American Society for Testing and Materials Special Technical Publication 381, 1964.
19. Forman, R. G., Experimental Program to Determine Effect of Crack Buckling and Specimen Dimensions on Fracture Toughness of Thin Sheet Materials, AFFDL-TR-65-146, January 1966.
20. Liu, H. W., Discussion to, Proceedings of the Crack Propagation Symposium, Cranfield, Vol. II, 1961.
21. Rice, J. R., Contained Plastic Deformation Near Cracks and Notches Under Longitudinal Shear, Brown University Report, July 1965.
22. Dugdale, D. S., "Yielding of Steel Sheets Containing Slits," Journal of the Mechanics and Physics of Solids, Vol. 8, 1960.
23. "Progress in Measuring Fracture Toughness and Using Fracture Mechanics, Fifth Report of Special Committee," Materials Research and Standards, March 1964.
24. Weiss, V., and Yukawa, S., "Critical Appraisal of Fracture Mechanics," American Society for Testing and Materials Special Technical Publication 381, 1964.
25. Third Annual Workshop in Fracture Mechanics, Universal Technology Corp., 1966.
26. Dixon, J. R., "Stress Distribution Around Edge Slits in a Plate Loaded in Tension--The Effect of Finite Width of Plate," Journal of Royal Aeronautical Society (T.N.), Vol. 66, No. 617, May 1962.
27. Forman, R. G. and Kobayashi, A. S., "On the Axial Rigidity of a Perforated Strip and the Strain Energy Release Rate in a Centrally Notched Strip Subjected to Uniaxial Tension," Journal of Basic Engineering, Vol. 86, 1964.
28. Isida, M. and Itagaki, Y., "Stress Concentration at the Tip of a Central Transverse Crack in a Stiffened Plate Subjected to Tension," Proceedings of the 4th U.S. National Congress of Applied Mechanics, Vol. 2, 1962.
29. Isida, M., "Crack Tip Stress Intensity Factors for the Tension of an Eccentrically Cracked Strip," Journal of Applied Mechanics, Transactions of ASME, Sept. 1966.

30. Gross, B., Srawley, J. E., and Brown, Jr., Stress Intensity Factors for a Single-Edge Notch Tension Specimen by Boundary Collocation of a Stress Function, NASA TN D-2395, August 1964.
31. Crichlow, W. J., "Stable Crack Propagation—Fail-Safe Design Criteria—Analytical Methods and Test Procedures," AIAA Paper No. 69-215, February 1969.
32. Broek, D., The Residual Strength of Cracked Sheet—Tests Interrupted After Intermediate Slow Crack Growth, NLR-TR M-2145, National Aerospace Laboratory, Amsterdam, July 1965.
33. Newman, J. C., Jr., "Fracture of Cracked Plates Under Plane Stress," paper presented to National Symposium on Fracture Mechanics, July 1967.
34. Crichlow, W. J., "The Ultimate Strength of Damaged Structures—Analysis Methods with Correlating Test Data," Full Scale Fatigue Testing of Aircraft Structures, edited by F. J. Plantema and J. Schijve, Pergamon Press, 1961.
35. Crichlow, W. J., "Limitations of Fatigue-Crack Research in the Design of Flight Vehicle Structures," American Society for Testing and Materials Special Technical Publication 415, 1967.
36. Neuber, H., Theory of Notch Stresses: Principles for Exact Stress Calculations, (J. W. Edwards, Ann Arbor, Mich., 1964).
37. Crack Propagation Prediction and Crack-Stopper Techniques for Stiffened and Unstiffened Flat Sheet in a Supersonic Transport Environment, ASD-TRD-63-773, September 1963.
38. Welborne, E. R., "The Correlation of Unstable Crack Length Data for Sheet Material," Aeronautical Quarterly, November 1961.
39. McEvily, A. J., Jr., Illg, W., and Hardrath, H. F., Static Strength of Aluminum-Alloy Specimens Containing Fatigue Cracks, NASA (NACA) TN 3816, October 1956.
40. Kuhn, P., Residual Strength in the Presence of Fatigue Cracks, paper presented to the Structures and Materials Panel-AGARD, 1967.
41. Irwin, G. R., "Crack Extension Force for a Part-Through Crack in a Plate," Journal of Applied Mechanics, Vol. 29, Transactions of American Society Mech. Eng., Vol. 84, Series E, December 1962.
42. Tiffany, C. F., Masters, J. N., and Shah, R. C., Fracture Control of Metallic Pressure Vessels, NASA Space Vehicle Design Criteria, (to be published)
43. Figge, I. E., Residual Strength of Alloys Potentially Useful in Supersonic Aircraft, NASA TN D-2613, February 1965.

44. Kuhn, P., and Figge, I. E., Unified Notch-Strength Analysis for Wrought Aluminum Alloys, NASA TN D-1259, 1962.
45. Tiffany, C. F., and Masters, J. N., "Applied Fracture Mechanics," American Society for Testing and Materials Special Technical Publication 381, 1964.
46. Kuhn, P., "Strength Calculations for Sheet-Metal Parts with Cracks," Materials Research and Standards, September 1968.
47. Bloom, J. M., The Effect of a Riveted Stringer on the Stress in a Sheet with a Crack or a Cutout, Office of Naval Research Report No. 20, June 1964, (AD 603693).
48. Grief, R., and Sanders, J. L., Jr., "The Effect of a Stringer on the Stress in a Cracked Sheet," Journal of Applied Mechanics, Vol. 32, Transactions of ASME, Vol. 87, Series E, 1965.
49. Kobayashi, A. S., Ziv, M., and Hall, L. R., "Approximate Stress Intensity Factor for an Embedded Elliptical Crack Near a Free Surface," International Journal of Fracture Mechanics, June 1965.
50. Anderson, R. B., and Sullivan, T. L., Fracture Mechanics of Through-Cracked Cylindrical Pressure Vessels, NASA TN D-3552, February 1966.
51. Hahn, G. T., Sarrate, M., and Rosenfield, A. R., "Criteria for Crack Extension in Cylindrical Pressure Vessels," International Journal of Fracture Mechanics, Vol. 5, No. 3, September 1969.
52. Kaufman, J. G., "Fracture Toughness of 7075-T6 and T651 Sheet, Plate and Multilayered Adhesive-Bonded Panels," Transactions of ASME, Journal of Basic Engineering, September 1967.
53. Bluhm, J. I., "Fracture Arrest," Fracture, An Advanced Treatise, Volume V, Fracture Design of Structures, H. Liebowitz, (ed.), Academic Press, 1969.
54. Romualdi, J. P. and Sanders, P. H., "Fracture Arrest by Riveted Stiffeners," Proceedings of Fourth Midwest Conference on Solid Mechanics, University of Texas Press, 1959-1960.
55. Tetelman, A. S., and McEvily, Jr., A. J., Fracture of Structural Materials, John Wiley and Sons, Inc., 1967.
56. Liebowitz, H., (ed.), Fracture, An Advanced Treatise, "Fracture of Non-metals and Composites," Vol. VII, Academic Press, to be published.
57. Smith, R. W., et al, Fatigue Behavior of Materials Under Strain Cycling in Low and Intermediate Life Range, NASA TN D-1574, April 1963.
58. Manson, S. S., Fatigue: A Complex Subject-Some Simple Approximations, NASA TN X-52084, 1965.

59. Donaldson, D. R., and Anderson, W. E., "Crack Propagation Behavior of Some Airframe Materials," Proceedings of the Crack Propagation Symposium, Cranfield, Vol. 2, September 1961.
60. Paris, P., and Erdogan, R., "A Critical Analysis of Crack Propagation Laws," Transactions of ASME, Journal of Basic Engineering, December 1963.
61. Paris, P., et al, "A Rational Analytic Theory of Fatigue," The Trend in Engineering, January 1961.
62. Paris, P. C., "The Fracture Mechanics Approach to Fatigue," in Fatigue-An Interdisciplinary Approach, Syracuse University Press, 1964.
63. Fatigue Crack Propagation, American Society for Testing and Materials Special Technical Publication, ASTM STP 415, June 1967.
64. Forman, R. G., et al, "Numerical Analysis of Crack Propagation in Cyclic-Loaded Structures," Transactions of ASME, Journal of Basic Engineering, Vol. 89, No. 3, September 1967.
65. Hudson, C. M., Effect of Stress Ratio on Fatigue-Crack Growth in 7075-T6 and 2024-T3 Aluminum-Alloy Specimens, NASA TN D-5390, August 1969.
66. Swanson, S. R., et al, "Crack Propagation in Clad 7079-T6 Aluminum Alloy Sheet Under Constant and Random Amplitude Fatigue Loading," American Society for Testing and Materials Special Technical Publications, ASTM-STP 415, June 1967.
67. Anderson, W. E., and James, L. A., Estimating Structural Cracking Behavior from Substitute Tests, Battelle Northwest Report BNWL-SA-2291, January 1969.
68. Smith, H. R., et al, "A Study of Stress Corrosion Cracking by Wedge-Force Loading," to be published in Journal of Engineering Fracture Mechanics.
69. Hartman, A., "On the Effect of Oxygen and Water Vapor on the Propagation of Fatigue Cracks in 2024-T3 Alclad Sheet," International Journal of Fracture Mechanics, 1, 1965.
70. Wei, R. P., "Application of Fracture Mechanics to Stress Corrosion Cracking Studies," paper presented to International Conference on Fundamental Aspects of Stress Corrosion Cracking, Ohio State University, September 1967.
71. "Proposed Method of Test for Plane-Strain Fracture Toughness of Metallic Materials," American Society for Testing and Materials Standards, Part 31, May 1969. 1099-1112.
72. Krafft, J., et al, "Effect of Dimensions on Fast Fracture Instability of Notched Sheets," Proceedings of the Crack Propagation Symposium, Cranfield, Vol. 1, September 1961.

73. Srawley, J. E., and Brown, Jr., W. F., "Fracture Toughness Testing Methods," American Society for Testing and Materials Special Technical Publication 381, 1964.
74. Heyer, R. H., and McCabe, D. E., "Plane-Stress Fracture Toughness Testing Using a Crack Line Loaded Specimen," paper presented to National Symposium on Fracture Mechanics, Lehigh University, August 1969.

BIBLIOGRAPHY*

CRACK PROPAGATION - (ENVIRONMENTAL EFFECTS)

Fatigue Crack Propagation, American Society for Testing and Materials Special Technical Publication (ASTM, STP-415), June 1967.

Proceedings of the Crack Propagation Symposium, Vols. I and II, Cranfield, 1961.

American Society for Testing and Materials Special Technical Publication, ASTM STP 462 (to be published).

Barrois, W., Critical Study on Fatigue Crack Propagation, Advisory Group for Aeronautical Research and Development, Report 412, June 1962.

Bradshaw, F. J., "The Effect of Gaseous Environment on Fatigue Crack Propagation," Scripta Metallurgica, Vol. 1, 1967.

Beachem, C. D., The Effects of Three Aqueous Environments on High-Stress Low-Cycle Fatigue of an 18% Nickel Maraging Steel, AD-475863L, June 1965.

Dahlberg, E. P., "Fatigue-Crack Propagation in High-Strength 4340 Steel in Humid Air," Transactions of ASM, Vol. 58, 1965.

Denke, P. H., Bentley, C. W., and Hunt, R. T., "Fracture Toughness and Crack Propagation Properties of Candidate Mach 3 Transport Materials," Society of Automotive Engineers Paper 650794, October 1965.

Figge, I. E., and Hudson, C. M., Crack Propagation, Delayed Failure, and Residual Static Strength of Titanium, Aluminum, and Stainless Steel Alloys in Aqueous Environments, NASA TND-3825, February 1967.

Hudson, C. M., Fatigue-Crack Propagation in Several Titanium and Stainless-Steel Alloys and One Superalloy, NASA TND-2331, October 1964.

Hudson, C. M., Studies of Fatigue Crack Growth in Alloys Suitable for Elevated-Temperature Applications, NASA TND-2743, April 1965.

Hudson, C. M., and Hardrath, H. F., Effects of Changing Stress Amplitude on the Rate of Fatigue-Crack Propagation in Two Aluminum Alloys, NASA TND-960, September 1961.

Meyn, D. A., "The Nature of Fatigue-Crack Propagation in Air and Vacuum for 2024 Aluminum," Transactions of the ASM, Vol. 61, 1968.

*It is recommended that those who are not engaged in fracture mechanics research consult with those who are familiar with the literature in this field for more definitive selections. This listing cannot be considered complete; however, it does represent a cross section of selected reports for additional information.

McEvily, Jr., A. J., and Illg, W., The Rate of Fatigue-Crack Propagation in Two Aluminum Alloys, NACA TN 4394, September 1958.

Pierce, W. S., Crack Growth in 2014-T6 Aluminum Tensile and Tank Specimens Cyclically Loaded at Cryogenic Temperatures, NASA TN D-4541, April 1968.

Schijve, J. and de Rijk, P., The Effect of Temperature and Frequency on the Fatigue Crack Propagation in 2024-T3 Alclad Sheet Material, NLR-TR M.2138, National Aero and Astronautical Research Institute-Amsterdam, January 1965.

Schijve, J. and de Rijk, P., The Crack Propagation in Two Aluminum Alloys in an Indoor and an Outdoor Environment Under Random and Programmed Load Sequences, NLR-TR M.2156, National Aerospace Laboratory NLR, The Netherlands, November 1965.

Smith, H. H., et al, "Fatigue Crack Growth Rates in Type 316 Stainless Steel at Elevated Temperatures as a Function of Oxygen Pressure," Transactions of the Metallurgical Society of AIME, Vol. 245, May 1969.

Spitzig, W. A., and Wei, R. P., "A Fractographic Investigation of the Environment on Fatigue-Crack Propagation in an Ultrahigh-Strength Steel," Transactions of ASM, Vol. 60, 1967.

Wei, R. P., "Fatigue-Crack Propagation in a High-Strength Aluminum Alloy," International Journal of Fracture Mechanics, Vol. 4, Nr. 2, June 1968.

Wei, R. P., and Landes, J. D., "Correlation Between Sustained-Load and Fatigue Crack Growth in High-Strength Steels," Materials Research and Standards, July 1969.

An Investigation of Low-Cycle Fatigue Failures Using Applied Fracture Mechanics, ML-TDR-64-53, May 1964.

Crack Strength and Crack Propagation Characteristics of High Strength Metals, ASD-TR-61-207, January 1962.

Crack Propagation Prediction and Crack-Stopper Techniques for Stiffened and Unstiffened Flat Sheet in a Supersonic Transport Environment, ASD-TDR-63-773, September 1963.

CRACK PROPAGATION - (THEORY AND CORRELATIONS)

Fatigue-An Interdisciplinary Approach, Proceedings of 10th Sagamore Army Materials Research Conference, Syracuse University Press, 1964.

Fatigue Crack Propagation, American Society for Testing and Materials Special Technical Publication, ASTM, STP-415, June 1967.

Proceedings of the Crack Propagation Symposium, Vols. I and II, Cranfield, 1961.

Proceedings of International Conference on Mechanisms of Fatigue in Crystalline Solids, ACTA Metallurgica, Vol. 11, July 1963.

Proceedings of First International Conference on Fracture, 1966.

Barrois, W., Critical Study of Fatigue Crack Propagation, Advisory Group for Aeronautical Research and Development, Report 412, June 1962.

Borris, L. J. (ed.) Fracture of Metals, Symposium on Fundamental Phenomena in the Material Science, 4th Boston, 1966, Plenum, New York, 1967.

Cotterell, B., "An Interpretation of the Mechanics of Crack Growth by Fatigue," Transactions of ASME, Journal of Basic Engineering, March 1965.

Erdogan, F., Crack Propagation Theories, NASA CR-901, December 1967.

Forman, R. G., et al, "Numerical Analysis of Crack Propagation in Cyclic-Loaded Structures," Transactions of ASME, Journal of Basic Engineering, Vol. 89, No. 3, September 1967.

Frost, N. E., and Dixon, J. R., "A Theory of Fatigue Crack Growth," International Journal of Fracture Mechanics, Vol. 3-No. 4, December 1967.

Grosskreutz, J. C., A Theory of Stage II Fatigue Crack Propagation, AFML-TR-64-415, March 1965.

Head, A. K., "The Growth of Fatigue Cracks," Phil. Mag., Ser. 7, Vol. 44, ND 356, September 1953.

Liu, H. W., "Fatigue Crack Propagation and the Stresses and Strains in the Vicinity of a Crack," Applied Materials Research, October 1964.

Liu, H. W., "Fatigue Crack Propagation and Applied Stress Range-An Energy Approach," Transactions of the ASME, Journal of Basic Engineering, March 1963.

Manson, S. S., Fatigue: A Complex Subject-Some Simple Approximations, NASA TMX 52084, 1965.

Paris, P. and Erdogan, F., "A Critical Analysis of Crack Propagation Laws," Transactions of ASME, Journal of Basic Engineering, December 1963.

Paris, P. C., et al, "A Rational Analytic Theory of Fatigue," Trend in Engineering, January 1961.

Schijve, J., Analysis of the Fatigue Phenomenon in Aluminum Alloys, NLR-TR M.2122, National Aero and Astronautical Research Institute, Amsterdam, April 1964.

Tetelman, A. S., and McEvily, Jr., A. J., Fracture of Structural Materials, John Wiley and Sons, 1967.

Valluri, S. R., et al, Further Considerations of a Theory of Crack Propagation in Metal Fatigue, paper 752A, Society of Automotive Engineers, September 1963.

Yang, C. T., "A Study of the Law of Crack Propagation," Transactions of ASME, Journal of Basic Engineering, September 1967.

Proceedings of the Air Force Conference on Fatigue and Fracture of Aircraft Structures and Materials, December 1969, to be published.

CRACK PROPAGATION-(DATA AND ANALYSIS)

Fatigue Crack Propagation, STP-415, American Society for Testing and Materials Special Technical Publication ASTM, June 1967.

Proceedings of the Crack Propagation Symposium, Vols. I and II, Cranfield, 1961.

Beachem, C. D., "Microscopic Fatigue Fracture Surface Features in 2024-T3 Aluminum and the Influence of Crack Propagation Angle upon Their Formation," Transactions of ASM, Vol. 60, 1967.

Broek, D., Crack Propagation and Residual Strength of Full Scale Wing Center Sections, NLR-TM S.612, National Aero and Astronautical Research Institute, Amsterdam, August 1964.

Broek, D., and Schijve, J., The Influence of the Mean Stress on the Propagation of Fatigue Cracks in Aluminum Alloy Sheet, NLR-TN M.2111, National Aero and Astronautical Research Institute, Amsterdam, January 1963.

Broek, D., and Schijve, J., The Effect of Sheet Thickness on the Fatigue-Crack Propagation in 2024-T3 Alclad Sheet Material, NLR-TR M. 2129, National Aero and Astronautical Research Institute, Amsterdam, April 1963.

Broek, D., Crack Propagation Properties of 2024-T8 Sheet Under Static and Dynamic Loads, NLR-TM M.2161, National Aero and Astronautical Research Institute, Amsterdam, March 1966.

Broek, D. et al, The Effect of Heat Treatment on the Propagation of Fatigue Cracks in Light Alloy Sheet Material, NLR-TR M.2134, National Aero and Astronautical Research Institute, Amsterdam, May 1963.

Brothers, A. J., and Yukawa, S., "Fatigue Crack Propagation in Low Alloy Heat Treated Steels," Transactions of ASME, Journal of Basic Engineering, March 1967.

Carman, C. M., and Katlin, J. M., "Low Cycle Fatigue Crack Propagation Characteristics of High Strength Steels," Transactions of ASME, Journal of Basic Engineering, December 1966.

Carter, T. J., Crack Propagation Tests on 2024-T3 Unstiffened Aluminum Alloy Panels of Various Length-Width Ratios, C.P. No. 952, Ministry of Technology, Aeronautical Research Council, 1967.

Catanach, Jr., W. M., and Erodogan, F., Fatigue Crack Propagation in Cylindrical Shells, NASA CR-1197.

Crooker, T. W., and Lange, E. A., "Low Cycle Fatigue Crack Propagation in A201B, A302B, and A517F Pressure Vessel Steels," Welding Journal, Research Supplement, July 1967.

Figge, I. E., and Hudson, C. M., Crack Propagation, Delayed Failure, and Residual Static Strength of Titanium, Aluminum, and Stainless Steel Alloys in Aqueous Environments, NASA TN D-3825, February 1967.

Forman, R. G., Digital Computer Program for the Analysis of Crack Propagation in Cyclic Loaded Structures, AFFDL-TR-67-5 (AD-815 615), April 1967.

Frost, N. E., and Dugdale, D. S., "The Propagation of Fatigue Cracks in Sheet Specimens," *Journal of the Mechanics and Physics of Solids*, Vol. 6, 1958.

Frost, N. E., and Greenan, A. F., "Cyclic Stress Required to Propagate Edge Cracks in Eight Materials," *Journal Mechanical Engineering Science*, Vol. 6, No. 3, 1964.

Frost, N. E., and Denton, K., "Effect of Sheet Thickness on the Rate of Growth of Fatigue Cracks in Mild Steel," *Journal Mechanical Engineering Science*, Vol. 3, No. 4, 1961.

Frost, N. E., and Phillips, C. E., "Some Observations on the Spread of Fatigue Cracks," *Proceedings of Royal Society of London, Series A*, Vol. 242, October 1957.

Grover, H., "Fatigue Crack Propagation in Sheet Specimens," *Materials Research and Standards*, August 1964.

Herrnstein, III, W. H., and McEvily, Jr., A. J., Effect of Decarburization on Notch Sensitivity and Fatigue-Crack Propagation Rates in 12MoV Stainless-Steel Sheet, NASA TN D-966, November, 1961.

Hudson, C. M., Fatigue-Crack Propagation in Several Titanium and Stainless-Steel Alloys and one Superalloy, NASA TN D-2331, October 1964.

Hudson, C. M., Investigation of Fatigue Crack Growth in Ti-8Al-1Mo-1V (Duplex-Annealed) Specimens Having Various Widths, NASA TN D-3879, March 1967.

Hudson, C. M., Studies of Fatigue Crack Growth in Alloys Suitable for Elevated-Temperature Applications, NASA TN D-2743, April 1965.

Hudson, C. M., and Hardrath, H. F., Effects of Changing Stress Amplitude on the Rate of Fatigue-Crack Propagation in Two Aluminum Alloys, NASA TN D-960, September 1961.

Illg, W., and McEvily, Jr., A. J., The Rate of Fatigue-Crack Propagation for Two Aluminum Alloys Under Completely Reversed Loading, NASA TN D-52, October 1959.

Kaufman, J. G., et al, Fracture Toughness, Fatigue and Corrosion Characteristics of 7075-T651, 7075-T7351 and 7079-T651 Aluminum Alloys, AFML-TR-65-170, May 1965.

Krafft, J. M., "On Prediction of Fatigue Crack Propagation Rate from Fracture Toughness and Plastic Flow Properties," *Transactions of ASM*, Vol. 58, 1965.

Liu, H. W., "Crack Propagation in Thin Metal Sheet Under Repeated Loading," Transactions of ASME, Journal of Basic Engineering, March 1961.

Manson, S. S., and Hirschberg, M. H., Low Cycle Fatigue of Notched Specimens by Consideration of Crack Initiation and Propagation, NASA TN D-3146, June 1967.

Manson, S. S. and Hirschberg, M. H., Crack Initiation and Propagation in Notched Fatigue Specimens, NASA TM X-52126, September 1965.

Martin, D. E., and Sinclair, G. M., "Crack Propagation Under Repeated Loadings," Proceedings of Third National Congress Applied Mechanics, 1959.

McEvily, Jr., A. J., and Illg, W., The Rate of Fatigue-Crack Propagation in Two Aluminum Alloys, NACA TN 4394, September 1958.

Meyn, D. A., "Observations on Micromechanisms of Fatigue-Crack Propagation in 2024 Aluminum," Transactions of ASM, Vol. 61, 1968.

Pelloux, R. M. N., "Fractographic Analysis of the Influence of Constituent Particles on Fatigue Crack Propagation in Aluminum Alloys," Transactions of ASM, Vol. 57, 1964.

Pierce, W. S., and Sullivan, T. L., Factors Influencing Low-Cycle Crack Growth in 2014-T6 Aluminum Sheet at -320°F (77K), NASA TN D-5140, April 1969.

Pierce, W. S., Crack Growth in 2014-T6 Aluminum Tensile and Tank Specimens Cyclically Loaded at Cryogenic Temperatures, NASA TN D-4541, April 1968.

Rawe, R. A., and Eitman, D. A., A Parametric Relationship Between Fatigue Life, Cyclic Stress, and Crack Length in Flat Panels and Cylinders, ASME paper No. 67-WA/AV-8, 1968.

Rolfe, S. T., and Munse, W. H., "Fatigue Crack Propagation in Notched Mild Steel Plates," Welding Journal, Research Supplement, June 1963.

Schijve, J., and de Rijk, P., The Effect of Temperature and Frequency on the Fatigue Crack Propagation in 2024-T3 Alclad Sheet Material, NLR-TR M. 2138, National Aero and Astronautical Research Institute, Amsterdam, January 1965.

Schijve, J., and Jacobs, F. A., Fatigue Crack Propagation in Unnotched and Notched Aluminum Alloy Specimens, NLR-TR M. 2128, National Aero and Astronautical Research Institute, Amsterdam, May 1964.

Schijve, J., et al, The Effect of the Sheet Width on the Fatigue Crack Propagation in 2024-T3 Alclad Material, NLR-TR M. 2142, National Aero and Astronautical Research Institute, Amsterdam, March 1965.

Schijve, J., et al, Fatigue Tests with Random and Programmed Load Sequences, With and Without Ground to Air Cycles. A Comparative Study on Full-Scale Wing Center Section, AFFDL-TR 66-143, 1966.

Smith, S. H., et al, Fatigue-Crack-Propagation and Fracture-Toughness Characteristics of 7079 Aluminum-Alloy Sheets and Plates in Three Aged Conditions, NASA CR-996, February 1968.

Wang, D. Y., Effect of Stress Ratio on Fatigue Crack Growth and Mode of Fracture in 2024-T4 and 7075-T6 Aluminum Alloys in the Low-Cycle Range, AFML-TR-66-216, December 1966.

Weibull, W., The Effect of Size and Stress History on Fatigue Crack Initiation and Propagation, ASD-TDR-62-785, August 1962.

Proceedings of the Air Force Conference on Fatigue and Fracture of Aircraft Structures and Materials, December 1969, to be published.

FRACTURE - (ENVIRONMENTAL)

Crack Propagation Prediction and Crack-Stopper Techniques for Stiffened and Unstiffened Flat Sheet in A Supersonic Transport Environment, ASD-TDR-63-773, September 1963.

Fracture Toughness Testing and Its Applications, American Society for Testing and Materials, Special Technical Publication, (ASTM STP 381), 1964.

Symposium on Stress-Corrosion Cracking of Titanium, American Society for Testing and Materials Special Technical Publication, (ASTM STP 397), 1965.

Anderson, R. B. and Sullivan, T. L., Fracture Mechanics of Through-Cracked Cylindrical Pressure Vessels, NASA TND-3252, February 1966.

Averback, B. L., et al, (ed), Fracture, The Technology Press of M.I.T. and J. Wiley and Sons, 1959.

Brown, B. F., "A New Stress-Corrosion Cracking Test for High-Strength Alloys," Materials Research and Standards, March 1966.

Calfo, F. D., Cryogenic Fracture Properties of Thin AISI 301 60-Percent Cold-Reduced Sheet at Various Angles to the Rolling Direction, NASA TND-5413, September 1969.

Calfo, F. D., Effect of Residual Stress on Fracture Strength of AISI 301 Stainless-Steel and Ti-5Al-2.5 Sn ELI Titanium Cracked Thin-Wall Cylinders NASA TN D-4777, September 1968.

Creager, M., and Paris, P. C., "Elastic Field Equations for Blunt Cracks with Reference to Stress Corrosion Cracking," International Journal of Fracture Mechanics, Vol. 3, No. 4, December 1967.

Figge, I. E., Residual-Static-Strength and Slow-Crack-Growth Behavior of Duplex-Annealed Ti-8Al-1Mo-1V Sheet, NASA TN D-4358, 1968.

Figge, I. E., Residual Static Strength of Several Titanium and Stainless-Steel Alloys and One Superalloy at -109°F, 70°F and 550°F, NASA TN D-2045, December 1963.

Figge, I. E., Residual Strength of Alloys Potentially Useful in Supersonic Aircraft, NASA TN D-2613, February 1965.

Hickel, R. O., et al, "A Summary of the Behavior of Materials at Cryogenic Temperatures," Metals Engineering Quarterly, May 1963.

Johnson, H. H., and Willner, A. M., "Moisture and Unstable Crack Growth in a High Strength Steel," Applied Materials Research, January 1965.

Mulherin, J. H., "Stress-Corrosion Susceptibility of High-Strength Steel, in Relation to Fracture Toughness," Transactions of ASME, Journal of Basic Engineering, December 1966.

Mulherin, J. H., The Influence of Environment on the Crack Propagation Characteristics of High Strength Aluminum Alloys, U. S. Army, Frankford Arsenal Report, R-1809, AD 632988, April 1966.

Orange, T. W., Fracture Toughness of Wide 2014-T6 Aluminum Sheet at -320°F, NASA TN D-4017, June 1967.

Petrak, G. J., Investigation of the Subcritical Crack Growth Life of Titanium in a Corrosive Environment, AFML-TR-68-271, 1968.

Piper, D. E., et al, "Corrosion Fatigue and Stress Corrosion Cracking in Aqueous Environments," Metals Engineering Quarterly, American Society for Metals, August 1968.

Sullivan, T. L., Texture Strengthening and Fracture Toughness of Titanium Alloy Sheet at Room and Cryogenic Temperatures, NASA TN D-4444, May 1968.

Sullivan, T. L., Uniaxial and Biaxial Fracture Toughness of Extra-Low-Interstitial 5 Al-2.5 Sn Titanium Alloy Sheet at 20°K, NASA TN D-4016, June 1967.

Tetelman, A. S., and McEvily, Jr., A. J., Fracture of Structural Materials, J. Wiley and Sons, 1967.

Van der Sluys, W. A., "The Effect of Moisture on Slow Crack Growth in Thin Sheets of SAE 4340 Steel Under Static and Repeated Loading," Transactions of ASME, Journal of Basic Engineering, March 1967.

Wei, R. P., "Application of Fracture Mechanics to Stress Corrosion Cracking Studies," paper presented at the International Conference on Fundamental Aspects of Stress Corrosion Cracking, September 1967.

Wei, R. P., and Landes, D., "Correlation Between Sustained-Load and Fatigue Crack Growth in High-Strength Steels," Materials Research and Standards, July 1969.

Yang, C. T., "Analysis of Static Crack Propagation at Room and Cryogenic Temperatures," Metals Engineering Quarterly, August 1966.

Yen, C. S., and Pendleberry, S. L., "Fracture Strength of High-Strength Steels Containing Shallow Cracks," Transactions of ASM, Vol. 55, 1962.

FRACTURE MECHANICS-(THEORY)

Fracture Toughness Testing and Its Applications, American Society for Testing and Materials Special Technical Publication (ASTM STP-381), 1964.

Averbach, B. L. et al, (ed.), Fracture, The Technology Press of M.I.T. and J. Wiley and Sons, 1959.

Broek, D., "The Energy Criterion for Fracture of Sheets Containing Cracks," Applied Materials Research, July 1965.

Griffith, A. A., "The Phenomena of Rupture and Flow in Solids," Philosophical Transactions of The Royal Society, 221A, (1920), 163, also, Metallurgical Classics, Transactions of American Society for Metals, Vol. 61, 1968, pps. 855-906.

Hahn, G. T., et al, "Model for Crack Propagation in Steel," Journal of the Iron and Steel Institute, August 1964.

Irwin, G. R., "Fracture," Handbuch der Physik, Flügge, S. (ed.), Vol. VI, 1958.

Irwin, G. R., "Crack-Extension Force for a Part-Through Crack in a Plate," Transactions of ASME, Journal of Applied Mechanics, December 1962.

Irwin, G. R., "Fracture Dynamics," Transactions of ASM, 40A, 1948.

Irwin, G. R., "Fracture Mechanics," in Structural Mechanics, Pergamon Press, 1960.

Irwin, G. R., "Theoretical Aspects of Fracture Failure Analysis," Metals Engineering Quarterly, February 1963.

Liebowitz, H., (ed.) Fracture, an Advanced Treatise, Vols. I-VII, Academic Press, 1968, 1969.

McClintock, F. A., A Criterion for Ductile Fracture by the Growth of Holes, M.I.T. Preprint No. 878, 1968.

McClintock, F. A., "Local Criteria for Ductile Fracture," The International Journal of Fracture Mechanics, Vol. 4, No. 2, June 1968.

Orowan, E., "Fundamentals of Brittle Behavior in Metals," in Fatigue and Fracture of Metals, The Technology Press of M.I.T. and J. Wiley and Sons, 1952.

Tetelman, A. S., and McEvily, Jr., A. J., Fracture of Structural Materials, J. Wiley and Sons, 1967.

Yokobori, T. et al, (ed.), International Conference on Fracture, Japan Society for Promotion of Sciences, Sendai, Japan, 1966.

FRACTURE- (DATA AND ANALYSIS)

*"Fracture Testing of High Strength Sheet Materials: A Report of a Special ASTM Committee," American Society for Testing and Materials Bulletin, January and February 1960.

*Fracture Toughness Testing and Its Applications, American Society for Testing and Materials Special Technical Publication (ASTM STP-381), 1964.

*Plane Strain Crack Toughness Testing of High Strength Metallic Materials, American Society for Testing and Materials Special Technical Publication (ASTM STP-410), 1967.

*"Progress in Measuring Fracture Toughness and Using Fracture Mechanics, Fifth Report of a Special ASTM Committee," Materials Research and Standards, March 1964.

*"Proposed Method of Test for Plane-Strain Fracture Toughness of Metallic Materials," American Society for Testing and Materials Standards, Part 31, May 1969.

*"The Slow Growth and Rapid Propagation of Cracks," Materials Research and Standards, May 1961.

Fracture Toughness and Tear Tests, Exhibit "C", ML TDR 64-238, October 1964.

Thick Section Fracture Toughness, Exhibit "B", ML TDR 64-236, October 1964.

*Allen, F. C., "Stress Analysis of Centrally Cracked Plates," Douglas Aircraft Division paper No. 5513, March 1969.

Anderson, R. B., and Sullivan, T. L., Fracture Mechanics of Through-Cracked Cylindrical Pressure Vessels, NASA TN D-3252, February 1966.

*Anderson, W. E., Some Designer-Oriented Views on Brittle Fracture, Battelle Northwest, BNWL-SA-2290, February 1969.

*Anderson, W. E., and James, L. A., Estimating Structural Cracking Behavior from Substitute Tests, Battelle Northwest, BNWL-SA-2291, January 1969.

Bloom, J. M., The Effect of a Riveted Stringer on the Stress in a Sheet with a Crack or a Cutout, AD-603693, June 1964.

Boyle, R. W., "A Method for Determining Crack Growth in Notched Sheet Specimens," Materials Research and Standards, August 1962.

*Recommended for greater in-depth understanding of fracture mechanics principles.

Bowie, O. L., and Neal, D. M., "Single Edge Crack in Rectangular Tensile Sheets," Transactions of ASME, Journal of Applied Mechanics, September 1965.

Boyle, R. W., et al, "Determination of Plane Strain Fracture Toughness with Sharply Notched Sheets," Welding Journal, Research Supplement, September 1962.

Broek, D., Static Tests on Cracked Panels of 2024-T3 Alclad Sheet Materials from Different Manufacturers, National Aerospace Laboratory NLR, The Netherlands, NLR-TN M.2164, August 1966.

Broek, D., The Effect of Finite Specimen Width on the Residual Strength of Light Alloy Sheet, National Aerospace Laboratory NLR, The Netherlands, NLR-TR M.2152, September 1965.

Broek, D., The Effect of the Sheet Thickness on the Fracture Toughness of Cracked Sheet, National Aerospace Laboratory NLR, Amsterdam, NLR-TR M.2160, January 1966.

Broek, D., The Residual Strength of Aluminum Alloy Sheet Specimens Containing Fatigue Cracks or Saw Cuts, National Aerospace Laboratory NLR, Amsterdam, NLR-TR M.2143, March 1966.

Broek, D., The Residual Strength of Cracked Sheet-Tests Interrupted After Intermediate Slow Crack Growth, National Aerospace Laboratory NLR, Amsterdam, NLR-TR M.2145, July 1965.

Broek, D. and Jacobs, F. A., The Static Strength of Aluminum Alloy Sheet Specimens Containing Blunt Notches, National Aerospace Laboratory NLR, Amsterdam, NLR-TR M.2149, August 1965.

Broek, D. and Nederveen, A., The Influence of the Loading Rate on the Residual Strength of Aluminum Alloy Sheet Specimens, National Aerospace Laboratory NLR, Amsterdam, NLR-TR M.2154, October 1965.

Brown, Jr., W. F., "Fracture Testing and ASTM," Materials Research and Standards, March 1967.

Calfo, F. D., Effect of Residual Stress on Fracture Strength of AISI 301 Stainless-Steel and Ti-5Al-2.5 Sn ELI Titanium Cracked Thin-Wall Cylinders, NASA TN D-4777, September 1968.

Cammett, J., et al, Residual Strains and Displacements Within the Plastic Zone Ahead of a Crack, AD 644815, November 1966.

Carman, C. M., Crack Resistance Properties of High Strength Aluminum Alloys, U.S. Army, Frankford Arsenal Report K-1789, December 1965.

Carman, C. M., et al, "Plane-Strain Fracture Toughness of High-Strength Aluminum Alloys," Transactions of ASME, Journal of Basic Engineering, December 1965.

Copley, L. G., and Sanders, Jr., J. L., "A Longitudinal Crack in a Cylindrical Sheet Under Internal Pressure," *International Journal of Fracture Mechanics*, Vol. 5, No. 2, June 1969.

Corten, H. T. and Shoemaker, A. K., "Fracture Toughness of Structural Steels as a Function of the Rate Parameter $\ln A/\dot{\epsilon}$ ", *Transactions of the ASME, Journal of Basic Engineering*, March 1967.

Cotterell, B., "On the Nature of Moving Cracks," *Transactions of ASME, Journal of Applied Mechanics*, March 1964.

Crichlow, W. J., "The Materials-Structures Interface, A Systems Approach to Airframe Structural Design," *AIAA/ASME 10th Structures, Structural Dynamics and Materials Conference*, New Orleans, 14-16 April 1969.

Crichlow, W. J., "The Ultimate Strength of Damaged Structure-Analysis Methods with Correlating Test Data," Full Scale Fatigue Testing of Aircraft Structures, Pergamon Press, 1960.

Crichlow, W. J., Stable Crack Propagation-Fail Safe Design Criteria-Analytical Methods and Test Procedures, AIAA paper No. 69-215, February 1969.

*Davis, R. A. and Quist, W. E., "Fracture Toughness, What it is, How to Design for it, How to Test for it," *Materials in Design Engineering*, November 1965.

Davis, S. O., et al, Center Notch Plane Strain K_{Ic} Fracture Toughness Properties of Several High-Strength Steel Alloys, AFML-TR-65-214, October 1965.

Davis, S. O., et al, Effect of Specimen Type and Crack Orientation of Fracture Toughness, AFML-TR-67-38, March 1967.

Davis, S. O., et al, Plane Strain Fracture Toughness Properties of Three Aluminum Alloys as a Function of Specimen Geometry, AFML-TR-65-150, July 1965.

Denke, P. H., et al, Fracture Toughness and Crack Propagation Properties of Candidate Mach 3 Transport Materials, Society of Automotive Engineers, Paper No. 650794, October 1965.

Dixon, J. R., "Stress Distribution Around Edge Slits in a Plate Loaded in Tension-The Effect of Finite Width of Plate," *Journal of the Royal Aeronautical Society*, Vol. 66, May 1962.

Dugdale, D. S., "Yielding of Steel Sheets Containing Slits," *Journal of Mech. and Physics of Solids*, Vol. 8, 1960.

Duncan, M. E., and Sanders, J. L., Jr., "The Effect of a Circumferential Stiffener on the Stress in a Pressurized Cylindrical Shell with a Longitudinal Crack," *International Journal of Fracture Mechanics*, Vol. 5, No. 2, June 1969.

Erdogan, F. and Shi, G. C., "On the Crack Extension in Plates Under Plane Loading and Transverse Shear," Transactions of ASME, Journal of Basic Engineering, December 1963.

Figge, I. E., Residual-Static-Strength and Slow Crack-Growth Behavior of Duplex-Annealed Ti-8Al-1Mo-1V Sheet, NASA TN D-4358, 1968.

Figge, I. E., Residual Static Strength of Several Titanium and Stainless-Steel Alloys and One Superalloy at -109°F, 70°F, and 550°F, NASA TN D-2045, December 1963.

Figge, I. E., Residual Strength of Alloys Potentially Useful in Supersonic Aircraft, NASA TN D-2613, February 1965.

Fisher, D. M., et al, Design and Use of Displacement Gage for Crack-Extension Measurements, NASA TN D-3724, November 1966.

Forman, R. G., Experimental Program to Determine Effect of Crack Buckling and Specimen Dimensions on Fracture Toughness of Thin Sheet Materials, AFFDL-TR-65-146, January 1966.

Forman, R. G., Study of Fatigue Crack Initiation from Flaws Using Fracture Mechanics Theory, AFFDL-TR-68-100, November 1967.

Forman, R. G., The Effect of Plastic Deformation on the Strain Energy Release Rate in a Centrally Notched Plate Subjected to Uniaxial Tension, AFFDL-TR-65-186, January 1966.

Forman, R. G., et al, Vulnerability of Aircraft Structures Exposed to Small Arms Fire Projectile Damage, AFFDL-TR-67-157, February 1968.

Gerberich, W. W., "A Discussion of Slow Crack Growth Associated with Plane-Strain Instability," Transactions of ASM, Vol. 59, 1966.

Gerberich, W. W., "Plastic Strains and Energy Density in Cracked Plates," Parts I and II," Society for Experimental Stress Analysis, 1965.

Gerberich, W. W., and Zacky, V. F., "On The Plane Stress Plastic Zone Correction in Fracture Mechanics," Welding Journal, Research Supplement, August 1968.

Glucklich, J. and Cohen, L. J. "Size as a Factor in the Brittle-Ductile Transition and the Strength of Some Materials," International Journal of Fracture Mechanics, Vol. 3, No. 4, December 1967.

Greenberg, H. D. and Clark, W. G., Jr., "A Fracture Mechanics Approach to the Development of Realistic Acceptance Standards for Heavy Walled Steel Castings," American Society for Metals, Metals Engineering Quarterly, August 1969.

Grief, R. and Sanders, J. L., Jr., "The Effect of a Stringer on the Stress in a Cracked Sheet," Transactions of ASME, Journal of Applied Mechanics, March 1965.

Gross, B., and Srawley, J. E., Stress-Intensity Factors by Boundary Collocation for Single-Edge-Notch Specimens Subject to Splitting Forces, NASA TN D-3295, February 1966.

Gross, E., et al, "Elastic Displacements for Various Edge-Cracked Plate Specimens," The International Journal of Fracture Mechanics, Vol. 4, No. 3, September 1968.

Gross, B., and Srawley, J. E., Stress-Intensity Factors for Three-Point Bend Specimens by Boundary Collocation, NASA TN D-3092, December 1965.

Hahn, G. T., and Rosenfield, A. R., "Experimental Determination of Plastic Constraint Ahead of a Sharp Crack Under Plane-Strain Conditions," Transactions of ASM, Vol. 59, 1966.

Hahn, G. T., and Rosenfield, A. R., "Local Yielding and Extension of a Crack Under Plane Stress," ACTA Metallurgica, Vol. 13, March 1965.

Hahn, G. T., and Rosenfield, A. R., "Plastic Zones Generated by Cracks Growing Under Load," The International Journal of Fracture Mechanics, Vol. 4, No. 2, June 1968.

Hanna, G. L., and Steigerwald, E. A., Influence of Work Hardening Exponent on Crack Propagation in High-Strength Materials, AFML-TR-66-139, October 1966.

Hartranft, R. J., and Sih, G. C., "Effect of Plate Thickness on the Bending Stress Distribution Around Through Cracks," Journal of Mathematics and Physics, Vol. XLVII, No. 3, September 1968.

Hoagland, R. G., "On the Use of the Double Cantilever Beam Specimen for Determining Plane Strain Fracture Toughness of Metals," Transactions of ASME, Journal of Basic Engineering, September 1967.

*Hofer, Jr., K. E., "Equations for Fracture Mechanics," Machine Design, February 1, 1968.

Hutchinson, J. W., "Singular Behavior at The End of a Tensile Crack in a Hardening Material," Journal of Mech. and Physics of Solids, Vol. 16, 1968.

Irwin, G. R., "Relation of Crack Toughness Measurements to Practical Applications," Welding Journal Research Supplement, November 1962.

Irwin, G. R., Relatively Unexplored Aspects of Fracture Mechanics, U. of Illinois, Theoretical and Applied Mech. Dept. Report, TAM No. 240, February 1963.

*Irwin, G. R., Liebowitz, H., and Paris, P. C., (eds.) Engineering Fracture Mechanics, Pergamon Press, (All Issues)

*Irwin, G. R., et al, Fracture Strengths Relative to Onset and Arrest of Crack Propagation, U.S. Naval Research Laboratory Report 5222, November 1958.

Isida, M., "Stress-Intensity Factors for the Tension of an Eccentrically Cracked Strip," Transactions of ASME, Journal of Applied Mechanics, September 1966.

Isida, M., et al, On the Crack Tip Stress Intensity Factor for the Tension of a Centrally Cracked Strip with Reinforced Edges, Department of Mechanics Report, Lehigh University, September 1965.

Isida, M., and Itagaki, Y., "Stress Concentration at the Tip of a Central Transverse Crack in a Stiffened Plate Subjected to Tension," Proceedings of the 4th U.S. National Congress of Applied Mechanics, Vol. 2, 1962.

Jones, R. E., Comparison of Fracture Toughness Values Obtained Using Semi-Infinite Aluminum Plates with Values Obtained Using Laboratory Size Specimens, AFML-TR-69-58, April 1969.

Ju, F. D., Stress Field in the Vicinity of an Irwin-Crack, AD 671 916, February 1968.

Kassir, M. K., and Sih, G. C., "External Elliptical Crack in Elastic Solid," The International Journal of Fracture Mechanics, Vol. 4, No. 4, December 1968.

Kaufman, J. G., et al, "Fracture Toughness of Aluminum Alloys," American Society for Metals, Metal Engineering Quarterly, August 1969.

Kaufman, J. G., "Fracture Toughness of 7075-T6 and -T651 Sheet, Plate, and Multilayered Adhesive-Bonded Panels," Transactions of ASME, Journal of Basic Engineering, September 1967.

Kies, J. A., The Resistance of Materials to Fracture Propagation and Gunfire Damage, U.S. Naval Research Laboratory Report 594, November 1956.

Kobayashi, A. S., et al, "Crack-Opening Displacements and Normal Strains in Centrally Notched Plates," Experimental Mechanics, April 1969.

Krafft, J. M., "Dynamic Mechanical Behavior of Metal at the Tip of a Plane Strain Crack," Paper presented at Southwest Research Institute Symposium on the Mechanical Behavior of Materials Under Dynamic Loads, San Antonio, September 1967.

Kramer, I. R., Study of Brittle Crack Propagation, ARL 69-0039, March 1969.

Kuhn, P., Residual Strength in the Presence of Fatigue Cracks, paper presented to Structures and Materials Panel-AGARD, 1967 (available from NASA-Washington).

Kuhn, P., "Strength Calculations for Sheet-Metal Parts with Cracks," Materials Research and Standards, September 1968.

Kuhn, P., and Figge, I. E., Unified Notch-Strength Analysis for Wrought Aluminum Alloys, NASA TN D-1259, May 1962.

Lauta, F. J., and Stiegerwald, E. A., Influence of Work Hardening Coefficient on Crack Propagation in High Strength Steels, AFML-TR-65-31, May 1965.

Li, Che-Yu, and Wei, R. P., "Calibrating the Electrical Potential Method for Studying Slow Crack Growth," Materials Research and Standards, August 1966.

*Liebowitz, H., (ed.), Fracture, an Advanced Treatise, Vols. I-VII, Academic Press, 1968, 1969.

Lorenz, P. M., "Some Parameters Affecting Measured Fracture Toughness of High-Strength Steel," Transactions of ASM, Vol. 54, 1961.

Mowbray, D. F., et al, "Fracture Toughness Determinations of A-302B and Ni-Mo-V Steels with Various Size Specimens," Transactions of the ASME, Journal of Basic Engineering, December 1966.

Oppel, G. U., and Hill, P. W., "Strain Measurements at the Root of Cracks and Notches," Experimental Mechanics, July 1964.

Packman, P. F., et al, "The Applicability of a Fracture Mechanics-Nondestructive Testing Design Criterion for Aerospace Structures," American Society for Metals, Metals Engineering Quarterly, August 1969.

*Paris, P. C., and Sih, G. C., "Stress Analysis of Cracks," American Society for Testing and Materials Special Technical Publication, (ASTM STP 381), 1964

Petrak, G. J., Evaluation of Three Point Fatigue-Cracked Bend Test Parameters, AFML-TR-68-327, November 1968.

Raymond, L., and Usell, R. J., "Fracture Mechanics in Cost-Effective Pressure Vessel Design," Journal of Spacecraft, Vol. 6, No. 6, June 1969.

Rice, J. R., Contained Plastic Deformation Near Cracks and Notches Under Longitudinal Shear, Division of Engineering, Brown University, July 1965.

Rice, J. R., Plastic Yielding at a Crack Tip, Division of Engineering, Brown University, March 1965.

Rice, J. R., Stresses Due to a Sharp Notch in a Work Hardening Elastic-Plastic Material Loaded by Longitudinal Shear, National Science Foundation Report NSF GK 286/1, December 1965.

Ripling, E. J., et al, "Measuring Fracture Toughness of Adhesive Joints," Materials Research and Standards, March 1964.

Roberts, R., and Rich, T., "Stress-Intensity Factors for Plate Bending," Transactions of ASME, Journal of Applied Mechanics, September 1967.

Rosenfield, A. R., et al, "Crack Extension and Propagation Under Plane Stress," International Conference on Fracture, Sendai, Japan, 1965.

*Shannon, Jr., J. L., "Fracture Mechanics-the Search for Safety in Numbers," Machine Design, September 28, 1967 and "Fracture Mechanics-Reducing Theory to Practice," Machine Design, October 12, 1967.

Sih, G. C., "Crack-Tip, Stress-Intensity Factors for Plane Extension and Plate Bending Problems," Transactions of ASME, Journal of Applied Mechanics, June 1962.

Sih, G. C., "On the Singular Character of Thermal Stresses Near a Crack Tip," Transactions of ASME, Journal of Applied Mechanics, September 1962.

Sih, G. C., "Stress Distributions near Internal Crack Tips for Longitudinal Shear Problems," Transactions of ASME, Journal of Applied Mechanics, March 1965.

Sih, G. H., et al, Three-Dimensional Stress Distribution near a Sharp Crack in a Plate of Finite Thickness, AFML-TR-66-242, November 1966.

Smith, S. H., et al, Fatigue-Crack-Propagation and Fracture-Toughness Characteristics of 7079 Aluminum-Alloy Sheets and Plates in Three Aged Conditions, NASA CR-996, February 1968.

Spitzig, W. A., "A Fractographic Feature of Plane-Strain Fracture in 0.45C-Ni-Cr-Mo Steel," Transactions of ASM, Vol. 61, 1968.

*Srawley, J. E., and Esgar, J. B., Investigation of Hydrotest Failure of Thiokol Chemical Corporation 260-inch-Diameter SL-1 Motor Case, NASA TM X-1194, January 1966.

Steigerwald, E. A., Plane Strain Fracture Toughness for Handbook Presentation, AFML-TR-67-187, (AD 821 626), July 1967.

*Steigerwald, E. A., "What You Should Know About Fracture Toughness," Metal Progress, November 1967.

Steigerwald, E. A., and Hanna, G. L., "Influence of Work-Hardening Exponent on the Fracture Toughness of High-Strength Materials," Transactions of the Metallurgical Society of AIME, Vol. 242, February 1968.

Sullivan, A. M., "New Specimen Design for Plane-Strain Fracture Toughness Tests," Materials Research and Standards, January 1964.

Sullivan, T. L., Texture Strengthening and Fracture Toughness of Titanium Alloy Sheet at Room and Cryogenic Temperatures, NASA TN D-4444, May 1968.

- *Tetelman, A. S., and McEvily, A. J., Jr., Fracture of Structural Materials, J. Wiley and Sons, 1967.
- *Tiffany, C. F., et al, Fracture Control of Metallic Pressure Vessels, NASA, Space Vehicle Design Criteria (Structures), to be published.
- Walker, E. K., A Study of the Influence of Geometry on the Strength of Fatigue Cracked Panels, AFFDL-TR-66-92, June 1966.
- Wang, D. Y., "An Investigation on Fatigue Crack Propagation and Failsafe Design of Stiffened Large Aluminum Alloy Plates with Various Crack Stoppers," Paper presented AIAA/ASME 10th Structures, Structural Dynamics and Materials Conference, New Orleans, April 1969.
- Wei, R. P., and Lauterbach, F. J., "Measuring Plane-Strain Fracture Toughness with Carbonitrided Single-Edge-Notch Specimens," Materials Research and Standards, July 1965.
- Weiss, V., et al, "Effect of Section Size on Notch Strength," Transactions of ASME, Journal of Basic Engineering, September 1966.
- Wells, A. A., "Application of Fracture Mechanics At and Beyond General Yielding," British Welding Journal, Vol. 10, 1963.
- Wells, A. A., "Fracture Control of Thick Steels for Pressure Vessels," British Welding Journal, May 1968.
- *Wessel, E. T., et al, Engineering Methods for the Design and Selection of Materials Against Fracture, AD 801 005, June 1966.
- Williams, M. L., and Swedlow, J. L., "The Association Between Crack-Opening Displacement and Fracture Toughness," Transactions of Metallurgical Society of AIME, Vol. 239, February 1967.
- *Williams, M. L., et al, (eds.) International Journal of Fracture Mechanics, Wolters-Noordhoff Publ., (All Issues).
- *Wilson, W. K., et al, Fracture Mechanics Technology for Combined Loading and Low-To-Intermediate Strength Metals, AD 682754, Clearinghouse, 1968.
- Wu, E. M., "Application of Fracture Mechanics to Anisotropic Plates," Transactions of the ASME, Journal of Applied Mechanics, December 1967.
- Yusuff, S., "Fracture Phenomena in Metal Plates," Aircraft Engineering, May 1962.
- Zinkham, R. E., "Anisotropy and Thickness Effects in Fracture of 7075-T6 and -T651 Aluminum Alloy," Engineering Fracture Mechanics, Vol. 1, 1968.
- Zinkham, R. E., "Longitudinal and Short Transverse Fatigue and Fracture Properties of Heavy Aluminum Alloy Plates, Produced by Forging and Rolling," Transactions of the Metallurgical Society of AIME. Vol. 245, July 1969.

Unclassified

Security Classification

DOCUMENT CONTROL DATA - R & D

(Security classification of title, body of abstract and indexing annotation must be entered when the overall report is classified)

1. ORIGINATING ACTIVITY (Corporate author) Northrop Corporation Aircraft Division Hawthorne, Calif.		2a. REPORT SECURITY CLASSIFICATION Unclassified	
		2b. GROUP	
3. REPORT TITLE Fracture Mechanics Guidelines for Aircraft Structural Applications			
4. DESCRIPTIVE NOTES (Type of report and inclusive dates) Final Report - January 1969 - November 1969			
5. AUTHOR(S) (First name, middle initial, last name) David P. Wilhem			
6. REPORT DATE December 1969		7a. TOTAL NO OF PAGES 196	7b. NO OF REFS 74
8a. CONTRACT OR GRANT NO F33615-69-C-1313		9a. ORIGINATOR'S REPORT NUMBER(S) NOR 69-142	
b. PROJECT NO 1467			
c. Task No. 146704		9b. OTHER REPORT NO(S) (Any other numbers that may be assigned to this report) AFFDL-TR-69-111	
d.			
10. DISTRIBUTION STATEMENT This document has been approved for release and sale; its distribution is unlimited.			
11. SUPPLEMENTARY NOTES		12. SPONSORING MILITARY ACTIVITY Air Force Flight Dynamics Laboratory Air Force Systems Command Wright-Patterson AFB, Ohio 45433	
13. ABSTRACT This document provides the guidelines, limitations, and modifications required to perform a structural, fracture analysis using Griffith-Irwin, fracture mechanics principles. It serves as an introduction to fracture mechanics for those personnel who are concerned with fracture strength estimates for aerospace structural applications. Illustrations and hypothetical examples are included which show how engineering solutions for critical crack size and fracture stress may be made. The critical stress intensity (fracture toughness) concept is used as a basic factor for the fracture analysis of materials. For most crack situations, a stress intensity factor can be computed which can be related to critical conditions and estimates made of critical crack lengths, stresses, and crack propagation behaviors. To provide a complete and accurate fracture analysis, the user is encouraged to become familiar with all aspects of the analysis and its limitations.			

14.	KEY WORDS	LINK A		LINK B		LINK C	
		ROLE	WT	ROLE	WT	ROLE	WT
	FRACTURE MECHANICS						
	FRACTURE MECHANICS GUIDELINES						
	FRACTURE ANALYSIS						
	FRACTURE TOUGHNESS						
	CRACK PROPAGATION						